Vinyl Chloride Precipitation Polymerisation: Charge Effects

by

Norman Ogilvy, G.R.S.C.

A thesis submitted for the Degree of Doctor of Philosophy

University of Edinburgh September 1985

To Ann

Acknowledgements

I am grateful to my supervisor, Dr. W. D. Cooper, for his constant encouragement and interest throughout the project.

I also thank I.C.I. plc., Petrochemical and Plastics Division and the S.E.R.C. for the provision of a C.A.S.E. award.

In particular I am grateful to Mr. E. L. Zichy, without whose initial experiments this work would not have been carried out, along with Dr. D. G. Rance and Mr. J. C. Wilson for their continued help and many useful discussions.

The assistance of the technical staff of the Chemistry Department is appreciated and the author is grateful to Ann for undertaking the typing.

Abstract

Previous studies of the bulk and suspension polymerisation of vinyl chloride monomer have been reviewed and in particular those results pertaining to the aggregation of the so called "primary" particles formed during the initial stage of polymerisation. In a recent study it was proposed that the primary particles carried a net negative charge and that the resulting electrostatic repulsion between these particles could account for their known colloidal stability. The aim of this work was to confirm and quantify the extent of this net negative charge and, if successful, to vary its magnitude to provide a means of control over the primary particle stability and hence the particle aggregation process.

For this investigation a combined polymerisation / microelectrophoresis cell was developed to withstand the pressure required to maintain vinyl chloride monomer in a liquified form at temperatures up to 343 K.

Dispersions of PVC particles in VCM were characterized in terms of their zeta potential, particle concentration, particle diameter and aggregate morphology, as determined by scanning electron microscopy.

The results obtained confirmed that the primary

particles consistantly carried a net negative charge in the region of 18 elementary charges. The particles also exhibited a critical maximum diameter above which aggregation occurred.

The theoretical stability of the primary particles was predicted by DLVO type calculations. A comparison of two and multiparticle interaction models has been presented. The experimentally observed primary particle stability was in agreement with the theoretical predictions.

Major changes in primary particle stability were achieved by the addition of low molecular mass compounds which modified the net charge on the particles over the range of 2 to 70 charges per particle. The rate of polymerisation was also shown to affect polymer morphology.

A mechanism for the development of particle structures in the initial stages of PVC production was proposed and ways in which this structure can be controlled discussed. Several suggestions for further work in this industrially important area were also made.

CONTENTS

Chapter 1	INTRODUCTION	1
1.1	Introduction.	2
1.2	A review of the precipitation polymerisation of VCM.	7
1.3	Outline of the project.	30
Chapter 2	THEORY OF COLLOID STABILITY.	34
2.1	Introduction.	35
2.2	Potential energy of repulsion.	36
2.3	Potential energy of attraction.	52
2.4	Total potential energy of interaction.	63
2.5	Kinetics of coagulation.	66
2.5.1	Rapid coagulation.	66
2.5.2	Slow coagulation and stability.	70
Chapter 3	EXPERIMENTAL METHODS.	76
3.1	Equipment and materials.	77
3.1.1	Introduction.	77
3.1.2	Materials.	78
3.1.3	Equipment for VCM handling.	79
3.1.4	Development of a combined polymerisation/electrophoresis cell.	81
3.1.5	Equipment for polymerisation/ electrophoresis experiments.	83

3.2	Techniques.	85
3.2.1	Preparation of PVC Latex.	85
3.2.1.1	VCM transfer to the Hone Cylinder.	85
3.2.1.2	Monomer transfer to the cell.	86
3.2.1.3	Polymerisation.	88
3.2.2	Elecrophoresis.	89
3.2.2.1	Theory.	89
3.2.2.2	Technique.	93
3.2.2.3	Evaluation of optical corrections and cell lengths.	95
3.2.3	Analysis of particle size and morphology.	100
3.2.3.1	Particle sampling method.	103
3.2.3.2	Scanning electron microscopy.	105
3.2.3.3	Image analysis.	106
Chapter 4	RESULTS AND DISCUSSION	109
4	Introduction.	110
4.1	Preliminary investigations using the combined cell.	111
4.1.1	Polymerisation.	111
4.1.2	Electrophoresis.	113
4.2	Experimental investigation of colloidal events during polymerisation.	121
4.2.1	Introduction.	121
4.2.2	PVC polymer morphology.	121

4.2.3	Particle size distribution.	130
4.2.4	Particle concentration.	141
4.2.5	Electrophoresis.	146
4.2.6	Primary particle charge.	158
4.3	Theoretical investigation of colloidal stability during polymerisation.	161
4.3.1	Particle charge regime during growth.	161
4.3.2	Theoretical investigation of primary particle stability.	163
4.4	Addition of low molecular mass additives.	170
4.4.1	Introduction.	170
4.4.2	Manoxol-OT.	172
4.4.3	Span-20.	175
4.4.4	Bis-(2-hydroxyethyl)-aminohexadecane.	184
4.5	VCM polymerisation reaction kinetics.	197
4.5.1	Introduction.	197
4.5.2	Calculation of polymerisation rates.	199
4.6	Summarising remarks.	205
4.7	Proposed mechanism for the precipitation polymerisation of VCM.	210
4.8	Suggestions for future work.	219
4.8.1	Equipment.	219
4.8.2	Experimental programme.	221
References		223
Appendixes		238

Chapter One

Introduction

1.1 Introduction

Commercial production of poly(vinyl chloride) (PVC) began in 1927 and since then the demand for this polymer has increased rapidly making PVC one of the highest tonnage polymers produced today (12 million tonne in 1980). PVC is utilized in numerous products ranging from clothing, furnishing and packaging to the formation of rigid pipe work, floor coverings and electric cable insulation as used in the construction industry. This variety of applications stems from the widely differing material properties achieved by the incorporation of formulation ingredients with the raw polymer.

Poly(vinyl chloride) may be produced by a bulk, suspension, emulsion or solution polymerisation. The low solubility of PVC in its monomer (VCM) results in phase separation at an early stage of the polymerisation. This creates colloidal sized particles which grow by a series of polymerisation and coagulation steps. As the monomer is consumed, particle aggregates fuse together to give a continuous porous network within a single polymer granule.

The final granule morphology, which encompasses the size, shape and internal structure of the granule, will be determined to a large extent by the nature and packing of the particles formed at earlier stages in the polymerisation. The morphology, and in particular the porosity of the final product, is of prime importance as it determines the extent of ingress of plasticiser to

soften the PVC before fabrication. More recently, with the recognition of the toxicity of VCM, the production of a more porous polymer granule has been sought to assist the ready removal of unreacted residual monomer (1).

The particles formed during the early stages of polymerisation range from approximately 20 nm to 1 μm diameter and thus span the typical size range for colloidal particles. The application of colloid stability theory to the results of an experimental investigation of these particles during their evolution should provide a mechanism for the control of granule morphology and hence porosity.

Lyophobic (dispersion medium hating) colloids such as PVC particles in VCM are, by definition thermodynamically unstable due to their high interfacial free energies. In the absence of particle interaction forces each collision brought about by Brownian motion and resulting in coagulation will lead to reduction of the interfacial free energy. Coagulation will continue to occur at a rate controlled by diffusion until the minimum total interfacial free energy for the system is reached. In practice however, many lyophobic colloids are found to be stable over considerable periods of time indicating the presence of a stabilising mechanism. This may be the adsorption of a layer of protective material giving rise to steric stabilisation or electrostatic repulsion due to electrically charged particles.

Derjaguin and Landau (2) and Verwey and Overbeek (3)

have independently developed a theory to predict the stability of two particles as they approach from infinite separation and are influenced by attractive and repulsive interparticle forces. The validity of the DLVO theory has been tested exhaustively over the last 30 years and it has successfully accounted for the observed stability of many aqueous and non-aqueous dispersions.

In this work the results of theoretical calculations are used to predict the experimentally observed stability of polymer particles produced during the polymerisation of vinyl chloride monomer.

In emulsion polymerisation, the monomer is dispersed as relatively stable droplets in water by the addition of emulsifying agents. The reaction is initiated by a water soluble initiator and the final product is a stable suspension or latex of PVC particles typically having diameters in the range 0.05-0.25 μm. These can be used directly or more commonly spray dried to give a polymer in powdered form.

In suspension polymerisation monomer droplets of about 100 μm diameter are dispersed in water by vigorous agitation. A protective colloid such as poly(vinyl alcohol) is used to prevent droplet coalescence. Unlike emulsion polymerisation, the free radical reaction is initiated by a monomer soluble initiator. The product is a free flowing powder made up of 50-250 μm diameter granules which usually originate from more than one monomer droplet.

The bulk or mass polymerisation of VCM is carried out in the absence of water or a solvent for the polymer and results in a dry granular powder which does not require expensive dewatering techniques. The product is also of high purity as it is not necessary to add emulsifiers or protective colloids. For these reasons considerable effort has been spent on developing a large scale commercial process such as the Pechiney-St. Gobian method (6) to overcome the heat transfer problem associated with this type of polymerisation.

The final method of solution polymerisation is mainly reserved for speciality copolymers because of the high production costs encountered in this process.

Unfortunately for the newcomer, the terminology used in the literature to describe PVC morphology is inconsistent and very confusing. In this work the polymer structures observed by electron microscopy have been assigned the terminology proposed by Allsopp (7), whose nomenclature is best suited to describe the colloidal events taking place in the formation of the particulate polymer granule. This terminology, along with the recently proposed IUPAC nomenclature (8), is given in Appendix (1) for cross referencing purposes.

In this work the bulk polymerisation of VCM was investigated. The mechanism and kinetics of bulk and suspension polymerisation are equivalent and so the results obtained also apply to the commercially more important suspension polymerisation. Indeed the suspension

polymerisation can be considered to be a series of individual bulk polymerisations occurring within each monomer droplet in the aqueous phase.

In these systems the phase separation and coiling of macro radicals occurs very early in the polymerisation to create "basic" particles of 10 to 20 nm. Basic particles lack colloidal stability and around a 1000 particles rapidly coagulate to give a "primary" particle. Primary particles are initially stable and grow to approximately 0.2 μm diameter by polymerisation. A second period of coagulation then occurs resulting in the formation of the "primary particle cluster or aggregate" containing initially 13 primary particles. Polymerisation continues within these clusters which fuse together as the monomer is consumed. The final product of the suspension polymerisation is a highly porous 100 μm diameter polymer granule.

The last decade has seen a rapid advance in the understanding of the microstructure of PVC and it has been suggested (9) that porosity may be controlled by the size at which the primary particles coagulate to form the primary clusters. The aim of this work is to confirm the nature of the stabilising mechanism operating on the primary particle and by modifying their colloidal stability control the size at which they coagulate. Hopefully this will lead to a relationship between PVC morphology and polymer porosity and allow for a more rational control of the industrial suspension and bulk polymerisations.

1.2 A review of the precipitation polymerisation of VCM.

A great deal of the early literature on VCM polymerisation concentrates on establishing the complex nature of the reaction kinetics. Reports pertaining to the morphological characteristics of the polymer are more limited. However, the recent interest in this area along with the application of specialised techniques has allowed rapid advances to be made in the understanding of the particulate structure of PVC. The majority of investigators of precipitation polymerisation have considered bulk polymerisation for experimental simplicity, rather than the more important industrial suspension process. This is of little consequence since Talamini and coworkers (10) showed the two processes to be mechanistically similar.

The polymerisation was considered by Bort (11) to take place in three stages, the first and third stages occur in a single phase and represent a homogeneous process. During the second stage two phases are present simultaneously and give rise to a heterogeneous system. The first stage lasts until the phase separation of the growing macro radicals from the monomer. This creates a heterogeneous system which consists of the liquid monomer and monomer swollen polymer phases. This stage lasts from less than 1% conversion to approximately 77% conversion at which point all free monomer is consumed. The third stage of the polymerisation is then entered in which, the

monomer trapped within the polymer continues to polymerise and the system reverts to a homogeneous process.

The results of a series of investigations (12-17) indicated that there was an acceleration of the bulk polymerisation rate with conversion. Bengough and Norrish (14) observed that this acceleration was due to the cocatalytic effect of the phase separated polymer. They showed that in the presence of a solvent for the PVC no rate acceleration occurred. This disproved the previously held views that either the initiation was controlled by two consecutive reactions via an initiator-monomer complex (15), or by the presence of inhibiting impurities (16,18).

The rate acceleration caused by the cocatalytic effect of 'dead' polymer was found to be proportional to the amount of polymer present raised to the power 2/3 ($[P]^{2/3}$) which suggested that the increased rate was linked to the surface area of the polymer. Their mechanism proposed that, in addition to the normal propagation step in the monomer, a growing radical could transfer to the surface of a polymer particle. Here the trapped radicals were relatively free from the termination reaction which occurs more frequently in the monomer. Thus as more radicals are transferred to the surface, the reaction rate increases. The revived polymer grows by the addition of monomer until the radical is terminated by chain transfer with the monomer, thus releasing a mobile free radical. The mechanism of Bengough and Norrish has been critisised (11) for ignoring the possibility of polymerisation inside

the monomer swollen particles of the polymer phase.

Mickley et. al. (19) considered separate reactions occurring in the monomer and polymer phases. For the polymer phase they proposed that at low conversions the rate was proportional to the polymer concentration [P] whilst at higher conversions a $[P]^{2/3}$ (surface area) dependency occurred. They explained their results in terms of a precipitation plus flocculation process in which primary particles are generated homogeneously in the monomer phase and are almost immediately deposited onto a large and nearly constant number of primary aggregates. A polymer concentration effect, on polymerisation rate, would arise if radical activity was trapped within the primary particle as it was incorporated into the aggregate or if radical activity was transferred from the liquid phase into the primary particle. They concluded that at low conversions the primaries in the still small aggregates would have ready access to both monomer and radical activity resulting in a first order polymer concentration dependancy. As the aggregates grew larger only the primary particles at the surface would have access to the monomer and free radical activity, resulting in a rate dependance of $[P]^{2/3}$.

Cotman et. al. (20) also found that the simple surface area relationship given by Bengough and Norrish was inadequate at low conversions and proposed an empirical equation to predict the power dependance of polymer concentration on polymerisation rate.

The failure of these attempts to adequately describe the cocatalytic effect of the polymer resulted in the development of a series of new kinetic models. Unlike the previous models, which considered polymerisation to occur only in the monomer phase or at the surface of the polymer, new kinetic schemes were proposed which assumed polymerisation to take place in both the liquid phase and throughout the entire swollen polymer phase.

Talamini and co-workers (10) showed the kinetic equivalence of the bulk and suspension polymerisation. Their model allowed initiation to occur in both the monomer and polymer phases. However, the possibility of radical transfer between phases was ignored. They interpreted the experimentally observed increase in polymerisation rate with conversion as arising from a faster rate of polymerisation in the polymer rich phase. As the amount of this phase increases with conversion so does the rate of polymerisation.

Abdel-Alim and Hamielec (21) further refined this model to allow for the consumption of the initiator and account for the change in volume which occurs with increasing conversion. Using several types of initiators they found their model accurately described the kinetics of bulk polymerisations to high conversions.

The most vulnerable assumption of the Talamini model is the lack of radical transfer from one phase to the other. Ugelstad (22,23) has extended the original model to allow radical adsorption and desorption from the

polymer phase, whilst Olaj (24,25) has approached the problem in a completely different way. Olaj proposed that radicals in the polymer rich phase remain there until termination occurs, whilst radicals formed in the monomer grow in the monomer until they phase separate to create polymer particles. These are incorporated into existing polymer particles where they continue to polymerise until they lose their radical activity through chain transfer or mutual termination. Olaj's model results in the rapid transfer of all the monomer initiated radicals to the polymer phase where eventually they are terminated. The increase in rate with increasing conversion arises from the increase in kinetic chain length, caused by the reduction in the rate of bimolecular termination as the volume of particles increases at constant rate of initiation.

The kinetic models of Olaj and Ugelstad are equivalent except at low conversions. Ugelstad claimed that his model, which allows for the mutual termination of radicals arising in the monomer phase, would give better agreement at low conversions. However, following the analysis of experimental results (26) Ugelstad (27) has indicated that Olaj's model is more reliable at low conversions.

A number of recent papers have discussed the experimental results of bulk and suspension polymerisation in terms of kinetic models. Both Kafarov et. al. (28) and Thiele et. al. (29) have proposed modified schemes

assuming reactions occurring in both phases and including radical transport between phases. Bulle and co-workers (30) have investigated the suspension polymerisation and compare their experimental results to a Talamini type model, without radical transfer between phases and a model similar to one proposed by Bort which takes into account the diffusion of radicals from the liquid to polymer phase. Both models are in reasonable agreement with the experimental results, the Bort model giving slightly better results.

A completely different mechanism has been proposed by Ray and Jain (31) who claim that primary particles of about 1 μm diameter formed during the initial stages of polymerisation are swollen to a negligible degree and reaction within the polymer phase is neglected. The polymerisation takes place in the monomer phase and within the pores of the aggregated primary particles at higher conversions. It is claimed that the autocatalytic effect arises from a decrease in the value of the diffusion controlled termination constant in the pores.

Although some difficulties still exist at low polymer conversions the kinetic models derived from the original Talamini model have been shown to be in good agreement with the experimental results of bulk and suspension polymerisations. During the extensive investigation of these kinetic schemes a great deal of circumstantial evidence was gained regarding the formation and nature of the polymer particles.

The results of the early investigation of Mickley (19) on the formation and fate of particles created during bulk polymerisation were later confirmed by Cotman (20). Their work indicated that the initially soluble macro radical grew to a critical length of between 25 to 32 monomer units. The polymer chain then coiled upon itself to produce what they termed a primary particle of about 10 nm diameter. At less than 0.1% conversion they observed a rapid reduction in particle number corresponding to the formation of aggregates. Cotman estimated that during this stage the particle number decreased from at least 25×10^{11} to 5×10^{11} particles per gram of VCM. By applying the results of Muller (32), who showed that the collision frequency was greater for dissimilar sized aggregates than like sized aggregates, they concluded that the larger aggregates would tend to scavenge primaries and smaller aggregates from suspension. The overall result was a near constant number of aggregates growing by deposition of primary particles or by the polymerisation of active radicals on the surface of the particles.

Bort et. al. (33-36) were amongst the first to investigate the relationship between reaction kinetics and particle morphology. They identified two types of particles, the microglobule and the macroglobule, the latter being a 1 - 2 μm diameter aggregate of microglobules. A mechanism, similar to those suggested by Mickley and Cotman, was proposed in which microglobules precipitated from the monomer at a low conversion and then

continued to grow either by the polymerisation of the monomer swelling them or by the incorporation of polymer from the monomer. The unstable microglobules continued to flocculate until they attained a critical size above which they remained stable to flocculation.

Bort showed, that at slow polymerisation rates, a considerable number of collisions resulting in coagulation of microglobules occurred before the critical particle diameter was reached. This resulted in a macroglobule containing many microglobules. Conversely, at high polymerisation rates, the microglobules reached the critical size before the coagulation of particles could occur, thus each macroglobule would arise from a single microglobule. Bort concluded that the number of microglobules produced was virtually independant of the polymerisation rate at approximately 1×10^{11} per cm^3 of VCM. Thus a constant number of microglobules were distributed between the macroglobules. The number of microglobules per macroglobule, and hence its morphology, being solely determined by the rate of polymerisation.

The particles described by Bort and coworkers were also observed by Tregan and Bonnemayer (37) who, at less than 1% conversion, found 0.1 μm diameter microglobules consisting of yet smaller nuclei. Above 5% conversion these microglobules became colloidally unstable and aggregated to give macroglobules of between 1 and 2 μm in diameter.

Behrens (38,39), observing ultra thin sections of PVC using electron microscopy, resolved 10 nm structures and proposed that these particles were the basic elements of the PVC polymer structure. Calculations based on molecule dimensions indicated that these basic particles contained between 5 and 10 macro radicals. Behrens confirmed that the 10 nm diameter basic particles existed in both the bulk and suspension polymerisation and grow uniformly to create 0.1 to 0.3 μm diameter microglobules (primary particles).

The problem of particle nucleation was considered by Boissel and Fischer (40) who followed the development of particles during the initial stages of bulk polymerisations using a turbidimetric device and electron microscopy. They found phase separation of the polymer from its monomer occurred at conversions as low as 0.001%. Previous estimates had indicated significantly higher values (11,41). Rance and Zichy (42) provide further evidence to suggest the early phase separation of the polymer. By considering the Flory interaction parameter for the VCM/PVC system (chi = 0.98) they calculated the solubility of the polymer in monomer to be limited to polymer chains consisting of approximately 10 monomer units.

The first particles observed by Boissel and Fischer from polymerisations at 323 K and 333 K were substantially spherical granules of less than 0.25 μm diameter. On reducing the temperature to 303 K the

particles were no longer spherical and contained a substructure. For a constant rate of radical formation the number of particles formed was found to decrease with increasing temperature. However, at a given temperature they observed that the number of particles remained constant up to a critical conversion, above which the granules aggregated to form complex structures, called grains, with a minimum diameter of 20 to 30 μm. At this point a far smaller population of granules appeared indicating, for the first time, the possibility of secondary nucleation. The critical conversion value was found to be strongly dependant on the rate of agitation. As the intensity of agitation was increased the critical conversion decreased (0.12% to 0.05%).

A mechanism for the polymerisation was presented in which precipitated macromolecules group together in packs of 5 to 10 to produce particles of 10 nm. These grow uniformly by polymerisation, without aggregation, up to a critical conversion, at which point they agglomerate to give the final 20-30 μm grain.

This mechanism deviates from those proposed by several other authors (19,20,42,43,44) in that there is no rapid aggregation of the 10 nm basic particles to give the 0.8 to 0.1 μm diameter primary particles which grow by polymerisation until a critical conversion is reached. Boissel and Fischer give no evidence for their mechanism and it is possible that their experiments failed to detect the rapid aggregation step of the 10 nm diameter basic

particles so early in the polymerisation (19,42).

An attempt to study the aggregation of basic particles to form primary particles has been reported (42). Particle nucleation in a bulk polymerisation was followed by photon correlation spectroscopy (PCS). No evidence of the basic 10 nm particles was found, the first observed structures already being primary particles of 0.08 μm diameter. The authors calculated that the aggregation of the basic particles took place within the first 10 to 20 seconds of polymerisation and occurred before PCS measurements could be recorded.

Singleton and co-workers (45) have, however, observed 10 nm structures in plasticised PVC using small angle X-ray diffraction and freeze fracture-replication electron microscopy. Following this, Soni et. al. (46) used a variety of electron microscope sample preparation techniques, including freeze fracture, ion etching and osmium tetroxide staining, to obtain evidence of the basic particle which they consider to consist of a crystalline core surrounded by a less ordered material, possibly of a fringed micelle structure.

Barclay (47) considered the formation and structure of PVC particles prepared by the commercial suspension and two stage bulk polymerisation. He found that the method of nucleation was common to both processes with the precipitation of 10 nm polymer particles from the monomer almost as soon as it was contacted by initiator. At less than 0.1% conversion these "nascent" particles

aggregate to form microgranules of up to 0·1 μm diameter. A period of growth was followed by coagulation at about 1% conversion to give microgranule clusters which continued to grow into the final PVC particles.

Many references (1,7,9,47,48,49) have been made to the important relationship between particle morphology and the final PVC polymer porosity. A porous polymer being required to degas readily and allow the rapid uptake of plasticiser. In suspension polymerisation the monomer phase is dispersed in water by vigorous agitation and the monomer droplets produced are prevented from coalescing by the addition of a protective colloid such as poly (vinyl alcohol), PVA, or a granulating agent. At low conversion a skin or membrane forms around the droplet which has been shown to be a PVA/PVC graft copolymer. Polymerisation of the monomer results in a polymer granule of 100 to 150 μm diameter, enclosed in a 0.5 μm thick membrane. These granules may have varying degrees of internal porosity. Barclay identified two types of pore, namely the small interstitial voids between microgranules or groups of microgranules and the much larger skin lined voids which may occur within the granule. In bulk polymerisation no membrane is formed around the particle and here the internal porosity arises from the interstices between the primary particles.

Several studies (1,7) have investigated the porosity of the bulk and suspension polymers using mercury porosimetry. Recently Bort et. al. (50), using a contact

standard porometry method, reported that for bulk produced PVC above 20% conversion there was an increase in small pore sizes but a net decrease in the pore parameters and porosity.

Krzewki and Sieglaff (48) have indicated the limitations of results obtained by mercury porosimetry and similar techniques. They point out that these methods measure only the average porosity and fail to indicate the distribution of pore sizes. Using scanning electron microscopy they identified five main types of granule morphology. These were characterised in terms of porosity and structural heterogeneity using a density fractionation method, silicone oil adsorption and SEM examination of fractured particles embedded in an epoxy resin. Their results indicated that within single resin particles a wide range of porosities may exist that would prevent the uniform uptake of formulation ingredients and profoundly effect compounding and processing operations.

The awareness of the link between morphology and processing behaviour has led to attempts to unravel the mechanism of particle formation and to develop methods of controlling PVC morphology. In suspension polymerisation it has been shown (44) that the interfacial tension between vinyl chloride and the aqueous phase has a marked effect on the total porosity. Non-porous granules are produced when the interfacial tension is relatively high due to the larger contractive force acting on the monomer droplets. Under conditions of high agitation and where

insufficient protective colloid is present, aggregation of monomer droplets occurs forming small skin lined voids between the aggregated droplets. Where the final granule is formed from a single droplet large internal voids result from a combination of droplet distortion caused by vigorous agitation and volume contractions which occur within the droplet during polymerisation. It was concluded that the size, shape and internal structure of suspension PVC was largely controlled by a balance of the amount of protective colloid, the interfacial tension and the rate of agitation within the reaction vessel.

Sanderson (1) considered the modification of PVC granule morphology by alteration of the reaction conditions. By considering suspension polymerisations over a temperature range of 323K to 343K it was found that both the granule porosity and molecular mass of the polymer were inversely proportional to the reaction temperature. Thus where polymerisation conditions, with the exception of temperature, are kept constant, high temperature polymerisations will result in high molecular mass polymers of high granule porosity. Conversely, at low temperatures low molecular mass polymers of low granule porosity result.

Constant stirring of the reactants during polymerisation is required, initially to create monomer droplets and then to assist heat transfer out of the exothermic reaction. The effect of the rate of agitation, at constant temperature, was therefore also studied. The

results showed that the final granule size was inversely proportional to the agitation rate whilst granule porosity was directly related. Thus, as stirring speed increased, the droplet size decreased and the porosity increased. These results were broadly in line with the earlier results of Johnson (51) who investigated the system to higher rates of agitation. At low stirrer speeds the PVC granules obtained were large, dense spheres. As the agitation increased, the size of the granules at first decreased, reached a minimum and then increased due to the agglomeration of monomer droplets. Throughout the process the granule porosity increased and it was concluded that it was impossible to control both granule size and porosity by agitation alone.

On considering the role of the protective colloid, Sanderson found that for identical polymerisation conditions variations in the chemical structure of the dispersing colloid produced polymer granules ranging from highly porous to virtually non-porous. Higher porosity PVC suspension granules can therefore be obtained by reducing the polymerisation temperature, increasing agitation and optimising the nature of the protective colloid.

Allsopp (7) investigated the growth mechanism of PVC granules at high polymer conversions by injecting additional monomer into a conventional suspension polymerisation before and after the loss of the free monomer phase. This occurs at about 70% conversion and is accompanied by a pressure drop. The results indicated that

the reduction in polymerisation rate after pressure drop was due to monomer starvation and it was postulated that the polymerisation only occurred at the surface of the polymer, the centre of the primary particles acting only as a monomer reservoir.

During the post-pressure drop polymerisation a detremental loss of overall porosity was observed and was attributed to the infilling of pores by increased polymerisation in the interstitial voids of the primary particles. This was caused by initiator precipitating onto the surface of the particles particularly in the pores of the primary particle aggregates, where the last residues of monomer would persist.

More recently Allsopp (52) presented a review of suspension polymerisation, concentrating on the macro to submacroscopic morphology of the PVC granule. Depending on the stability of the VCM droplet suspended in water, three possible polymerisation mechanisms are proposed, each giving rise to a characteristic macro-morphology. By route one, high droplet protection is achieved by intermediate interfacial tension and low rates of agitation, the droplet remains stable to coalescence throughout the polymerisation and forms a spherical granule of low porosity. In route two an intermediate level of protection is applied (low interfacial tension) and high agitation rates are employed. Here the droplets undergo a controlled coalescence during the polymerisation to produce irregular granules of smaller size and higher porosity. Subtle

changes in the process are used to produce polymers to a variety of specifications. Route three is avoided in the commercial process. If insufficient droplet protection is present droplet coalescence is unhindered resulting in a continuous polymer structure throughout the reaction vessel.

The control of the macroscopic polymer morphology is now fairly well understood. Changes in the bulk polymer properties, such as apparent density and granule size and size distribution can be related to macroscopic structural changes. Some properties however, for example surface area, porosity and processing characteristics, vary widely with virtually no change in the macro scale appearance of the granule. These properties are the result of micro and submicroscopic structures within the granule and methods of controlling these properties are much less well understood.

As we have already seen, the porosity to a large extent arises from the interstitial voids between individual, or aggregates of, primary particles. Zichy (9) reaffirmed this finding and proposed that the major factors influencing the morphology and hence porosity of the polymer was the size of the primary particles at the last aggregation step or the conversion at which this occurred. Zichy, using a spinning drop apparatus, studied the morphological changes taking place within a suspended monomer droplet.

A mechanism of particle formation, similar to that

of Fitch (53), was suggested in which soluble oligomeric radicals precipitate as polymer particles. Oligomers formed after the first particles could either themselves grow to a critical size and precipitate or be captured by existing particles. As the particle number increases the probability of capture increases until all oligomers formed in the monomer are incorporated. Particle growth then occurs by polymerisation of the monomer swollen particles or, in the absence of a net repulsive force, by the coagulation of particles to form aggregates.

Using Smoluchowski's theory of diffusion controlled flocculation, Zichy calculated the expected average particle diameter at 2% conversion to be 10 μm, whereas in practice the observed particle diameter was only about 0.1 μm. This indicated the presence of a net repulsive force between particles which prevented their coagulation to form 10 μm diameter particles.

Two types of polymerisations, one of which contained a colloid stabiliser for the primary particles, were taken to 28% conversion. On examining the polymer produced by electron microscopy, in the presence of particle stabiliser spherical particles of 0.8μm diameter were found, whilst the polymer formed in the absence of stabiliser consisted of aggregates of spherical particles onto which further polymer had grown. These aggregates appeared to contain 13 primary particles in which a central particle was surrounded by 12 touching neighbours. This is to be expected as Hoare (54) has shown that the

cohesive strength of a 13 particle cluster represents one of the more stable arrangements of particles in clusters.

Zichy concluded that the major factors influencing the final morphology of the fully polymerised polymer and hence its porosity, was the size of the primary particle aggregate which was controlled to a large extent by the monomer conversion and diameter of the primary particles at the aggregation step. The modification of the onset of primary particle aggregation by the control of their colloid stability could lead to a degree of morphology and porosity control.

Dunn and Chong (55) applied DLVO theory to the problem of particle formation during the polymerisation of vinyl acetate. The polymer particles which precipitated were initially unstable and coalesced rapidly forming aggregates which then remained stable with respect to like sized aggregates. However they continued to coagulate with smaller newly formed particles which, in the polymerisation of vinyl acetate, were produced throughout the reaction. They reported that the DLVO theory successfully accounted for the dependance of particle size on polymerisation variables and that the rate of particle coalescence during the reaction depends primarily on the stabilisation of the polymer particles rather than the rate of polymerisation.

Ottewill et. al. (56) indicated the important role of colloidal stability on the control of particle size in the formation of polymer latices. In the absence of

emulsifiers, it was shown that in aqueous systems the ionic strength and the incorporation of ionisable surface groups to give electrostatic stabilisation played a major role in controlling particle size.

Wilson and Zichy (57) have described an experiment to ascertain whether electrostatic stabilisation could account for the observed stability of PVC particles produced by suspension polymerisation. A pendant drop of VCM surrounded by an aqueous phase was polymerised until turbid. The resulting PVC particles were allowed to sediment leaving a clear layer of monomer at the top of the drop. By applying a potential difference of 1.5 V across the droplet the boundary between the clear monomer and PVC particles moved, the direction of movement indicating that the PVC particles carried a net negative charge. Uncertainty in the magnitude of the electric field between the electrodes meant that no quantitative measurement of the electrophoretic mobility of PVC particles in monomer could be made.

As a result of this work, Speirs (58),(59) investigated the electric charge on the growing primary particles to establish whether it was of sufficient magnitude to account for the observed stability behaviour. Following the development of a microelectrophoresis technique capable of operating at the autogeneous pressure of VCM, Speirs confirmed that a net negative charge existed on the PVC particles dispersed in VCM and obtained a zeta potential of -83 mV which corresponded to

approximately 41 elementary charges per particle.

Evidence for the existence of basic particles was also obtained by electron microscopy following the photochemical polymerisation of VCM.

It was proposed that the sharp onset of flocculation of primary particles in the polymerisation was characteristic of a system which contains a constant total charge. Theoretical DLVO type calculations, to predict the stability behaviour of primary particles, indicated that the classical two particle interaction approach was inappropriate since the double layer thickness was of the same order as the average interparticle separation. When the particle concentration effect was allowed for, by considering multi-particle interactions, a closer agreement between experimental and theoretical results was achieved.

More recently Davidson and Witenhafer (60) observed that PVC particles inside an unagitated suspension droplet remained stable up to 2% conversion and formed regular arrays which they suggested was indicative of electrostatic stabilisation since particles stabilised by entropic or mechanical means would not exhibit this behaviour. Using a moving boundary electrophoresis apparatus designed for use at high pressure, an electrophoretic mobility of $-1.78 \times 10^{-18} m^2 V^{-1} sec^{-1}$ was recorded which corresponds to a zeta potential of approximately -120mV.

The origin of charge on the PVC particles is still

the subject of speculation. Both Rance and Zichy (61) and Davidson and Witenhafer (60) have proposed that the most probable source of negatively charged ions in VCM at the start of polymerisation is chloride ions, which may specifically adsorb at the VCM/PVC interface. The chloride ions may be present either by the dehydrochlorination of PVC or from the hydrochloric acid produced through a side reaction. It has been shown (62) that residual oxygen present in the reactor readily reacts with VCM in the presence of radicals to produce vinyl chloride peroxide which subsequently decomposes to give hydrochloric acid as one of the products. Once all the oxygen has been consumed it was suggested that the ionic species present in the system (Cl^-, OH^-, H_3O^+ ions) will remain constant thus giving rise to a constant total charge to be distributed amongst the fixed number of PVC particles.

Further evidence to suggest that the chloride ion is responsible for the observed electrophoretic behaviour has been obtained (60) by an aqueous extraction of the charging species from initially stable particles produced in a bulk polymerisation. This resulted in the aggregation of the particles and hydrochloric acid being detected in the aqueous phase. Furthermore it was proposed that in a suspension polymerisation the charging species were not lost to the aqueous phase but retained by the pericellular membrane which surrounds the polymerising droplets.

An alternative explanation for the negative charge has been provided by Fowkes and Heilscher (63) in

terms of "anion states" on the polymer resulting from electron injection from "donor states" of the surrounding medium.

The exact origin of the electrical charge on the PVC particles is unclear. However the ability to modify the magnitude of this charge could result in a method of controlling PVC morphology with commercial gains in ease of polymer processing. Consequently the literature contains very few reports pertaining to the nature of additives used in the modification of PVC polymer morphology and their possible link with the colloidal stability of the primary particles.

Zichy (9) reported that polymerisations containing an "experimental stabilizer" prevented aggregation of primary particles at conversions up to 28% whereas in the unstabilised polymerisation aggregation of the primary particles occurred at much lower conversion.

Other investigators (64) have shown that bulk polymerisations carried out at 323K in the presence of up to 4% methanol resulted in a transition from large agglomerates of microglobules to smooth spherical particles. Their results indicated that agglomerate morphology was dependent on polymerisation temperature and amount of methanol present.

Bort et. al. (65) established that the surfactants sucrose distearate and sucrose dipalmitate modified the kinetics and morphology of PVC polymerisations.

During the course of this work Tornell and Uustalu

(66) investigated the influence of Span-20 and a range of polymeric additives on primary particle nucleation and agglomeration during the bulk polymerisation of VCM. They observed that the polymeric additives stabilized the primary particles against agglomeration but this failed to have any effect on particle size.

The addition of 0.2% sorbitan monolaurate (Span-20) resulted in a decrease in primary particle size at the point of aggregation. No mechanism for its action was proposed.

1.3 Outline of the project.

The previous work of Speirs (58) in a C.A.S.E. Award at Edinburgh University laid the foundations for this study.

The initial objective of this present work was to confirm Speirs' finding that the PVC particles carried a net negative charge. An investigation would then be undertaken to quantify the magnitude and sign of this charge as polymerisation conditions were systematically varied. The results of this study could indicate that the observed behaviour of primary particle stability prior to aggregation might be successfully explained in terms of electrostatic stabilisation. Then by the addition of low molecular mass compounds it was hoped that the magnitude of the charge on the primary particles could be varied to

control the onset of primary particle aggregation. This control could then be utilized to produce a polymer with a wide variety of morphologies and lead to a PVC polymer with greater porosity and more consistant processing properties.

Since VCM is a carcinogenic gas at atmospheric pressure and room temperature it has to be held under excess pressure to maintain it in a liquid form and precautions taken to prevent its escape.

The observation of particle charge required microelectrophoresis equipment capable of withstanding the autogeneous pressure of VCM at temperatures up to 343K and yet still possess optical characteristics suitable for dark field microscopy.

Furthermore it was found that the electrophoresis cell had to be constructed from quartz rather than borosilicate glass before van der Minne and Hermanie's (67) criteria for regular electrophoresis could be achieved.

The microelectrophoresis results of Spiers indicated that a PVC structure dispersed in VCM monomer carried in the region of 41 elementary charges per particle. Attempts were made to evaluate this charge on the growing primary particle, however, no correlation between particle radius, particle charge nor period of polymerisation was found and it was suggested that reproducible polymerisations were not being obtained. Spiers experimental investigation was severely hampered by

the difficulties encountered in the polymerisation, transference and measurement of the electrophoretic mobility of PVC particles dispersed in the liquified monomer.

To overcome the difficulties encountered by Spiers a combined polymerisation/electrophoresis cell was envisaged. The evolution of this cell along with the procedures of monomer purification, polymerisation and polymer dilution to produce a PVC particle concentration low enough for microelectrophoresis are dealt with in Chapter 3.

Particle nucleation, growth and its associated polymer morphology as characterised by scanning electron microscopy and image analysis techniques are dealt with in Chapter 4. The primary particle concentration and its associated charge are evaluated as a function of monomer conversion and as a result of this investigation a charge regime during particle growth is proposed.

Employing this charge regime the theoretical primary particle stability could be predicted using DLVO type calculations. By introducing the experimental data of particle concentration, radius and zeta potential into the theoretical calculations it would be possible to predict the likelihood of primary particles carrying sufficient charge to confer the observed stability behaviour during the polymerisation process.

Assuming a good correlation between the theoretical predictions and the experimental results, the

stability calculations can be utilised to predict the PVC morphology resulting from varying the primary particle charge. This is followed by an experimental investigation of the role of low molecular mass compounds in modifying the electric charge on the primary particles. Methods of controlling the colloidal stability of the growing particles are then discussed.

Finally, on the control of polymer morphology, the important relationship between reaction kinetics and the colloidal stability of the particles is discussed in terms of the effects of varying both polymerisation temperature and initiator concentration.

A mechanism for the development of particle structures in the initial stages of PVC production is proposed and ways in which these structures can be controlled discussed. Several suggestions for further work in this industrially important area are then made.

Chapter Two

Theoretical aspects of colloidal stability

2.1. Introduction

Dispersion stability has been the subject of many useful reviews (3,68 - 72) with several articles devoted to colloidal stability in non-aqueous systems (73 -77). However, on reviewing the literature on dispersion stability, it became apparent that the majority of investigations, both practical and theoretical deal with aqueous systems. Consequently dispersion stability in low permittivity media are less well understood.

In this chapter the theoretical aspects of colloidal stability are considered. Lyklema, in his extensive review (73), discusses some of the difficulties encountered in non-aqueous systems and in the following sections, where necessary, the major differences between dispersions in aqueous and low permittivity media are highlighted.

A general and quantitative theory for the stability of lyophobic colloids has been proposed by Derjaguin and Landau (2) and independently, by Verwey and Overbeek (3). The so called DLVO theory has been explored exhaustively in the last 40 years, particularly in aqueous systems, and although several difficulties remain (78), the theory is, in principle, correct and in agreement with many experimental facts in both aqueous and non-aqueous systems.

According to the DLVO theory the interaction between colloidal particles is a superposition of the

electrostatic repulsion arising from the overlap of the electrical double layers, V_R; and the attraction arising from the van der Waals forces, V_A. The theory excludes the possible effects of polymeric material adsorbed at the particle/medium interface. As no polymeric surfactants have been used in the initial bulk polymerisations of VCM, DLVO theory is expected to be applicable to this system.

The electrophoretic study by van der Minne and Hermanie (67) indicated the existance of the electrical double layer in non-aqueous media such as hydrocarbons, thus realising the valuable work of Fuoss and Kraus (79) and La Mer and Downes (80) on ionic dissociation of electrolytes in low permittivity media. The investigation of Koelmans and Overbeek (81) on the relationship between zeta potential and the stability of non-aqueous dispersions showed the possible applicability of DLVO theory in non-aqueous systems. The study has since been verified by Parfitt et. al. (82) and Romo (83) using a wide variety of materials in non-aqueous media.

2.2 Potential energy of repulsion

In general when two phases are brought into contact a difference in potential develops between them. If one of the phases is a polar liquid, e.g. water, its dipolar molecules will tend to orientate at the interface and generate a potential difference. In the presence of ions or ionogenic groups, the electric charges will tend to

distribute themselves in a non-uniform manner at the interface. There are several mechanisms by which non-ionic particles may acquire a surface electrical charge.

a) ionisation of surface groups such as carboxyl and sulphate.

b) Preferential adsorption of ions from the dispersion medium or desorption from the particle surface.This also includes the adsorption of ionic surfactants.

c) Dipolar molecule orientation at the particle surface.

To maintain the overall electrical neutrality of the colloidal system this surface charge must be compensated by an equal but opposite charge (counter-ions) in the dispersion medium.

This balancing charge arises from an excess of counter-ions over co-ions (same charge as surface) near to the particle surface.

Together, the surface charge and its associated counter-ions constitute the electrical double layer. The distribution of ions in the electrical double layer is determined by a balance between thermal and electrical forces.

On this basis both Gouy (84) and Chapman (85) independantly proposed a quantitative treatment for the diffuse electrical double layer. Several assumptions were

made in the model.

a) The particle charge is uniformly spread over the surface.

b) The ions in the diffuse double layer are dimensionless point charges.

c) The dispersion medium influences the double layer only through its dielectric constant which has a uniform value at all points throughout the diffuse layer.

The concentration of ions in solution around the surface is given by the Boltzmann equation

$$n_+ = n_o \exp[-ze\psi/kT] \qquad (2.2.1)$$

and

$$n_- = n_o \exp[+ze\psi/kT] \qquad (2.2.2)$$

where n_+ and n_- are the respective number of positive and negative ions per unit volume at points where the potential is ψ. n_o is the corresponding bulk concentration of each ionic species of valency z. T, k and e represent absolute temperature, Boltzmann constant and proton charge respectively.

For a dispersion medium containing a single symmetrical electrolyte of valency z the net volume charge density ρ at points where the potential is ψ can be expressed as

$$\rho = ze(n_+ - n_-) \qquad (2.2.3)$$

Combining equations (2.2.1) and (2.2.3) yields

$$\rho = zen_o(\exp[-ze\psi/kT]-\exp[+ze\psi/kT]) \qquad (2.2.4)$$

$$\rho = 2zen_o\sinh(ze\psi/kT) \qquad (2.2.5)$$

The Poisson equation

$$\Delta\psi = -\rho/\varepsilon \qquad (2.2.6)$$

describes the relationship between the potential ψ and the charge density ρ, at all points in a medium of permittivity ε around a charged surface. Δ is the Laplace operator and equals $(\partial 2/\partial x^2 + \partial^2/\partial y^2 + \partial^2/\partial z^2)$, x,y and z representing the cartesian co-ordinates. ε is equal to $\varepsilon_o \varepsilon_r$ where ε_r is the relative permittivity (dielectric constant) of the dispersion medium and ε_o is the permittivity of a vaccuum ($8.854 \times 10^{-12} Fm^{-1}$).

Combining equations (2.2.5) and (2.2.6) gives

$$\Delta\psi = (2zen_o/\varepsilon)\sinh(ze\psi/kT) \qquad (2.2.7)$$

Equation (2.2.7) is most readily solved when the surface is flat, since the potential need only be evaluated in one direction, perpendicular to the surface. Furthermore, if the potential is small such that $ze\psi/kT < 1$ the Debye-Hückel approximation that

$$\exp(ze\psi/2kT) \cong 1+ze\psi/2kT \qquad (2.2.8)$$

may be used. Equation (2.2.7) then simplifies to

$$\frac{\partial^2 \psi}{\partial x^2} = \frac{2z^2e^2n_o}{\varepsilon kT} \psi \qquad (2.2.9)$$

or $$\frac{\partial^2 \psi}{\partial x^2} = \kappa^2 \psi \qquad (2.2.10)$$

where $$\kappa = \left(\frac{2z^2e^2n_o}{\varepsilon kT}\right)^{\frac{1}{2}} \qquad (2.2.11)$$

One solution of equation (2.2.10) is

$$\psi = \psi_o \exp(-\kappa x) \qquad (2.2.12)$$

where x is the distance from the surface and ψ_o is the potential at the surface. There is no exact analytical solution of equation (2.2.10) however numerous attempts to improve upon the Debye-Hückel approach have been published (86-92).

From equation (2.2.12) it is evident that the rate of exponential decay of potential from the particle surface is governed by the value of κ . Non-aqueous systems differ from aqueous in two respects, viz. the permittivity ε and electrolyte concentration, both of which influence the value of κ. Increasing ionic strength causes an increase in κ as a result of which the potential falls off more rapidly with distance. This is often referred to as "compression of the double layer". The reciprocal double layer thickness $1/\kappa$ although not

extending to the point where $n_+ = n_- = n$ is frequently used for comparative purposes. Indeed it is constructive to compare $1/\kappa$ values for typical aqueous and non-aqueous systems. For an aqueous system containing a 1:1 electrolyte at a concentration of 10^{-3} mole l^{-1} the double layer thickness is approximately 10 nm; for a similar electrolyte in dispersion medium of $\varepsilon_r=2$ with an ionic concentration of about 10^{-11} mole l^{-1}, $1/\kappa$ approaches 100 μm. Figure 2.2.1 indicates the much slower potential decay away from the surface in the diffuse double layer for dispersions in low permittivity media. For such diffuse double layers, even in dilute dispersions, the overlap of the double layer with those of adjacent particles is possible, thus reducing the stability of the dispersion below that predicted by the DLVO theory, in which, two particles approach from infinite separation.

The simple picture of the Gouy and Chapman diffuse double layer predicts a capacity of the double layer that is higher than that measured experimentally, leading to absurdly high ionic concentrations in the environment of the surface. Stern (93) recognized that the discrepancy arose from the assumptions that:-

(a) the electrolyte ions could be regarded as point charges and

(b) that the solvent could be treated as a structureless dielectric of constant permittivity.

The finite size of the ions limits their maximum

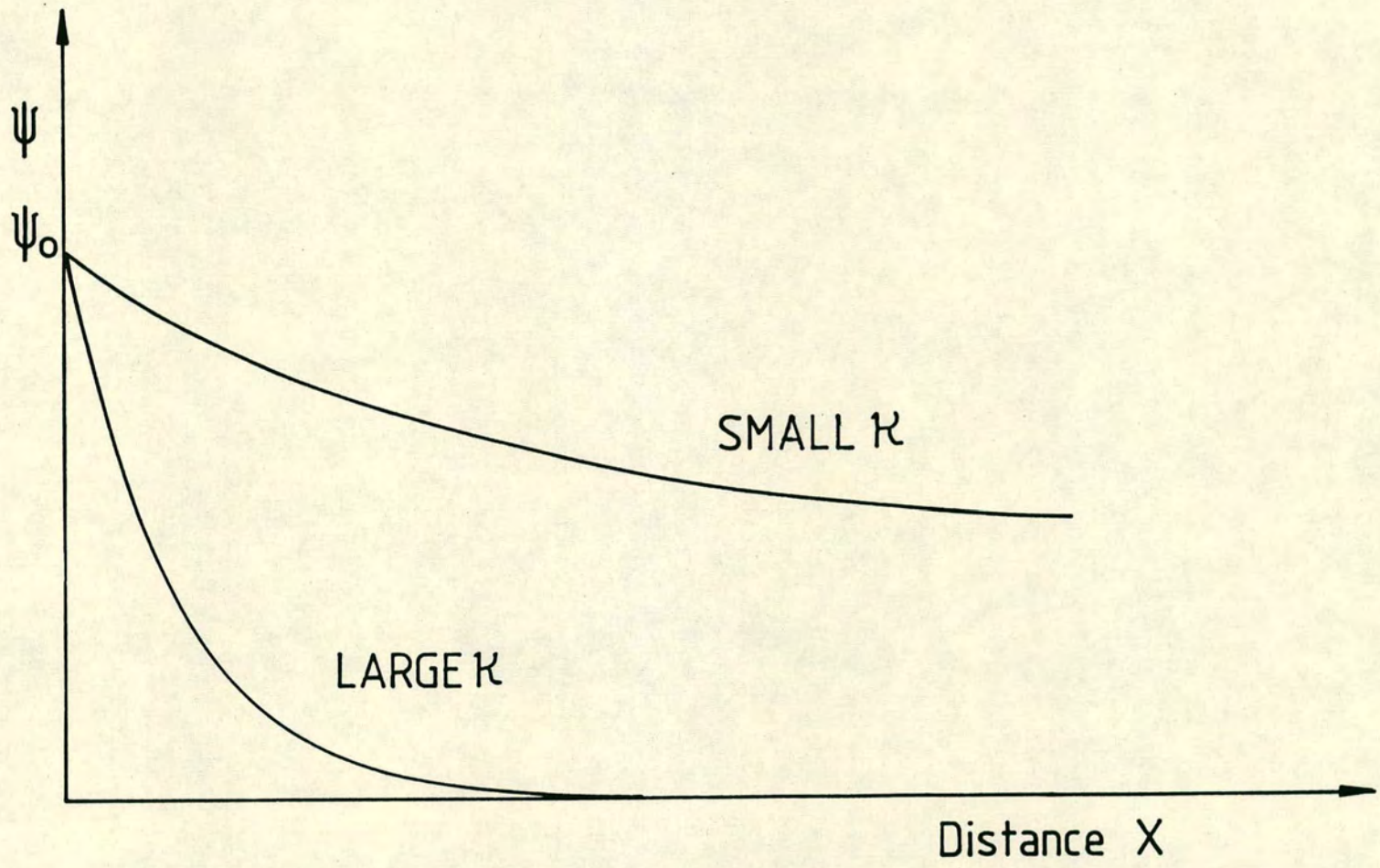

Fig. 2.2.1. Schematic diagram indicating the influence of κ on the rate of potential decay in the diffuse double layer.

concentration at the surface and distance of closest approach. Furthermore, the high electric field near the wall (10^6 to 10^8 Vm^{-1}) produces some ordering of solvent dipoles.

Stern considered the possibility of specific ion adsorption and proposed a model in which the electric double layer is divided into two regions; as indicated schematically in figure 2.2.2. The inner layer within the Stern plane contains specifically adsorbed ions attached to the surface, partly by electrostatic and partly by van der Waals forces, strongly enough to overcome thermal agitation. In this layer the potential decays linearly as in a classical parallel plate condenser from ψ_o at the particle surface to ψ_δ at the Stern plane. This plane is located at a distance δ from the surface and represents the centre of any specifically adsorbed ions. Beyond the Stern plane the potential falls from ψ_δ to zero, in this diffuse region the decay may be represented by the Gouy and Chapman theories.

The Stern model was further refined by Grahame (94) who distinguished between the outer Helmholtz plane corresponding to the Stern plane, through the centres of the solvated ions at the surface and the inner Helmholtz plane which runs through the centres of desolvated specifically adsorbed ions.

More elaborate procedures, using a continuously variable dielectric permittivity have been examined by Buff and Goel (95) and more recently by Levine et. al.

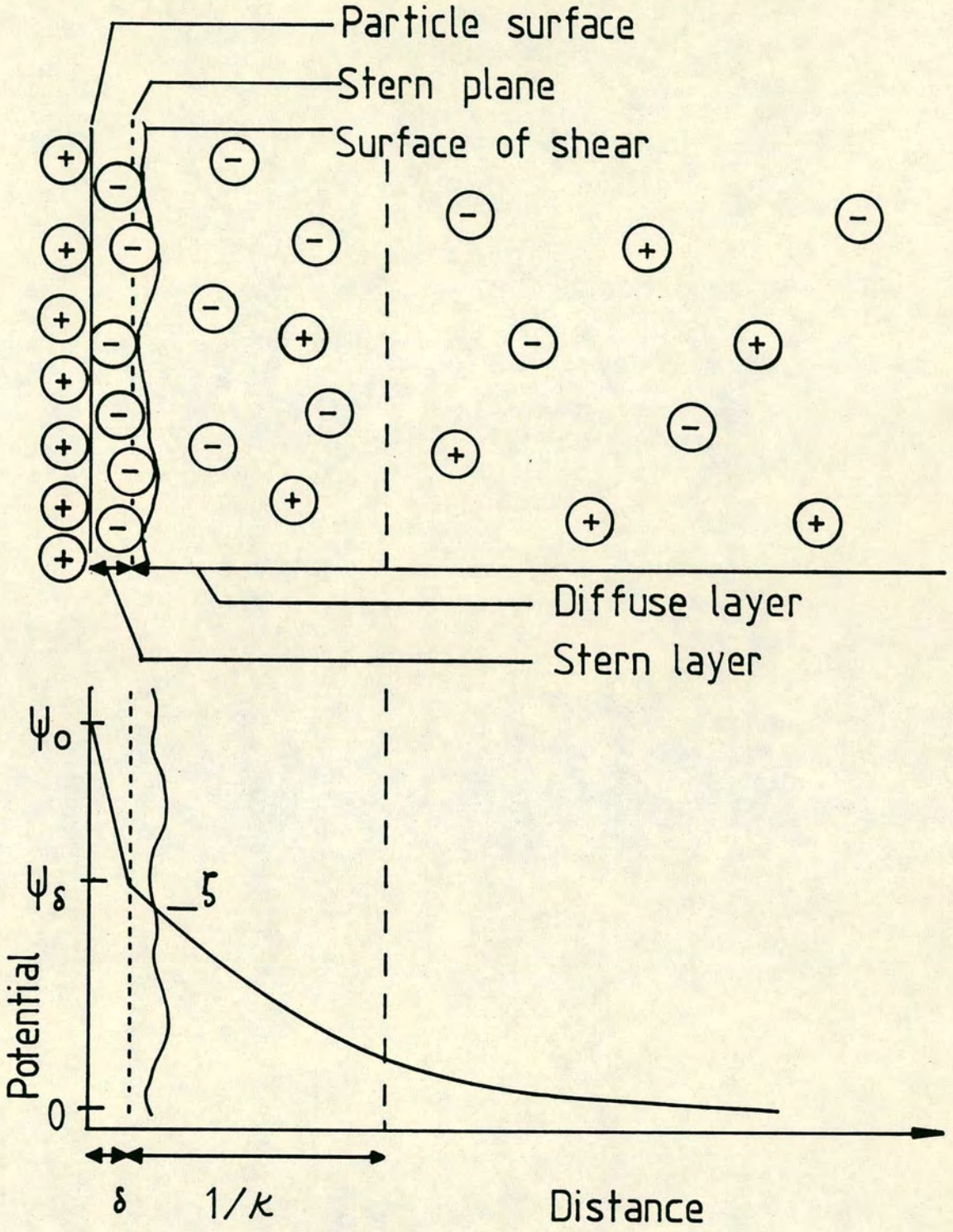

Fig. 2.2.2. Schematic representation of the Stern model of the electric double layer

(96) (97) thus allowing the ψ function to become smoother in the interfacial region.

Further information on the refinements of the electrical double layer are dealt with in the excellent review by Hunter (98).

The overlap of Gouy-Chapman type diffuse double layers of colloidal particles gives rise to a potential energy of repulsion, V_R. Calculation of V_R involves evaluating the change in free energy as two particles approach from infinite separation. For spherical particles several methods have been proposed depending on the value of κa, where κ is defined by equation (2.2.11) and a is the particle radius.

The potential energy for repulsion will first be considered for systems in which the double layer thickness is small with respect to the particle size ($\kappa a >> 1$). Then for small κa values ($<<1$), which are more typical of low permittivity dispersion media, such as used in this study.

Interaction of Two Dissimilar Double Layers.

The potential at any point in the electrical double layer around a colloidal particle according to the Gouy-Chapman model is given by

$$\Delta\psi = (zen_o/\varepsilon) \sinh(ze\psi/kT) \qquad (2.2.7)$$

Assuming a low potential (<25mV), the Debye-Huckel approximation allows this expression to be simplified to

$$\Delta\psi = \kappa^2\psi \qquad (2.2.13)$$

which for infinite flat plates can be expressed as

$$\partial^2\psi/\partial x^2 = \kappa^2\psi \qquad (2.2.14)$$

since variations need only be considered in the x direction.

$$\psi = A_1 \cosh(\kappa x) + A_2 \sinh(\kappa x) \qquad (2.2.15)$$

where A_1 and A_2 are constants.

For two dissimilar plates of potentials ψ_{o1} and ψ_{o2} a distance 2d apart, the boundary conditions $\psi=\psi_{o1}$ at $x = o$ and $\psi = \psi_{o2}$ at $x = 2d$ are satisfied. Thus from equation (2.2.15).

$$\psi = \psi_{o1} \cosh(\kappa x) + \left(\frac{\psi_{o2}-\psi_{o1}\cosh(2\kappa d)}{\sinh(2\kappa d)}\right) \sinh(\kappa x) \qquad (2.2.16)$$

which describes the distribution of potential as a function of distance between the plates.

Verwey and Overbeek (3) have shown that for small, constant surface potentials the total free energy is given by

$$G = -\tfrac{1}{2}\sigma\psi_o \qquad (2.2.17)$$

where is the surface charge density. Thus for the system of two plates separated by a distance 2d, the free energy is given by

$$G_{2d} = -\tfrac{1}{2}(\sigma_1\psi_{o1} + \sigma_2\psi_{o2}) \qquad (2.2.18)$$

where σ_1 and σ_2 are the surface charge densities of the separate double layers. The surface charge density

$$\sigma = -\varepsilon(d\psi/dx)_{x=o} \tag{2.2.19}$$

thus

$$\sigma_1 = -\varepsilon\kappa[\psi_{o2}\ \text{cosech}(2\kappa d) - \psi_{o1}\ \coth(2\kappa d)] \tag{2.2.20}$$

and

$$\sigma_2 = +\varepsilon\kappa[\psi_{o2}\ \text{cosech}(2\kappa d) - \psi_{o1}\ \coth(2\kappa d)] \tag{2.2.21}$$

Substituting σ_1 and σ_2 into equation (2.2.18) yields

$$G_{2d} = \frac{\varepsilon\kappa}{2}[2\psi_{o1}\psi_{o2}\ \text{cosech}(2\kappa d) - (\psi_{o1}^2 + \psi_{o2}^2)\ \coth(2\kappa d)] \tag{2.2.22}$$

which at large separations

$$G_\infty = -\frac{\varepsilon\kappa}{2}(\psi_{o1}^2 + \psi_{o2}^2) \tag{2.2.23}$$

The difference between equation (2.2.23) and (2.2.22) represents the free energy change occurring when two plates are brought from infinite separation to 2d. The potential energy of interaction, V_I, between infinite, flat double layer is described by

$$V_I = \Delta G = \frac{\varepsilon\kappa}{2}((\psi_{o1}^2 + \psi_{o2}^2)(1 - \coth(2\kappa d)) + 2\psi_{o1}\psi_{o2}\ \text{cosech}(2\kappa d)) \tag{2.2.24}$$

The potential energy of repulsion between spherical particles of radius much greater than the double layer thickness ($\kappa a >> 1$) has been addressed by Derjaguin (99). The interaction of the double layers is assumed to be made up from contributions from infinitesimally small parallel rings each of which may be considered as a flat plate. V_R for spherical particle interaction is then given by

$$V_R = \int_o^\infty 2\pi h V_I dh \qquad (2.2.25)$$

where h is the radius of the ring as shown in Figure 2.2.3 and V_I is defined by equation (2.2.24).
From the geometry of Figure 2.2.3

$$H - H_o = a_1 + a_2 - \sqrt{a_1^2 - h^2} - \sqrt{a_2^2 - h^2} \qquad (2.2.26)$$

which on differentiation yields

$$dH = \left(\frac{1}{(a_1^2 - h^2)^{\frac{1}{2}}} + \frac{1}{(a_2^2 - h^2)^{\frac{1}{2}}}\right) h dh \qquad (2.2.27)$$

when $h << a_1$ and $h << a_2$.

$$h dh \quad \left(\frac{a_1 a_2}{a_1 + a_2}\right) dh \qquad (2.2.28)$$

By substitution equation (2.2.25) becomes

$$V_R = \frac{2\pi a_1 a_2}{a_1 + a_2} \int_{H_o}^\infty V_I(H) dH \qquad (2.2.29)$$

where 2d = H the distance between plates. Equation (2.2.29)

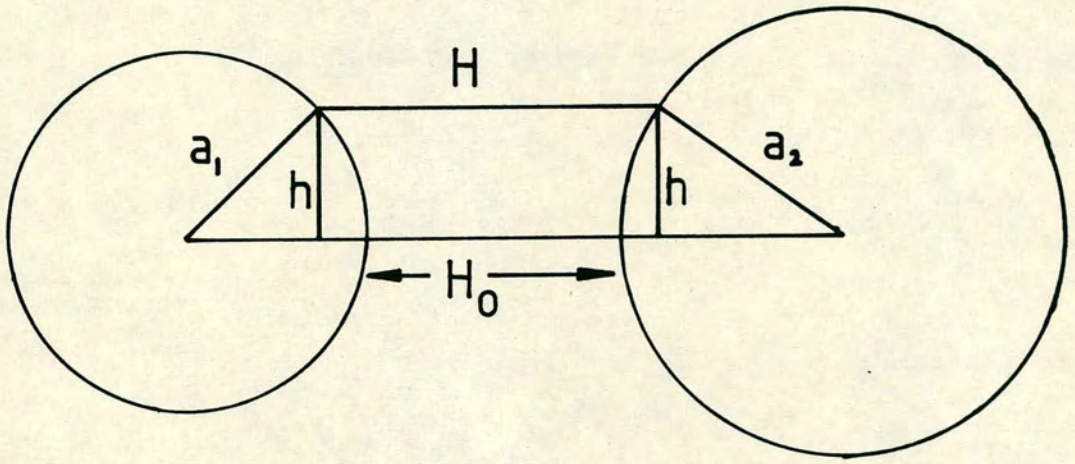

Fig. 2.2.3. Geometrical construction used in the calculation of the interaction between two dissimilar spherical particles from the interaction of two infinite flat plates.

may be evaluated analytically to yield

$$V_R = \frac{\varepsilon\pi a_1 a_2(\psi_{o1}^2 + \psi_{o2}^2)}{(a_1 + a_2)}\left(\frac{2\psi_{o1}\psi_{o2}}{(\psi_{o1}^2+\psi_{o2}^2)}\right)$$

$$\ln\left(\frac{1 + \exp(-\kappa H_o)}{1 - \exp(-\kappa H_o)}\right) + \ln(1-\exp(-2\kappa H_o))) \quad (2.2.30)$$

Or in the case of identical spherical particles where $a_1 = a_2 = a$ and $\psi_{o1} = \psi_{o2} = \psi_o$ equation (2.2.30) reduces to

$$V_R = 2\varepsilon\pi a\psi_o^2 \ln(1 + \exp(-\kappa H_o)) \quad (2.2.31)$$

In view of the assumptions made in the derivation of equations (2.2.30) and (2.2.31), namely the use of the Debye-Hückel and the Derjaguin's approximations, these expressions are only entirely valid for low potentials (<25mV) and for conditions such that the double layer thickness is small in comparison to the particle radius. When $\kappa a > 10$ the error in the interaction potential is about 5%, but it increases to approximately 30% when κa is reduced to 2.

Hogg, Healy and Fuerstenau (100) have published a tabulated comparison of interaction energies predicted from the full expression (101) with those of the approximated expression, equation (2.2.24). They reported that, as expected, for potentials less than 25 mV, the agreement was extremely good, whilst even at 75 mV to 100 mV the divergence was not excessive, except at very small interplate separations. Practically however, this is of little significance since van der Waals attractive

forces usually dominate at short range.

In conclusion the main criterion for the applicability of equations (2.2.30) and (2.2.31) is the value of κa, provided the potential is reasonably low. At higher potentials the graphical procedure proposed by Verwey and Overbeek (3) is more accurate.

When κa is small ($\kappa a << 1$), as is the case when the electrolyte concentration in the dispersion medium is low, the extent of the double layer is greater than the particle dimensions (see above). For this case, the Poisson-Boltzmann equation (2.2.7) must be solved for all three dimensions to obtain the electric field in the double layer around the spherical particles. Mathematically this is a formidable problem unless the problem is simplified by again using the Debye-Hükel approximation and assuming that the potential ψ_o, is small.

$$\Delta\psi = \kappa^2\psi \qquad (2.2.13)$$

The solution of equation (2.2.13) can be expressed in the form of an infinite series. Having taken the first three terms of these series, Verwey and Overbeek (3) have invoked Gauss's theorem (2.2.32)

$$Q = -\int_{o}^{\omega_1} \varepsilon \left(\frac{\partial\psi}{\partial r_1}\right) \qquad d\omega_1 \qquad (2.2.32)$$

$r_1 = a \qquad \Theta = \text{constant}$

to relate the surface potential and charge Q, of the particles by equation (2.2.33).

$$\psi_o = \frac{Q[1 + \frac{e^{-\kappa a(s-2)}}{2\kappa as}(1 - e^{-2\kappa a})\{1 + \lambda_1(1 + \frac{1}{\kappa as}) + \lambda_2(1 + \frac{3}{\kappa as} + \frac{3}{(\kappa as)^2})\}]}{4\pi a\varepsilon(1 + \kappa a)\{1 - \delta(1 + \alpha)\}}$$

(2.2.33)

where $S = R/a$ and $\lambda_1, \lambda_2, \alpha$ and δ are parameters which may be solved from the equations given by Verwey and Overbeek(3).

During the interaction of colloidal particles through a Brownian collision two types of encounter have been considered, the constant surface charge or constant surface potential interaction. If the surface charge density is assumed to remain constant the surface potential must increase during the encounter. In the case where the surface potential on the particles remains constant, according to the theory, the surface charge density should decrease. In this situation a rapid desorption of ions from the surface must occur during the interaction. For dispersions in low permittivity media it is difficult to establish which mechanism prevails, however, it has been suggested that ion desorption would be slow due to the high solvation energies for ions in hydrocarbon media (73). Fortunately, DLVO type stability calculations are relatively insensitive to which type of approach is adopted.

If it is assumed that the surface potential remains constant then the potential energy of repulsion of

two spherical particles at a distance R apart is given by (3)

$$V_R = \psi_o(Q_\infty - Q_R) \qquad (2.2.34)$$

ψ_o = constant

where Q_∞ and Q_R are the particle charges at a separation of infinity and R respectively. Elimination of Q using equation (2.2.33) yields

$$V_R = \frac{\psi_o^2 \, 4\pi\varepsilon a^2 e^{-\kappa H}}{2a + H} \beta \qquad (2.2.35)$$

ψ_o = constant

where ε, a, κ, H and ψ_o are as defined previously and β is given by equation (2.2.36)

$$\beta = \frac{1 + \alpha}{1 + \frac{e^{-\kappa a(s-2)}}{2\kappa as}(1 - e^{-2\kappa a})(1 + \alpha)} \qquad (2.2.36)$$

β, and the analagous parameter γ (applicable under conditions of interaction at constant surface charge density), allow for the distortion of the diffuse double layer as particles approach during interaction. Tables of β, given by Verwey and Overbeek (3) for several values of κa indicate that β varies between $\cong$ 0.6 and 1 as a function of interparticle separation. Using these values

of β in equation (2.2.35) it is possible to calculate the repulsive interaction energy, V_R, for identical spheres when κa is small. Unfortunately an extension to describe dissimilar spheres has not been published.

When the ionic concentration of the dispersion medium is reduced, the limiting form of equation (2.2.35) has been proposed as a satisfactory approximation.

$$V_R = \frac{\psi_o^2 a^2 4\pi \varepsilon}{2a+H} \qquad (2.2.37)$$

which is Coulomb's law for point charges. Examination of equation (2.2.37) reveals that only a small surface charge is required to produce a large repulsive energy. Surface charges of about 10 per particle are predicted for typical zeta potentials when $\kappa a \ll 1$. Indeed Osmond (102) has questioned the validity of a continuous double layer on colloidal particles carrying so few charges.

In conclusion Verwey and Overbeeks expression (2.2.35) is valid for systems in which $\kappa a < 3$. When $\kappa a > 10$ the Derjaguin approximation is valid and equation (2.2.30) may be used to calculate V_R. In order to describe the intermediate region Verwey and Overbeek (3) have suggested the use of a graphical interpolation approach.

Recently a more accurate method, which is applicable for κa values down to 5 has been developed by McCartney and Levine (103) The mathematical approach involves expressing the potential in terms of a distribution of electric dipoles on the two spherical

particles and constructing an integral equation which governs the dipole distribution. This new approach is superior to the corresponding Derjaguin expression having an error of less than 3% for all separations where $\kappa a >> 5$.

Bell, Levine and McCartney (104) have proposed an alternative means of evaluation the repulsive potential energy for intermediate κa values. They extend the integral method to enable the case of dissimilar sized spheres of unequal potentials to be evaluated. Using the linear superposition approach (L.S.A.), which assumes that the potential between two particles is given to a good approximation by the sum of the potentials by either particle in the absence of the other, it was shown that it was possible to combine the L.S.A. at large separations with the Derjaguin formula at small separations ($\kappa H < 3$) to accurately predict V_R over a wide range of κa values.

By careful selection of a suitable expression it is possible to evaluate V_R with reasonable accuracy for most combinations of κa and potential. Before the total interaction of two colloidal particles can be assessed the potential energy of attraction must be predicted.

2.3 Potential energy of attraction.

In the absence of a stabilising mechanism all lyophobic colloids coagulate, implying that a net attractive force exists. This attractive interaction between colloidal particles has its origins in the van der

Waals forces, originally inferred from the properties of non-ideal gases and liquids (105). The recent interest in the calculation of electrodynamic attractive interactions has resulted in the publication of numerous review articles (106-110).

Three distinct forces of attraction between pairs of atoms or molecules are now recognised. These are:-

(a) Debye forces (111) arise as a result of the interaction between a permanent and an induced dipole. These forces are essentially independant of temperature since the induced dipoles alignment is invarient with respect to that of the inducing dipole. The force is short range, being inversely proportional to the sixth power of the separation. In this case, the potential energy of attraction, V_D, is given by

$$V_D = -(\mu_1^2 \alpha_2 + \mu_2^2 \alpha_1)/r^6 \qquad (2.3.1)$$

where; α_1 and α_2 are the polarizabilities of the apolar species respectively,

μ_1 and μ_2 are the dipole moments,

and r is the intermolecular distance.

(b) Keesom forces (112) arise from the interaction of permanent dipoles and, unlike Debye forces, are temperature dependent since increasing temperature destroys the alignment of the dipoles. Like Debye forces they are inversely proportional to the sixth power of separation. The potential energy of attraction between dipolar molecules is given in equation (2.3.2).

$$V_K = -2\mu_1^2\mu_2^2/3kTr^6 \qquad (2.3.2)$$

(c) London dispersion forces (113). Wang (114) showed that even two non-polar atoms attract each other. Although the time average dipole moment of an atom may be zero, it will still exhibit instantaneous finite dipole moments due to the non-symmetrical distribution of the electrons around the nucleus. This fluctuating electric dipole induces a corresponding dipole moment in a neighbouring atom, the resultant interaction between the atoms being one of attraction. The attractive energy is proportional to the mean square fluctuation of the electronic distribution and the more polarisable a molecule the stronger the attraction. London gave the following expression for the attractive potential energy between two identical non-polar atoms;

$$V_L = -3h\nu\alpha^2/4r^6 \qquad (2.3.3)$$

where; h is Planck's constant and

ν is the characteristic dispersion frequency of the atom given by the Drude equation.

$$\nu^2 = e^2/4\pi^2 m\alpha \qquad (2.3.4)$$

e and m are the charge and mass of the electron respectively. Dispersion forces are essentially independant of temperature and like both Debye and Keesom forces are inversely proportional to the sixth power of the separation.

Although all three types of interaction contribute to the total van der Waals attractive potential energy, only in the case of London dispersion forces are the separate interatomic interactions additive (to a first approximation) for macroscopic bodies. London dispersion forces between colloidal particles are therefore relatively long range and strong, whereas the Debye and Keesom forces, which are not additive, are weak and relatively insignificant.

In 1937 Hamaker (115) derived the London dispersion energy for two spherical particles as a function of diameter, interparticle separation and particle composition. For two spheres of unequal radii a_1, a_2,

$$V_A = -A/12\left[\frac{y}{(x^2+xy+x)} + \frac{y}{(x^2+xy+x+y)} + \frac{2\ \ln(x^2+xy+x)}{(x^2+xy+x+y)}\right] \quad (2.3.5)$$

where; V_A is the attractive potential energy,

H is the interparticle separation,

x is the ratio H/a_1 and y the ratio a_2/a_1,

A is the interaction parameter (Hamaker constant).

When $a_1 = a_2 = a$ i.e. the spheres are of equal radius,

$$V_A = -A/12\left[\frac{1}{(x^2+2x)} + \frac{1}{x^2+2x+1} + 2\ln\frac{x^2+2x}{x^2+2x+1}\right] \quad (2.3.6)$$

Finally when $x \ll 1$ i.e. $H \ll a$ equation (2.3.6) reduces to

$$V_A = \frac{-Aa}{12H} \qquad (2.3.7)$$

From equations (2.3.5) to (2.3.7) it is apparent that the potential energy of attraction depends on the product of an interaction parameter and a geometric term. The evaluation of the Hamaker constant poses the greatest obstacle in the calculation of attractive potential energies. Two methods of calculating the Hamaker constant have been proposed, these are frequently referred to as the microscopic and macroscopic approaches.

Microscopic approach

The method developed by Hamaker, is based on the assumption of additivity of intermolecular dispersion forces. This requires the interparticle separations to be sufficiently large for the interacting materials to appear as a continuous medium and not as an array of discreet molecules. The Hamaker constant A_{12} for two bodies of different materials at short distances in vacuum is given by

$$A_{12} = \pi^2 q_1 q_2 B_{12} \qquad (2.3.8)$$

where; q_1 and q_2 are the number of atoms of types 1 and 2 per unit volume of material

B_{12} is the London constant for the attraction between the atoms.

Various approximations for B_{12} have been given by several authors. For a simple case, such as two hydrogen atoms

$$B_{12} = B_{11} = 3\alpha_o^2 h\nu_o/4 \qquad (2.3.9)$$

where ν_o is the frequency of the electron in its ground state, which is related to the static polarisability α_o by

$$\nu_o^2 = e^2/4\pi^2 m_e \alpha_o \qquad (2.3.10)$$

where e is the charge on the electron

m_e is the mass of the electron

Eisenschitz and London (116) derived the following expression for more complex atoms

$$B_{12} = \frac{3he^4}{32\pi^4 m_e^2} \sum_1 \sum_2 \frac{f_1 f_2}{\nu_1 \nu_2 (\nu_1+\nu_2)} \qquad (2.3.11)$$

where f_1 and f_2 are the "oscillator strengths" corresponding to transition frequencies ν_1 and ν_2 in atoms 1 and 2. The summations are taken over all such transitions for both atoms.

By combining the expression for the polarisibility of an atom at frequency ν,

$$\alpha_1(\nu) = \frac{e^2}{4\pi^2 m_e} \Sigma_1 \frac{f_1}{\nu_1^2 - \nu^2} \qquad (2.3.12)$$

with the Lorentz- Lorentz equation,

$$R_1 = \frac{(n_1^2-1)}{(n_1^2+2)} \frac{M_1}{\rho_1} = 4\pi N_A \alpha_1(\nu)/3 \qquad (2.3.13)$$

a relationship giving the variation of refractive index of the material with frequency is obtained.

$$R_1 = \frac{e^2 N_A}{3\pi m_e} \Sigma_1 \frac{f_1}{\nu_1^2 - \nu^2} \qquad (2.3.14)$$

Where; n_1 is the refractive index of material 1 at frequency ν,

M_1 is the molecular mass,

ρ_1 is the density,

N_A is the Avogadro number.

For many materials, the variation of refractive index with frequency can be represented by a dispersion equation with only one term. For such dispersions equation (2.3.14) simplifies to

$$R_1 = \frac{n_1^2 - 1}{n_1^2 + 2} \frac{M_1}{\rho_1} = \frac{e^2 N_A}{3\pi m_e} \frac{S_1}{\nu_{1\nu}^2 - \nu^2} \qquad (2.3.15)$$

where $s = \Sigma f$ and may be regarded as the "effective number of dispersion electrons", and $\nu_{1\nu}$ is the characteristic frequency. Values of s_1 and $\nu_{1\nu}$ may be obtained from linear dispersion plots of $(n_1^2 + 2/n_1^2 - 1)$ against ν^2. Such values have been tabulated (117) (118) for a number of substances.

If one term dispersion equations apply to materials of type 1 and 2 equation (2.3.11) may be written as

$$B_{12} = \frac{3he^4}{32\pi^4 m_e^2} \frac{s_1 s_2}{\nu_{1\nu}\nu_{2\nu}(\nu_{1\nu} + \nu_{2\nu})} \qquad (2.3.16)$$

Using this equation, provided suitable dispersion data are available, the London constant can be evaluated and used in equation (2.3.8) to obtain the Hamaker constant.

From equation (2.3.15) when $\nu = 0$ and by making use of the relationships

$$\varepsilon_{10} = n_{10}^2 \qquad (2.3.17)$$

$$N_{10} = N_o \rho_1 / m_1 \qquad (2.3.18)$$

where n_{10} is the limiting refractive index in the visible wavelength region, Gregory (106) has given the following expression, which allows the Hamaker constant to be calculated directly

$$A_{12} = \frac{27}{32} \frac{h_{1\nu}\nu_{2\nu}}{(\nu_{1\nu} + \nu_{2\nu})} \frac{\varepsilon_{10} - 1}{\varepsilon_{10} + 2} \frac{\varepsilon_{20} - 1}{\varepsilon_{20} + 2} \qquad (2.3.19)$$

Equations (2.3.8) and (2.3.19) are only applicable to particles interacting across a vacuum. When the particles are immersed in a fluid medium, the attractive force is reduced by comparing particle medium interactions. To account for any intervening medium

Hamaker (115) proposed a modified Hamaker constant, such that,

$$A_{132} = A_{12} + A_{33} - A_{13} - A_{23} \qquad (2.3.20)$$

where A_{132} is the modified Hamaker constant for interaction across a medium, 3, and the subscripts 1 and 2 refer to the different particle materials.

Schenkel and Kitchener (119) following a remark by Verwey and Overbeek (3), corrected for the attenuation of the electromagnetic field by the intervening dielectric medium by dividing the value of A_{132} by the dielectric constant of the dispersion medium. Gregory (106) has shown that this simple division overestimates the attenuation and Visser (107) comments that the Schenkel Kitchener correction should be ignored. As we shall see, the effect of the intervening medium can only be adequately predicted by use of the Lifshitz (120) macroscopic approach.

Retardation effect

Since the London interaction is a consequence of electromagnetic radiation, which is propagated at the speed of light (3×10^8 ms^{-1}) between the colloidal particles and the period of fluctuation of an instantaneous dipole is about 10^{-15}-10^{-16}s once two particles are separated by more than approximately 30 nm the dipoles in the separated particles become out of phase. This is known as the retardation effect and it

results in a reduction of the force of attraction. Casimir and Polder (121) using quantum electrodynamics, showed that at very large separations the distance dependence term in the London equation changed from the sixth to the seventh power, so reducing the magnitude of the attractive interaction. Tabor (110) has summarised the effect of retardation. In general, strong non-retarded forces are expected for separations less than 30 nm, retarded forces for separations between about 100 nm to 1000 nm and extremely weak non-retarded forces at separations greater than this.

Macroscopic or continuum approach.

The London - Hamaker microscopic approach yields attractive interactions which are in reasonable agreement with experimental observations. The theory is however restricted by several assumptions:-

a) Pairwise additivity of the intermolecular interactions is valid.

b) The presence of an intervening medium may be dealt with by the use of an arbitary dielectric constant at a single frequency.

c) All electronic dipole fluctuations, which contribute to the attraction, occur about one characteristic frequency.

The calculation of van der Waals forces based on these assumptions are only strictly valid for highly rarified gases. In condensed systems if atom 1 in A exerts a force

in atom 1 in B the presence of neighbouring atoms in A and B is bound to influence the interaction between A1 and B1.

A radical solution to these inadequecies has been given by Lifshitz et. al. (120) (122) who treated the bodies and intervening medium in terms of their bulk or macroscopic properties, specifically their dielectric constants as a function of frequency. Retardation and propagation through a dense medium are implicit in the theory. The attraction was assumed to be due to a fluctuating electromagnetic field in the gap, arising from spontaneous electric and magnetic polarisations within the media. The general equation derived by Lifshitz was difficult to handle and has been rendered more tractable by Ninham and Parsegian (123) and others (124) (125).

When interaction parameters are calculated using the bulk or macroscopic approach, unlike the microscopic approach, it is found that "A" is not constant for any given system, but rather it is a function of separation and temperature.

Gregory (106) has concluded that if sufficient optical data are available the macroscopic approach is preferable. However for materials of fairly low dielectric constant it was found that the microscopic and macroscopic treatments were in good agreement. Furthermore, for dispersions in low permittivity media, such as the subject of this investigation, V_R tends to dominate the total potential energy of interaction. Exact values of V_A are often not required (126). Here the use of single valued

Hamaker constant is adequate for DLVO type calculations.

2.4. Total Potential Energy of Interaction.

The total potential energy of interaction V may be obtained by the summation of the attractive and repulsive potential energies viz:

$$V_T = V_A + V_R \qquad (2.4.1)$$

The character of total interaction energy as a function of interparticle separation is therefore determined by the relative contributions from V_A and V_R. The potential energy of repulsion, arising from the overlap of electric double layers, decays exponentially with increasing particle separation and operates over a range of the order of the thickness of the double layer. The van der Waals attraction exhibits an approximately inverse relationship with interparticle separation. Consequently attraction predominates at small and frequently at large interparticle distances. At very small separations Born repulsion arises from the overlap of electron clouds resulting in a deep primary minimum in the total potential energy curve. At intermediate separations the double layer repulsion may predominate, depending on the relative magnitude of the two potential energies.

The general form of the potential energy curves for the interaction of two colloidal particles as a function of separation is shown schematically in Figure 2.4.1.

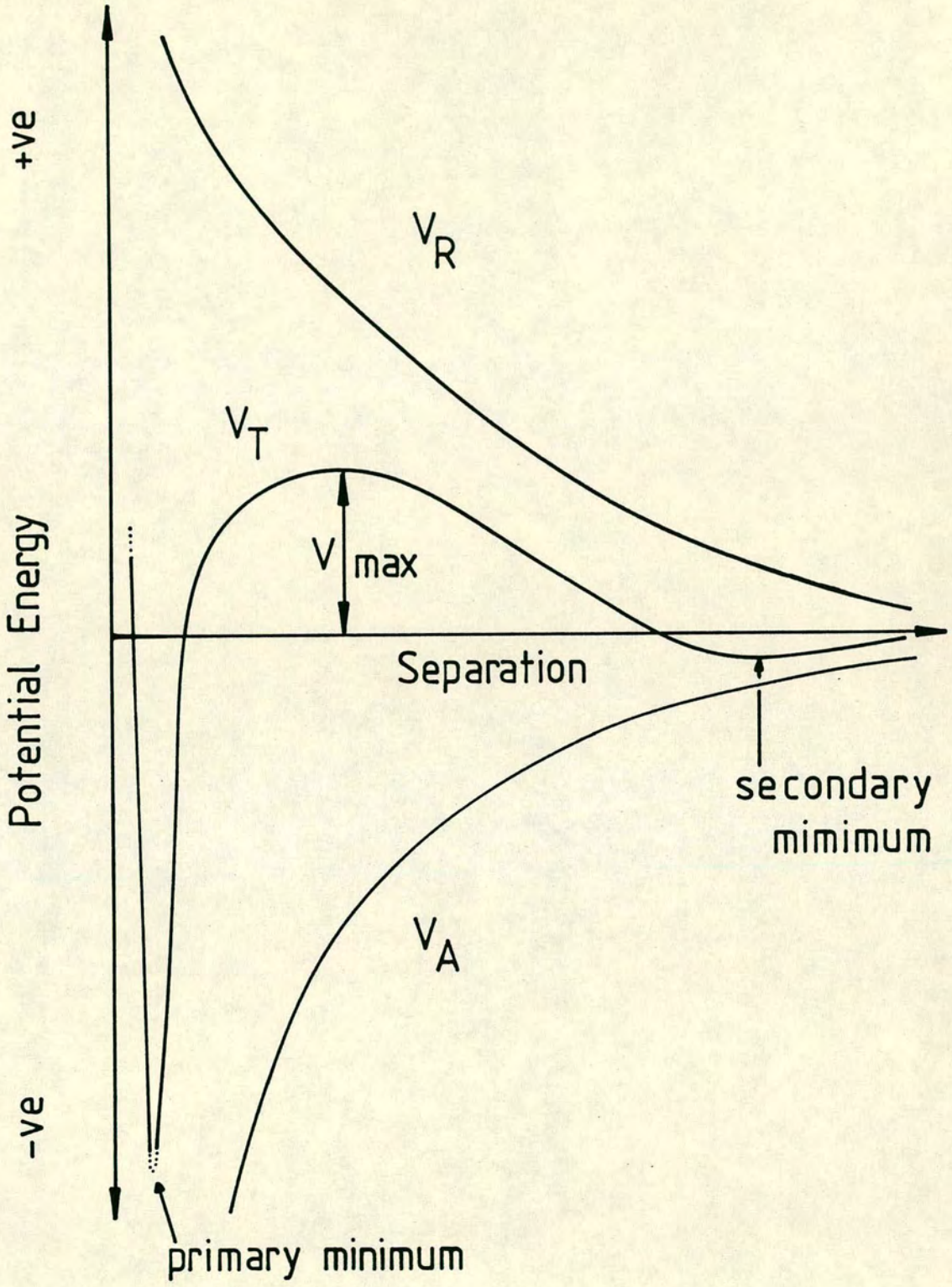

Fig. 2.4.1. Schematic potential energy diagram of two interacting particles.

Three important features characterise the V_T curve with regard to colloidal stability, the depth of the primary minimum, the height of the potential energy barrier, V_{max}, and the presence and depth of any secondary minimum. In general the primary minimum is very deep compared to the thermal energy, kT, and particles once coagulated into it are very difficult to redisperse. The colloidal stability of a dispersion against primary minimum coagulation is determined to a certain extent by the height of the potential energy barrier. If V_{max} is large in comparison to kT the system will be stable. Often at large separations, the V_R term decays more rapidly than V_A and a secondary minimum appears in the V_T curve. In contrast to the primary minimum, the secondary minimum is usually relatively shallow and particles flocculate reversibly into it forming loose aggregates which are readily redispersed by shear.

Potential energy curves such as those presented in Figure 2.4.1 may be used to demonstrate pictorially the influence of the various governing parameters on colloidal stability. For a given system the nature of the V_A curve is invarient. The form of the V_T curve is thus determined by changes in V_R, such as Stern potential, ψ_δ, or double layer thickness, $\frac{1}{\kappa}$. The effect of particle size at constant surface potential is illustrated in Figure 2.4.2. Smaller particles are less stable than larger ones with respect to primary minimum coagulation.

Figure 2.4.3 indicates that at constant particle

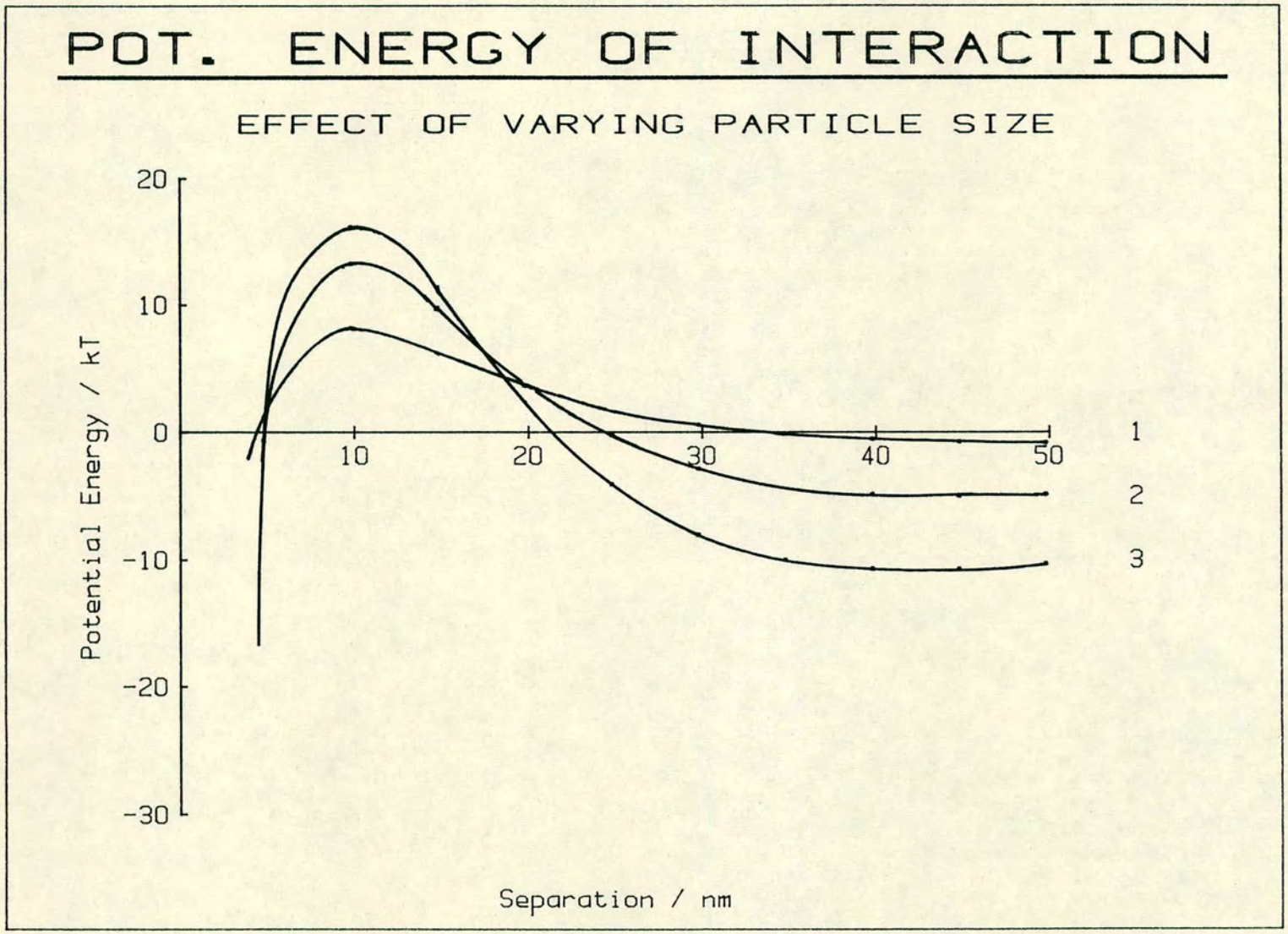

KEY

1 a = 100 nm

2 a = 300 nm

3 a = 500 nm

Psi = 25 mV

A = 1E-19 J

Kappa = 1E8 m^{-1}

Dielectric Const = 78.3

Figure 2.4.2

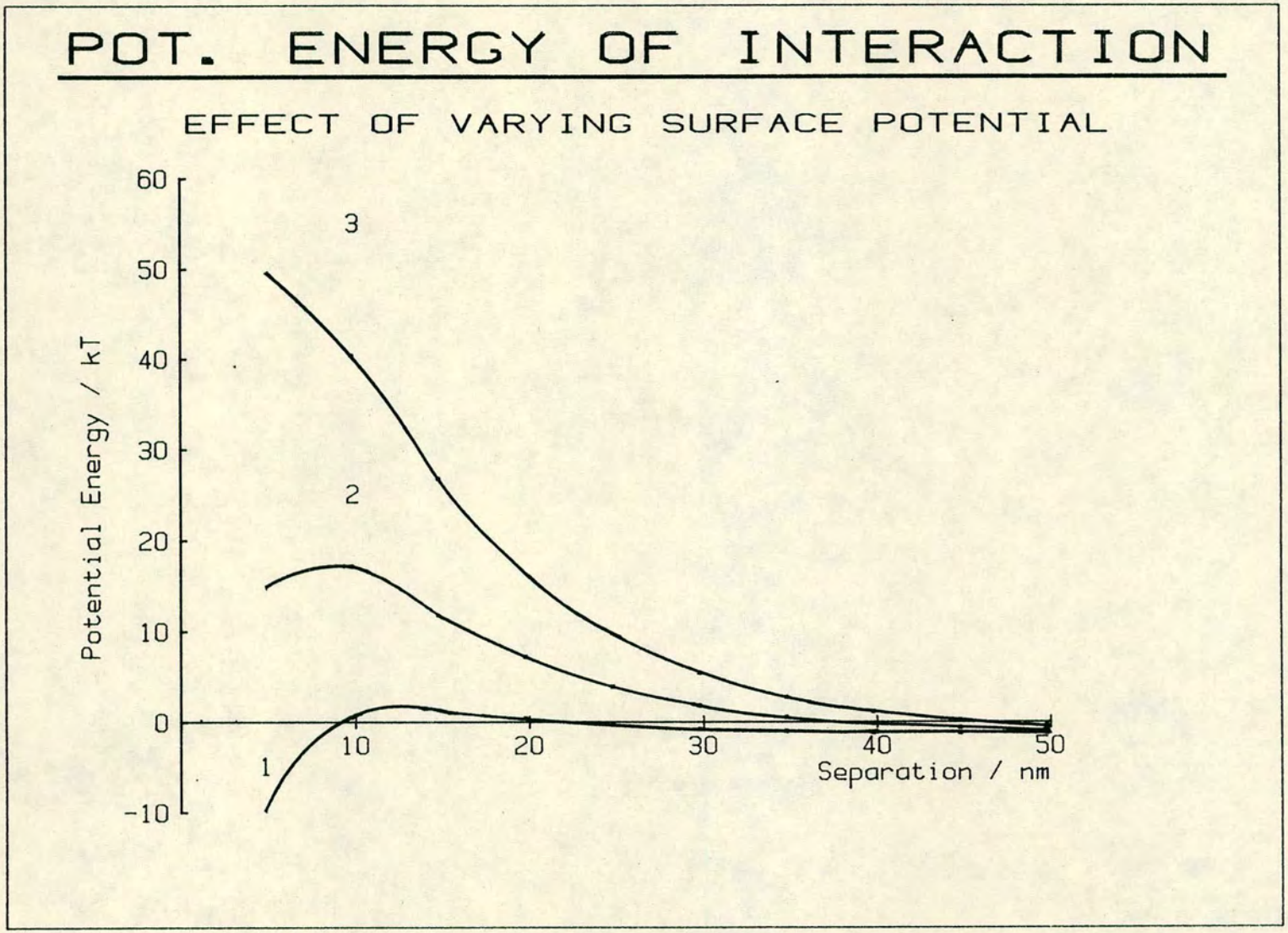
POT. ENERGY OF INTERACTION
EFFECT OF VARYING SURFACE POTENTIAL
Potential Energy / kT
60
50
40
30
20
10
0
-10
10
20
30
40
50
Separation / nm
1
2
3
KEY
1 Psi = 20 mV
2 Psi = 30 mV
3 Psi = 40 mV
a = 100 nm
A = 1E-19 J
Kappa = 1E8 m-1
Dielectric Const = 78.3

Figure 2.4.3

size increasing Stern potential, ψ_δ, increases colloidal stability.

Compression of the double layer leads to a reduction in distance over which the repulsive force operates. Thus lyophobic colloids may be coagulated by increasing electrolyte concentration. Figure 2.4.4 indicates the effect of varying double layer thickness on V_T curves.

For dispersions in low permittivity media, such as PVC in VCM, free ion concentrations tend to be low, giving rise to thick double layers. In such cases the V_R term dominates the total potential energy curve at all but the smallest interparticle separations, so that the accurate evaluation of the V_A term is of less importance than in high permittivity media (73).

The force encountered by colliding colloidal particles is given by the slope of the V_T curve. Figure 2.4.5 shows that for dispersions in low permittivity media although the repulsive term is long range the force experienced by interacting particles is low compared to the short range but strong force encountered in aqueous systems.

The adsorption of macromolecules at the particle/medium interface can lead to an additional barrier to coagulation and a further term, V_S, must be included in the expression for V_T.

$$V_T = V_A + V_R + V_S \qquad (2.4.2)$$

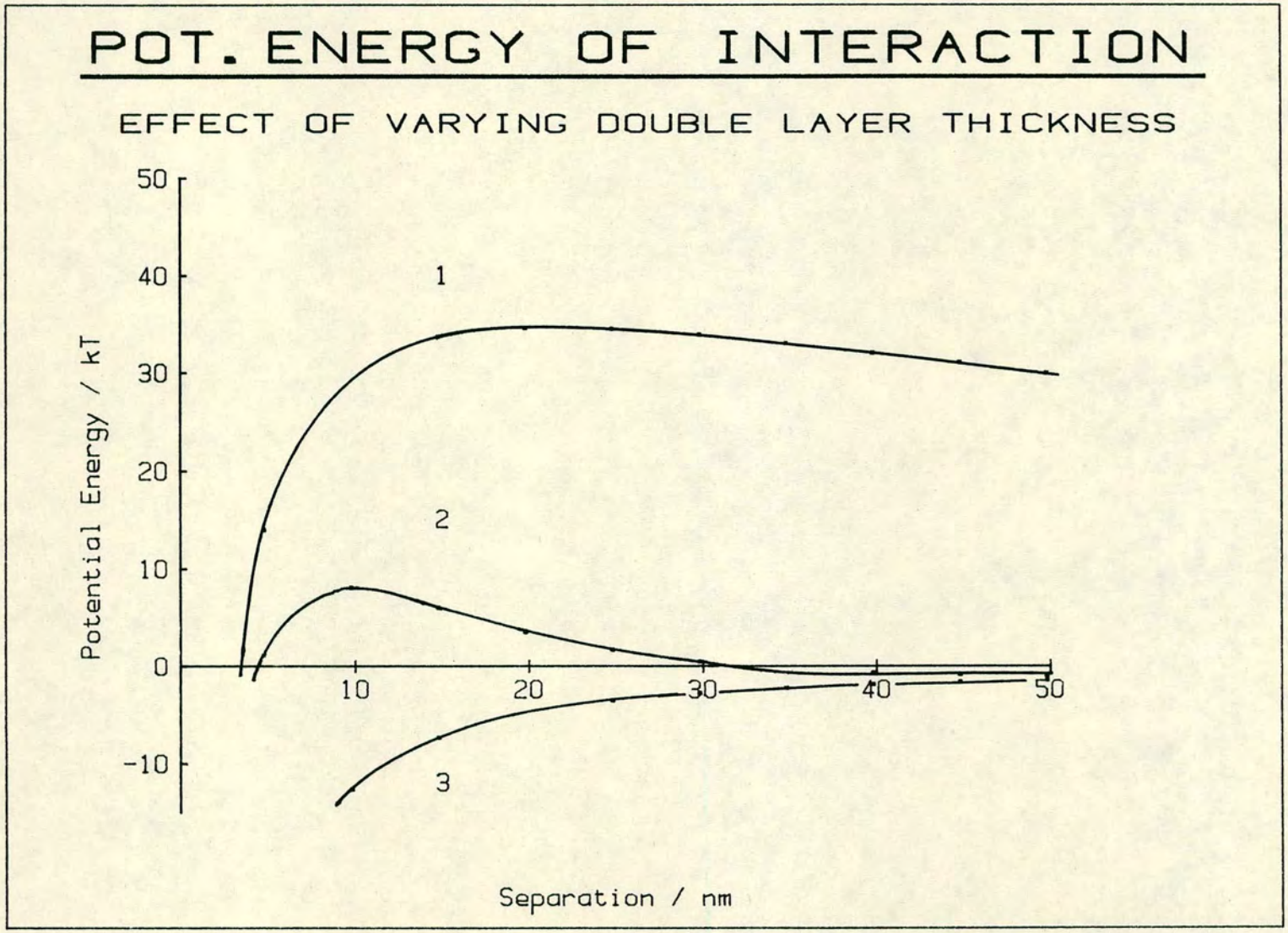

KEY

1 Kappa = 1E7m^{-1}

2 Kappa = 1E8m^{-1}

3 Kappa = 1E9m^{-1}

Psi = 25 mV

a = 100 nm

A = 1E-19 J

Dielectric Const = 78.3

Figure 2.4.4

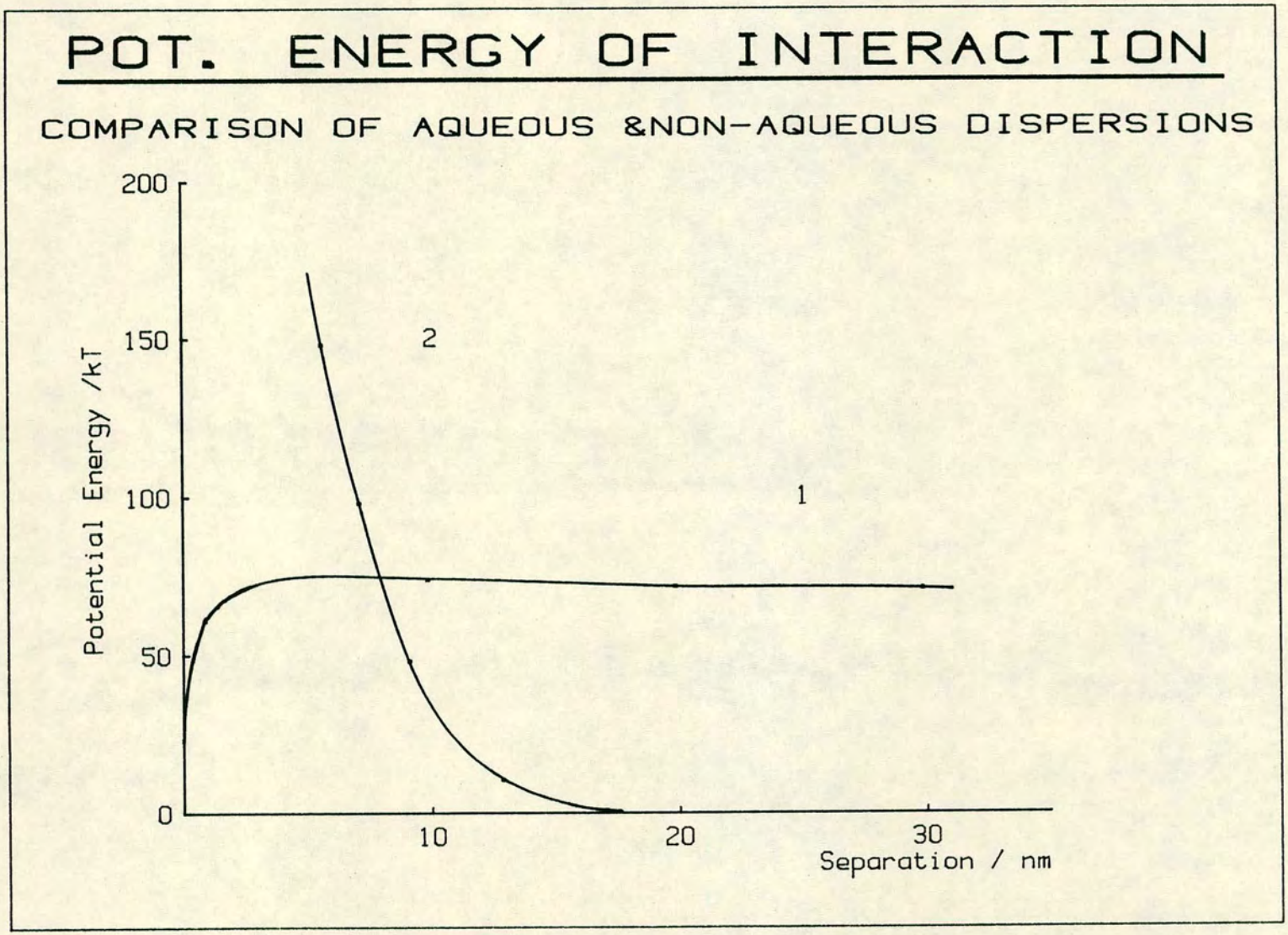

Data from reference (61)

Figure 2.4.5

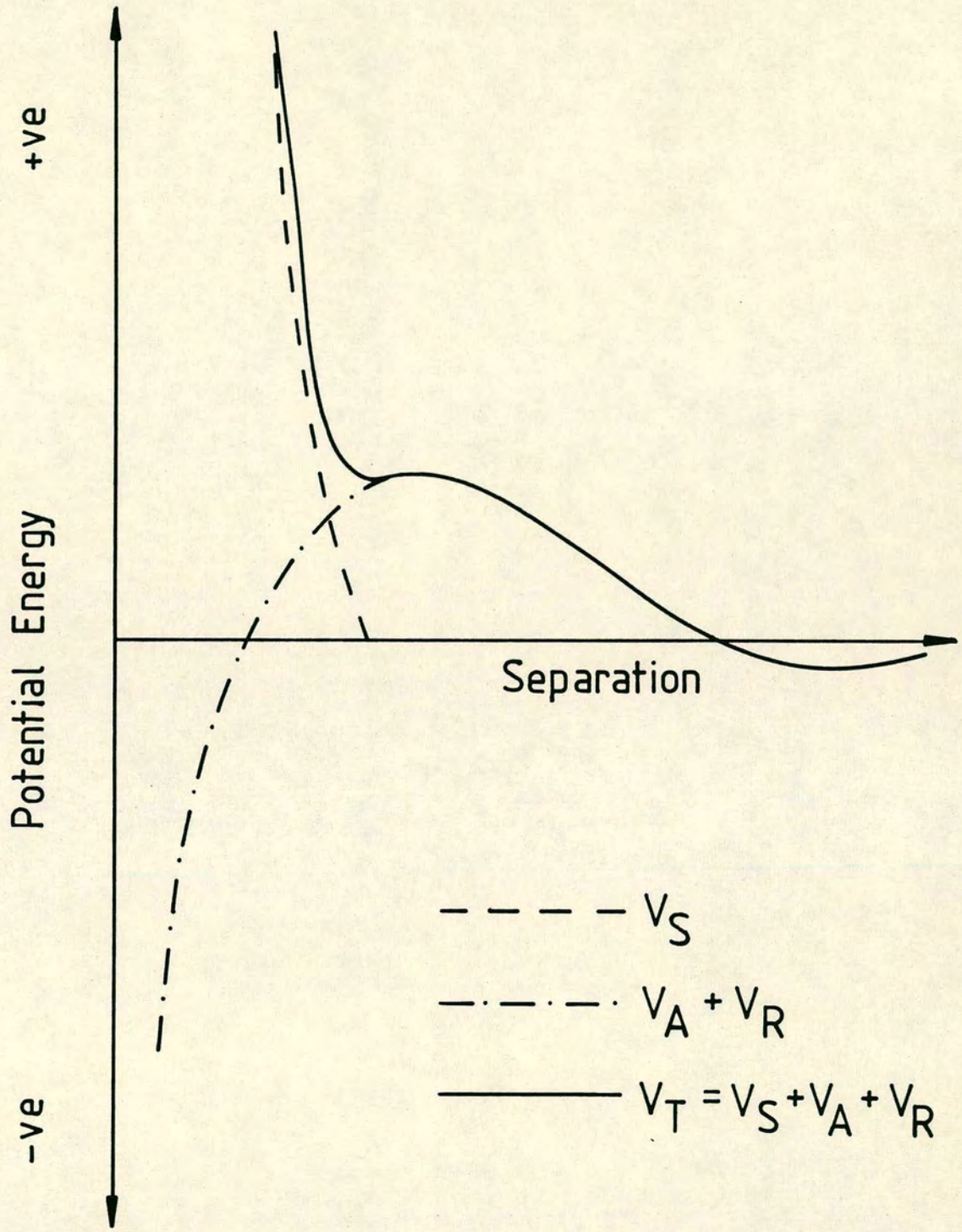

Fig. 2.4.6. Schematic potential energy diagram showing the influence of a steric stabilization term V_S.

V_S allows for the decrease in entropy and the corresponding increase in free energy resulting from chain interaction during particle collision. A qualitative picture of inclusion of the V_S term on an electrostatically stabilised dispersion has been given by Lyklema (73) and is presented in Figure 2.4.6.

The total potential energy curves indicate whether or not a particular dispersion may be expected to be stable but give no indication of the rate of coagulation. To obtain such information a study of the kinetics of coagulation is required.

2.5 Kinetics of coagulation

2.5.1 Rapid coagulation

The rate at which a dispersion coagulates depends on the frequency with which particles interact and, on interaction, whether their thermal energy is sufficient to overcome the repulsive potential energy barrier. Von Smoluchowski (127) considered the simplest form of coagulation in which spherical particles experience no interaction forces until they collide, at which point they become irreversibly coagulated. Under these conditions coagulation is entirely diffusion controlled and proceeds at the so called "rapid rate".

Using Fick's first Law of Diffusion, Von Smoluchowski calculated the number of particles, J,

diffusing through a closed spherical surface towards a fixed central particle. Under steady state conditions this was constant and equal to the number of particles colliding with the central one, giving;

$$J = 4\pi Dr^2 \frac{\partial N}{\partial r} \qquad (2.5.1.1)$$

where D is the diffusion coefficient of the particles,
r is the distance from the centre of the fixed particle and
N is the number of fixed particles per unit volume.
Under the boundary conditions $N = N_o$ where $r = \infty$; and $N = 0$ when $r = R$ equation (2.5.1.1) yields

$$J = 4\pi DRN_o \qquad (2.5.1.2)$$

where R is the sum of the particle radii and
N_o is the initial particle number.
If the central particle is also subject to Brownian motion the diffusion coefficient in equation (2.5.1.2) must be modified to account for the relative motion of the two particles. Since the particles move independently of each other

$$D_{12} = D_1 + D_2 \qquad (2.5.1.3)$$

which for particles of equal size

$$D_{11} = 2D_1 \qquad (2.5.1.4)$$

Equation (2.5.1.2) therefore becomes

$$J = 8\pi D_1 R N_o \qquad (2.5.1.5)$$

where J now represents the number of collisions with one particle. The rate at which primary particles disappear by coagulation is therefore given by;

$$\frac{-dN}{dt} = 8\pi D_1 R N_1^2 \qquad (2.5.1.6)$$

where N_1 is the primary particle number at time t. Equation (2.5.1.6) only describes the beginning of the coagulation process, where collisions only occur between primary particles. As coagulation proceeds multiple particles are formed and in order to account for the disappearance of all types of particles, equation (2.5.1.7) is modified to

$$\frac{-dN}{dt} = 4\pi DRN^2 \qquad (2.5.1.7)$$

where N is the number of particles of all types.

The diffusion coefficient, D, for Brownian motion is given by

$$D = kT/6\pi\eta a \qquad (2.5.1.8)$$

where k is the Boltzmann constant, T, the absolute temperature, η the viscosity of the dispersion medium and a the particle radius. As R is approximately equal to 2a equation (2.5.1.7) may be written as;

$$\frac{-dN}{dt} = \frac{4kT}{3\eta} N^2 \qquad (2.5.1.9)$$

or

$$\frac{-dN}{dt} = k_o N^2 \qquad (2.5.1.10)$$

where

$$k_o = \frac{4kT}{3\eta} \qquad (2.5.1.11)$$

Coagulation proceeds as a second order reaction, the rate constant being k_o. This expression is only strictly applicable to dispersions of monodisperse spheres. Consequently it is most accurate in describing the initial stages of coagulation before significant multiplet formation has occurred.

Overbeek (128) and Muller (32) (129) have extended the analysis to cover both the effect of polydispersity and non-sphericity on the rate of coagulation. Their results indicated that the probablity of collision between particles of differing size was always greater than that between monodisperse particles. Indeed, it was shown that the probability of collision is increased by a factor of about 3 when the ratio of the two particle radii is 10. However, provided the deviation from ideality is not too excessive, the predicted rapid rate constants agree reasonably well with those determined experimentally.

2.5.2 Slow coagulation and stability.

Rapid rate coagulation only occurs in the absence of a net repulsive force between colloidal particles. In the presence of a potential energy barrier, V_{max}, only a proportion of particle encounters leads to permanent contact and the rate at which particles coagulate is reduced.

Fuchs (130) extended the rapid rate theory to the case where appreciable interaction occurs between particles. For diffusion in a field of force

$$J = 4\pi r^2 (D_1 \frac{\partial N}{\partial r} + \frac{N}{\rho} \frac{dV_T}{dr}) \qquad (2.5.2.1)$$

where $V_T(r)$ is the total potential energy of two particles as a function of the separation r and

ρ is the frictional constant of the particles.

On solving equation (2.5.2.1) subject to the normal boundary conditions, J, the number of collisions with one particle per unit time is given by

$$J = \frac{8\pi D_1 N_o}{\int_{2a}^{\infty} \frac{\exp(V_T/kT)}{r^2} \, dr} \qquad (2.5.2.2)$$

Comparing this equation with equation (2.5.1.5) and putting R =2a we can see that the total potential energy V_T reduces the coagulation by a factor,

$$W = 2a \int_{2a}^{\infty} \exp (V_T/kT) \frac{dr}{r^2} \qquad (2.5.2.3)$$

and where s= r/a

$$W = 2 \int_2^{\infty} \exp (V_T/kT) \frac{ds}{s^2} \qquad (2.5.2.4)$$

where W is defined as the stability ratio and is equal to the ratio of the rate constant for rapid coagulation, k_o, to the rate constant for slow coagulation, k

$$W = \frac{k_o}{k} \qquad (2.5.2.5)$$

McGowan and Parfitt (131) have proposed a modified form of equations (2.5.2.3) and (2.5.2.4) to allow for the significant van der Waals attractive forces experienced by the particles before contact, giving;

$$W = \frac{\int_{2a}^{\infty} \exp (V_T/kT) dr/r^2}{\int_{2a}^{\infty} \exp (V_A/kT) dr/r^2} \qquad (2.5.2.6)$$

$$W = \frac{\int_{2}^{\infty} \exp(V_T/kT) ds/s^2}{\int_{2}^{\infty} \exp(V_A/kT) ds/s^2} \qquad (2.5.2.7)$$

From the knowledge of the relevant potential energy curves it is therefore possible to theoretically predict a value of W by numerical integration.

Spielman (132) has criticised the assumption of additivity of single particle Brownian diffusion coefficients, equation (2.5.1.3), to explain the relative

diffusion of two particles during collision. In practice, the viscous motion of two neighbouring particles is quite different from that of a single particle (133) (134). Equation (2.5.1.3) is strictly only valid when the particles are widely separated and its use is questionable at the considerably smaller separation typically important in colloidal interactions. Spielman has proposed a modified Brownian relative diffusion coefficient, D_{12},

$$D_{12} = kT/f \qquad (2.5.2.8)$$

where k and T are as defined earlier and

f is given by;

$$f = \frac{K_1K_2 - \lambda_1\lambda_2}{K_1 + K_2 - \lambda_1 - \lambda_2} \qquad (2.5.2.9)$$

in which K_1, K_2, λ_1, and λ_2 are positive hydrodynamic resistance coefficients and are functions of parameters describing the fluid viscosity and the dimensions and separation of the particles. Incorporation of the viscous effects into the stability ratio expression yields

$$W = \frac{\int_2^\infty (D_{12}^\infty/D_{12}) \exp(V_T/kT) ds/s^2}{\int_2^\infty (D_{12}^\infty/D_{12}) \exp(V_A/kT) ds/s^2} \qquad (2.5.2.10)$$

where $D_{12}^\infty = D_1 + D_2$ and is equal to the relative diffusion coefficient in the absence of viscous interactions.

The inclusion of the Spielman correction for viscous interactions always results in a retardation of the predicted coagulation rate. For thin double layers this reduction in rate may be as much as a factor of 10, however for thick double layers, such as investigated in the current study of PVC dispersed in VCM, the reduction is less significant.

The DLVO theory of colloid stability has been extended by Hogg, Healy and Fuerstenau (135) for the case of heterocoagulation between two spherical colloidal particles differing in both surface potential and radius. For a dispersion containing particles of types 1 and 2 there are three possible interactions between particles each of which give rise to an individual stability ratio, W_{11}, W_{22} and W_{12}, which corresponding to the 1 - 1, 2 - 2, and 1 - 2 interactions respectively. The probability of these encounters are given by;

$$P_{11} = n^2 \qquad (2.5.2.11)$$

$$P_{22} = (1-n)^2 \qquad (2.5.2.12)$$

$$P_{12} = 2n(1-n) \qquad (2.5.2.13)$$

where n is the fraction of particles of type 1 present in the polydisperse system. The overall stability ratio of the dispersion, W_T, is then given by;

$$\frac{1}{W_T} = \frac{n^2}{W_{11}} + \frac{(1-n)^2}{W_{22}} + \frac{2n(1-n)}{W_{12}} \qquad (2.5.2.14)$$

Cooper et. al. (136) found suitable agreement between experimental results and theoretical predictions based on this extension of DLVO theory. More recently (137) improved formulas, used in this approach, for the interaction of dissimilar double layers have been published.

Cooper (137) has extended the work to Hogg et. al. (135) to cover distributions of particle radii, and surface potentials. In this approach a correction is made for the enhanced probability of collision between dissimilarly sized particles. This is based on Muller's (32) (129) extended Smoluchowski's coagulation rate expression for polydisperse systems as discussed earlier. The overall stability ratio W_T is now given by the summation of all possible particle interactions of probability P_{ij} and stability ratio W_{ij}.

$$\frac{1}{W_T} = \Sigma \left(\frac{P_{ij}}{W_{ij}}\right) \qquad (2.5.2.15)$$

By considering Gaussian distributions, it was shown that at constant surface potential the least stable particles dominate the overall stability of a polydisperse system, whilst at constant particle radius small variations in surface potential had a profound influence on the stability of the system.

In 1981, Prieve and Lin (138) considered the stability of polydisperse systems, they too considered Gaussian distributions of particle radii and surface

potential. They conclude that a distribution in Stern potential has a much greater effect on W_T than a distribution in particle size. For example, a standard deviation in Stern potential equal to 10% of the mean was found to reduce W_T by orders of magnitude.

Chapter Three

Experimental methods

3.1 Equipment and materials.

3.1.1 Introduction.

Vinyl chloride monomer (VCM) is a gas at normal room temperatures and atmospheric pressure (b.p. 259.4 K) and is easily liquified using moderate pressures. For the handling, polymerisation and electrophoresis experiments specialised equipment was required which was capable of maintaining the monomer in liquid form. At 343 K, the highest polymerisation temperature used, the saturated vapour pressure rises to 1.2 MPa but to prevent the possibility of equipment failure and exposure to the toxic monomer all the apparatus was constructed to withstand pressures in excess of 2.1 MPa.

In 1974 a higher incidence of a rare liver cancer, angiosarcoma was found in workers exposed to vinyl chloride monomer and since then the permitted exposure limits have progressively reduced towards zero exposure. The current Occupational Safety and Health Administration (OSHA) limit (139) allows exposure up to 1 ppm over an eight hour period. Continuous monitoring, using a Sippin pump, during a typical days VCM handling revealed a 0.1 ppm exposure level. The volume of VCM used in any one experiment was kept sufficiently low, such that, in the event of a complete equipment failure, the amount of VCM on dilution would be below the 1 ppm level. To reduce the exposure risk further Draeger monitoring was carried out at important stages of the experimental procedure, and all

monomer transfer steps carried out in a fume cupboard.

3.1.2 Materials.

Vinyl chloride monomer (VCM) (CH_2CHCl) was supplied in a 25 kg storage cylinder by I.C.I. plc, Petrochemical and Plastics Division. The monomer was purified by two separate distillation steps. It has been proposed (61) that traces of water in VCM may play an important role in the mechanism of producing a charged stabilised system. Indeed, Speirs, in the previous work had found it impossible to dry the monomer to a constant level and suggested that the inconsistent results that he obtained were caused by the variation in water content. However, in this work, no special attempt was made to remove residual traces of water and the irreproducible results as found by Spiers were not obtained. Furthermore, the use of dry VCM would be unrealistic of the industrial aqueous polymerisation process.

Lauroyl peroxide ($[CH_3(CH_2)_{10}CO]_2O_2$) BDH Laboratory Grade was recrystallised from water and stored in a desiccator, before use as a free radical initiator.

Low molecular weight additives, bis-(2-hydroxyethyl) -aminohexadecane ($C_{16}H_{33}N[CH_2CH_2OH]_2$), which was prepared using Fluka reagents, and Span-20 (Sorbitan monolaurate), were supplied by I.C.I. plc. These reagents were stored in a vacuum desiccator over P_2O_5 and used without further purification. Manoxol-OT (Aerosol-OT) (di-2-ethylhexyl

ester of sodium sulphosuccinic acid) BDH General Laboratory Reagent was Soxlet extracted using sodium dried ether for 8 hours. The purified Manoxol-OT was stored over P_2O_5 in a vacuum desiccator and a water level of <0.2% was found by Karl Fischer titration.

Methanol (CH_3OH) BDH Specially Dried was used as a solvent for the addition of low molecular weight additives to the polymerisation.

Tetrahydrofuran ($[CH_2]_4O$) Fisons Standard Laboratory Grade was used as a solvent for polyvinyl chloride.

Nitrogen gas (N_2) BOC White Spot was used for pressurising and purging the equipment of oxygen.

Water was triply distilled from all glass apparatus and had a specific conductivity of less than 1.2×10^{-6} cm^{-1} Ω^{-1}.

3.1.3 Equipment for VCM handling.

The equipment for monomer transfer had to be capable of withstanding pressures in excess of 2.1 MPa and was designed so that it could be purged of contaminants and evacuated before monomer was handled.

The pressure rig described and used by Speirs contained many redundant features and involved the VCM passing through various mixing chambers "en route" to the electrophoresis cell. To reduce the possibility of leaks and contamination the original rig was used in a modified

form so that it only controlled the purging and evacuation of the system. For the monomer transfer a new rig was constructed with the advantage of an almost direct link between the storage vessel and the cell outlet.

Due to VCM's corrosive properties all components on the handling rigs which came into contact with monomer were made of stainless steel. The Hone valves were connected by 1/16" outside diameter narrow bore tube and connected by Wade or specially produced couplings.

The equipment is shown schematically in Figure 3.1.3.1. It consists of a nitrogen inlet via a regulator 1 and a pressure gauge calibrated from 0-600 psi which allows the system to be pressurised and purged of contaminants by opening valves 2, 4 and 5. The system can be evacuated by opening valve 3 to the Speedivac rotary pump or VCM disposed of by connecting the scrubbing tower. At the end of each run any unreacted monomer was converted to the formic and chloroformic acids by passing through a scrubbing tower containing an alkaline potassium permanganate solution.

The vinyl chloride monomer is held in a small 25 cm^3 stainless steel Hone cylinder containing two inlet valves (6 and 7) and transfer of the monomer to cell outlet is achieved by opening valves 5 and 6. The cell outlet delivery tube is in the form of a loop and is an essential feature, as it is capable of sufficient movement to allow the electrophoresis cells to be attached without shearing off the cell inlet stem.

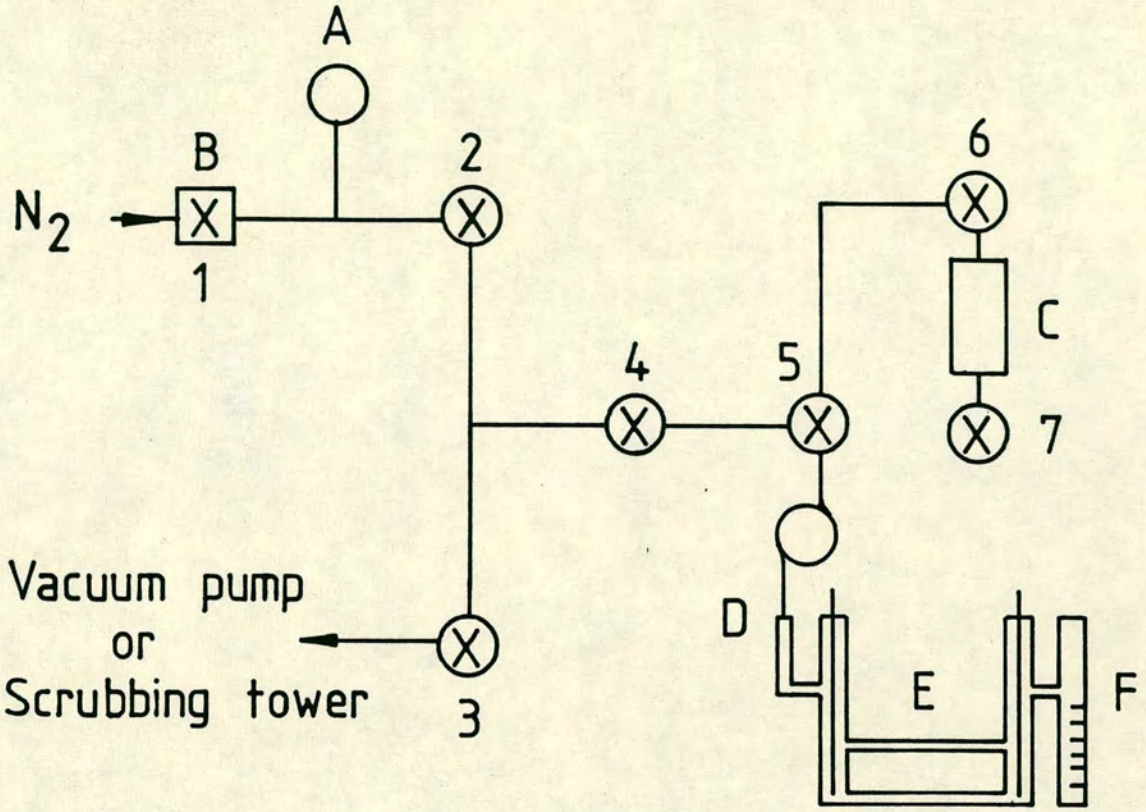

KEY

A. Pressure gauge
B. Nitrogen regulator
C. Hone cylinder
D. Ball valve
E. Electrophoresis cell
F. Polymerisation limb
Ⓧ Hone valves

Fig. 3.1.3.1. Schematic representation of the monomer transfer equipment

3.1.4 Development of a combined polymerisation/ electrophoresis cell.

The original electrophoresis cell used by Speirs is shown in Plate 3.1.4.1A and was constructed from borosilicate glass, later apparatus was built in quartz to a similar design. The cells consisted of two electrode compartments which were joined by a thick walled capillary and a wide bore cross-tube to allow equalisation of pressure throughout the cell. The front and back faces of the capillary were ground flat to reduce optical distortion during microscopic investigation. Platinized platinum electrodes were fitted to the cells by quartz to metal graduated seals, the platinum black layer having first been deposited by electrolysis of a chloro-platinic acid solution containing a trace of lead acetate. Entry and exit of VCM was accomplished through the side arms, the cells being made pressure tight by the compression of Viton washers between the cell and ball valve assemblies held in brass blocks by locking rings. Using these cells several problems were encountered and considerable refinement was necesssary before they could be used reliably to investigate the colloidal events occurring during the early stages of polymerisation.

In the previous work the initial aim of trying to carry out polymerisation and electrophoresis in the same cell proved impossible except at extremely low

polymer conversions. At higher conversions too large a particle concentration was produced for electrophoresis measurements using dark field microscopy.

To resolve this problem polymerisation was carried out in a test tube cell and then transferred to the thick walled microelectrophoresis cell which contained diluent vinyl chloride monomer. This transfer through valves and fine bore tubing resulted in orthokinetic coagulation of the dispersion by shear forces and raised doubts about the validity of the measured zeta potential and associated particle morphology. To overcome shear coagulation a trial modification was made to one of the glass electrophoresis cells by connecting a wide bore polymerisation limb to one of the glass side arms. (See Plate 3.1.4.1B). Initial experiments showed that it was possible to polymerise monomer in the side limb and then dilute the concentrated dispersion, without shear coagulation, by pouring a small amount of latex into diluent monomer held in the electrophoresis section of the cell.

The addition of a polymerisation limb necessitated a new method of sealing the cell, this was achieved by compressing a metal ferrule within a 6 mm Swagelok nut and cap onto the metal portion of a quartz to metal graduated seal. The other inlet was sealed using the brass clamping blocks. Plate 3.1.4.1B. Neither of these methods were ideal, the brass blocks were cumbersome and a series of cell failures occurred at the quartz to metal graduated seal. These breakages were caused by shearing forces being

A

B

Plate 3.1.4.1 Development of the combined Electrophoresis/polymerisation cell.

C

D

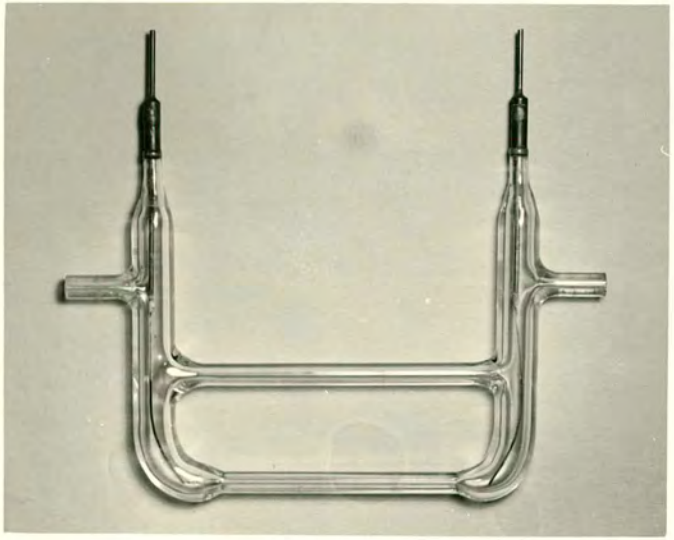

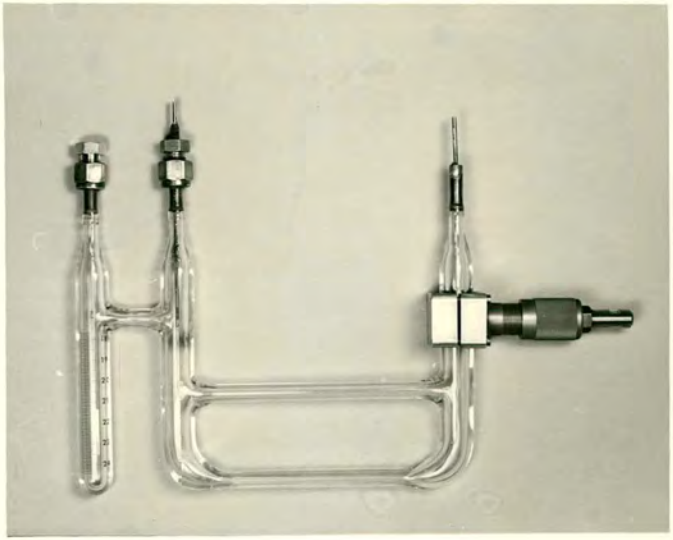

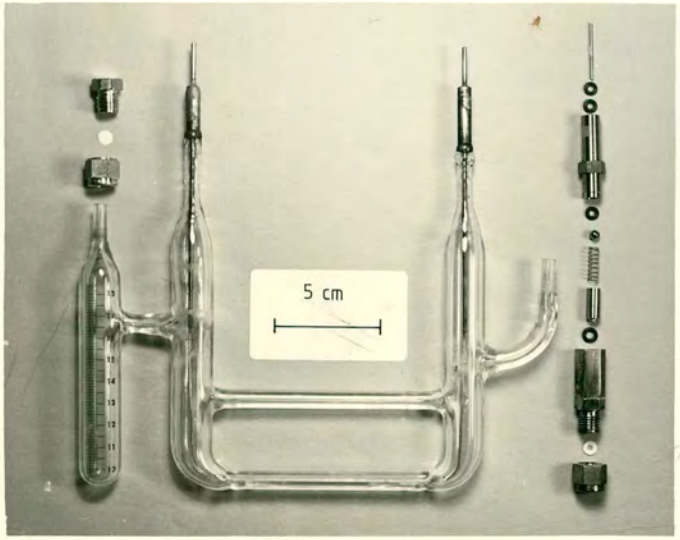
5 cm

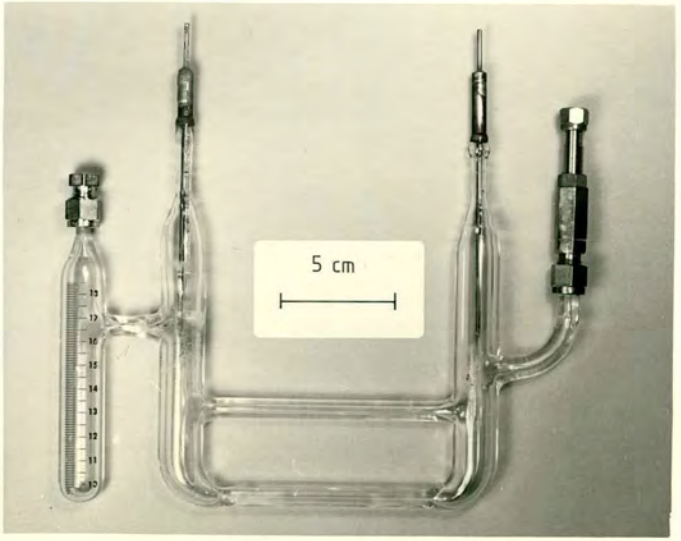
5 cm

transmitted directly to the seal on tightening the Swagelok cap to obtain a pressure tight cell.

A similar shearing problem has been encountered in sealing glass chromatography columns and here the problem has been resolved by the use of PTFE ferrules which give pressure tight systems at moderate temperature and pressures. This development rendered the quartz to metal seal obsolete and since the brass side valve block was cumbersome and restricted cell movement within the electrophoresis tank it, too, was replaced. A further advantage was that the ball valve could be mounted at either side of the cell, thus allowing monomer to be introduced directly into the polymerisation limb or electrophoresis section of the cell.

The modification involved grinding quartz inlet stems of about 2.5 cm in length, with an external diameter of 0.6 cm and internal diameter of greater than 0.2 cm to allow access for a sampling microslide. The final version of the quartz cell along with the components of the ball valve assembly is shown in Plate 3.1.4.1C and the assembled cell in Plate 3.1.4.1D.

3.1.5 Equipment for polymerisation/electrophoresis experiments.

Polymerisation and electrophoresis measurements were carried out in a modified Perspex tank mounted vertically to a Rank Brothers Particle Microelectro-

phoresis Apparatus. The standard tank was increased in height and width, the former to prevent convection currents during electrophoresis caused by poor thermostating and the latter to allow tubidimetric measurements to be recorded during polymerisation. The water in the tank was maintained at the required temperature ±0.1 K using an external thermostat unit (Haake Constant Temperature Circulator - Type FK10). A schematic diagram of the equipment is presented in Fig. 3.1.5.1. Automatic control of its two operating modes (polymerisation or electrophoresis) was achieved via a relay system.

For polymerisation the relay was in the 'on' position and controlled the polymerisation temperature via contact thermometer C1 mounted in the Perspex tank. It also activated the turbidimetric device which consisted of a quartz iodide light source L1, whose output could be focused through the polymerisation limb of the cell using a converging lens. The light intensity passing through the dispersion was detected by a photo-cell (Evans Electroselenium Ltd.) and decreased as a function of extent of reaction. The photo-cell output voltage was measured on a digital electrometer (Keithley - Type 616) and recorded as a function of polymerisation time on a Servoscribe chart recorder.

The turbidimetric recordings were used to determine the length of induction period prior to particle formation, which was shown by a sharp increase in

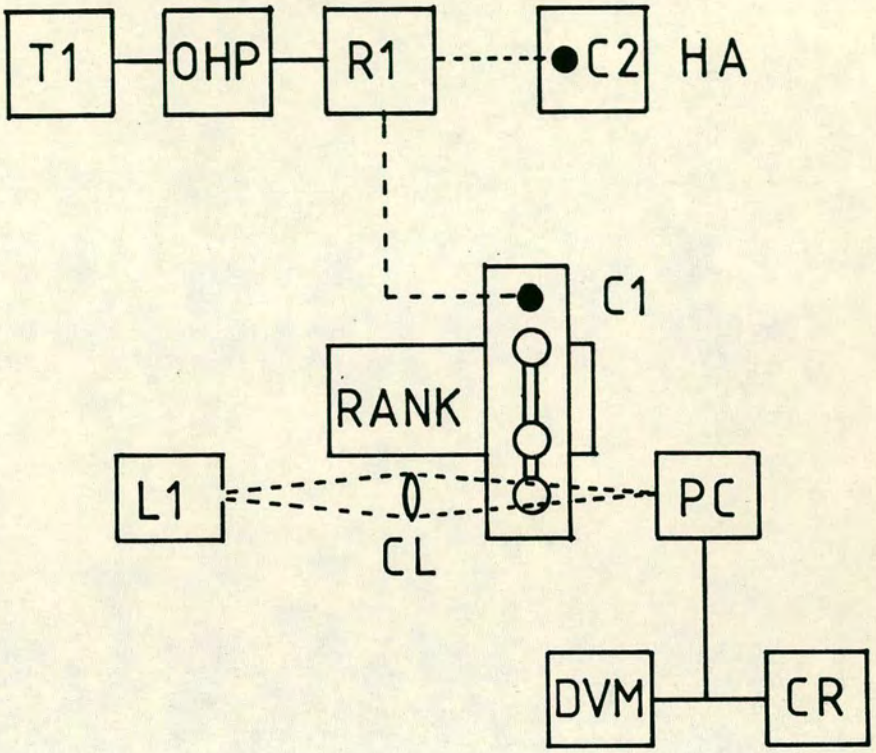

KEY

T1	Timer
OHP	Over temperature protection circuit
R1	Relay
HA	Haake constant temperature circulator
C1	Contact thermometer (polymerisation)
C2	Contact thermometer (electrophoresis)
L1	Light source
CL	Converging lens
PC	Photocell
DVM	Digital volt meter
CR	Chart recorder

Fig. 3.1.5.1 Schematic representation of the polymerisation / electrophoresis equipment

turbidity. Furthermore, by comparison with earlier traces, they gave a useful indication of the rate and extent of reaction during the polymerisation.

At the desired conversion the reaction was rapidly quenched by switching the relay system off, this transferred temperature control to contact thermometer C2 which was set at 293.1 K for the electrophoresis measurements. For polymerisations at 308.1 K the polymerisatiom rate was sufficiently slow that adequate quenching could be achieved using the Haakes internal compressor unit alone. At higher temperatures and more rapid reaction rates the quenching process was aided by pumping iced water through the system. The relay also switched off the turbidimetric device, thus recording the final tubidity and polymerisation time. For low temperature polymerisations with their long reaction times the addition of a timing device and an overheat protection circuit allowed the process to be automated and the polymerisation events recorded for examination before electrophoresis.

3.2 Techniques.

3.2.1 Preparation of PVC Latex.

3.2.1.1 VCM transfer to the Hone cylinder.

Prior to polymerisation small volumes of pure VCM were obtained by distillation from the 25 kg storage cylinder into the small Hone cylinder. A flexible braided

steel pipe was connected by a Wade coupling between the storage cylinder and the top valve, 6, of the Hone cylinder. The lower cylinder valve, 7, was connected to a Speedivac rotary pump and the cylinder and connecting pipe evacuated for 5 minutes. Nitrogen at 0.25 MPa was then admitted to the cylinder and the system again evacuated for 5 minutes. This procedure adequately removed air from the apparatus, which would retard the onset of polymerisation.

The Hone cylinder was cooled to 195 K with liquid nitrogen and the valve on the large storage cylinder opened. After 5 minutes the Hone cylinder typically contained about 23 g of condensed vinyl chloride monomer and by transferring the cylinder into a water bath at 293 K excess VCM was allowed to distil back into the storage cylinder. The valve on the storage cylinder was then closed and any residual monomer trapped in the connecting pipe condensed into the Hone cylinder by cooling in liquid nitrogen. The top Hone valve, 6, was then closed and the cylinder brought to room temperature using a water bath.

3.2.1.2 Monomer transfer to the cell.

The transfer of monomer, prior to polymerisation, went through several stages of development. The final and most reliable method is described below. Initiator (typically 0.05 to 0.15% (wt/vol) was weighed into a long

necked weighing boat and fed directly to the base of the polymerisation limb. Any low molecular weight additives and a microslide to collect a sample for electron microscopy were also added at this stage.

The ball valve components were assembled using forceps to avoid contamination and a short length of tube inserted into the assembled valve. As the cell was attached to the cell outlet of the transfer rig, the short tube was depressed and pushed to hold open the ball valve. The joint was sealed with Viton O rings. Plate 3.2.1.2.1A.

By opening valves 1,2,4 and 5 the cell was purged for 5 minutes with nitrogen at 0.15 MPa to remove oxygen and water vapour. The polymerisation limb was then sealed using a Swagelok cap. Before transferring monomer, the cell was pressure tested by increasing the nitrogen pressure to 1.3 MPa. Valve 5 was closed and the cell removed from the rig and checked for leaks and the correct operation of the ball valve mechanism. On reattaching the cell to the rig the electrophoresis section of the cell was placed in an ice/water slush bath, keeping the polymerisation limb outside the bath and at room temperature. The thermal gradient formed between the cell and the monomer stored in the Hone cylinder was sufficient to allow VCM to distill into the electrophoresis section of the cell. Whilst the cell cooled, three cycles of purging were carried out by opening valves 1,2,4 and 5, pressuring to 1.3 MPa, then evacuating for 5 minutes by closing valve 2 and opening valve 3 to the rotary pump.

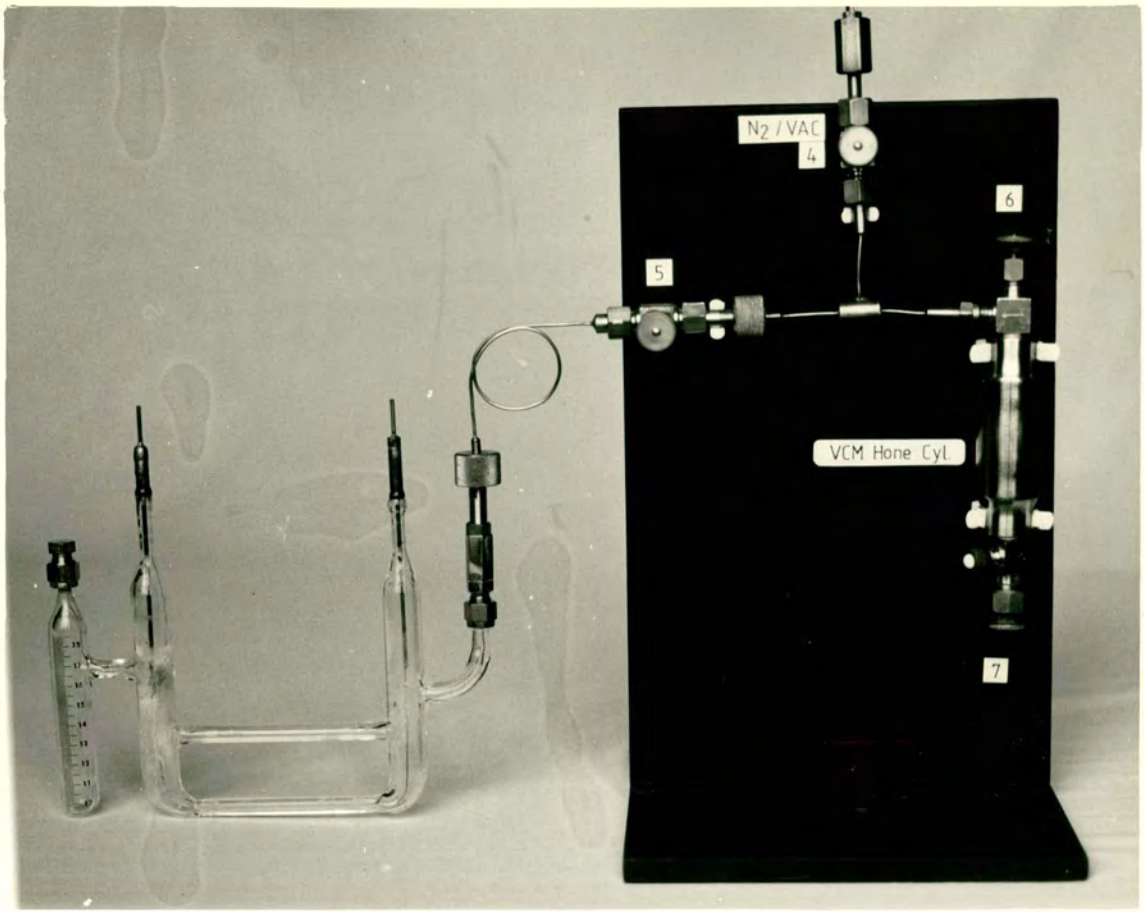
N2 / VAC
4
5
6
VCM Hone Cyl.
7

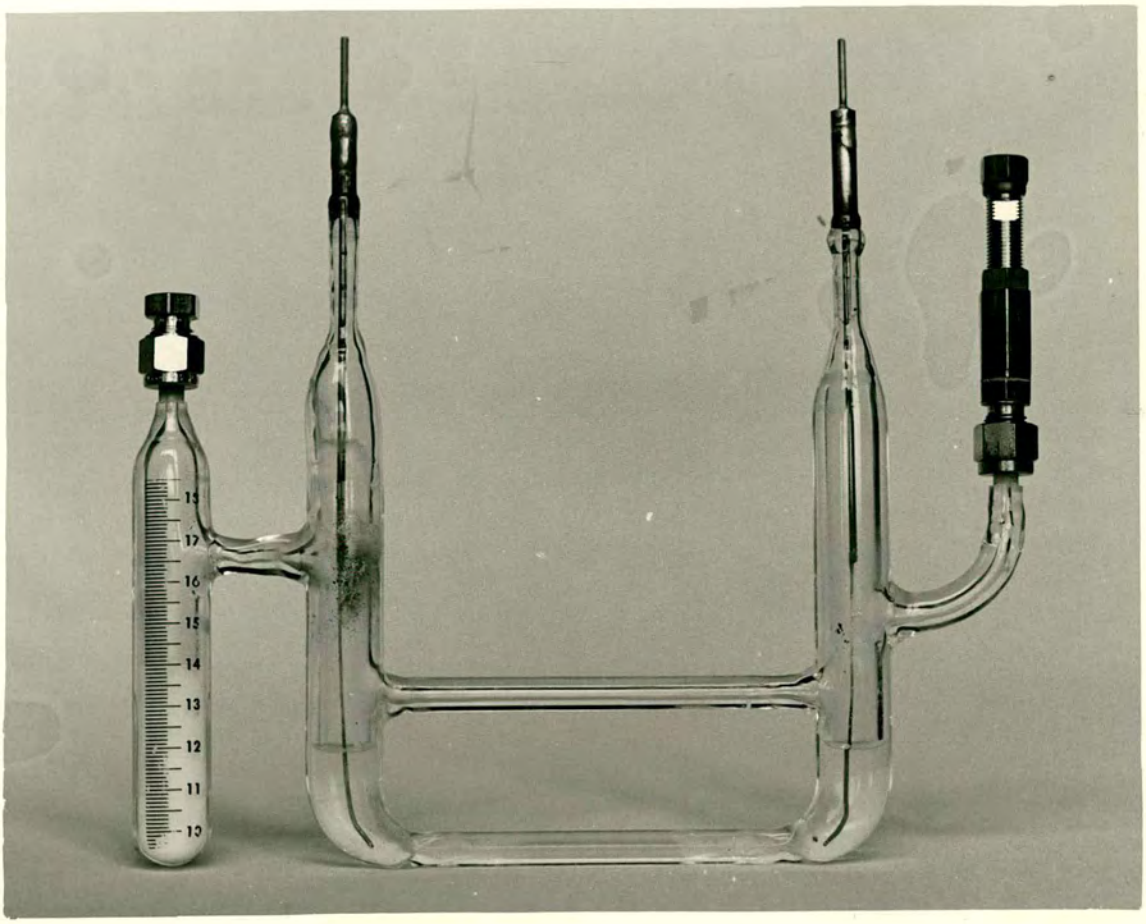
18
17
16
15
14
13
12
11
10

After the third cycle the cell was evacuated for a further 10 minutes. These purging sequences adequately removed volatile contaminants from the cell.

The original rig was then isolated from the transfer rig by closing valve 4 and monomer condensed into the electrophoresis section by opening the Hone cylinder valve 6. The rate of distillation was controlled so that no VCM condensed onto the initiator within the polymerisation limb. Monomer was collected until it reached the level of the strengthening cross member of the cell and distillation completed by closing valve 6 then 5. The cell was removed from the transfer rig and sealed using a Wade cap. Plate 3.2.1.2.1B. A final check for minor VCM leaks using a Draeger pump was carried out before removing the cell for the polymerisation step.

3.2.1.3 Polymerisation.

Small scale polymerisations, typically 5 cm^3 of VCM, were carried out in the side limb of the cell. So that the volume of monomer within the polymerisation limb could be accurately determined, a graduated scale was attached to the outside of the limb. This was calibrated by weighing small volumes of water into the limb and recording the corresponding scale reading so that a plot of mass of water against scale reading could be drawn. A least squares analysis of the data gave expressions of the type; Quartz cell 8

$$V = 1.0029 \times (1.148 \times \text{scale reading} - 10.934) \quad (3.2.1.3.1)$$

Where V is the volume of liquid in cm^3.

Before commencing each reaction the thermostat bath was brought to the required temperature and the turbidimetric device (as described in section 3.1.5) set to give a 'blank' reading of 0.360 V. Using the calibrated scale, the required amount of monomer was poured into the polymerisation limb and mixed with the initiator.

The cell was then immersed in the thermostated tank and accurately positioned so that the light beam of the turbidimetric device passed through the centre of the polymerisation limb. The time taken for turbidity to appear was noted and the turbidity trace recorded. A typical trace is shown in Fig. 3.2.1.3.1. At the desired conversion the reaction was quenched and automatically equilibrated to 293.1 K for electrophoresis measurements. Plate 3.2.1.3.1shows the concentrated polymer latex with diluent monomer held in the electrophoresis section of the cell.

3.2.2 Electrophoresis

3.2.2.1 Theory

There are four electrokinetic phenomena, electrophoresis, electro-osmosis, streaming potential and sedimentation potential, each of which involves a relative

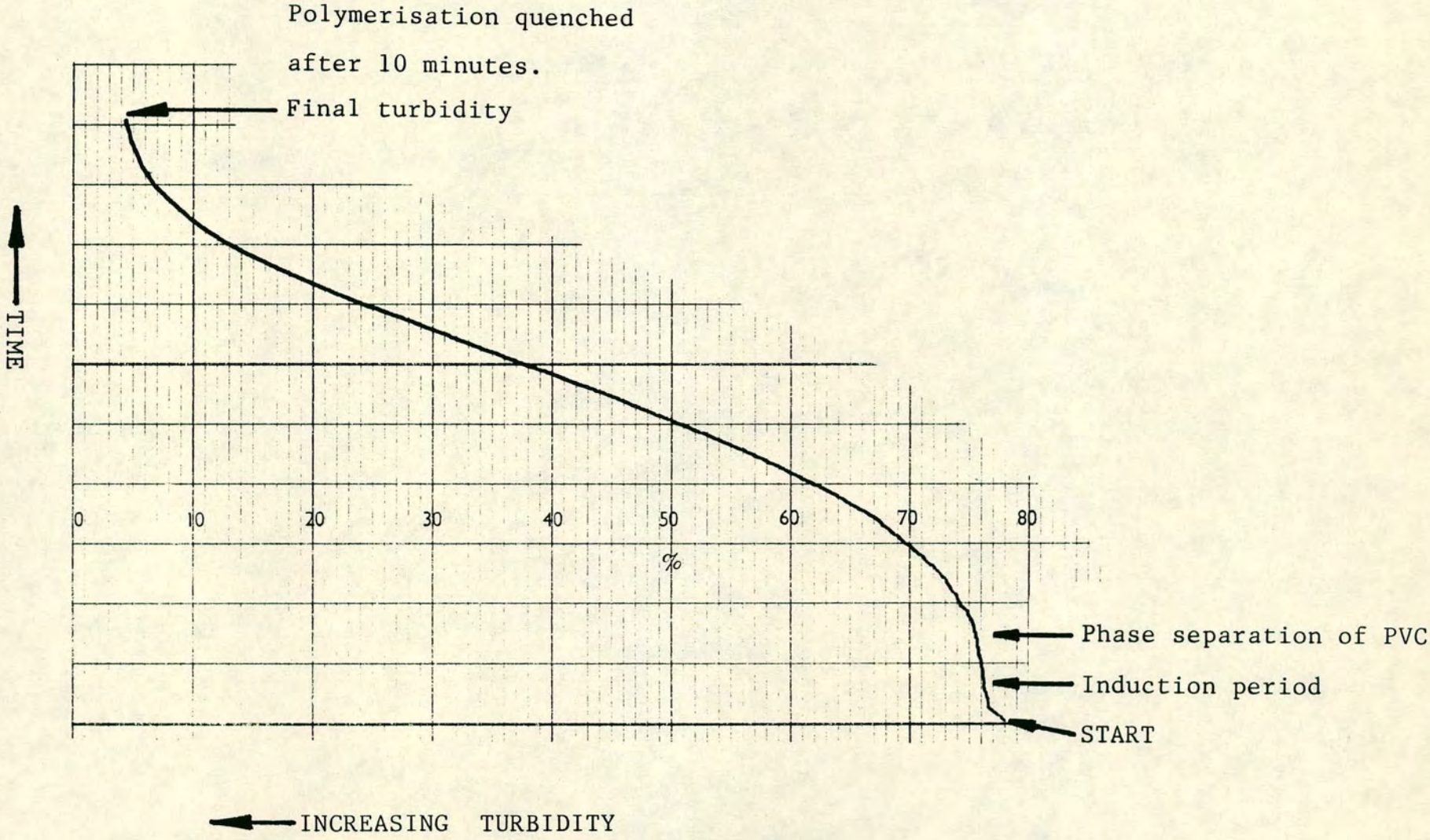

Fig. 3.2.1.3.1 Polymerisation turbidity trace.

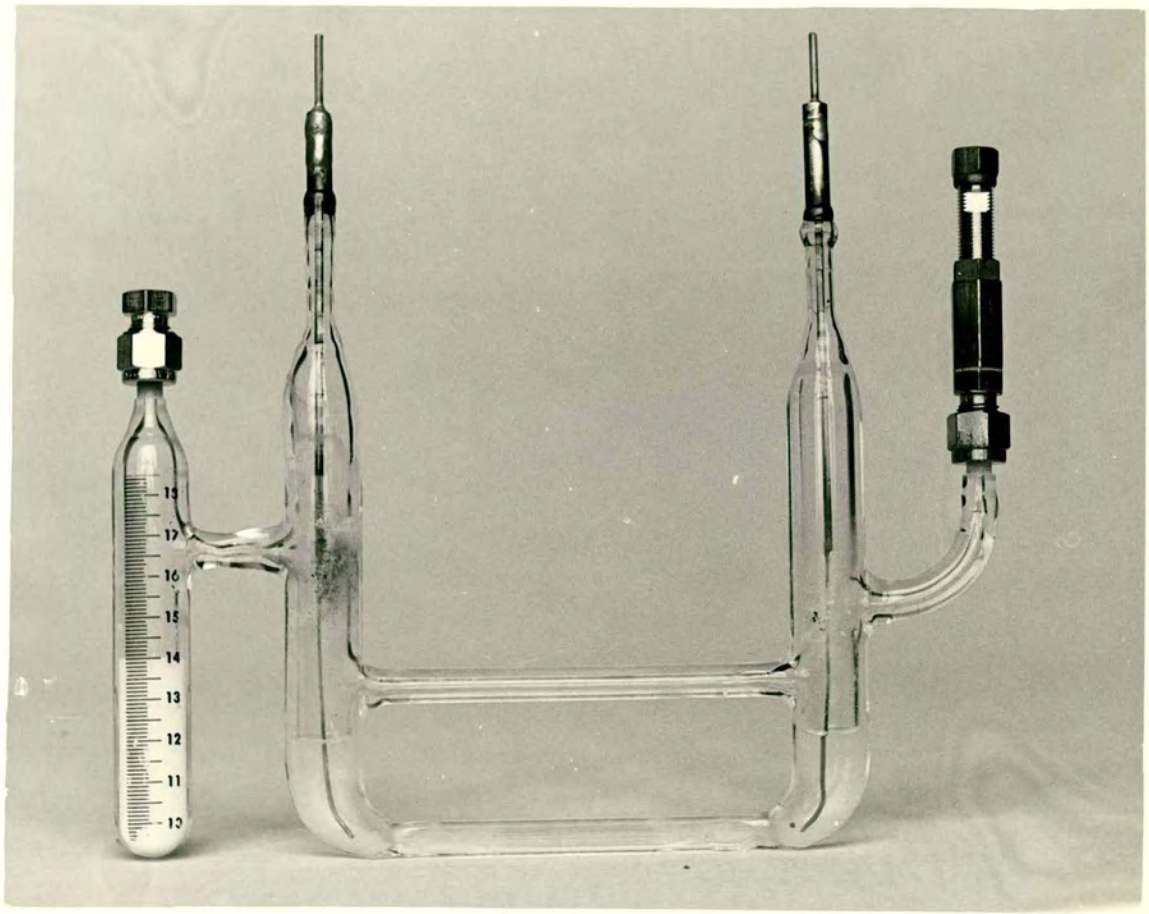
18
17
16
15
14
13
12
11
10

tangential motion between the rigid and mobile parts of an electric double layer. Electrophoresis involves the migration of charged, suspended material under the influence of an applied electric field. The resultant electrophoretic velocity is proportional to the sign and magnitude of the potential at the surface of shear between the particle and its double layer. This potential is called the zeta potential (ζ) and bears no direct relationship to ψ_o or ψ_δ although it is often assumed to be approximately equal to ψ_δ. (See Fig. 2.2.2).

Of the several experimental techniques available for the measurement of electrophoretic mobilities, only microelectrophoresis can be applied in this study because of the elevated pressures required to liquify the gaseous monomer. In microelectrophoresis the movement of individual particles under the influence of a known electric field is followed directly in a dark field microscope. The measurement of the electrophoretic velocity is complicated by the presence of a surface charge on the cell walls which gives rise to an electro-osmotic flow of liquid in the vicinity of the cell walls. Since there can be no net transport of liquid in a closed cell, a compensating return flow of liquid down the centre of the cell occurs resulting ideally in a parabolic liquid velocity pattern in the capillary. There are two depths, the so-called "stationary levels", at which the net liquid flow is zero. Only at these points can the electrophoretic velocity be observed directly. At any

other depth in the cell the observed velocity is the resultant of the liquid velocity V_L at that depth and the true electrophoretic velocity, V_E.

The liquid velocity V_L at a distance r from the centre of a cylindrical capillary of radius a is the sum of the electro-osmotic velocity V_{EO} and the return flow which obeys Poiseuille's law, such that

$$V_L = V_{EO} - C(a^2-r^2) \qquad (3.2.2.1.1)$$

where C is a constant. For no overall liquid transport

$$\int_o^a V_L \ (2\pi r) \ dr = 0 \qquad (3.2.2.1.2)$$

The solution of equations (3.2.2.1.1) and (3.2.2.1.2) gives

$$C = 2V_{EO}/a^2 \qquad (3.2.2.1.3)$$

so that

$$V_L = V_{EO} \left(\frac{2r^2}{a^2} - 1\right) \qquad (3.2.2.1.4)$$

At the stationary levels $V_L = 0$ and for a cylindrical capillary this occurs at $(r/a)^2 = 0.5$ i.e. at a distance of 0.293a from the front and rear capillary walls.

The observed velocity, V_{OBS}, of a particle at any depth in the cell is given by

$$V_{OBS} = V_E + V_L = V_E + V_{EO}\left(\frac{2r^2}{a^2} - 1\right) \quad (3.2.2.1.5)$$

From a linear plot of V_{OBS} against $(r/a)^2$

$$V_{EO} = \text{slope}/2 \quad (3.2.2.1.6)$$

$$V_E = \text{intercept} + V_{EO} \quad (3.2.2.1.7)$$

Thus electrophoretic velocity may be determined either from the observed particle velocity as a function of depth through the cell, or by direct measurement at the stationary levels at $(r/a)^2 = 0.5$.

Several equations applicable to different κa values have been proposed to calculate zeta potentials from electrophoretic velocity data. For the case of PVC particles dispersed in VCM, κa is $<<1$ and the Hückel equation (140) was used.

$$u = \frac{\zeta \varepsilon}{1.5\ \eta} \quad (3.2.2.1.8)$$

where u is the electrophoretic mobility and is equal to the electrophoretic velocity divided by the applied potential gradient ε and η are the permittivity and viscosity of the dispersion medium. The expression was derived from Stokes equation and allows for the so-called electrophoretic retardation. Under the influence of the applied electric field the counter ions flow in the

opposite direction to the particles and, in so doing, impart a liquid flow which reduces the electrophoretic velocity of the particles. This movement distorts the originally symmetrical double layer and, due to the finite time required for its restoration by diffusion and conduction, a retarding potential difference is formed. This is the relaxation effect and is not accounted for in the Hückel equation but can be safely neglected in dispersions where $\kappa a < 0.1$ (141) which is the case in the present investigation of PVC particles suspended in VCM.

The calculation of zeta potentials has been the subject of several refinements which have been reviewed by Hunter (98). The recent computer solution of O'Brien and White (142) has not been employed here since at low κa values their approach yields zeta potentials with little deviation from those obtained by the Hückel equation.

3.2.2.2 Technique

The construction of the cell and the preparation of the polymer latex has already been discussed in sections 3.1.4 to 3.2.1. A small amount of the concentrated dispersion was gently poured into diluent monomer held in the electrophoresis portion of the cell. There it was thoroughly mixed before being mounted vertically in the thermostated tank of the Rank electrophoresis apparatus.

Electrophoresis measurements were made at

293.1 K ± 0.1 K and to prevent convection currents forming by the distillation of monomer around the cell the room was maintained to a similar temperature. To minimise further the problem of convection within the cell, two heat filters (Ealing Beck Ltd.) were positioned between the microscope lamp and the dark ground condenser assembly. The scattered light observed from the particles depended upon the extent of polymerisation and, at a total magnification of 200x, ranged from a faint mist in which no individual particle could be observed to single bright spots against a dark background.

A d.c. potential of up to 450 V could be applied to the cell using a voltage stabilised power supply, the magnitude and reversibility of this potential being checked with a high impedance digital voltmeter. Particles were timed over a series of squared graticules in one eye piece using a digital stop clock accurate to 0.02 s. To minimise operator timing errors, Brownian motion errors and electrode polarisation, the number of squares crossed was chosen so that the times were between 4 and 10 seconds. Furthermore, the potential gradient was reversed after each timing to avoid the build up of electrode reaction products and to compensate for any horizontal particle drift.

The observed velocity was obtained by recording eight concordant particle timings at up to nine levels throughout the front half of the cell. The product of the mean reciprocal time taken to traverse one graticule

square by the length of that square gave the observed particle velocity and a linear graph of V_{OBS} against $(r/a)^2$ plotted. Using a least squares analysis to give the slope and intercept the electrophoretic and electro-osmotic velocities were calculated from equations (3.2.2.1.7) and (3.2.2.1.6) respectively.

To disclose any variation in electrophoretic velocity as a function of time, measurements were also made directly at the stationary level at the start and on completion of an electophoresis session.

Division of the electrophoretic velocity by the applied potential gradient yields the electrophoretic mobility and the corresponding zeta potentials were calculated from the Hückel equation (eqn. 3.2.2.1.8).

3.2.2.3 Evaluation of optical corrections and cell lengths.

Optical corrections.

During the design of the electrophoresis cell conflicting requirements were met regarding the optical capillary. The thin walled Van Gils type cells (143) which suffer only minor optical distortions could not withstand the elevated pressures required to liquify the monomer. The cells were therefore constructed with thick walled Mattson type capillaries (144), which induced complex optical distortions in the particle image. The flat outer and curved inner walls of the capillary act as a

plano-concave lens which has the effect of shifting the apparent position of levels within the cell.

A correction was first proposed by Henry (145) but more recently Hall (146) has shown that the analysis was inadequate due to the complexity of the astigmatism. Each point within the cell gives rise to two virtual images, when focused just inside the near wall these two images are close together and appear as a point source. In the rear half of the cell the images are widely spaced and appear as poorly defined elongated spheres. In practice it was impossible to make measurements in the rear half of the cell because of this astigmatism and data was only collected at a series of optically corrected levels in the front half of the cell.

The corrections were evaluated using a rearranged form of the expression given by Smith (147)

$$V = \frac{n_3\ au}{n_1\ a-u(n_1-n_2)} + \frac{d}{n_2}(n_3-n_2) \qquad (3.2.2.3.1)$$

where V is the apparent location of the point relative to the true position

u is the actual distance from the front inner wall to the required point of observation

a is the capillary radius

d is the minimum wall thickness

n_1 is the refractive index of the liquid in the cell (1.364 for VCM at 293 K)

n_2 is the refractive index of the cell material (quartz 1.46)

n_3 is the refractive index of the medium immersing the microscope lens (air).

The capillary radius "a" could only be measured indirectly. The minimum flat flat distance of the cell was measured using a micrometer, whilst the minimum wall thickness was measured by setting the cell vertical and perpendicular to the light source, at the central plane of the capillary. The thickness was then measured by focussing alternately on the inner and outer walls of the capillary, the difference in micrometer readings multiplied by the refractive index (n_2) gave the wall thickness. The minimum wall thickness was obtained by moving in 1 mm steps along the observable portion of the capillary. The capillary radius a was then calculated by subtracting the two minimum wall thicknesses from the flat flat distance.

Table 3.2.2.3.1 contains the data for each of the cells.

The optical corrections for the quartz cells calculated from equation (3.2.2.3.1) are given in Table 3.2.2.3.2:

Table 3.2.2.3.1 Flat flat distance, wall thicknesses and capillary radius for each cell

Cell type	Flat flat distance/μm	Minimum wall thicknesses/μm		Capillary Radius/μm
Glass	6983	2799	2732	726
Modified Glass	7001	2691	2917	697
Quartz Mark 1 & 3	6934	2114	2200	1310
Quartz Mark 2,4,5,6 & 8	6259	2655	2580	512
Quartz Mark 7 & 9‡	-	-	-	500

‡ Cell failed before measurements taken and cell not repaired until experimental work had ceased.

Table 3.2.2.3.2 Distance to be moved from the apparent position of the front inner wall to focus various $(r/a)^2$ values

$(r/a)^2$	Distance to be moved/μm	
	Quartz Cell Mark 1 & 3	Quartz Cell Mark 2,4,5,6 & 8
0.9	49.5	19.2
0.8	100.6	39.3
0.7	155.1	60.6
0.6	213.1	83.3
0.5	275.6	107.7
0.4	344.1	134.5
0.3	421.0	164.5
0.2	514.7	199.7
0.1	626.5	244.9
0	897.3	367.8

Cell lengths

To enable the conversion of electrophoretic velocity to mobility the potential gradient applied during electrophoresis had to be evaluated. (The potential gradient equals the applied voltage divided by the cell length). This requires a knowledge of the cell length which was obtained conductimetrically via the cell constant.

The resistance of three separate KCl solutions of known concentration was measured in the cells using a Wayne Kerr Bridge. The cell constants were found by

multiplying the mean resistance by the specific conductance of KCl solution. The cell lengths were then calculated from the product of the cell constant by the capillary cross-sectional area and the results are shown in Table 3.2.2.3.3.

3.2.3 Analysis of particle size and morphology

The analysis of particle size and morphology was a major aspect of this work and allowed the visual characterisations of the various particle types and the resulting morphological changes brought about by varying the colloidal stability of the system. One prerequisite to image analysis was the development of a reliable sampling technique which would not cause drastic changes in particle morphology by flocculation.

Various methods of sizing colloidal polymer particles are available. In this study electron microscopy was used because it can measure highly polydisperse particle size distributions over any size range within the colloidal domain. In reviewing particle sizing of polymer laticies Fitch (148) suggested that electron microscopy should be considered as a method of last resort. This is because the particles (a) tend to aggregate and separate according to size during sample preparation, (b) tend to degrade under the electron beam, and (c), are low in

Table 3.2.2.3.3 Cell constant, Cross sectional area and Cell length for each cell

Cell type	Cell constant/m^{-1}	10^6 x Cross sectional area/m^2	10^2 x Cell length/m
Glass	59940	1.656	9.92
Modified Glass	63380	1.526	9.67
Quartz Mark 1 & 3	16970	5.391	9.15
Quartz Mark 2,4,5,6 & 8	119300	0.823	9.82
Quartz Mark 7 & 9	114400	0.78	9.0

density and therefore difficult to distinguish from the background when they are small. Furthermore, hundreds or thousands of particles must often be measured to obtain statistically significant results. In spite of all these shortcomings electron microscopy is a popular method of particle sizing because the actual particles can be seen. Since particle morphology as well as particle size is an important part of this investigation, methods of overcoming these deficiencies (a-c) have been developed and are discussed in later sections.

The many factors influencing the results obtained by electron microscopy have been discussed by Bradford and Vanderhoff (149)(150). More specifically PVC particles over the range of 0.05 μm - 1.0 μm have been studied by Davidson and others (151)(152) using transmision electron microscopy. They found that particles of less than 0.05 μm diameter could not be observed and that the PVC particle diameter shrank by 20% in the electron beam. These concurrent effects can result in both a decrease and an increase in the mean particle diameter (shrinkage causes the mean to decrease but the loss of small particles results in a larger mean). The contribution of each effect to the overall mean is dependent on the original particle size distribution. By using a vertical shadowing technique, they observed that when exposed to the TEM electron beam, using a 100 kV accelerating voltage, the shadowed latex particles produced shadows which were 20% larger than their corresponding particles. A comparison of

the shadow diameters with results obtained by other techniques (fractional creaming, Joyce Loebl Disc Centrifuge, Micrometric sedigraph, optical arrays and Coulter counter) showed good agreement over the size range 0.5 - 1.0 μm. However for particles of less than 0.1 μm they found electron microscopy the most reliable technique (153).

In the present work scanning electron microscopy (SEM) was employed since it has several advantages over transmission electron microscopy when used to analyse the morphology of PVC particles. The technique utilised much lower electron beam currents and accelerating voltages, so that specimen heating and degradation are not normally a problem. Consequently, using the SEM technique no particle shrinkage was observed.

3.2.3.1 Particle sampling method

In the previous work at Edinburgh it proved difficult to obtain a representative sample of the PVC latex for electron microscopy. Speirs found that during sampling the high shear forces in transferring dispersed latex particles through valves and narrow bore tubing resulted in orthokinetic flocculation of these particles.

This problem has been resolved by simply including a glass microslide (2x20 mm) within the polymerisation limb, onto which a thin layer of PVC particles was deposited during the evaporation of the unreacted monomer.

This sampling method was satisfactory for polymer conversions up to 3%, above this too thick a layer was deposited for electron microscopy.

The percentage yield of polymer was then determined gravimetrically. The PVC was solvent extracted from the polymerisation limb with two 10 cm^3 aliquots of hot tetrahydrofuran into a weighing bottle where the solvent was evaporated. The PVC was dried to constant weight in an oven at 353 K and the percentage yield (wt/vol) calculated. The quantitative efficiency of this extraction was confirmed by control experiments.

Before use the microslides were cleaned using a surfactant cleaning solution (RBS 25) in an ultrasonic bath. (Dawe Soniclean 500W Generator.) This was followed by copious rinsing using double distilled water with further ultrasonic treatment. The microslides were then oven dried and stored in a desiccator until required. The inclusion of the microslide caused no variation in the rate of polymerisation.

The possibility of preferential adsorption of certain types of particle onto the glass microslide surface was investigated by sampling latex particles onto a microslide which had been vertically half gold coated. The image analysis of micrographs from the two areas showed no significant difference, suggesting that there was no preferential adsorption of particular types of latex particles.

3.2.3.2 Scanning electron microscopy

Prior to SEM examination the PVC sample had to be mounted and the specimen gold coated. The microslide carrying the deposited sample was cut into three sections and using double sided adhesive tape mounted on a 10 mm diameter electron microscope stub. The specimen was then gold coated in a Cool Sputter Coater (Polaron Equipment Ltd. Type E5100 Series 11) to give a coating thickness of approximately 20 - 25 nm.

The main reason for gold coating is to increase both the thermal and electrical conductivity of the specimen, PVC is particularly non-conducting (a major industrial use is wire insulation) and an uncoated sample would charge up under the incident electron beam causing a loss of resolution due to increased astigmatism and picture brightness. The gold coating also prevents undue heating which in extreme conditions could cause thermal degradation of the specimen. Furthermore, the coating provides greater mechanical stability, increased secondary electron emission and increased contrast by reducing beam penetration into the sample.

Micrographs were initially taken on a Cambridge Stereoscan 604 but later micrographs were obtained on a Cambridge S250 due to the development of an elusive scanning fault. The resolution of these machines was better than 10 nm at 25 kV and this was sufficient to cover the entire range of particle sizes of interest to

this study. To avoid operator bias micrographs were taken from six predetermined regions of the microslide to give a comprehensive record of the particle types present. Micrographs were recorded on a fine grain film (Kodak Panatomic X) using a 35 mm camera and processed in a fine grain developer (Kodak Microdol X) to give negatives of maximum definition.

3.2.3.3 Image analysis

Image analysis involved an initial preview of the micrographs to record the type and morphology of the particles present. This was followed by a more detailed analysis of particle size in which some or all of the following parameters would be measured.

(i) The unflocculated primary particle diameter.
(ii) The primary floc diameter.
(iii) The primary and primary floc diameter to give an overall particle size distribution.
(iv) The diameter of primary particles within the floc structure.

For the majority of polymer batches analysis of type (iii) was adequate, however, if overlap of the primary and primary floc distributions occurred, individual analyses of types (i) and (ii) became necessary.

Particle diameters were measured on a Vickers

Magiscan Image Analyser to give number and volume average particle diameters (D_n and D_v) and their standard deviations (σ_n and σ_v). Statistically valid distributions were accumulated for each polymer batch by measuring particle diameters until the Magiscan upper limit of 1000 particles had been reached. Histograms of the particle size distribution of the sample: (a) the most frequently occurring value (called the mode), (b) the spread or dispersion of the data about this value, and (c) the skewness, or lack of symmetry about the most frequently ocurring value.

Size distribution functions and average sizes have been discussed in detail by Herdan and Smith (154). In this study, the number, surface area and volume averages have been calculated since in the comparison of a series of samples by means of an improperly chosen average size, there may be no correlation of the physical properties with the average size found. For instance the presence of a secondary nucleation of particles could be missed by using a volume averaging technique, such as light scattering, since the large number of small particles would make little contribution to the total volume of the sample and thus have virtually no influence on the total volume average value.

When the particle size distributions of both the primary and primary flocs is measured (type iii) the Magiscan output reports only the overall mean and standard deviations. To obtain this data for each type of particle

the individual distributions were fed into a computer programme ("Diameter". Listed in Appendix 2) which makes use of the following statistical relationships.

Number average $$D_n = \frac{\Sigma n_i D_i}{\Sigma n_i} \quad (3.2.3.3.1)$$

Surface area average $$D_{sa} = \frac{\Sigma n_i D_i^3}{\Sigma n_i D_i^2} \quad (3.2.3.3.2)$$

Volume (weight) average $$D_v = \frac{\Sigma n_i D_i^4}{\Sigma n_i D_i^3} \quad (3.2.4.4.3)$$

Number standard deviation $$\sigma_n = \frac{\Sigma n_i D_i^2}{\Sigma n_i} - D_n^2 \quad (3.2.3.3.4)$$

Volume standard deviation $$\sigma_v = \frac{\Sigma v_i D_i^2}{\Sigma v_i} - D_v^2 \quad (3.2.3.3.5)$$

where n_i is the number of particles of class diameter D_i

The degree of skewness = (mean - mode) (3.2.3.3.6)

The programme output values of the three averages and the standard deviations along with the modal value and skewness of the distribution.

One final parameter considered in the image analysis was the polydispersity of the primary particles and this was calculated from the ratio of D_n to D_v, which for a monodisperse system is unity.

Chapter Four

Results and discussion

4. Introduction

In this Chapter results of experimental and theoretical investigations are presented and discussed.

In section 4.1 the reproducibility of polymerisation and confirmation of reliable electrophoresis are considered.

The following section, 4.2, describes the characterisation of PVC particles dispersed in vinyl chloride monomer. The effects of particle charge, concentration and electrophoretic mobility on particle morphology are presented. From these a particle charge regime, operating during the initial stages of polymerisation, is proposed.

Section 4.3 discusses the theoretical particle stability using the DLVO type calculations dealt with in Chapter 2. The experimental data and proposed charge regime are used in theoretical calculations designed to elucidate whether the observed stability behaviour of the primary particles could be explained in terms of electrostatic stabilisation. By variation of particle charge changes in PVC morphology can be predicted.

A later section describes the effect of low molecular mass compounds on primary particle charge. Methods of controlling the colloidal stability of the growing particles are also discussed.

Finally, on the control of polymer morphology, the important relationship between reaction kinetics and

colloidal stability of PVC particles is discussed. A mechanism is then proposed for the development and control of PVC morphology.

4.1 Preliminary investigations using the combined cell.

4.1.1. Polymerisation.

As a preliminary to the investigation of particle charge as a function of particle radius and polymerisation temperature, a polymerisation rate was sought which provided an "observation window" in which the growth and flocculation of primary particles could be monitored simultaneously. Too large a polymerisation rate would result in very rapid particle growth and only a short time scale in which to observe trends in the colloidal events. Alternatively too small a polymerisation rate, although providing a long "observation window", would make it impossible on safety grounds to complete the production, investigation and disposal of a PVC batch during normal working hours.

The early experiments were initiated with Liladox (dicetyl peroxydicarbonate) using a concentration of 0.05% (wt/vol). The rates of polymerisation obtained at 343 K were varied and irreproducible. During one of these polymerisations the side limb of the Quartz cell (mark 1) exploded and following a review of the polymerisation method the process was modified in two ways. Firstly the maximum polymerisation temperature was reduced to 333 K so

lowering the saturation vapour pressure of VCM from 1.2 MPa to 1.0 MPa and secondly the Liladox initiator was replaced with lauroyl peroxide since in small scale polymerisations the latter has been reported to give more reproducible polymerisation kinetics (155).

Using the criteria given earlier for the longest "observation window", the optimum lauroyl peroxide initiator concentration of 0.1% (wt/vol) was calculated so that the majority of polymerisations would require a reaction time of between five and sixty minutes over the intended investigation temperature range of 308 K to 333 K To confirm reproducible polymerisation in the combined cell and to expose any variation in reaction rate during the project, the rate of polymerisation was monitored for each polymerisation. The initial reaction rate was investigated by terminating a series of polymerisations at different extents of polymerisation, up to a maximum of 4% conversion. The polymer yield was determined by the gravimetric method described earlier. The initial stages of VCM polymerisation follow first order reaction kinetics and the polymerisation rate was obtained from the appropriate graphical plot as described in section 4.5.2. For a reaction mixture containing 0.1% lauroyl peroxide at 323.1 K the first order polymerisation rate constant was $(3.74 \pm 0.09) \times 10^{-6}\ s^{-1}$ and this compares favourably with the value of $3.80 \times 10^{-6}\ s^{-1}$ obtained by Rance and Zichy (42).

The experimental work of Speirs was abandoned

because of an unexplained reduction in the observed polymerisation rate by a factor of between two and ten times over the initial value. It was suggested that the reaction became increasingly inhibited by unknown species on the test tube cell wall. Continuous monitoring of reaction rate during this work showed that the observed reaction rate constant remained unchanged throughout the life of Quartz cell (mark 2) and its subsequent versions. This indicated that the rate retarding feature of Speirs' test tube cell had not been incorporated into the combined cell developed for this work.

4.1.2. Electrophoresis

This work confirmed the earlier findings of Speirs that reliable electrophoresis of PVC particle aggregates suspended in VCM cannot be observed in a borosilicate glass electrophoresis cell. When electrophoresis measurements were attempted, two types of phenomena were observed. In the first, immediately after the application of the electric field, no particle motion was observed, then, gradually over a period of 3 to 5 seconds, the particle velocity increased until a uniform velocity was obtained. On removing the potential gradient across the cell the particle velocity slowly decreased taking a similar time to decay. The second phenomenon which occurred at higher potential gradients involved irregular particle movements. Immediately the field was applied the

particles moved rapidly over two to three graticule squares and then reversed direction and moved off in a slow regular manner. On reversing the field a similar movement in the reversed direction was observed. The magnitude of these initial jumps was proportional to the applied potential gradient for values in excess of a critical value.

These two phenomena have been observed and discussed by van der Minne and Hermanie (67). The delayed particle velocity is due to the time necessary to charge the small capacitor formed by the electrophoresis cell. In order to build up the electric field a small amount of current has to pass through the electrolyte, which in this case is VCM monomer. The time taken to establish the electric field is related to the magnitude of R x C, where R/Ω is the resistance of the electrolyte and C/F is the capacitance of the cell. The magnitude of R and C are large and small respectively and calculations show that a charging time of a few seconds is to be expected. This accounts for the observed increase in particle velocity during the period in which a uniform field is established. The second effect of irregular jerky particle movement was observed by Pohl (156) who called it dielectrophoresis. It arises from the formation of inhomogeneous fields. A more rigorous treatment of the relationship between electrophoresis and dielectrophoresis has been given by Parreira (157).

Under ideal conditions the application of the

potential gradient creates a homogeneous field at a rate determined by the conductivity of the dispersion medium. However, in low permittivity media, where significant conduction along the capillary walls may be possible, a strongly divergent field can be formed initially due to the termination of lines of force on the cell walls. The irregular motion observed during dielectrophoresis is caused by the migration of particles of higher permittivity than the dispersion medium to the position of highest field strength in the non-uniform field. Acceptable electrophoresis will only commence when sufficient current has passed through the dispersion medium to allow a homogeneous field, in which the lines of force are parallel to the capillary, to be formed between the electrodes.

Two mechanisms have been proposed for surface conductance along the cell walls. This may arise from the relatively high conductivity of borosilicate glass (67,158) in which network modifying sodium ions act as ionic conductors. Furthermore, traces of water in the monomer tend to accumulate at the glass surface where they are held by hydrogen bonding to the silanol groups present in the reasonably hydrophilic glass surface. A second method of surface conduction is then possible by proton transfer through the surface layer of water molecules.

To achieve reliable electrophoresis, conductance through the cell wall must be eliminated. Van der Minne and Hermaine proposed a definitive cell design for use in

low dielectric media in which the use of quartz rather than glass was recommended. Quartz has a simpler composition (158), since it contains fewer interstitial metal ions and surface silanol groups. The former reduces the conductivity of quartz by roughly a factor of 100 over glass whilst the lower silanol group content reduces the adsorption of trace water at the cell/VCM interface. Further suggestions for the cell design included the use of a wide bore capillary (2 mm) to reduce the possibility of divergent fields terminating on the walls and increasing the cell wall resistance by diminishing the wall thickness. Finally, the use of low potential gradients aid regular electrophoresis since inhomogeneous fields arise at high field strengths. The mark 1 combined quartz cell contained a 2 mm diameter capillary and a relatively low field strength of 18 V cm^{-1} was applied during electrophoresis. The use of thin capillary walls was not possible because of the elevated pressures required to liquify the monomer.

During the limited electrophoresis measurements made in the mark 1 cell, prior to its explosion, the problem of dielectrophoresis was not encountered. The replacement cell (mark 2) built by ICI Plc contained a 1 mm diameter capillary and initial attempts to obtain electrophoresis resulted in both delayed particle motion and dielectrophoresis. After considerable experimentation reliable electrophoresis was obtained for the majority of polymer batches by treating both the internal and external

surfaces of the cell with a solution of dichlorodimethylsilane before each polymerisation. This rendered the quartz cell wall hydrophobic by replacing silanol groups -SiOH with - Si - O - $Si(Me)_2$- O -. Surface conductance along the wall was minimised by keeping traces of water dispersed throughout the monomer.

To overcome the difficulties encountered with the 1 mm diameter capillary, quartz cell mark 3 was constructed with the 2 mm capillary. As predicted, no dielectrophoresis problem was encountered but vertical convection currents were present within the cell. At the front of the cell particles rose vertically, at the centre there was little movement and at the rear of the cell particles fell vertically. The convection current was caused by local heating from the illuminating light source and although the positioning of a second heat filter between the cell and light source reduced the convection current, electrophoresis measurements were rendered meaningless as the observed particle motion was always the resultant vector of the component due to the migration under the applied field and the component due to the vertical convection current. Vertical convection currents had been a problem in the original cell but these were overcome by the addition of a single heat filter and by using the minimum light intensity necessary to observe the particles undergoing electrophoresis. For reasons which will be discussed in a later section, it became imperative to use the maximum illuminating power to resolve the

scattered light from the particles and this gave rise to the increased convection currents within the cell. The problem of convection currents in the 2 mm diameter capillary could not be resolved by the addition of further heat filters as this reduced the light intensity making it impossible to observe the small particles, so reluctantly, all further versions of the cells were constructed with 1 mm diameter capillaries despite their associated problems of dielectrophoresis.

Electrophoresis results occasionally showed that the electrophoretic velocity of the particles decreased after approximately 20 to 25 minutes. Speirs also reported this loss of mobility and attributed it to particle adsorption on the cell walls. If the cell was dried with acetone (Analar) the cell walls were rendered positive and rapid adsorption of the negatively charged particles occurred. However, oven drying of the cell, after copious rinses with water, produced negatively charged walls and greatly reduced particle adsorption.

The extensive particle adsorption on the walls reduced the charge carrier content of the dispersion medium and greatly increased charge transport along the capillary walls by both the adsorbed particles and counterions. Under these conditions the potential drop was mainly between the electrodes and the capillary wall rather than between the two electrodes via the electrolyte. The observed decrease in particle velocity about 20 minutes after initial reliable electrophoresis

arose because the particle adsorption on the walls became sufficient to provide a conductive path along the walls reducing the actual potential drop across the dispersion medium. The original mobility could be restored by redispersing the particles by agitation of the cell contents, thus confirming the mechanism suggested.

To assess any systematic variation in particle mobility as a function of elapsed time from starting electrophoresis, particle timings were first obtained at the front stationary level and then again at frequent intervals during the electrophoresis run. Timings were also obtained at various depths within the cell, so that, a van Gils plot of electrophoretic velocity against $(r/a)^2$ could be constructed. A straight line was obtained but frequently its slope increased slightly during electrophoresis corresponding to the walls becoming more positive by the mechanism proposed earlier. No variation in electrophoretic velocity at the stationary level was found suggesting that the two wall potentials were gradually increasing with time, and at the same rate. Thus the regular distribution of electrophoretic velocities within the cell remained, as predicted by eqn.(3.2.2.5) and the electrophoresis results were therefore not invalidated by the increasing wall potentials.

These preliminary investigations have shown that the measurement of electrophoretic mobilities of dispersions in low permittivity media are frought with difficulties and great care is necessary to ensure that

reliable electrophoretic data are obtained. The following criteria for reliable electrophoresis are considered essential (67):-

(1) Motion should be uniform and rectilinear between the electrodes.

(2) The electrophoretic velocity should be independent of position in the electric field.

(3) The electrophoretic velocity should be directly proportional to the applied field strength, and should reverse exactly on reversal of the field.

Only after implementing the experimental procedures given above could these criteria be fulfilled.

The first and second criteria were met once the problems of vertical convection currents and dielectrophoresis had been eliminated. The electrophoretic velocity was measured over the observable section of the capillary and no systematic variation in electrophoretic velocity was found. Finally the electrophoretic velocity at the stationary level was measured as a function of the applied potential and a typical result shown in Fig 4.1.2.1. The graph shows a straight line going through the origin confirming the third criteria, that the electrophoretic velocity should be proportional to the applied field strength.

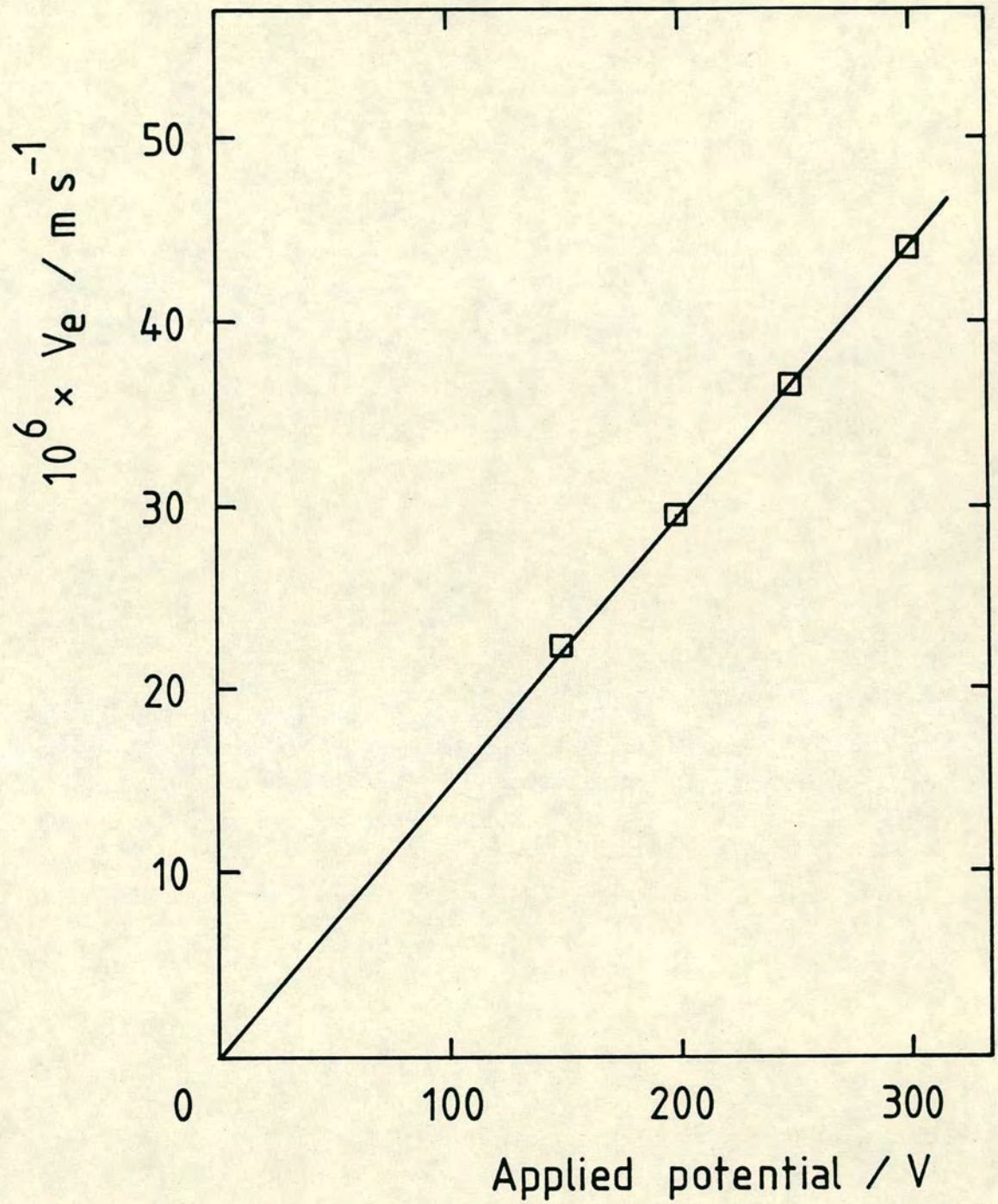

Fig.4.1.2.1. Applied potential against electrophoretic velocity for a PVC dispersion in the combined quartz cell

4.2 Experimental investigation of colloidal events during polymerisation.

4.2.1 Introduction

The following sections describe the characterisation of PVC particles dispersed in vinyl chloride monomer. Having completed the preliminary investigations in the combined cell, the effects of particle size, particle concentration and electrophoretic mobility on polymer morphology were determined and are discussed here.

These parameters could not be measured during polymerisation and resulted in a batch process being adopted, in which polymerisations were quenched at the desired conversion and the experimental data collected. During these investigations 160 batches of polymer were produced spanning the range of 0 to 4% conversion.

The results presented in this section relate to polymerisations carried out at 323.1 K containing 0.1% (wt/vol) lauroyl peroxide initiator.

4.2.2 PVC polymer morphology.

Polymer morphology was assessed by scanning electron microscopy. The technique and methods of analysing the photomicrographs were discussed in section 3.2.3.

During the course of this study, in excess of 1200 micrographs were taken to record the colloidal events occurring during the initial stages of the polymerisation. In this way a thorough understanding of the development of PVC polymer morphology was obtained. The large number of micrographs recorded makes it impossible to present each micrograph. However the statistical data derived from the image analyses is presented in tabular form. To enable the reader to visualise the types of particles formed and the changes in polymer morphology that occur during polymerisation, typical micrographs are presented in Plates (4.2.2.1 to 4.4.2.12). This series covers the formation and fate of the colloidally sized particles and represents monomer conversion over the range of 0.1% to 3% (wt/vol).

The first particles to appear are the basic particles which are believed to result from the polymerisation of a single radical. These particles phase separate at approximately 10^{-3}% conversion and have a diameter of about 10 - 20 nm.

Speirs (58) has obtained micrographic evidence of basic particles. These were observed in a very slow polymerisation, initiated photochemically.

No photomicrographic evidence of the basic particles was obtained in the present study. Under the conditions employed in this investigation, the coagulation of the basic particles to primary particles was estimated to occur within 10 to 20 seconds of initiating the

polymerisation (42). Consequently, the first particles observed were already primary particles, the basic particles being too short lived to be detected.

Plates 4.2.2.1 to 4.2.2.4 indicate the various forms of primary particles during polymerisation. The particles produced were substantially of a spherical nature. As the polymerisation proceeds the particles were observed to aggregate to form doublets, triplets and then multibody aggregates. See Plates 4.2.2.5 to 4.2.2.8.

The fully formed primary particle aggregates are shown in Plates 4.2.2.9 to 4.2.2.11. Structures resembling those proposed by Zichy (9) based on the most stable 13 particle cluster arrangement (54) were observed.

Plate 4.2.2.12 indicates the fate of the primary particle aggregates. As the monomer is consumed the aggregates fuse together to give a continuous polymer network.

As discussed earlier, the ease of polymer processing and removal of residual monomer will depend upon the porosity of the final polymer. From this series of micrographs it can be seen that porosity can arise from the interstitial voids between individual, or aggregates of, primary particles. These will be affected by the size of the particles and conversion at which the aggregation step occurs.

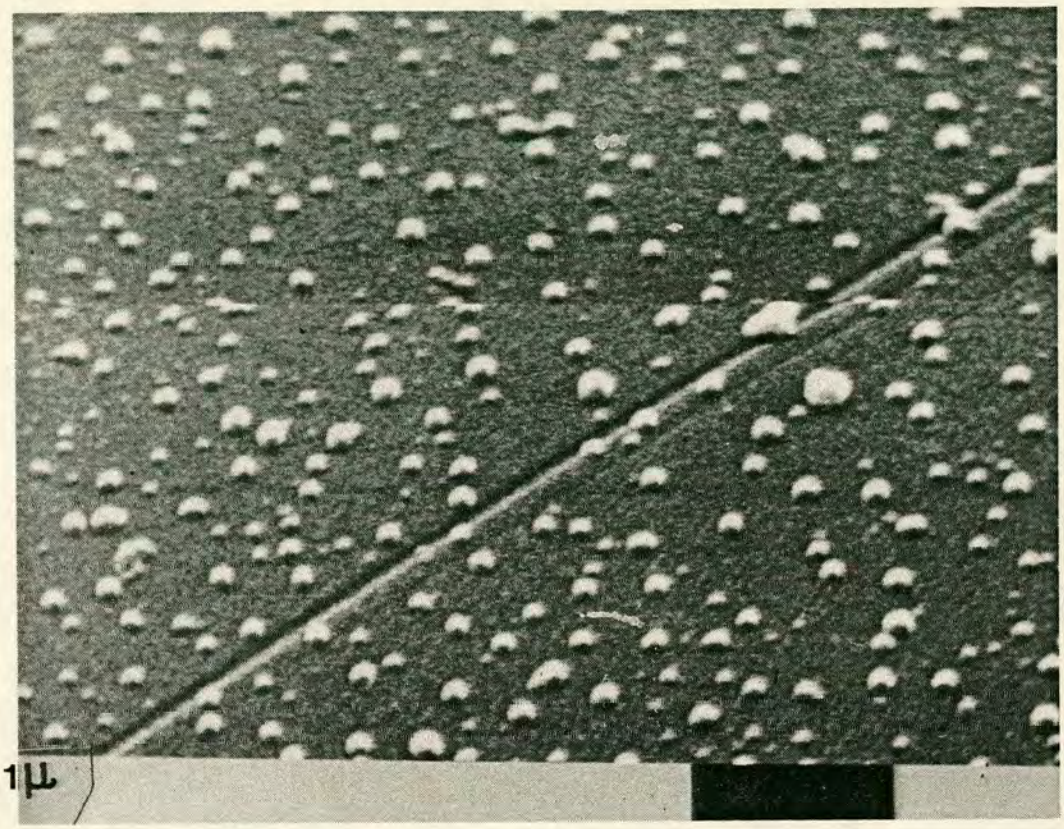

PLATE 4.2.2.1 PVC PRIMARY PARTICLES

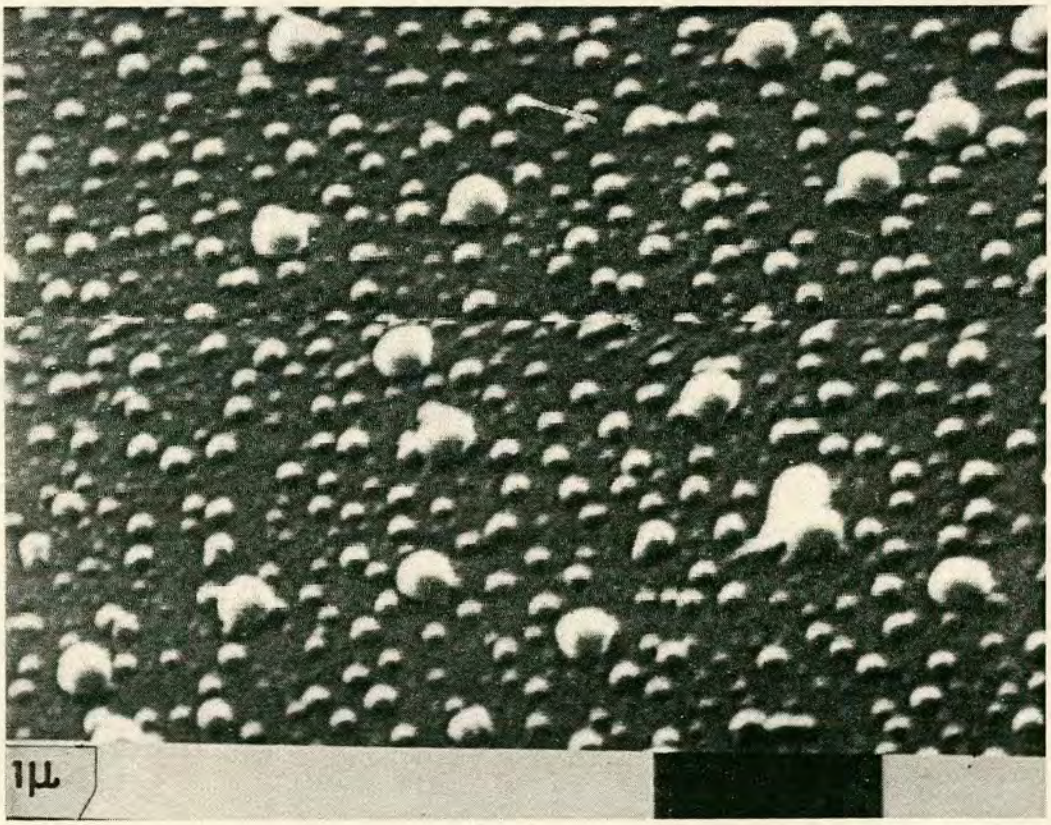

PLATE 4.2.2.2 PVC PRIMARY PARTICLES

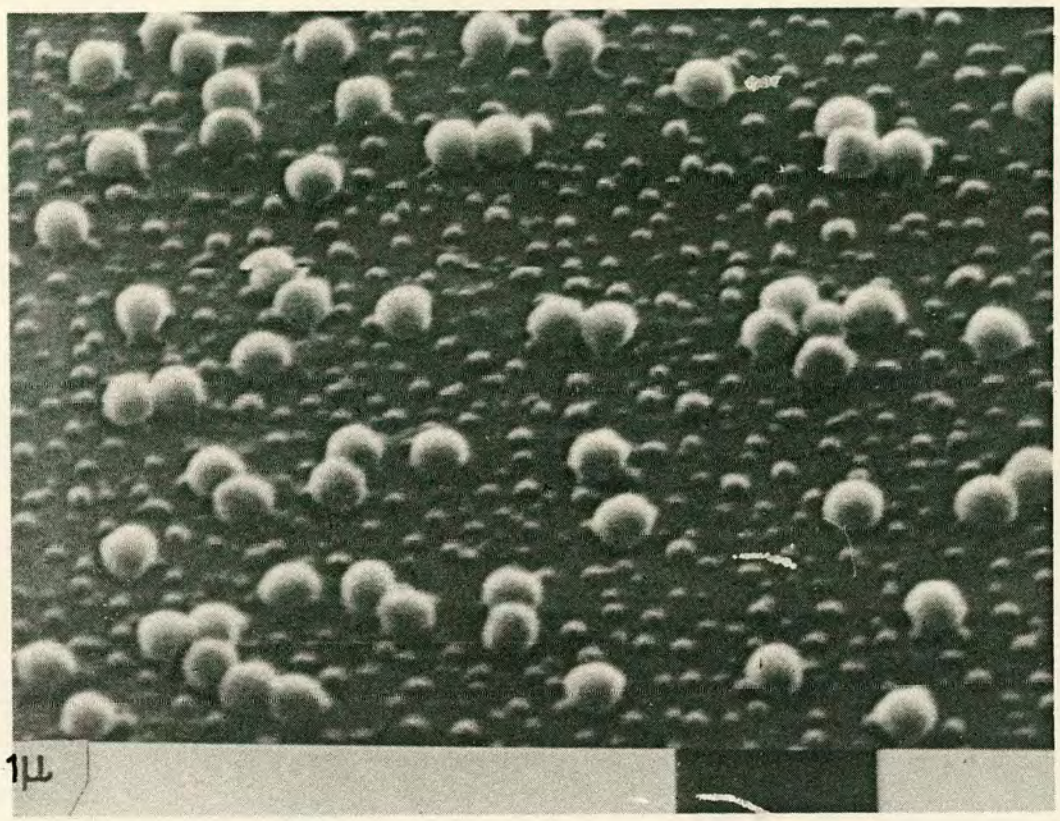

PLATE 4.2.2.3 PVC PRIMARY PARTICLES

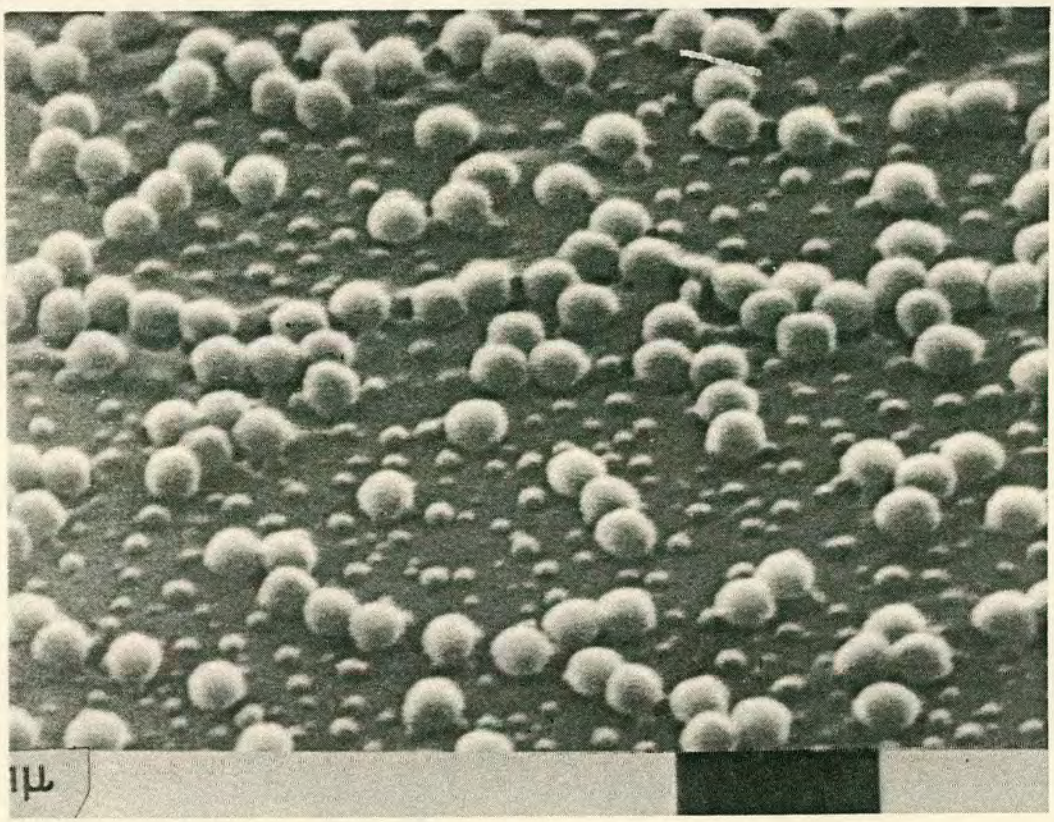

PLATE 4.2.2.4 PVC PRIMARY PARTICLES

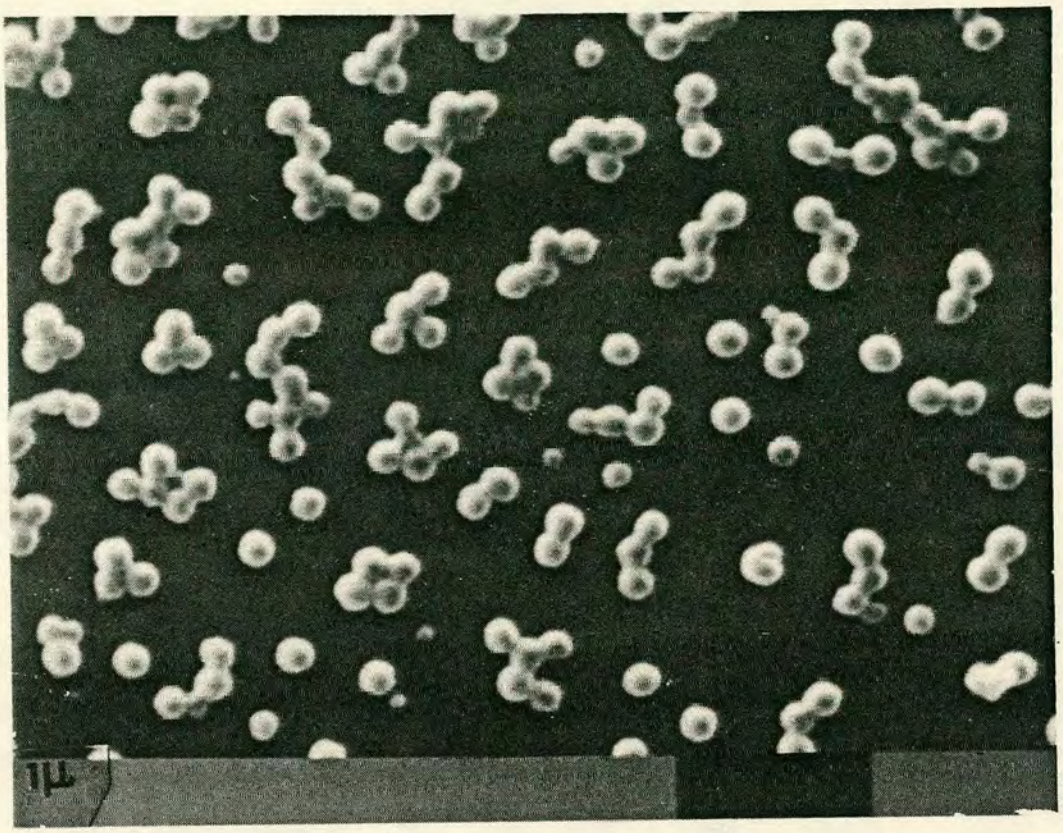

PLATE 4.2.2.5 COAGULATING PRIMARY PARTICLES

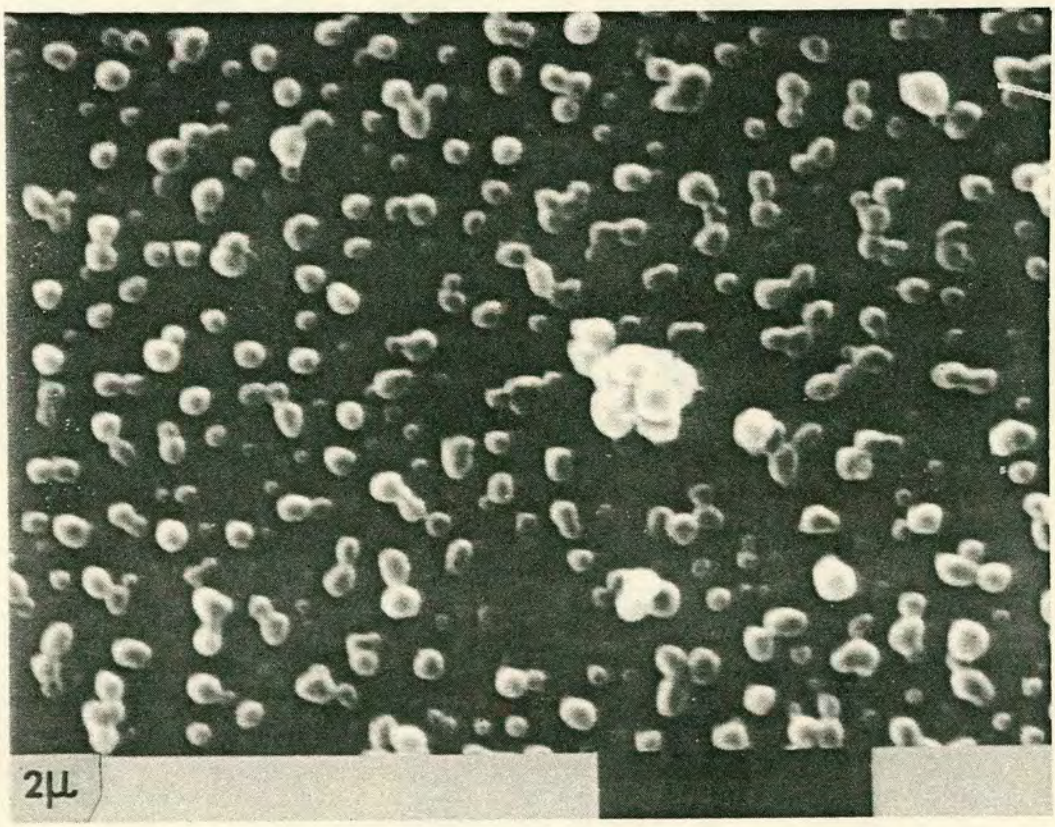

PLATE 4.2.2.6 COAGULATING PRIMARY PARTICLES PLUS ONE PRIMARY PARTICLE AGGREGATE

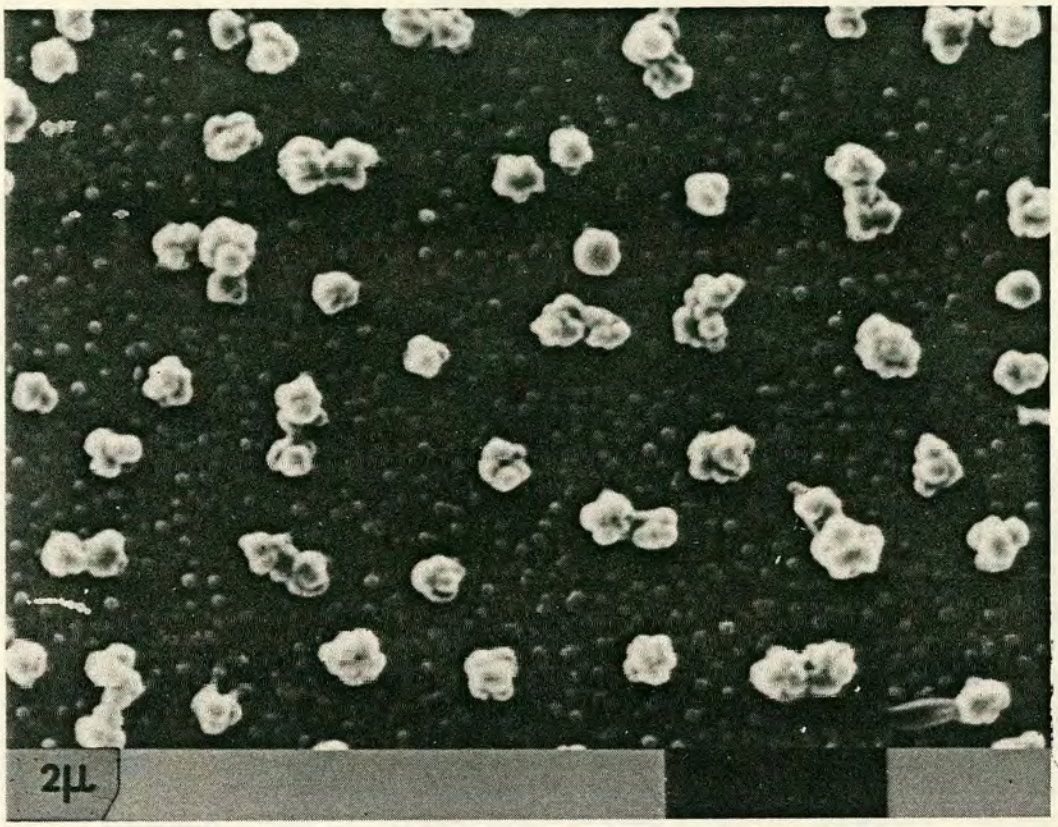

PLATE 4.2.2.7 PRIMARY AND PRIMARY PARTICLE AGGREGATES

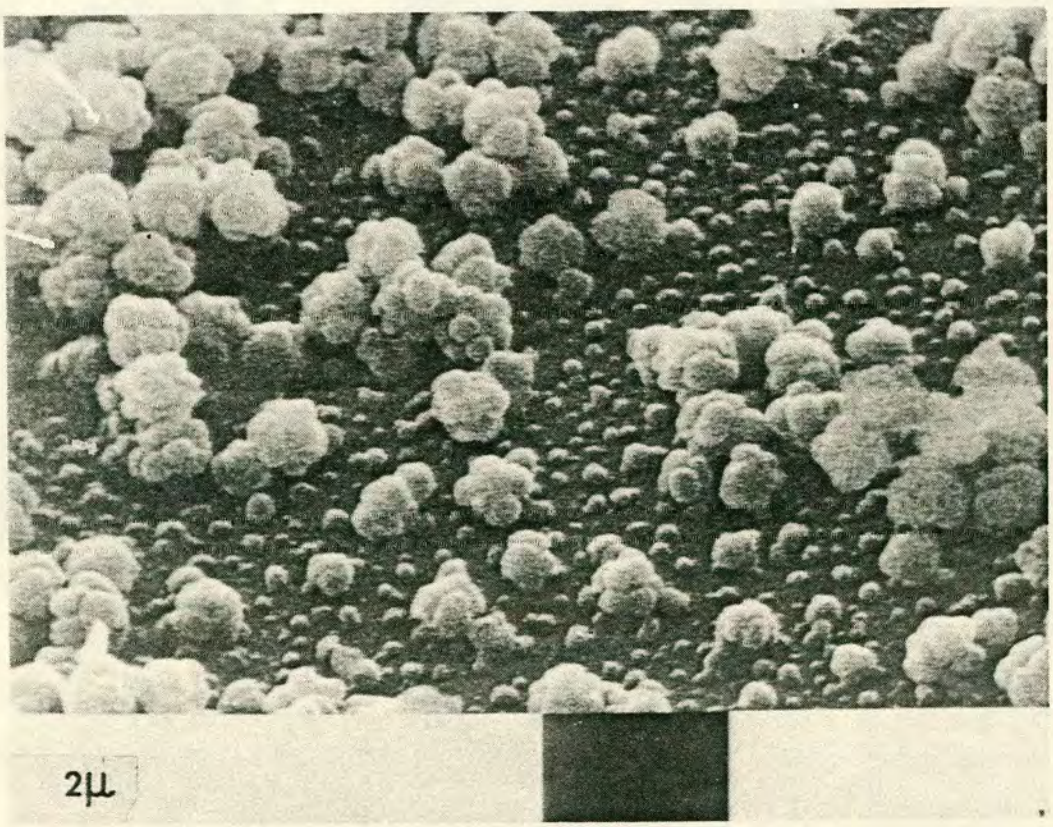

PLATE 4.2.2.8 PRIMARY AND PRIMARY PARTICLE AGGREGATES

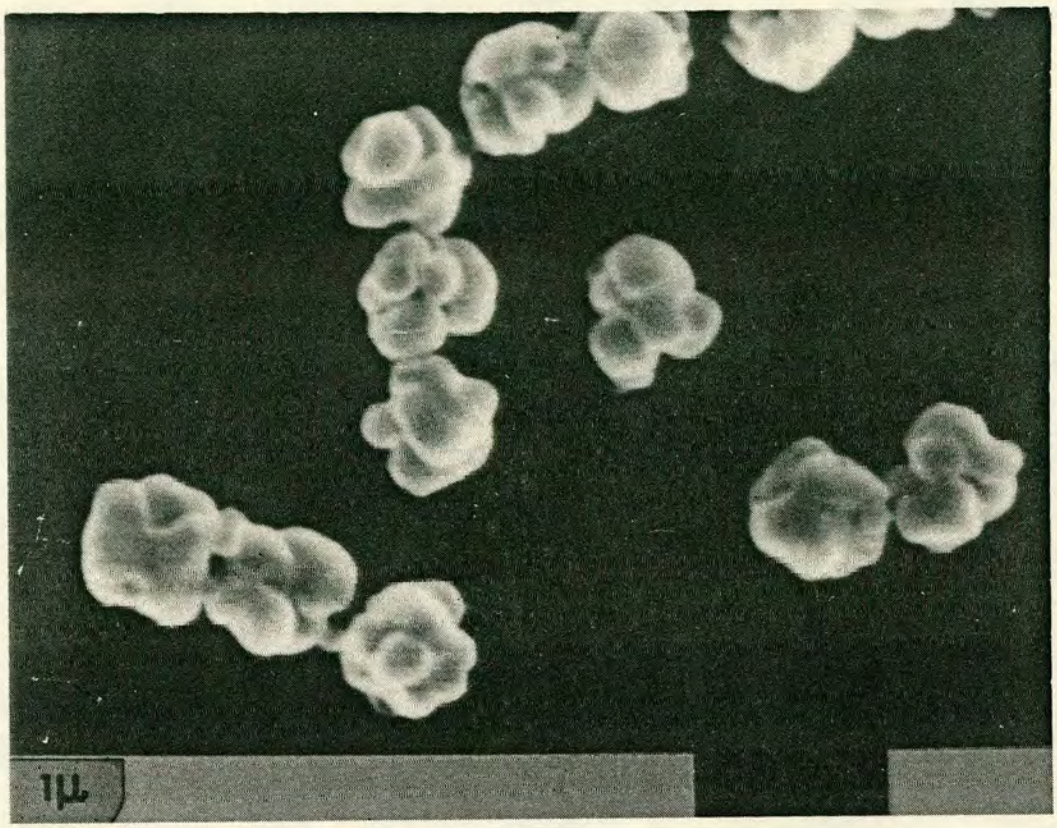

PLATE 4.2.2.9 PRIMARY PARTICLE AGGREGATES

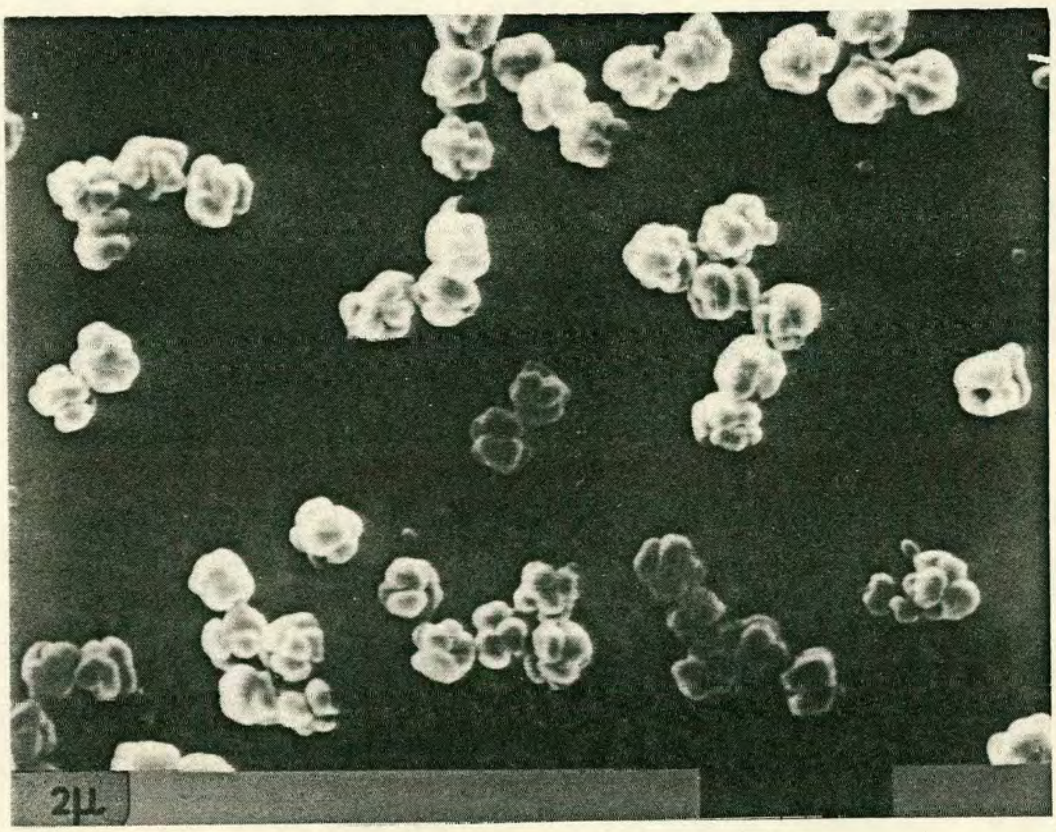

PLATE 4.2.2.10 PRIMARY PARTICLE AGGREGATES

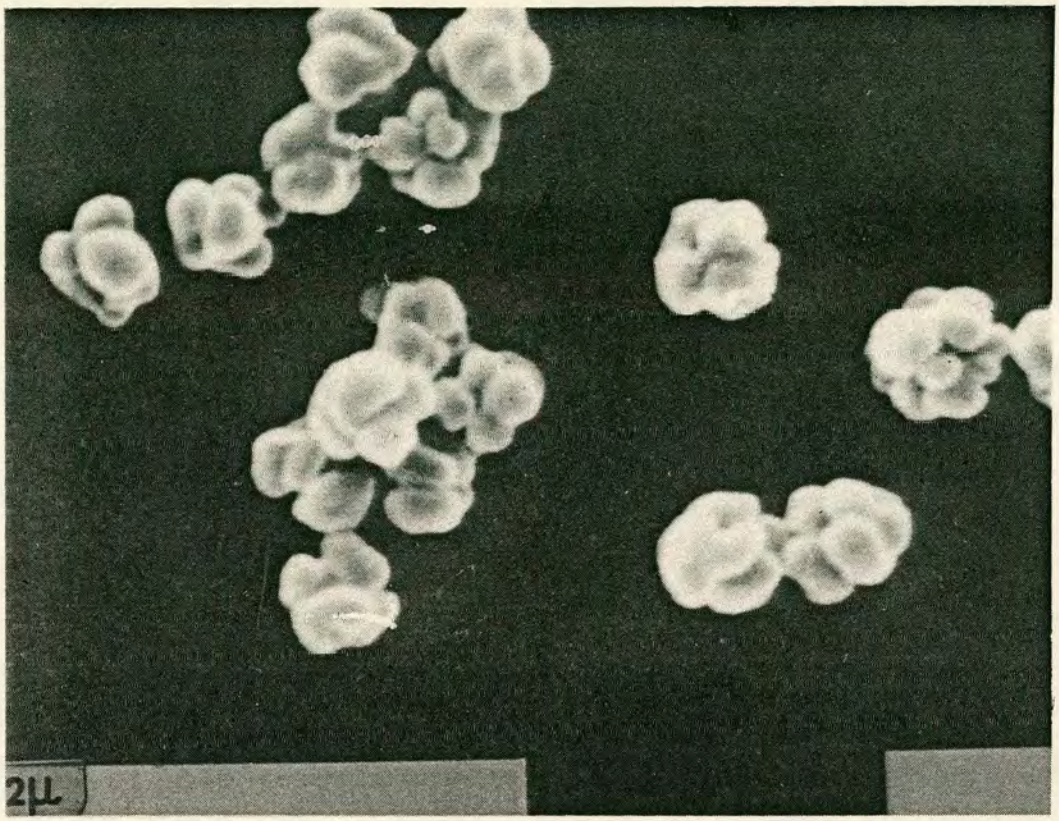

PLATE 4.2.2.11 PRIMARY PARTICLE AGGREGATES

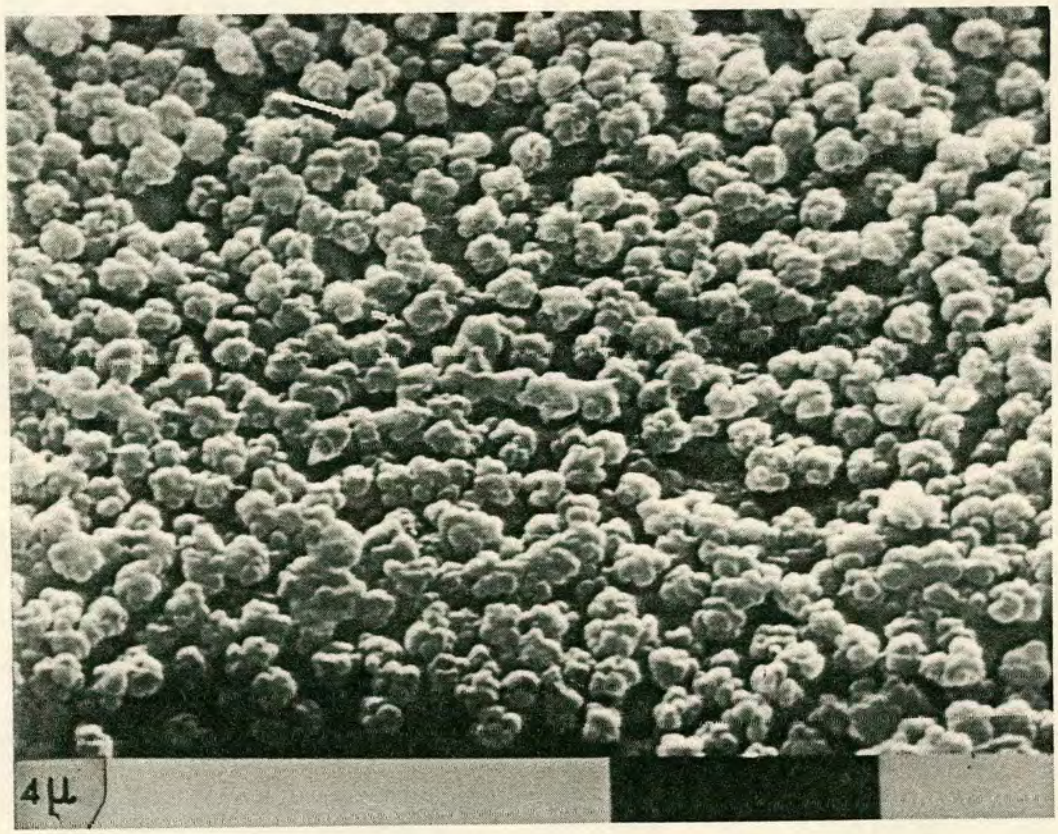

PLATE 4.2.2.12 PVC PRIMARY PARTICLE AGGREGATES LOCKING INTO A CONTINUUM

4.2.3 Particle size distribution.

Section 3.2.3.3 dealt with the image analysis of the SEM micrographs. Particle size analysis involved measuring some or all of the following parameters:-

(i) The unflocculated primary particle diameter

(ii) The primary particle aggregate diameter

(iii) The primary and primary aggregate diameter to give an overall particle size distribution

(iv) The diameter of the primary particles within the primary particle aggregate.

Figures 4.2.3.1 to 4.2.3.4 are examples of type (iii) histograms generated on the Vickers Magiscan Image Analyser.

Particle size distributions calculated on a number and volume basis are shown in Figures 4.2.3.1 & 4.2.3.2 for polymer batch 151. At this monomer conversion (0.16% (wt/vol)) the distribution represents single primary particles which appear to be stable to aggregation. The primary particles range in diameter from 0.02 μm to 0.32 μm and are not highly monodisperse (polydispersity $D_n/D_v = 0.7 - 0.8$).

Batch 28 represents a system in which some of the first formed primary particles have already coagulated to give primary particle aggregates (Figures 4.2.3.3 and 4.2.3.4). In this example the two distributions are

DIAMETER /µm	FREQUENCY	
0.000	0.	
0.020	2.	
0.040	24.	*******
0.060	58.	******************
0.080	96.	******************************
0.100	152.	**
0.120	165.	**
0.140	169.	**
0.160	129.	**
0.180	96.	******************************
0.200	43.	************
0.220	33.	*********
0.240	22.	******
0.260	5.	*
0.280	2.	
0.300	1.	
0.320	1.	
0.340	0.	
0.360	0.	
0.380	0.	
0.400	0.	
0.420	0.	
0.440	0.	
0.460	0.	
0.480	0.	
0.500	0.	
0.520	0.	
0.540	0.	
0.560	0.	
0.580	0.	
0.600	0.	
0.620	0.	
0.640	0.	
0.660	0.	
0.680	0.	
0.700	0.	
0.720	0.	
0.740	0.	
0.760	0.	
0.780	0.	
0.800	0.	
0.820	0.	
0.840	0.	
0.860	0.	
0.880	0.	
0.900	0.	
0.920	0.	
0.940	0.	
0.960	0.	
0.980	0.	

MEAN = 0.143 µm STD. DEVIATION = 0.047 µm

Figure 4.2.3.1. Vickers Magiscan NUMBER AVERAGE Particle Size Distribution for Polymer Batch 151

DIAMETER /µm	FREQUENCY	
0.000	0.	
0.020	0.	
0.040	1.	
0.060	5.	*
0.080	18.	*****
0.100	52.	***************
0.120	93.	**************************
0.140	146.	**
0.160	163.	**
0.180	169.	**
0.200	101.	*****************************
0.220	103.	******************************
0.240	88.	*************************
0.260	25.	*******
0.280	15.	****
0.300	9.	**
0.320	11.	***
0.340	0.	
0.360	0.	
0.380	0.	
0.400	0.	
0.420	0.	
0.440	0.	
0.460	0.	
0.480	0.	
0.500	0.	
0.520	0.	
0.540	0.	
0.560	0.	
0.580	0.	
0.600	0.	
0.620	0.	
0.640	0.	
0.660	0.	
0.680	0.	
0.700	0.	
0.720	0.	
0.740	0.	
0.760	0.	
0.780	0.	
0.800	0.	
0.820	0.	
0.840	0.	
0.860	0.	
0.880	0.	
0.900	0.	
0.920	0.	
0.940	0.	
0.960	0.	
0.980	0.	

MEAN = 0.186 µm STD. DEVIATION = 0.049 µm

Figure 4.2.3.2. Vickers Magiscan VOLUME AVERAGE

Particle Size Distribution for Polymer Batch 151

DIAMETER /µm	FREQUENCY	
0.000	0.	
0.020	0.	
0.040	2.	*
0.060	24.	**********
0.080	44.	**********
0.100	63.	**********
0.120	91.	**********
0.140	97.	**********
0.160	71.	**********
0.180	34.	**********
0.200	18.	*********
0.220	16.	********
0.240	2.	*
0.260	0.	
0.280	4.	**
0.300	2.	*
0.320	2.	*
0.340	14.	*******
0.360	22.	**********
0.380	42.	**********
0.400	53.	**********
0.420	61.	**********
0.440	71.	**********
0.460	57.	**********
0.480	63.	**********
0.500	53.	**********
0.520	42.	**********
0.540	20.	**********
0.560	18.	*********
0.580	6.	***
0.600	4.	**
0.620	0.	
0.640	2.	*
0.660	2.	*
0.680	0.	
0.700	0.	
0.720	0.	
0.740	0.	
0.760	0.	
0.780	0.	
0.800	0.	
0.820	0.	
0.840	0.	
0.860	0.	
0.880	0.	
0.900	0.	
0.920	0.	
0.940	0.	
0.960	0.	
0.980	0.	

MEAN = 0.314 µm STD. DEVIATION = 0.016 µm

Figure 4.2.3.3. Vickers Magiscan NUMBER AVERAGE Particle Size Distribution for Polymer Batch 28.

DIAMETER /µm	FREQUENCY	
0.000	0.	
0.020	0.	
0.040	0.	
0.060	0.	
0.080	1.	
0.100	1.	
0.120	3.	*
0.140	6.	**
0.160	6.	**
0.180	4.	*
0.200	3.	*
0.220	3.	*
0.240	1.	
0.260	0.	
0.280	2.	
0.300	1.	
0.320	1.	
0.340	10.	***
0.360	19.	*******
0.380	43.	**********
0.400	64.	**********
0.420	85.	**********
0.440	113.	**********
0.460	103.	**********
0.480	129.	**********
0.500	123.	**********
0.520	107.	**********
0.540	57.	**********
0.560	57.	**********
0.580	21.	********
0.600	16.	******
0.620	0.	
0.640	9.	***
0.660	10.	***
0.680	0.	
0.700	0.	
0.720	0.	
0.740	0.	
0.760	0.	
0.780	0.	
0.800	0.	
0.820	0.	
0.840	0.	
0.860	0.	
0.880	0.	
0.900	0.	
0.920	0.	
0.940	0.	
0.960	0.	
0.980	0.	

MEAN = 0.478 µm STD. DEVIATION = 0.081 µm

Figure 4.2.3.4. Vickers Magiscan VOLUME AVERAGE Particle Size Distribution for Polymer Batch 28.

clearly defined, the primary particles exist up to 0.24 μm This simple bimodal distribution was not always observed. Figures 4.2.3.5 and 4.2.3.6 show distributions which contain both free primary particles and aggregated primaries, but due to the presence of these small particle aggregates, the primary particle cut off point is not clearly defined. To resolve the free primary particle and primary particle aggregate distributions, separate image analyses of types (i) and (ii) were required, using the computer programme discussed in Appendix (2).

A comparison of the particle size distributions on a number and volume basis shows the importance of choosing the correct method of particle sizing. For example, in the distribution given in Figure 4.2.3.5 nearly 50% of the particles are <0.2 μm, however they only contribute 0.5% to the total volume of the sample (Figure 4.2.3.6). Thus these small particles have virtually no influence on the total volume average value (D_V). Indeed the volume average is so insensitive to small particles that in this case, the presence of 50% of particles <0.2 μm makes no change in the volume average diameter.

D_V all particles = 0.63 μm ± 0.11 μm

D_V all particles >0.2 μm = 0.63 μm ± 0.11 μm

For this reason the use of a volume averaging technique, such as light scattering, could fail to detect the presence of primary particles or a secondary nucleation phase, in a system where large primary particle aggregates have already formed.

DIAMETER /µm	FREQUENCY	
0.000	4.	*
0.020	38.	**********
0.040	117.	**********
0.060	92.	**********
0.080	61.	**********
0.100	29.	**********
0.120	29.	**********
0.140	25.	**********
0.160	19.	********
0.180	19.	********
0.200	13.	*****
0.220	15.	******
0.240	17.	*******
0.260	15.	******
0.280	10.	****
0.300	6.	**
0.320	4.	*
0.340	10.	****
0.360	10.	****
0.380	4.	*
0.400	4.	*
0.420	19.	********
0.440	6.	**
0.460	19.	********
0.480	25.	**********
0.500	19.	********
0.520	40.	**********
0.540	23.	**********
0.560	61.	**********
0.580	46.	**********
0.600	48.	**********
0.620	19.	********
0.640	27.	**********
0.660	15.	******
0.680	23.	**********
0.700	21.	********
0.720	13.	*****
0.740	10.	****
0.760	4.	*
0.780	8.	***
0.800	4.	*
0.820	2.	
0.840	0.	
0.860	2.	
0.880	2.	
0.900	0.	
0.920	0.	
0.940	0.	
0.960	0.	
0.980	0.	

MEAN = 0.341 µm STD. DEVIATION = 0.253 µm

Figure 4.2.3.5. Vickers Magiscan NUMBER AVERAGE Particle Size Distribution for Polymer Batch 66.

DIAMETER /µm	FREQUENCY	
0.000	0.	
0.020	0.	
0.040	0.	
0.060	0.	
0.080	0.	
0.100	0.	
0.120	1.	
0.140	1.	
0.160	1.	
0.180	1.	
0.200	1.	
0.220	2.	
0.240	2.	*
0.260	3.	*
0.280	2.	*
0.300	2.	
0.320	1.	
0.340	4.	*
0.360	5.	**
0.380	2.	*
0.400	3.	*
0.420	14.	******
0.440	5.	**
0.460	18.	********
0.480	27.	************
0.500	23.	**********
0.520	55.	**************************
0.540	36.	*****************
0.560	104.	**
0.580	88.	**
0.600	102.	**
0.620	44.	*********************
0.640	69.	*********************************
0.660	41.	********************
0.680	70.	**********************************
0.700	70.	**********************************
0.720	45.	**********************
0.740	41.	********************
0.760	18.	********
0.780	38.	******************
0.800	21.	**********
0.820	11.	*****
0.840	0.	
0.860	13.	******
0.880	14.	******
0.900	0.	
0.920	0.	
0.940	0.	
0.960	0.	
0.980	0.	

MEAN = 0.629 µm STD. DEVIATION = 0.115 µm

Figure 4.2.3.6. Vickers Magiscan VOLUME AVERAGE Particle Size Distribution for Polymer Batch 66.

Eventually all the primary particles aggregate. Figures 4.2.3.7 and 4.2.3.8 show a typical distribution in particle size for primary particle aggregates. In polymer batch 26 they span from 0.36 μm to 0.96 μm diameter.

By quenching polymerisations at increasing monomer conversions it was observed that the primary particles remained stable to aggregation until they attained a critical diameter above which they coagulated. Tables 4.2.3.1. to 4.2.3.4. record the statistical data obtained from the particle size distributions for polymer batches formed at 323.1 K containing 0.1% (wt/vol) lauroyl peroxide. The parameters recorded were discussed in Section 3.2.3.

The tabulated diameters are the apparent diameters of the PVC particles. During polymerisation each particle is swollen with monomer and is composed of 2 parts polymer to 1 part monomer (159). Evaporation of the monomer during sampling decrease their volume by 1/3. The actual particle diameter may be calculated by multiplying the apparent diameter by 1.145, to allow for the shrinkage occurring on particle sampling.

The primary particle diameter (volume average, D_v) as a function of monomer conversion is shown in Figure 4.2.3.9. Several important features of the VCM polymerisation process are revealed in this figure.

The previous assumption (42) (58) that the primary particles were highly monodisperse, appears to be incorrect. The standard deviation on the mean primary

DIAMETER /µm	FREQUENCY	
0.000	0.	
0.020	0.	
0.040	0.	
0.060	0.	
0.080	0.	
0.100	0.	
0.120	0.	
0.140	0.	
0.160	0.	
0.180	0.	
0.200	0.	
0.220	0.	
0.240	0.	
0.260	0.	
0.280	0.	
0.300	0.	
0.320	3.	*
0.340	3.	*
0.360	3.	*
0.380	6.	***
0.400	3.	*
0.420	9.	*****
0.440	9.	*****
0.460	9.	*****
0.480	23.	**********
0.500	35.	**********
0.520	76.	**********
0.540	47.	**********
0.560	73.	**********
0.580	73.	**********
0.600	81.	**********
0.620	81.	**********
0.640	81.	**********
0.660	52.	**********
0.680	78.	**********
0.700	67.	**********
0.720	52.	**********
0.740	47.	**********
0.760	17.	**********
0.780	15.	********
0.800	20.	**********
0.820	17.	**********
0.840	0.	
0.860	3.	*
0.880	12.	*******
0.900	0.	
0.920	3.	*
0.940	3.	*
0.960	0.	
0.980	0.	

MEAN = 0.635 µm STD. DEVIATION = 0.100 µm

Figure 4.2.3.7. Vickers Magiscan NUMBER AVERAGE Particle Size Distribution for Polymer Batch 26.

DIAMETER /µm	FREQUENCY	
0.000	0.	
0.020	0.	
0.040	0.	
0.060	0.	
0.080	0.	
0.100	0.	
0.120	0.	
0.140	0.	
0.160	0.	
0.180	0.	
0.200	0.	
0.220	0.	
0.240	0.	
0.260	0.	
0.280	0.	
0.300	0.	
0.320	0.	
0.340	0.	
0.360	1.	
0.380	1.	
0.400	1.	
0.420	3.	*
0.440	3.	*
0.460	3.	*
0.480	10.	*****
0.500	17.	********
0.520	41.	**********
0.540	28.	**********
0.560	49.	**********
0.580	54.	**********
0.600	67.	**********
0.620	74.	**********
0.640	81.	**********
0.660	57.	**********
0.680	94.	**********
0.700	87.	**********
0.720	74.	**********
0.740	71.	**********
0.760	29.	**********
0.780	26.	**********
0.800	39.	**********
0.820	36.	**********
0.840	0.	
0.860	7.	***
0.880	30.	**********
0.900	0.	
0.920	8.	****
0.940	9.	****
0.960	0.	
0.980	0.	

MEAN = 0.681 µm STD. DEVIATION = 0.100 µm

Figure 4.2.3.8. Vickers Magiscan VOLUME AVERAGE Particle Size Distribution for Polymer Batch 26.

Table 4.2.3.1. Overall particle size distribution data.

Type (iii) analysis.

Batch No.	% Conversion (wt/vol)	Mean diameter number basis Dn /μm	Standard deviation σn/μm	Mean diameter volume basis Dv /μm	Standard deviation σv/μm	Poly-dispersity Dn/Dv
23	0.54	0.231	0.147	0.436	0.109	0.53
24	0.96	0.264	0.165	0.499	0.125	0.53
27	0.24	0.149	0.055	0.211	0.063	0.71
29	1.60	0.790	0.227	0.987	0.243	0.80
32	2.03	0.448	0.280	0.746	0.133	0.60
33	0.49	0.133	0.119	0.476	0.139	0.28
34	0.41	0.191	0.156	0.445	0.090	0.43
39	0.42	0.235	0.086	0.286	0.036	0.82
40	0.71	0.304	0.184	0.522	0.120	0.58
41	0.42	0.236	0.105	0.331	0.071	0.71
42	0.64	0.189	0.123	0.370	0.090	0.51

Table 4.2.3.1. cont. Overall particle size distribution data.

Type (iii) analysis.

Batch No.	% Conversion (wt/vol)	Mean diameter number basis Dn /μm	Standard deviation σn/μm	Mean diameter volume basis Dv /μm	Standard deviation σv/μm	Poly-dispersity Dn/Dv
43	0.42	0.286	0.114	0.362	0.056	0.79
58	1.00	0.311	0.214	0.583	0.112	0.53
59	0.16	0.181	0.098	0.335	0.134	0.54
60	0.86	0.238	0.126	0.358	0.081	0.66
62	0.52	0.317	0.183	0.553	0.166	0.57
67	0.09	0.119	0.053	0.178	0.057	0.67
69	0.19	0.210	0.091	0.302	0.086	0.70
70	0.40	0.204	0.186	0.473	0.088	0.43
71	0.16	0.221	0.169	0.453	0.117	0.49
151	0.08	0.143	0.047	0.186	0.049	0.77

Table 4.2.3.2. Particle size distribution data (shrunken) for primary particles.

Type (i) analysis.

Batch No.	Mean diameter number basis Dn/ μm	Standard deviation σn/μm	Mode /μm	Skew	Mean diameter surface area Ds /μm	Mean diameter volume basis Dv /μm	Standard deviation σv/μm	Mode /μm	Skew	Poly-dispersity Dn/Dv
24	0.151	0.047	0.15	0.02	0.178	0.190	0.044	0.19	0.00	0.79
28	0.142	0.039	0.14	-0.05	0.162	0.171	0.038	0.15	0.55	0.83
41	0.106	0.034	0.09	0.47	0.127	0.135	0.029	0.13	0.17	0.79
42	0.109	0.038	0.11	-0.03	0.133	0.143	0.033	0.13	0.39	0.76
58	0.132	0.041	0.11	0.54	0.155	0.165	0.038	0.15	0.39	0.80
60	0.098	0.044	0.11	-0.27	0.135	0.151	0.044	0.11	0.93	0.65
62	0.131	0.044	0.12	0.25	0.158	0.167	0.034	0.17	-0.09	0.78

Table 4.2.3.2. Particle size distribution data (shrunken) for primary particles.

Type (i) analysis, continued.

Batch No.	Mean diameter number basis Dn/ μm	Standard deviation σn/μm	Mode /μm	Skew	Mean diameter surface area Ds /μm	Mean diameter volume basis Dv /μm	Standard deviation σv/μm	Mode /μm	Skew	Poly-dispersity Dn/Dv
67	0.118	0.051	0.15	-0.63	0.156	0.168	0.041	0.15	0.44	0.70
70	0.070	0.047	0.05	0.51	0.138	0.168	0.058	0.21	-0.72	0.44
151	0.143	0.047	0.15	-0.15	0.172	0.186	0.048	0.19	-0.08	0.77
152	0.143	0.041	0.13	0.32	0.170	0.180	0.049	0.17	0.20	0.79
153	0.102	0.036	0.08	0.61	0.128	0.141	0.041	0.13	0.27	0.72

Table 4.2.3.3. Particle size distribution data (shrunken) for primary particle aggregates.

Type (ii) analysis.

Batch No.	Mean diameter number basis Dn/ μm	Standard deviation σn/μm	Mode /μm	Skew	Mean diameter surface area Ds /μm	Mean diameter volume basis Dv /μm	Standard deviation σv/μm	Mode /μm	Skew	Poly-dispersity Dn/Dv
23	0.400	0.077	0.41	-0.13	0.429	0.442	0.076	0.41	0.42	0.90
24	0.463	0.088	0.49	-0.31	0.495	0.508	0.079	0.49	0.23	0.91
26	0.635	0.100	0.62	0.15	0.672	0.681	0.100	0.68	0.01	0.93
29	0.582	0.106	0.59	-0.08	0.620	0.638	0.105	0.63	0.08	0.91
32	0.678	0.138	0.68	-0.01	0.730	0.751	0.117	0.79	-0.33	0.90
34	0.357	0.069	0.29	0.97	0.383	0.395	0.068	0.39	0.07	0.90
40	0.448	0.110	0.47	-0.20	0.499	0.521	0.062	0.53	-0.15	0.86
42	0.348	0.069	0.33	0.26	0.373	0.385	0.066	0.39	-0.08	0.90
43	0.328	0.068	0.36	-0.47	0.353	0.362	0.055	0.37	-0.15	0.91

Table 4.2.3.4. Particle size distribution data (shrunken) for primary particles within primary particle aggregates. Type (iv) analysis.

Batch No.	Mean diameter number basis Dn/ μm	Standard deviation σn/μm	Mode /μm	Skew	Mean diameter surface area Ds /μm	Mean diameter volume basis Dv /μm	Standard deviation σv/μm	Mode /μm	Skew	Poly-dispersity Dn/Dv
29	0.328	0.070	0.32	-0.03	0.358	0.372	0.073	0.36	0.03	0.88
32	0.287	0.076	0.26	0.22	0.327	0.344	0.076	0.30	0.45	0.83
33	0.236	0.050	0.20	0.51	0.257	0.266	0.050	0.26	-0.07	0.89
34	0.184	0.042	0.17	0.21	0.203	0.211	0.041	0.21	-0.10	0.87
105	0.182	0.050	0.15	0.44	0.210	0.224	0.056	0.79	-10.4	0.81

particle diameters are large and often primary particles were found to span the entire size range over which they exist. Values for polydispersity are given in Table 4.2.3.2. which range from 0.4 to 0.8. A monodisperse system would return a value of unity.

Figure 4.2.3.9. also indicates a striking feature of the PVC polymerisation, the presence of a critical primary particle diameter. When the hitherto stable primaries exceed a certain critical diameter by polymerisation, they coalesce to form primary particle aggregates. The equation for the best straight line was:

Mean primary particle diameter;

$$D_v = 3.69 \times 10^{-9} \times \%\text{conversion} + 1.65 \times 10^{-7} \text{ m.}$$

The near zero gradient (3.69×10^{-9}) confirms that the mean critical diameter is virtually independent of conversion.

At the onset of coagulation (0.1% conversion (wt/vol)) the mean critical diameter of the primary particles was $(1.65 \pm 0.12) \times 10^{-7}$ m. This diameter represents the shrunken particle size, the corrected diameter for the monomer swollen primary particle is $(1.89 \pm 0.13) \times 10^{-7}$ m.

This value represents the mean maximum size at which the free primary particles can exist. Further growth by polymerisation results in the loss of primary particle stability to coagulation, and the formation of primary

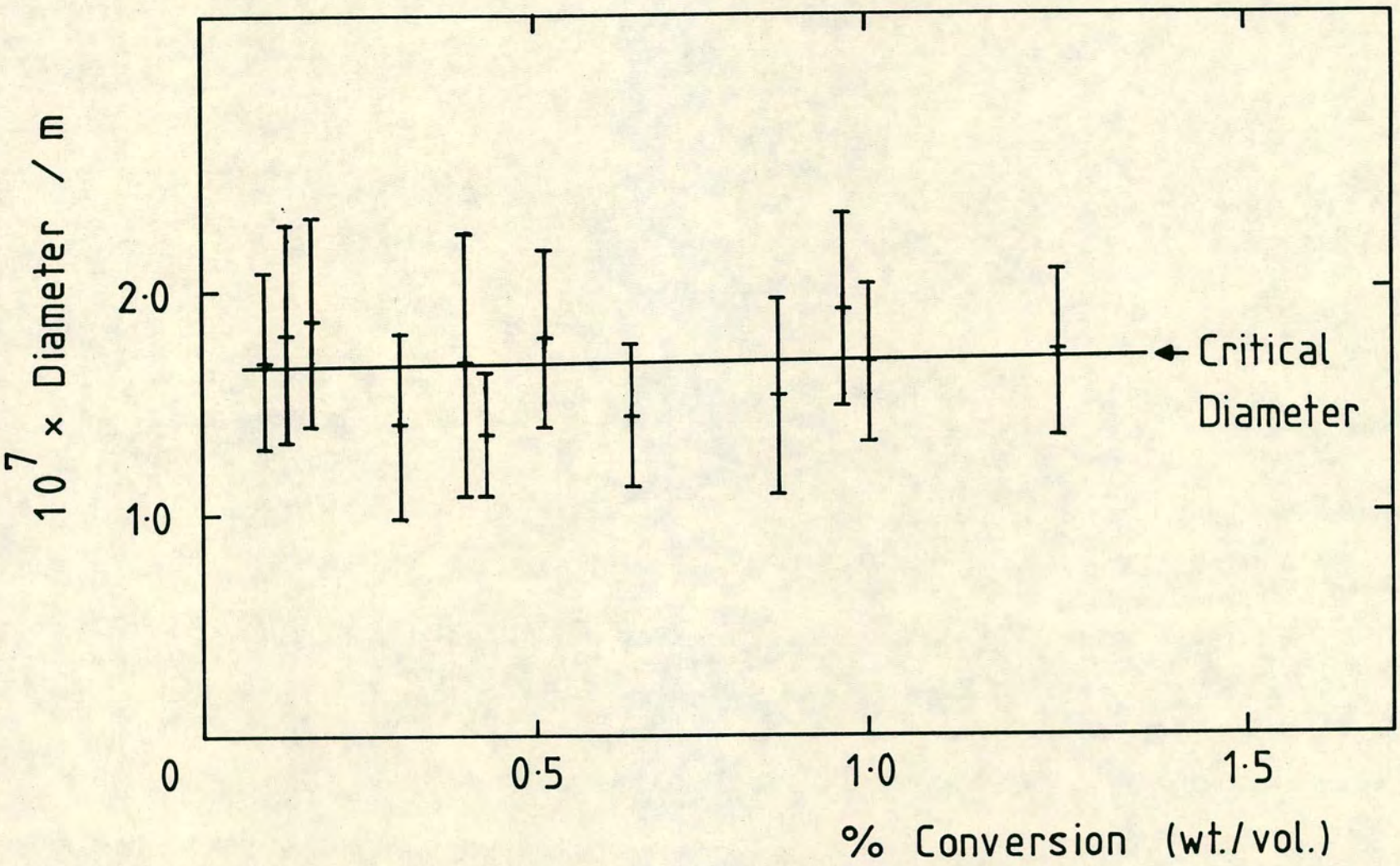

Fig.4.2.3.9 Primary particle diameter (shrunken Dv) as a function of monomer conversion

particle aggregates.

During this investigation the results of a separate study (42), using an alternative technique (photon correlation spectroscopy) indicated a critical primary particle diameter of 1.8×10^{-7} m, which tends to support the value of 1.89×10^{-7} m determined by scanning electron microscopy in this study. See Appendix (3).

Figure 4.2.3.10. shows the growth of the primary particle aggregate with monomer conversion. The aggregates appear at less than 0.4% conversion (wt/vol). Once formed the aggregates grow, by polymerisation, in a direction perpendicular to any polymer/monomer interface (9). The maximum aggregate diameter measured was found to be approximately 8×10^{-7} m at 2% conversion. In the commercial production of PVC the aggregates continue to grow and attain diameters ranging from 1×10^{-6} to 10×10^{-6} m in the final product.

The fate of the primary particles once encorporated within the primary particle aggregate is shown in Figure 4.2.3.11. The primary particles continue to increase in size by the polymerisation of the monomer in the swollen primaries and by the surface deposition of polymer.

Analysis of the primary particle size distribution, within the primary particle aggregates, indicates that the aggregates only contain primary particles that exceed the critical primary particle diameter. This provides further evidence to suggest that

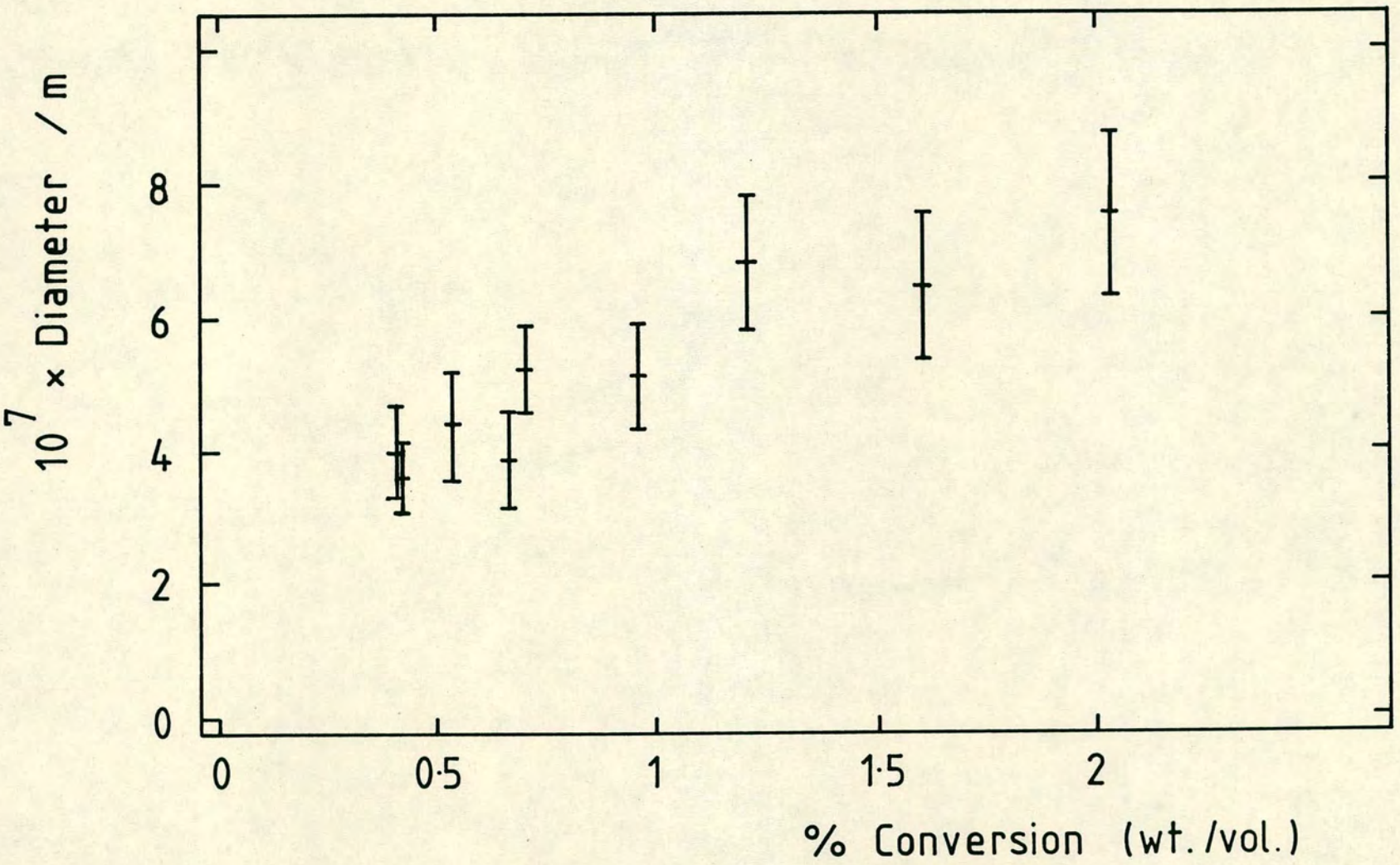

Fig. 4.2.3.10. Aggregate diameter as a function of monomer conversion

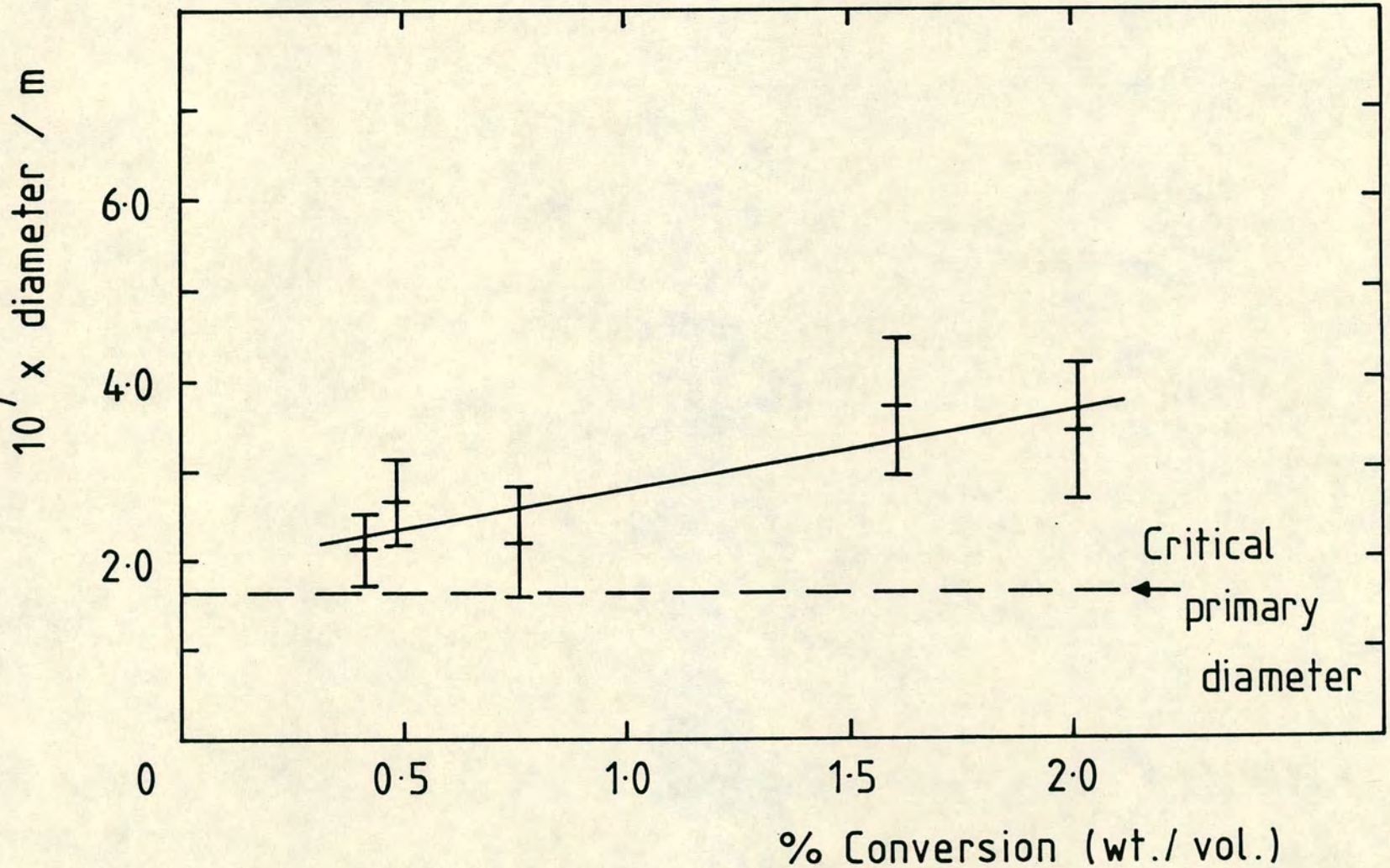

Fig. 4.2.3.11. Primary particle diameter within aggregates (shrunken Dv.) as a function of monomer conversion

the smaller primary particles are stable to coagulation until the critical diameter of 1.9×10^{-7} m has been exceeded.

4.2.4 Particle concentration

The final primary particle number per unit volume (particle concentration) was determined for each polymer batch. By following particle concentration as a function of monomer conversion the onset of primary particle coagulation could be observed. Furthermore by varying the polymerisation conditions or adding polymer modifiers, changes in primary particle concentration could be studied.

Unfortunately particle concentrations could not be assessed during polymerisation using the present experimental technique. Final particle concentration was determined for each polymer batch. The difficulties encountered in reproducing a coagulating polymerising system have been reported by Fitch (148). Indeed, it was impossible to determine the rate of primary particle coagulation from particle concentrations obtained from different polymerisations. This prevented a quantitative assessment of the stability of the dispersion from being obtained.

The particle concentration could not be measured directly by particle counting in the electrophoresis cell. Ultramicroscopy involves observation of the light

scattered by particles. The light intensity is a function of the particle volume and of the refractive index difference between the particles and the medium (160). Since the primary particle has a small volume and the refractive indices of VCM and PVC/VCM gel are similar (ca 1.4), dispersions of swollen primary particles in VCM cannot be seen clearly enough to allow direct particle counting.

An indirect method, described by Fitch (53), was used to estimate the particle concentration. The particle number was obtained by dividing the total mass of the polymer produced by the mass of one particle. Where the system is polydisperse, the average mass of a particle is used for the denominator.

$$\text{Particle Number } N = \frac{\text{Mass of polymer (Mp)}}{\text{Mass of one particle (mp)}} \qquad (4.2.4.1)$$

The average mass of one particle, assuming the particles to be spherical and having a bulk density of $1.4 \times 10^6 g\ m^{-3}$, is given by:

$$mp = \rho \frac{4}{3}\pi r^3 \qquad (4.2.4.2)$$

where r is the mean particle radius.

As the primary particle concentration, rather than the overall particle concentration is required, Fitchs' relationship was modified to give the mass of polymer due to primary particles divided by the mass of one primary

particle.

When all the particles exist as primary particles eqn. (4.2.4.1) holds. However, as coagulation occurs the total mass of polymer produced is a combination of the mass of primary particles and primary particle aggregates. The contribution of the primary particles to the total mass of polymer produced was obtained from the ratio of the primary particles to primary particle aggregates. This ratio was calculated from the particle size distributions obtained on the volume (weight) basis. The primary particle concentration was then given by eqn. (4.2.4.3.)

$$\text{Particle concentration /particles m}^{-3} = \frac{Mp \times R \times C}{1.4 \times 10^{6} \times 4/3\ \pi\ (r)^{3}} \qquad (4.2.4.3)$$

where Mp is mass of polymer produced

R is primary/aggregate ratio

and C is a constant (2×10^{5}); to give the number of particles per m^{-3}.

Using this equation primary particle concentrations were calculated at various monomer conversions using mean primary particle diameters based on a number and volume average basis. The tabulated data are given in Table 4.2.4.1.

It can be seen that the estimated particle concentration on both the number and volume average basis, decrease with increasing monomer conversion. The scatter

Table 4.2.4.1. Primary particle concentrations estimated from equation 4.2.4.3.

Batch No.	Mass of polymer/g	% Conversion (wt/vol)	Primary: Aggregate ratio	10^{-17} x Particle Number/m^3	
				Number basis	Volume basis
151	0.0081	0.16	1.00	7.56	3.43
152	0.0063	0.13	1.00	5.88	2.95
86	0.0133	0.27	1.00	9.20	2.19
81	0.0081	0.16	1.00	4.27	1.43
134	0.0097	0.19	0.089	1.23	0.73
153	0.0145	0.29	0.059	2.20	0.83
34	0.0204	0.41	0.031	2.08	0.82
41	0.0210	0.42	0.025	1.21	0.58
43	0.0210	0.42	0.002	0.36	0.21
62	0.0262	0.52	0.018	0.57	0.28
66	0.0391	0.78	0.009	1.02	0.13
26	0.0601	1.20	0	0	0
29	0.0800	1.60	0	0.02	0.01

in the estimated values results from the difficulties in reproducing the same coagulation and polymerisation kinetics in separate polymerisations. Figure 4.2.4.1 is a plot of the particle concentration calculated from D_v, as a function of monomer conversion. It shows that at the lowest accessible region of the polymerisation, the initial primary particle number is approximately 3×10^{17} m^{-3}. This estimated value was later confirmed in a separate study using PCS where the initial primary particle number was reported to be 2.9×10^{17} m^{-3}.

The good correlation between the two techniques suggests that the indirect estimation of particle numbers was valid for this system and would allow the comparison of particle concentrations as polymerisation conditions were varied, during the attempts to modify polymer morphology.

The graph also indicated that the onset of primary particle coagulation occurs very early in the polymerisation (approximately 0.2% (wt/vol)). This coagulation process occurs over a very narrow monomer conversion. By 0.5% conversion over 90% of the primaries have coagulated to form primary particle aggregates. The process being completed at less than 2% conversion. This critical conversion is much lower than that reported by several other investigators (11,19,20,41) who found the primary particles to exist up to 10% conversion. The low value found in this study is however in agreement with the findings of Boissel and Fischer (40), who report a

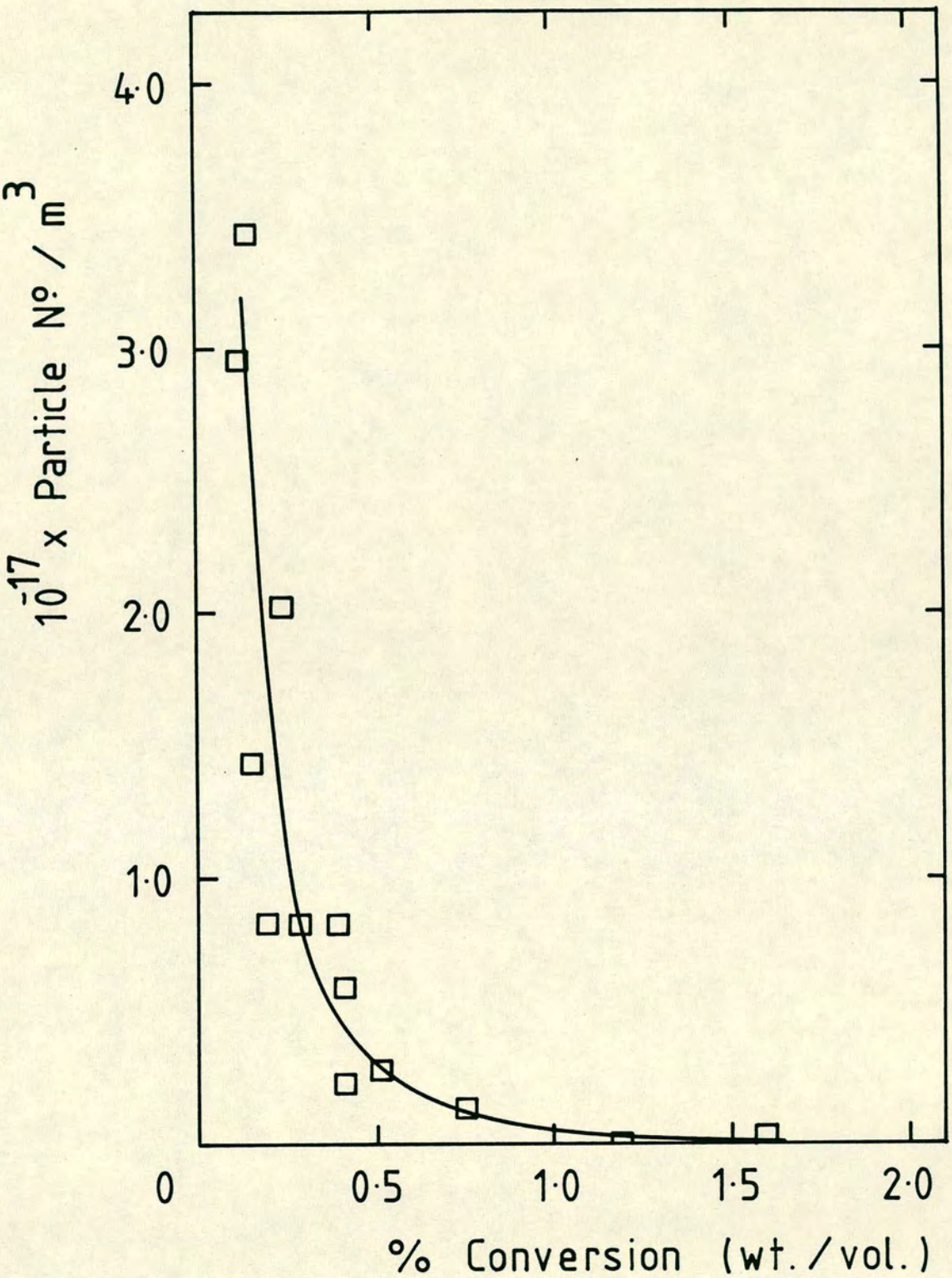

Fig. 4.2.4.1 Primary particle number as a function of monomer conversion for polymerisations at 323 K containing 0·1 % lauroyl peroxide.

critical conversion of 0.12% at low agitation speeds.

Their investigation showed that the critical conversion was strongly dependent on agitation rate. They concluded that the disparity between their low critical conversion and those reported in the literature, arose from the use of non-agitated systems, where critical conversion values are found to be much higher.

4.2.5 Electrophoresis

The development of the combined polymerisation/ electrophoresis cell and the preliminary investigations performed were discussed in a earlier section.

The experimental results presented in the preceeding sections has confirmed the proposals of Zichy (9) and Speirs (58), that once formed, the primary particles remain stable to coagulation and grow by polymerisation. They found that the primary particles carried a net negative charge and proposed that the observed stability of the primary particles might result from electrostatic stabilisation.

Speirs indicated that for a system that contained a finite charge, the primary particles would eventually exceed the diameter where the charge stabilisation would be sufficient to confer colloidal stability. The primary particles would then coagulate to form primary particle aggregates. A charging regime of this type dictates that the particles grow with a constant number of charges per

particle (Q).

where $Q = 4\pi\varepsilon_o \varepsilon_r \zeta a/e$ (4.2.5.1.)

and ε_o is the permittivity of a vacuum.

ε_r is the relative permittivity of VCM at the temperature at which the electrophoresis measurements were obtained.

ζ is the particle zeta potential.

a is particle radius.

e is the proton charge (1.6021×10^{-19}C).

From this relationship (161) it can be seen that as the particle radius, "a", increases, the zeta potential must decrease. The remaining parameters being constants.

In order to investigate the mechanism by which the primary particles acquire their stability to aggregation it was nescessary to see how the charge per primary particle varied as the polymerisation proceeded. This involved terminating identical polymerisations at different degrees of conversion and measuring the zeta potential and particle radius. The data obtained from polymerisations carried out over the range of 0 - 3% (wt/vol) conversion are summarised in Table (4.2.5.1).

Table 4.2.5.1 Results from polymerisations at 323 K.

Batch	Period of Polym/min	% Conversion (wt/vol)	$10^3 \times \zeta$ /V
27	10	0.24	-97
23	20	0.54	-95
33	20	0.49	-79
24	40	0.96	-90
26	60	1.20	-101
29	80	1.60	-137
32	100	2.03	-81
31	160	3.37	-80

These results confirm the findings of Speirs (59) and Davidson and Witenhafer (60) that the particles carry a negative zeta potential. Furthermore, the primary particles appear to remain net negatively charged throughout their lifespan.

Figure 4.2.5.1 presents the experimental zeta potential data as a function of monomer conversion. No correlation between zeta potential and monomer conversion is apparent from this figure. The predicted decrease in zeta potential with conversion does not appear to occur. This lack of correlation was also reported by Speirs, whose results are reproduced in Table 4.2.5.2. The values of percentage monomer conversion presented have been

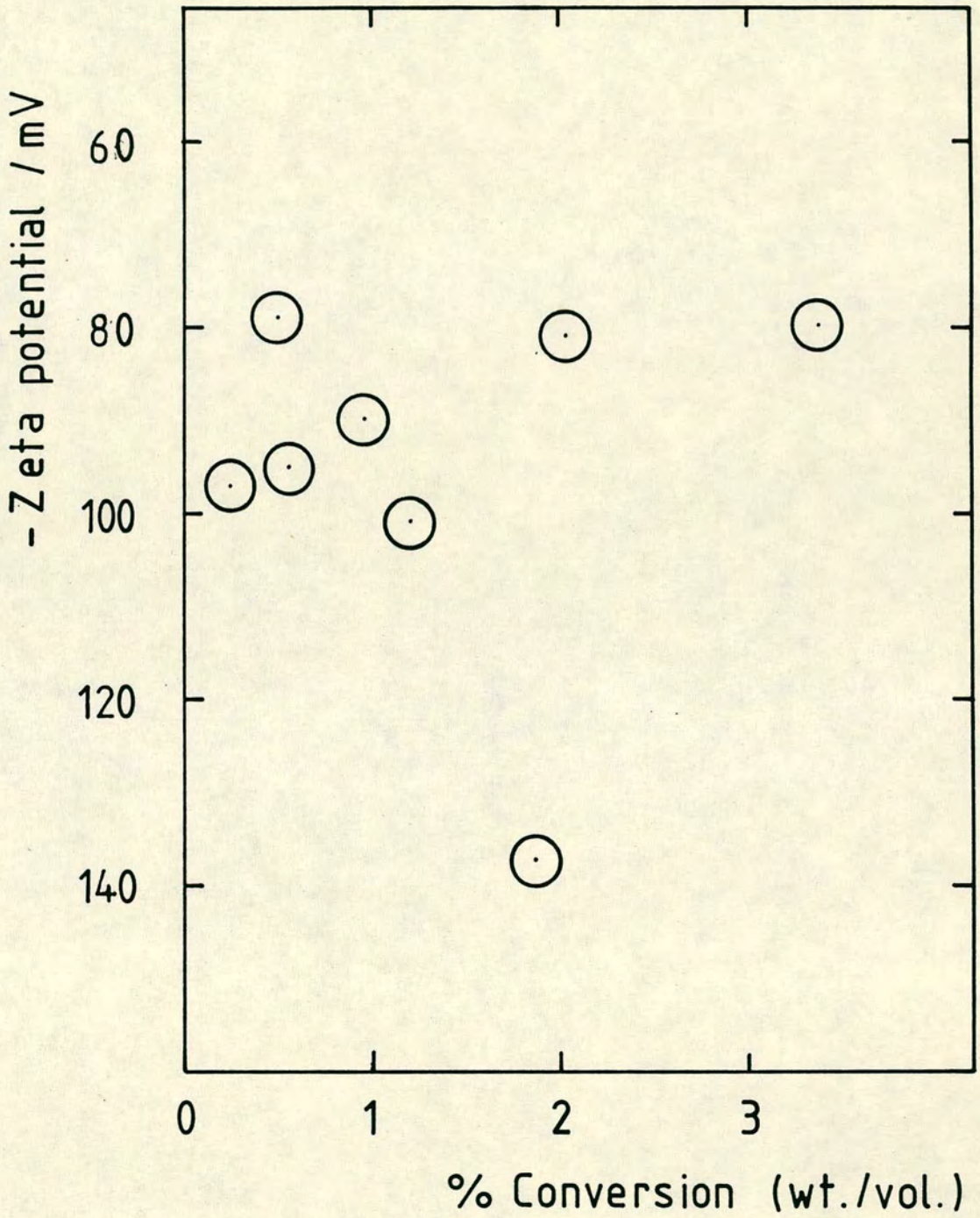

Fig. 4.2.5.1. Zeta potential as a function of monomer conversion. Batches 23-33.

calculated from the polymerisation rate constants given by Speirs.

Table 4.2.5.2 Results obtained by Speirs from polymerisations at 343 K.

Period of Polym/min	Estimated % Conversion	$10^3 \times \zeta$ /V	$10^8 \times a$ /m	Q
4	1.2	-85	15	42
6	2.1	-67	11	24
8	2.9	-97	16	48
10	3.6	-61	17	34

During this initial study the zeta potential obtained during a single electrophoresis run was found to vary with time. Observation of the particles during electrophoresis measurements indicated that the intensity of the scattered light also decreased with time. These features suggested that the nature of the particles, under observation, were changing with time.

Further evidence to confirm this, was obtained from the electron micrographs. In previous studies (42) (58) it had been assumed that the primary particles were monodisperse, and remained colloidally stable to high monomer conversions (10%). The electron micrographs disproved these assumptions. (See Plate 4.2.2.6). The onset of primary particle coagulation occurred at

approximately 0.1 - 0.2% (wt/vol) conversion. Furthermore, because the primary particles are polydisperse, some reach their critical diameter and coagulate to provide a heterogeneous dispersion containing both primary particles and primary particle aggregates.

The uncertainty over the nature of the particles observed during electrophoresis made it impossible to determine Q, the number of charges per primary particle, from the electrophoretic data in Table 4.2.5.1. The zeta potential measured was either that of a combination of the primary and primary particle aggregates, or of the primary particle aggregates. The latter is certainly the case for high monomer conversions e.g. batches 26 to 31, where no free primary particles were observed by electron microscopy.

The observed decrease in intensity of scattered light during microelectrophoresis measurements arose from the sedimentation of the larger aggregates. These conceal the smaller and much fainter primary particles. For this reason no correlation was found between zeta potential and extent of conversion for polymer batches 23 to 33. It is also tentatively suggested that Speirs electrophoresis difficulties and lack of correlation may be attributed to observation of coagulated rather than free primary particles, since his investigations covered polymerisations over the monomer conversion range 1 to 4%.

To enable the evaluation of the stabilising

mechanism operating on the primary particles, the interference resulting from the presence of primary particle aggregates had to be resolved. The experimental difficulties of handling the condensed monomer and the known susceptability of the dispersion to orthokinetic coagulation (58) prevented the use of centrifugation to remove the larger aggregates.

The situation was resolved by allowing the aggregates to sediment out under gravity. The rate at which swollen PVC particles sediment in liquid vinyl chloride was estimated using Stokes' equation (162) :-

$$\text{Sedimenting velocity} = \frac{2a^2(\rho P - \rho L)g}{9\eta} \qquad (4.2.5.2)$$

where a is particle radius assuming spherical particles.

ρP is density of the swollen polymer particle

$(1.239 \times 10^6 \text{ g m}^{-3})$

ρL is density of the liquid monomer

$(0.917 \times 10^6 \text{ g m}^{-3})$

η is the viscosity of the dispersion medium

$(1.9 \times 10^{-4} \text{ Pas})$

g is the acceleration due to gravity

On transferring a small portion of the concentrated dispersion from the polymerisation limb into the diluent monomer in the electrophoresis cell, the particles are suspended throughout the monomer dispersion medium. From a knowledge of the vertical distance from the top of the

cell capillary to the stationary level (distance to sediment) the maximum time required for a PVC particle to sediment to below the horizontal electrophoresis observation plane can be estimated from eqn.(4.2.5.3)

$$\text{Sedimentation time} = \frac{\text{distance to sediment}}{\text{velocity of sedimentation}} \qquad (4.2.5.3)$$

Figure 4.2.5.2. is a plot of particle radius against the sedimentation time. It shows, for example, that particles of $>3 \times 10^{-7}$ m have fallen below the electrophoresis observation plane within 100 seconds. The critical primary particle diameter was taken as 1.25×10^{-7} m, however as more particle size data were obtained this figure was reduced to 1×10^{-7} m. From the graph it is apparent that the electrophoretic velocity of the primary particles, in the absence of primary particle aggregates, can only be obtained when the dispersion is left to sediment for approximately 6000 seconds (100 minutes).

Consequently, a series of polymerisations (polymer batches 39 to 43) were terminated after periods of polymerisation spanning 3 to 60 minutes. Electrophoretic measurements were evaluated after allowing the dispersion to sediment for 100 minutes.

Immediately after transfer of the latex to the main body of the electrophoresis cell, the particles appeared as bright single specks of light. By measuring the time taken for individual particles to sediment over

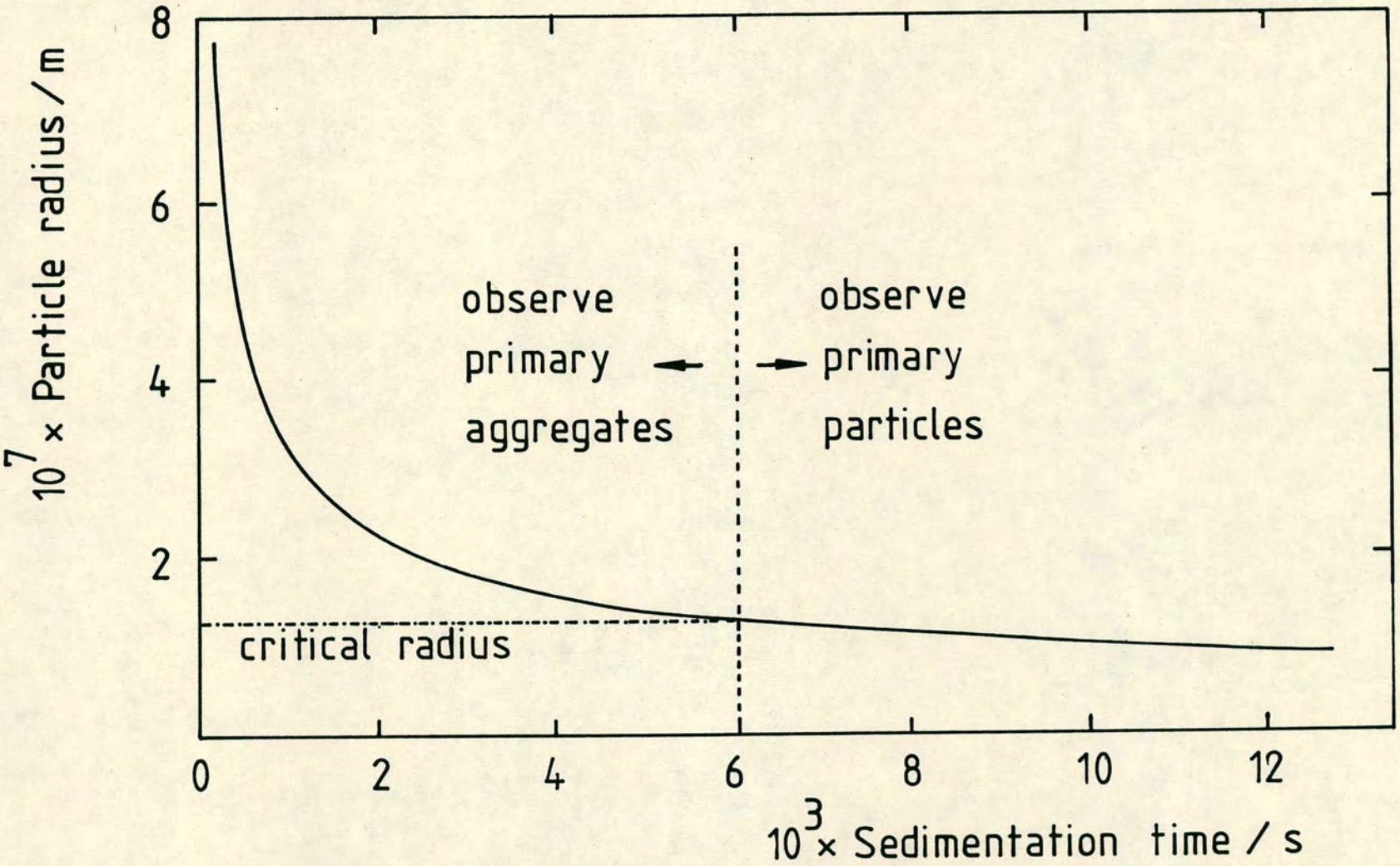

Fig.4.2.5.2. Maximum radius of particle observed as a function of sedimentation time.

several graticule squares, the particle diameters were calculated using eqn. (4.2.5.2) The estimated diameters compared favourably with those measured by S.E.M.

Within 10 to 15 minutes the bright single specks were below the observation region, revealing the primary particles as a faint mist in which it was difficult to observe single particles. Maximum illuminating power was required to resolve these faint particles. This gave rise to localised convection currents within the capillary of the electrophoresis cell, which was constructed with the 2 mm diameter capillary (see Table 3.2.2.3.1 for details). The addition of further heat filters between the cell and light source reduced the light intensity rendering particle observation impossible. Reluctantly the cell was reconstructed with a 1 mm diameter capillary. Convection currents were not a problem in the new cell, however, dielectrophoretic problems, which are enhanced in narrow bore capillaries, frequently prevented any electrophoretic measurements.

To confirm that the zeta potential was now independent of time, the electrophoretic mobility of PVC Batch 39 was measured at frequent intervals over a period of 18 hours. The zeta potentials obtained (-80, -90, -83, -92 and -80 mV) remained reasonably stable over this period compared with the wide variation found in the non-sedimented polymer batches 23 to 33.

Electrophoretic measurements were attempted initially on polymer batches 39 to 43 to assess the

sedimentation method.To confirm the trends observed in these preliminary experiments further polymerisations (batches 56 to 66) were also investigated using this technique. The results are tabulated in Table 4.2.6.1 and are discussed later in section 4.2.6.

PVC dispersions (batches 44 to 54) were produced at a lower polymerisation temperature (308 K) in an attempt to find an alternative to the sedimentation method. The initiator concentration was maintained at 0.1% (wt/vol). It was hoped that by reducing the rate of polymerisation the time taken for the primary particles to attain their critical diameter would be extended. Rance et. al. (42) have indicated that under these polymerisation conditions the onset of coagulation occurs after 20 minutes of polymerisation. Whereas the results obtained at Edinburgh, presented in section 4.2.4, clearly show that at the higher temperature of 323 K, the primary particles reach their critical diameter in polymerisation of less than 10 minutes duration.

By reducing the polymerisation temperature a longer observation period should be available in which primary particle charge, in the absence of aggregated primaries, could be investigated. Using this method the sedimentation period was not required.

A series of polymer batches were terminated after 5 to 20 minutes of polymerisation. It was observed that whilst measuring the electrophoretic behaviour of the PVC particles, the turbidity of the concentrated dispersion

within the polymerisation limb increased.

At 293 K it was unlikely that further polymerisation was a significant factor, a more likely reason for the increase in turbidity was the coagulation of the primary particles. This was confirmed when the morphology of the PVC produced was analysed by electron microscopy. This revealed a complex polymer morphology consisting of single primary particles and large aggregates of primary particles indicating that coagulation had indeed occurred. See Plates 4.2.5.1. and 4.2.5.2.

The ageing of the PVC dispersion in the polymerisation limb made it impossible to determine whether the coagulation of the primary particles occurred during polymerisation, or whilst electrophoresis was being carried out.

Negative zeta potentials were evaluated for PVC dispersions produced at 308 K. However these data could not be used to unravel the charging mechanism on the primary particles, since it was impossible to distinguish the nature of the particles measured in the electrophoresis experiments. Unlike the primary particle aggregates produced at 323 K, which are large and sediment rapidly, the primary particle aggregates produced at 308 K were of sufficiently small diameter (approximately 0.2 μm) not to sediment at an appreciable rate. For this reason the sedimentation method discussed earlier could not be used to distinguish between the primary particles and

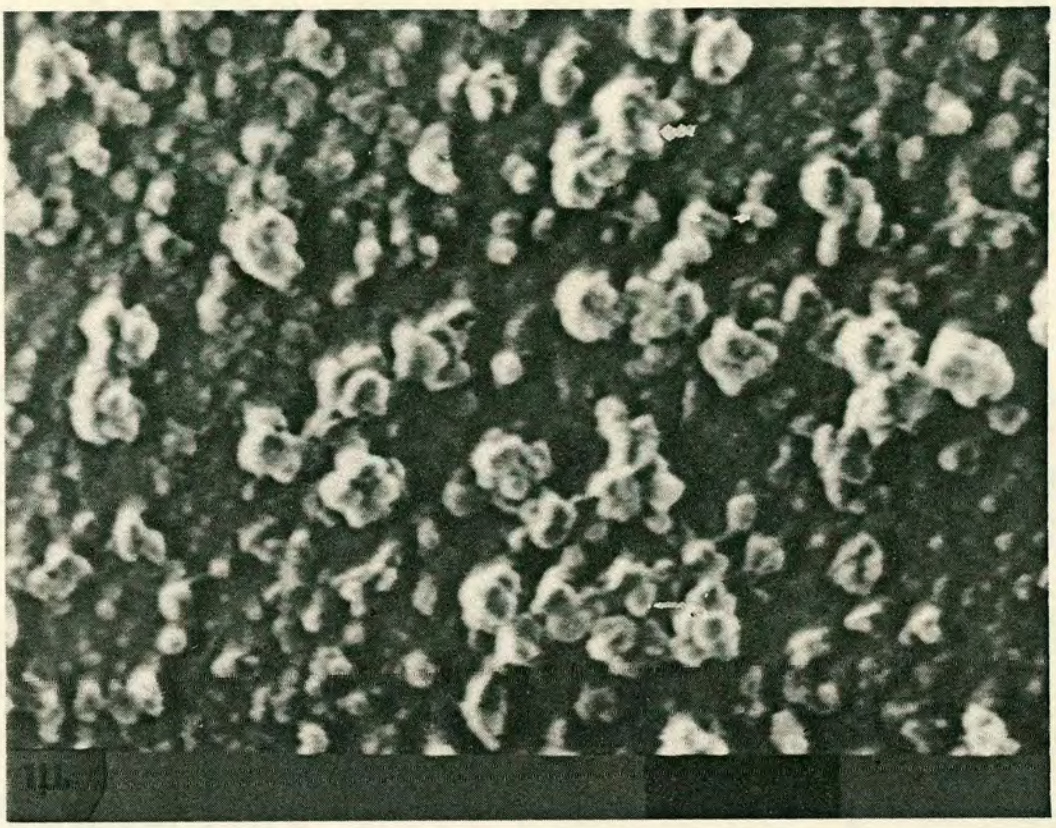

PLATE 4.2.5.1 PVC PARTICLES PRODUCED AT 293 K

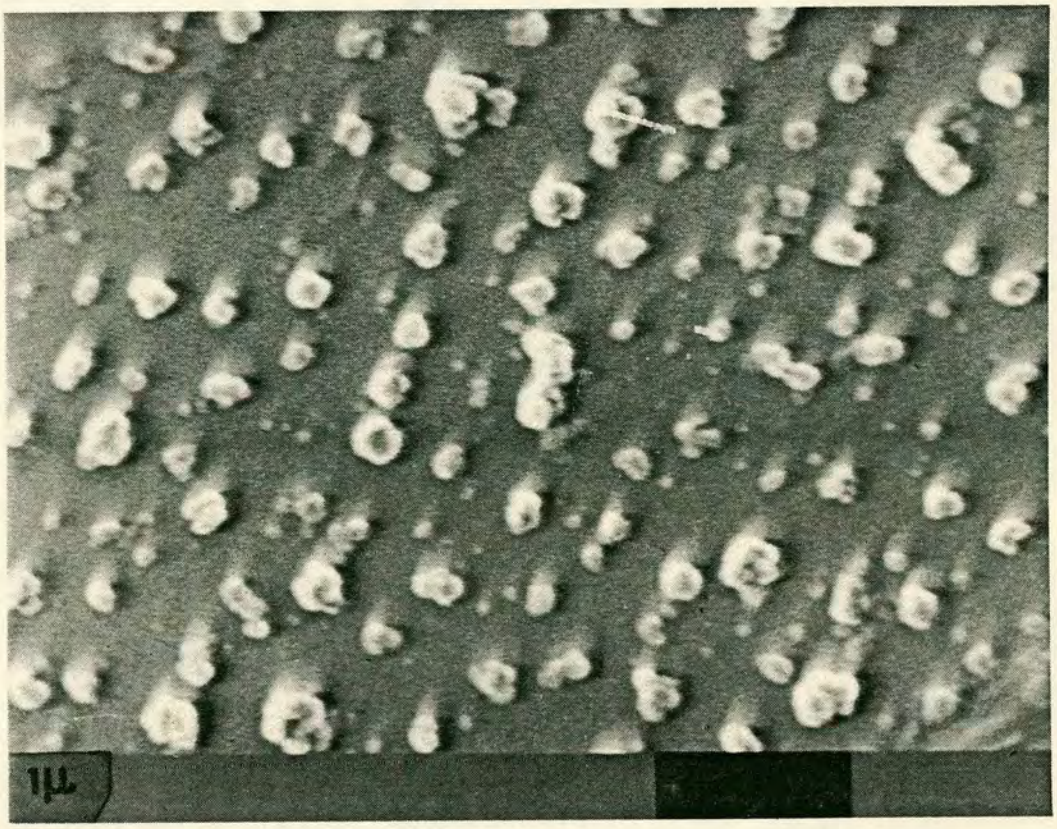

PLATE 4.2.5.2 PVC PARTICLES PRODUCED AT 293 K

primary particle aggregates, produced in the lower temperature polymerisations.

As the problem of dispersion ageing did not appear to occur in dispersions produced at 323 K, it was decided to abandon the low temperature polymerisations and return to polymerisations at 323 K. This required the use of the sedimentation method to remove the obscurring primary particle aggregates. This finally allowed the investigation of primary particle charge as a function of monomer conversion.

PVC batches 56 to 66 were prepared at a polymerisation temperature of 323 K. The electrophoretic mobility was evaluated after the sedimentation period. Of these only runs 59 and 62 generated valid electrophoresis data. Considerable difficulties (as discussed in section 4.1.2), were encountered in obtaining reliable electrophoresis. Furthermore, batches 63 and 64 failed to polymerise. These failures coincided with changing the bottled oxygen free nitrogen (OFN) supply used to flush the system of residual oxygen. An alternative source of OFN reinstated the correct polymerisation rate, suggesting that an impurity in the nitrogen was responsible for the lack of reaction.

The measurement of the electrophoretic properties of PVC particles dispersed in a condensed toxic gas of low permittivity proved to be a formidable task. Furthermore the "observation window" in which primary particles were expected to remain stable to coagulation proved to be much

shorter than 12% conversion predicted by earlier investigators (9).

During this study, electrophoretic mobility of stable primary particles could only be evaluated over the very limited monomer conversion range 0.16% to 0.67% (wt/vol). For this reason the experimental investigation, of bulk polymerisations in the absence of primary particle stabilisers, was terminated in favour of polymerisations containing small amounts of low molecular mass stabilisers. The presence of primary particle stabilising agents, such as Tetronic 707 (£85), have been shown to produce particles stable to much higher monomer conversions. By investigating a range of low molecular mass additives it was hoped that larger primary particle size range could be achieved, enabling a greater insight into the role of colloidal stability, if any, on the morphological development of PVC during bulk polymerisations. These investigations are discussed in a later section.

4.2.6 Primary particle charge

The combination of electrophoretic and particle size data obtained during the initial stages of polymerisation reveals valuable information on the mechanism of nucleation and formation of basic particles, along with the rapid formation of primary particles and their eventual loss of stability to form aggregates.

Table 4.2.6.1. Results of polymerisations at 323K.

Batch Number	Polymerisation Time / Minutes	% Conversion (wt/vol)	10^8 x Swollen Primary Particle Diameter / m		10^3 x -Zeta Potential / V	Number of Elementary Charges / Particle	
			Dn	Dv		Q (Dn)	Q (Dv)
43	3	0.42	7.79	9.39	96	12 ± 3	15 ± 3
59	10	0.16	11.7	14.7	113	21 ± 4	27 ± 3
41	20	0.42	12.1	15.6	90	18 ± 5	23 ± 6
62	20	0.52	15.0	19.1	85	21 ± 5	26 ± 5
39	30	0.42	8.59	10.4	85	12 ± 3	14 ± 3
42	45	0.67	12.5	16.4	76	15 ± 4	20 ± 4
40	60	0.71	*	*	*	*	*

* No primary particles observed.

The data obtained from the experiments at 323 K involving the prior sedimentation of the aggregates are summarised in Table 4.2.6.1. The total charge per primary particle (Q), in elementary charges, was calculated from equation (4.2.5.1.) for both number and volume average primary particle diameters.

From the table it is immediately apparent that the primary particles remain negatively charged during polymerisation. In addition, the number of charges per primary particle remains reasonably constant throughout their lifespan. The mean values being given below:-

$$Q\ (D_n) = 16 \pm 4$$

$$Q\ (D_v) = 20 \pm 5$$

From this result it is tentatively proposed that the stable primary particles grow with a constant number of elementary charges per particle. As the growing primary particle exceeds the critical size, above which, the electrostatic repulsion between particles is insufficient to confer colloidal stability, coagulation occurs resulting in the formation of primary particle aggregates. This proposed mechanism and a discussion of the possible charging regimes is given in the next section.

Also worthy of note is the very low number of elementary charges required to produce stable PVC particles in VCM. Comparison (61) between the number of charges at the plane of shear in the PVC/VCM system and that of charges at the surface of similarly sized aqueous polymer particles reveals that approximately one hundredth

of the charge density is required for the PVC/VCM dispersion.

In the following section, DLVO type calculations are used to model PVC particle stability during polymerisation. From these it will be seen whether the experimentally observed colloidal events correlate with the theoretical predictions.

4.3 Theoretical investigation of colloidal stability during polymerisation.

4.3.1 Particle charge regime during growth.

It has been shown that the PVC primary particles grow by polymerisation until they lose their colloidal stability at a critical diameter of approximately 0.2 μm. Coagulation then occurs with the appearance of primary particle aggregates. By monitoring both particle diameter and electrophoretic mobility as a function of monomer conversion, the total charge on the primary particle was found to remain reasonably constant during its lifespan. To test whether this experimental observation was consistent with theoretical predictions, a series of calculations were performed under various charge regimes. The following charge mechanisms during polymerisation were considered:-

a) The surface potential of each particle remains constant during particle growth, which corresponds to the formation of a thermodynamic

equilibrium between potential determining ions adsorbed on the particles and those in solution in the dispersion medium.

b) The surface charge density of each particle remains constant during particle growth, by which the number of potential determining ions present on each particle is limited sterically by their finite size.

c) The total charge on each particle remains constant during growth. This corresponds to the charge on the PVC particle being determined by a constant number of irreversibly bound charged surface groups, or to a finite total charge in the system being evenly distributed over a constant number of primary particles.

Using DLVO type calculations (Appendix (4)) the primary particle stability was predicted for particle growth under each of the charge mechanisms described above. Figure 4.3.1.1 shows the variation in stability ratio, W, as a function of particle radius for the three charge regimes. From this figure it is immediately apparent that under both constant surface potential and constant surface charge density regimes the stability of the primary particles is predicted to increase during particle growth. In contrast, under the constant particle charge regime the colloidal stability of the primary particles is predicted to decrease during particle growth.

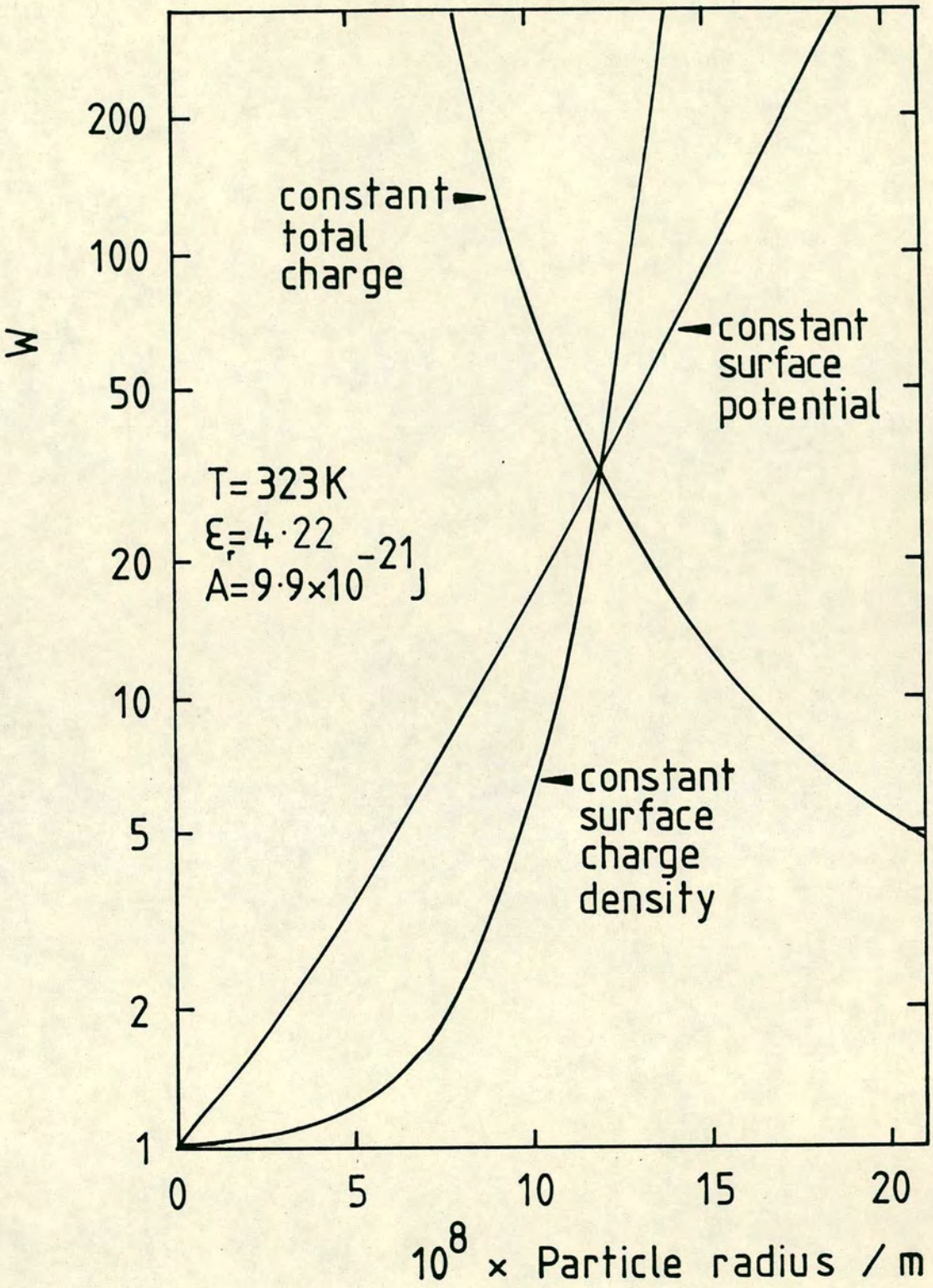

Fig. 43.1.1. Effect on stability ratio of particle growth under three different charge regimes.

This mechanism is consistent with the results presented in section 4.2.6, in which primary particles appear to grow at a constant charge in the region of 16 - 20 elementary charges per particle. All subsequent theoretical calculations were therefore based on the regime of particle growth at constant particle charge.

4.3.2 Theoretical investigation of primary particle stability.

The previous work on precipitation polymerisation of VCM at Edinburgh concentrated, because of experimental difficulties, on investigating the theoretical effect of varying colloidal parameters on particle stability. In this study the emphasis is now placed, more firmly, on seeing whether the observed primary particle behaviour reported earlier in this chapter, could be accounted for by a mechanism involving electrostatic stabilisation and, in particular, to indicate whether the experimentally determined number of charges per primary particle (Q = 16 - 20) would be sufficient to give this stabilisation.

The exploritory work of Speirs (58) has formed the foundations of the present theoretical calculations. Computer programmes were utilised to calculate the theoretical stability ratio, W, for the interaction of spherical particles under various experimental conditions. The programme uses the numerical integration technique

discussed in section 2.5.2 to calculate stability ratios from equation (2.5.2.10). Details of the programme are given in Appendix (4). The effect various parameters have on dispersions of PVC in VCM have already been reported (58) and are only dealt with briefly below.

It was confirmed that the effect of varying the type of V_R expression on stability ratio W was relatively small in comparison to the effect of varying the particle potential or charge. The simple Coulombs' expression (equation 2.2.37) predicts the highest stability whilst the Verwey and Overbeek β expression (equation 2.2.35) the lowest.

Likewise, as expected, the variation of the Hamaker constant proved to be negligible (126), negating the need for Liftshitz type calculations to determine Hamaker constants for the PVC/VCM system. In all subsequent calculations the value of A for swollen PVC particles interacting across a pure monomer was taken to be 9.9×10^{-21}J (155). For the range of free ionic concentrations likely to be present in VCM the effect of varying double layer thickness was also very small.

In contrast to these parameters Figure 4.3.2.1 shows that the magnitude of the primary particle charge plays a dominant role in determining the dispersion stability. Indeed this parameter completely overwhelms the effect of other variables and is thus expected to control the stability of PVC primary particles during polymerisation.

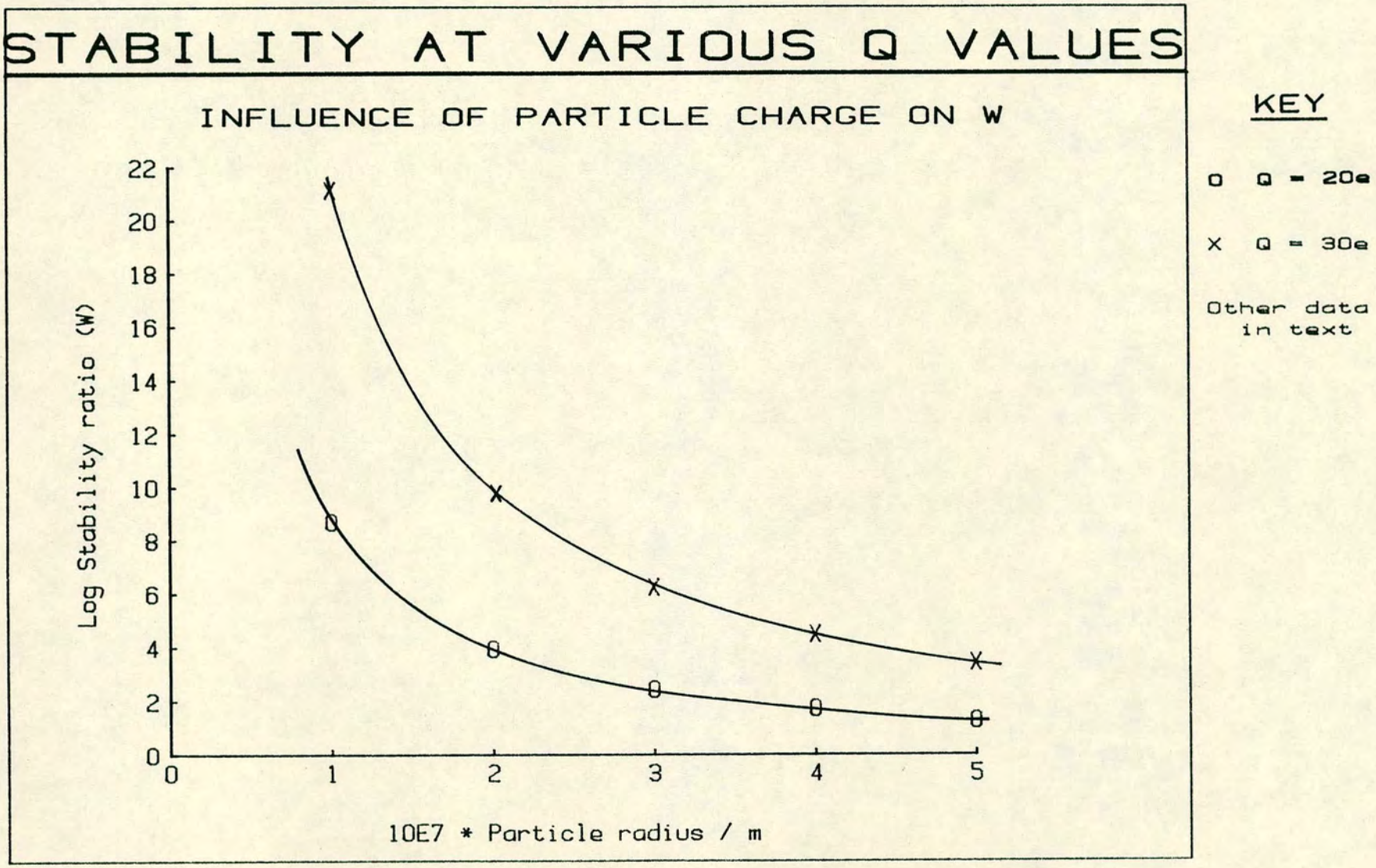
STABILITY AT VARIOUS Q VALUES
INFLUENCE OF PARTICLE CHARGE ON W
Log Stability ratio (W)
22
20
18
16
14
12
10
8
6
4
2
0
0
1
2
3
4
5
10E7 * Particle radius / m
KEY
O Q = 20e
X Q = 30e
Other data in text

Figure 4.3.2.1

In conclusion, these preliminary calculations indicated that for a model based purely on electrostatic stabilisation of the primary particles, the particle charge would be the most important factor in controlling their stability. This is determined entirely by their radius and zeta potential. Furthermore, the only charge mechanism capable of accounting for the observed primary particle life cycle was that proposed by Zichy (9) in which the particles grow with a constant number of charges per particle, until the surface charge becomes so diffuse that the surface potential is low enough to allow coagulation.

In dispersions of low permittivity media the predicted stability ratio is frequently found to be in excess of that for the experimental system (58). Parfitt (126) has shown that the effect of particle concentration must be allowed for in such systems and states that for a particle concentration of 10% the potential energy barrier to coagulation is typically reduced by about 50%. Albers and Overbeek (164) have proposed that the potential energy barrier is lowered in low permittivity media where the average interparticle separation becomes of the same order as the double layer thickness. For this reason the particle concentration effect was included in the investigation of primary particle stability during polymerisation. The model based on the work of Albers and Overbeek has been criticised by Levine et. al. (165) in a later series of papers where a more mathematically

rigorous approach has been adopted. However, as will be discussed shortly, the particle concentration effect was found to be less important in this study, and, for this reason, the more easily applied approach of Albers and Overbeek was considered adequate for estimating the stability of the PVC dispersions during particle growth. The model is discussed along with a detailed outline of ALOV, the computer programme in Appendix (4).

The fate of the growing primary particle was considered at the polymerisation temperature of 323 K, where the relative permittivity and Hamaker constant were taken to be 4.22 and 9.9×10^{-19} J (155). Stability ratios were predicted as a function of particle radius using data generated during the experimental investigation. For this temperature a suspension polymerisation droplet of 1 mm diameter, as assumed by the programme, would contain about 1.67×10^{8} primary particles, based on the particle concentration of 3.2×10^{17} m^{-3} determined earlier.

Figure 4.3.2.2, drawn for a primary particle carrying a total of 12 elementary charges (Q = 12) indicates the relationship between stability ratio (W) and particle radius. Two cases were considered, firstly for the interaction of two particles in the absence of other particles and secondly after allowance for multiparticle interactions. It is apparent from Figure 4.3.2.2 that for the experimental conditions under consideration the particle concentration effect is minimal and only leads to a marginal reduction in stability. This, at first sight,

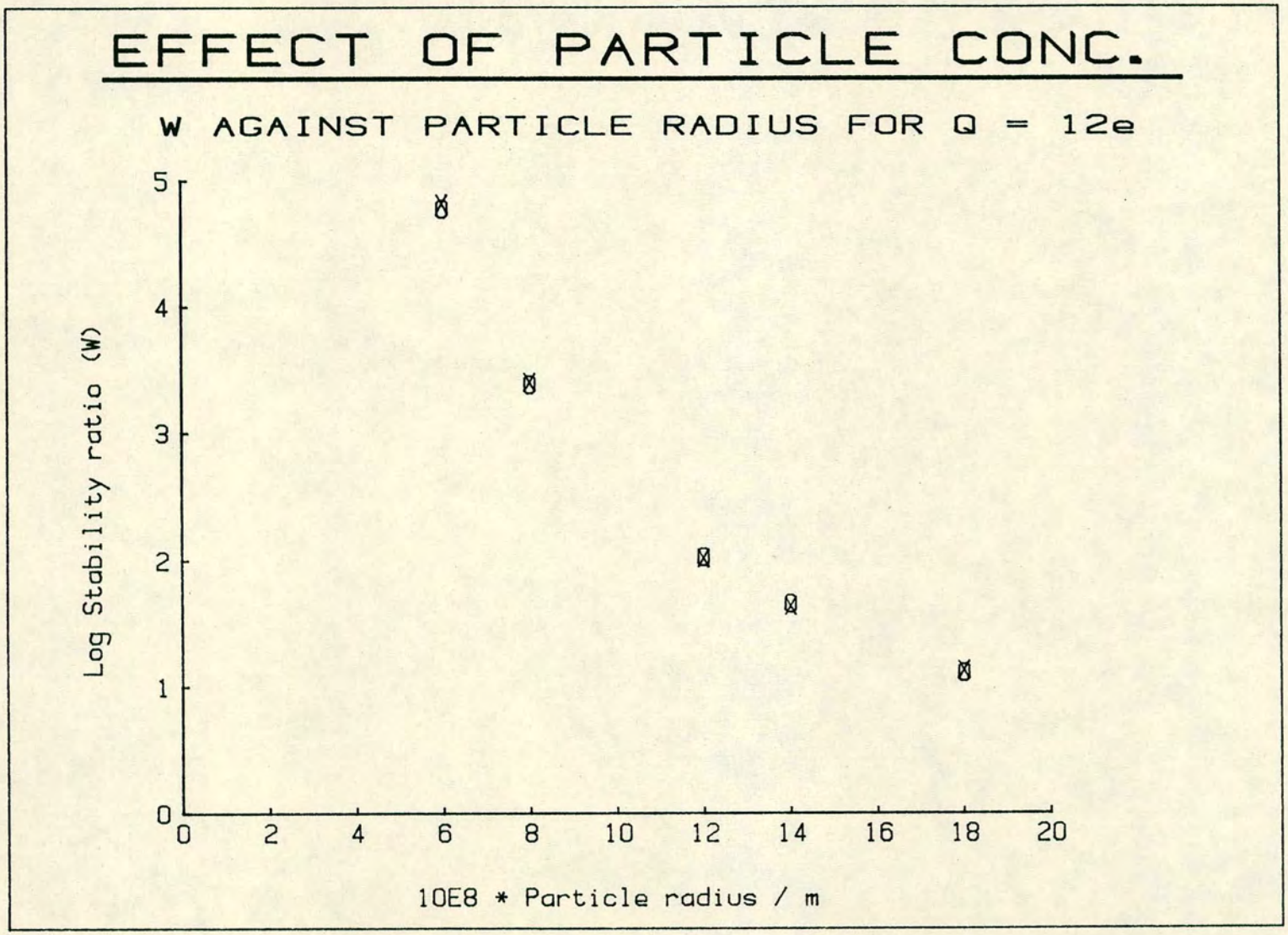
EFFECT OF PARTICLE CONC.
W AGAINST PARTICLE RADIUS FOR Q = 12e
Log Stability ratio (W)
0
1
2
3
4
5
0
2
4
6
8
10
12
14
16
18
20
10E8 * Particle radius / m
KEY
X Multi_particle interaction
O Two-particle interaction
Other data in text

Figure 4.3.2.2

is in sharp contrast with the work of Speirs where the particle concentration effect considerably reduced the stability of the dispersion. This disparity arises from the fact that the critical primary particle diameter was found in this and other studies (42) to be much lower than was previously assumed by Speirs. The volume fraction of the dispersion was therefore greatly reduced by the presence of much smaller primary particles and thus it was concluded that the particle concentration effect was less important in these calculations.

It was now necessary to use ALOV to predict theoretically the critical coagulation diameter of primary particles under typical polymerisation conditions and compare the results with the experimentally measured critical sizes.

Figure 4.3.2.3 was calculated assuming identical conditions as Figure 4.3.2.2. It shows how the stability of a growing primary particle, after allowing for the particle concentration effect, would vary as a function of particle radius at various particle charges. By examination of Figure 4.3.2.3 it is confirmed that, under a model in which the primary particles grow at constant total charge, they pass from stability to instability by growth over a very small range of particle radius. Furthermore, over this range, which is typical for free primary particles, very few charges per particle are required to stabilise the monomer swollen PVC particles dispersed in VCM.

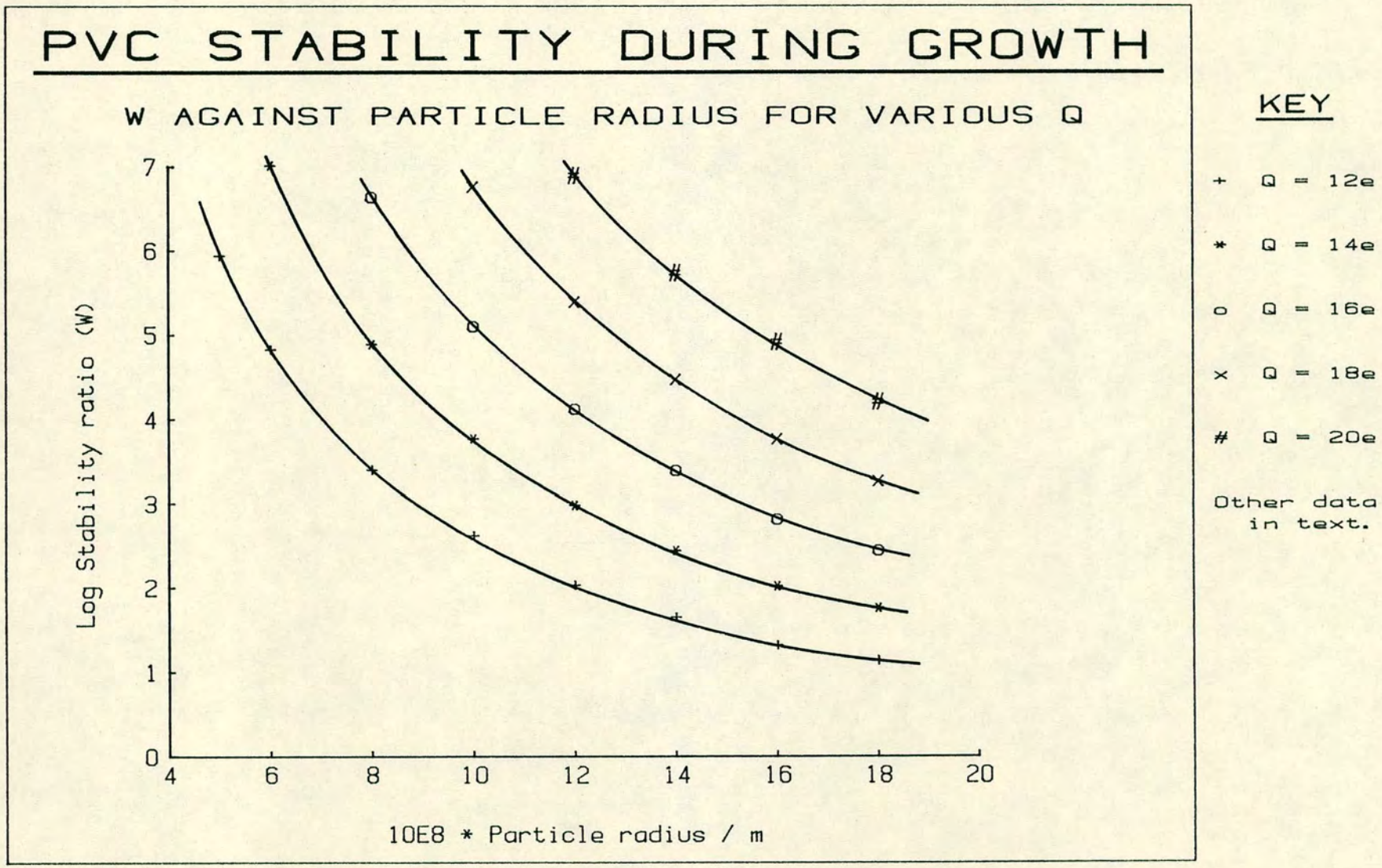
PVC STABILITY DURING GROWTH
W AGAINST PARTICLE RADIUS FOR VARIOUS Q
Log Stability ratio (W)
0
1
2
3
4
5
6
7
4
6
8
10
12
14
16
18
20
10E8 * Particle radius / m
KEY
+ Q = 12e
* Q = 14e
o Q = 16e
x Q = 18e
Q = 20e
Other data in text.

Figure 4.3.2.3

Before any quantitative comparison between theoretical prediction and experimental observation can be made a criterion for stability must be defined. There is no sharp distinction between a stable and unstable dispersion, rather a transition is observed from long term stability through slowly coagulating to unstable. Frequently the height of the potential energy barrier, Vmax, has been equated to dispersion stability although the values tend to be somewhat arbitary and depend on the stability criterion applied. Verwey and Overbeek (3) estimate a Vmax of approximately 15 kT in order to retard aggregation by a factor of 10^5 over rapid coagulation. Vold (166) considers 10 kT as "sufficient" whilst Crowl and Malati (167) accept 5 - 10 kT as "tolerable". From these examples it can be seen that a wide range of values have been quoted as representing a stable dispersion, however, most references to stability equate a Vmax value of 15 kT, or more, as representing a stable system. Fortunately the stability ratio W at the onset of coagulation of polymerising PVC primary particles has been determined by photon correlation spectroscopy (42). This value will be utilized in this study and a stability ratio of less than 10,000 will be taken to represent an unstable dispersion, Such a value of W corresponds to a potential energy barrier in the region of 11 kT. Likewise a stability ratio in excess of 500,000 (approximately 15 kT) will be taken to represent a stable system.

Following the method of Wiese and Healy (168), it

was felt that the most informative way of representing the theoretical results was in the form of a domain diagram. The domain diagram was constructed for a fixed value of Hamaker constant, primary particle number, relative permittivity and temperature and indicates the variation in primary particle radius corresponding to W = 10,000 and W = 500,000 as a function of particle charge. The diagram thus maps out the combinations of particle radius and charge corresponding to stability, instability and intermediate stability. It then allows the number of charges per particle to be predicted as the primary particles grow beyond the experimentally determined mean critical primary particle diameter of approximately 0.2 μm and, in doing so, pass from a region of stability into an unstable state and coagulation.

The domain diagram was constructed from plots of W as a function of particle radius for several values of particle charge. (See Figure 4.3.2.3). The particle radius corresponding to W = 10,000 and W = 500,000 for each of the particle charges was then taken directly from the graph of W against particle radius, and used to plot the domain diagram of radius against particle charge.

Using identical conditions as for Figure 4.3.2.3 a domain diagram was drawn for the polymerisation conditions investigated during this study. Figure 4.3.2.4 presents this domain diagram and indicates the stable, intermediate stability and unstable regions as the primary particles grow at various particle charges. Examination of this

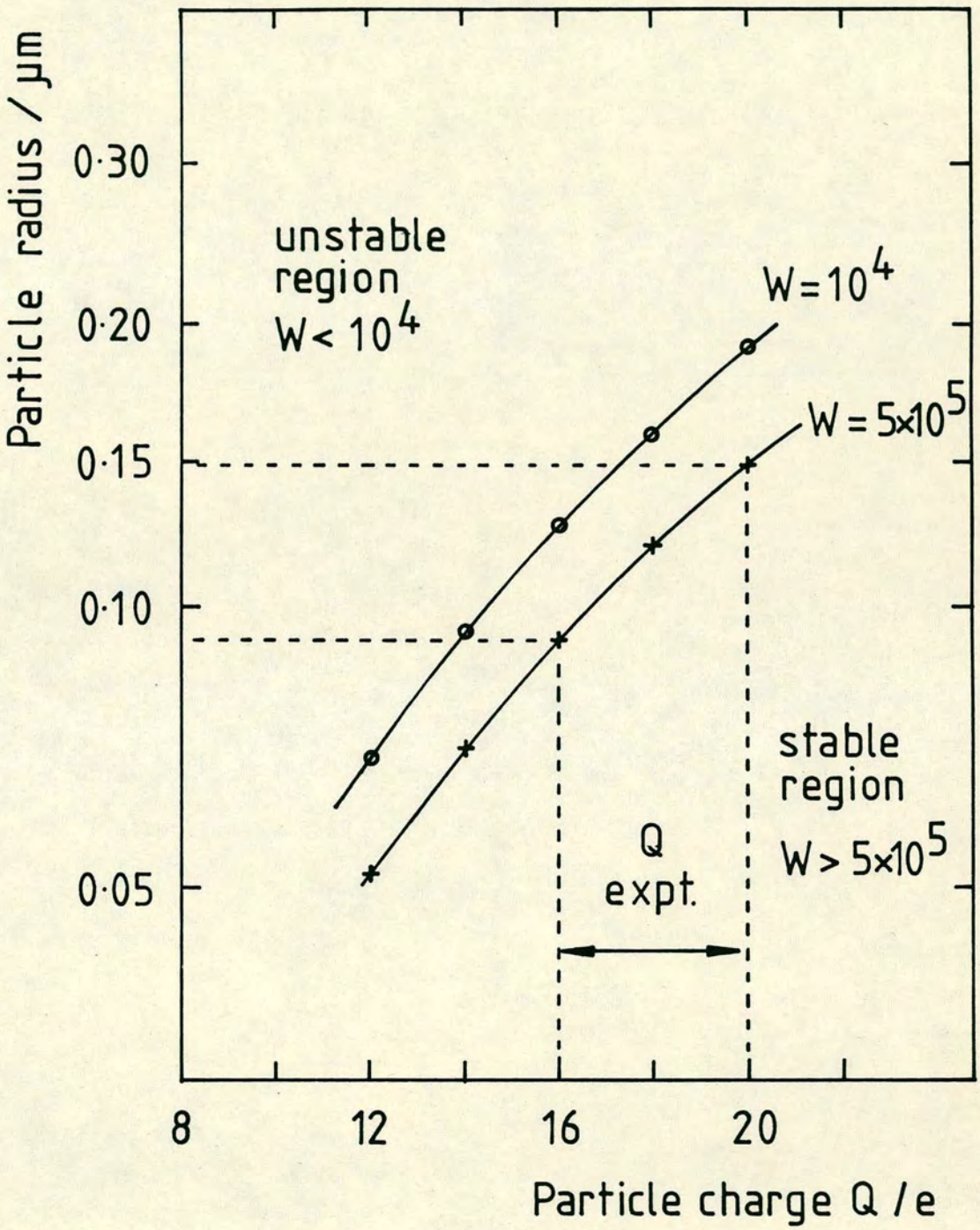

Fig. 4.3.2.4. Domain diagram constructed using ALOV, for polymerisations at 323 K, showing the predicted primary particle radius.

figure reveals that a primary particle, at the mean critical primary particle radius of 0.1 μm, would require approximately 17 elementary charges to remain stable to coagulation. This lies within the experimentally determined range of 16 to 20 charges per particle.

In conclusion, it is encouraging that there is a general agreement between the experimental and theoretical work. Furthermore, it is confirmed that the measured primary particle charge is sufficient to account for the known stability behaviour of the primary particles by a mechanism of electrostatic stabilisation.

4.4 Addition of low molecular mass additives.

4.4.1 Introduction

This section describes a study of the influence that low molecular mass monomer soluble additives have on colloid stability in the early stages of PVC polymerisation. By investigating a range of compounds it was hoped that the magnitude of the charge on the PVC primary particles could be varied to control the onset of primary particle aggregation. This would give a greater insight into the role of colloid stability on the morphological development of PVC during bulk polymerisations. A series of experiments were envisaged to elucidate the effect of increasing and decreasing the primary particle charge on the critical primary particle diameter and onset of aggregation. If control of the

colloid stability could be obtained this could then be utilised to produce a polymer with a wide variety of morphologies and possibly lead to a PVC polymer with greater porosity and more consistent processing properties. Due to the potential commercial gains of such a process the literature contains very few reports pertaining to the nature of additives used in the modification of PVC polymer morphology and their possible link with the colloidal stability of the primary particles.

Zichy (9) reported that polymerisations containing an "experimental stabiliser" prevented aggregation of primary particles at conversions up to 28%. It was hoped that other low molecular mass monomer soluble additives could be identified and their role in the early stages of VCM polymerisation elucidated.

Three potential modifiers, Manoxol-OT, Span-20 and bis-(2-hydroxyethyl)-aminohexadecane were investigated in polymerisations at 323 K using lauroyl peroxide at 0.1% (wt/vol) as a free radical initiator. Details of the chemical nature and preparation of these additives are given in Chapter 3. Several methods of introducing these additives at ppm levels into the small scale polymerisations were investigated. The most accurate method appeared to be the preparation of concentrated standards of the additives in a volatile solvent (Karl Fischer grade methanol). Then using µl quantities, ppm levels of the additives were injected onto a small portion

of the glass sampling microslide. The volatile solvent was then evaporated and the microslide introduced into the polymerisation limb of the combined quartz polymerisation/ electrophoresis cell. One advantage of using this method was the separation of the additive from the free radical initiator during the work up prior to polymerisation.

It was first necessary to screen these potential charge modifiers to reveal any morphological activity. Following this it was envisaged that suitable additives would be investigated; firstly at a constant monomer conversion, to evaluate the electrophoretic mobility as a function of additive concentration to reveal suitable treatment levels; secondly, carry out a programme of polymerisation at a constant additive concentration to determine the critical particle size at aggregation and any morphological changes to the PVC polymer structure.

4.4.2 Manoxol-OT

From a knowledge of the number of charges per primary particle and the particle concentration in earlier polymerisations, it was estimated that sub-ppm levels of low molecular mass additives should be effective in modifying the charge on the PVC primary particle. To allow for any adsorption on the walls of the polymerisation vessel, reactions containing Manoxol-OT over a concentration range of 1 to 100 ppm were investigated.

To assess the effectivness of Manoxol-OT in

altering primary particle characteristics a series of polymerisations were quenched at a constant monomer conversion of 0.1% (wt/vol). Previous experiments at this conversion had shown the primary particles to exist in an unaggregated state and it was hoped that electrophoresis measurements would be possible in the absence of primary particle aggregates.

Polymer batches 78, 75, 76 and 77 containing 1, 10, 50 and 100 ppm Manoxol-OT were polymerised to 0.1% monomer conversion. Electrophoresis measurements were evaluated before and after a sedimentation period of 100 minutes. No significant difference in particle mobility was found suggesting the absence of primary particle aggregates. Indeed, on examination, the SEM micrographs revealed no aggregated material, nor any obvious morphological changes brought about by the presence of Manoxol-OT. The shrunken primary particle diameter (D_v) for these polymer batches was typically 0.15 μm which is in good agreement with that found in earlier polymerisations at this monomer conversion (see Figure 4.2.3.9). The particles were found to carry a net negative charge. The electrophoresis data, along with the image analysis data (type 3 analysis), for each batch of polymer are presented in Table 4.4.2.1. Both number and volume based mean diameters and standard deviations for the shrunken polymer particles are tabulated.

The combination of electrophoretic and particle size data obtained at a constant monomer conversion

Table 4.4.2.1. Summary table for polymerisation at 323 K containing various concentrations of Manoxol-OT.

Batch No.	Manoxol-OT level /ppm	Mean and Standard Deviation shrunken diameter				- Zeta Potential /mV	Q_{Dn}	Q_{Dv}
		Dn/μm	σn/μm	Dv/μm	σv/μm			
78	1	0.069	0.029	0.101	0.040	73	14± 6	20± 8
75	10	0.074	0.043	0.150	0.055	74	10± 6	21± 8
76	50	0.088	0.040	0.148	0.054	83	14± 6	23± 9
77	100	0.082	0.042	0.152	0.056	85	13± 7	24± 9

reveals that the number of elementary charges per primary particle remains reasonably constant and independent of Manoxol-OT additions. This effect is shown in Figure 4.4.2.1 where primary particle charge, at constant monomer conversion, is plotted as a function of Manoxol-OT level. Extrapolation to zero Manoxol-OT concentration reveals a value of Q = 20 which was the value found for polymerisations in the absence of low molecular mass additives (Section 4.3.6).

In conclusion, at the concentrations investigated, the presence of Manoxol-OT had either no, or only slight, effect on particle charge, size and morphology. It is tentatively suggested that either Manoxol-OT has a very limited solubility, or remains undissociated in the low permittivity VCM monomer and was therefore unable to contribute to the charge stabilisation of the PVC primary particle. Thus the investigation of this low molecular mass additive was terminated in favour of other potential polymer modifiers.

4.4.3 Span-20

Span-20 (sorbiton monolaurate), a viscosity improver, being of non-ionic nature was not expected to furbish extra charged species within the polymerisation. Addition of Span-20 has been shown by Saharova et. al. (169) to modify the particle concentration in the early stages of the polymerisation of VCM. It was therefore

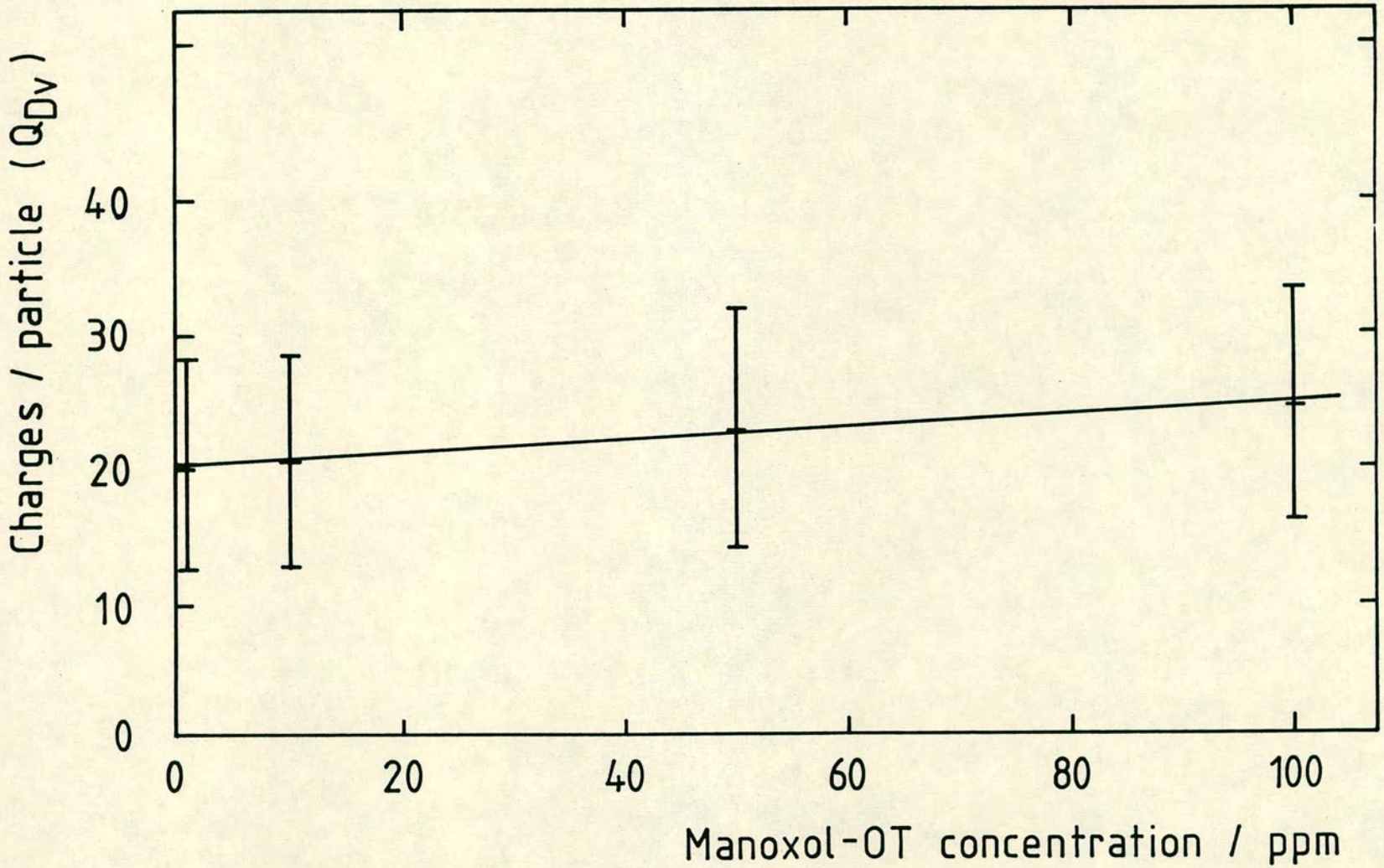

Fig. 4.4.2.1. Number of elementary charges / particle as a function of Manoxol - OT concentration.

expected that the addition of Span-20 would increase the number of PVC particles and shed light on the charging mechanism operating in this system.

Polymer batches 87 and 88 containing Span-20 at 10 ppm were polymerised to 0.09 and 0.18% (wt/vol) conversion respectively. It was observed that the monomer in the polymerisation limb became turbid much earlier than in the absence of Span-20. Electrophoresis measurements proved to be impossible with no regular movement of the faint particles on application of the applied field, indicating little or no charge present on the PVC particles. During electrophoresis measurements it was observed that the particle number appeared to decrease with a much coarsed dispersion being produced. From these initial findings it was concluded that the stabilising mechanism operating on the PVC particles is reduced in the presence of Span-20, resulting in an unstable dispersion and early aggregation of the particles.

Unfortunately scanning electron microscopy proved to be very difficult on samples containing Span-20 as the more volatile components tended to evaporate under the electron beam reducing picture quality. Plate 4.4.3.1 shows the two types of particles produced in polymer batch 87. The polymer produced consists of small free particles of less than 0.1 μm diameter and almost spherical larger particles of approximately 0.2 μm. These, on closer examination, appear to be composed of smaller particles and some appear to have undergone further polymer growth

and infilling at the VCM/PVC interface.

To enhance this change in polymer morphology a series of experiments were conducted at a Span-20 concentration of 0.2% (vol/vol) up to a monomer conversion of 2.8% (wt/vol).

The morphological development of PVC particles is shown in a series of SEM micrographs, Plates 4.4.3.2 to 4.4.3.6. At a monomer conversion of 0.38% (wt/vol) the PVC particles produced in batch 114 have a volume average diameter of 0.09 ± 0.02 μm and are much smaller than those produced in the absence of Span-20. See Plate 4.4.3.2. It is difficult to resolve the aggregated state of the primary particles at this conversion, due partly to their small size but mainly the adverse effects of much higher levels of Span-20 on microscopy. Comparison of this micrograph with Plate 4.4.3.1 indicates the drastic morphological change brought about by increasing the Span-20 concentration to 0.2% (vol/vol).

Plates 4.4.3.3 and 4.4.3.4 show the aggregated PVC particles at 1.4% (wt/vol) monomer conversion. Image analysis of the almost spherical particles indicated a volume average diameter of 0.22 μm ± 0.06 μm. Considerable fusion and infilling between the particles has occurred by this stage of the polymerisation as further polymer growth occurs perpedicular to any PVC/VCM interface (9). No free primary particles were observed above 0.38% (wt/vol) conversion. By 2.8% particle identity is being lost through the deposition of further polymer over the primary

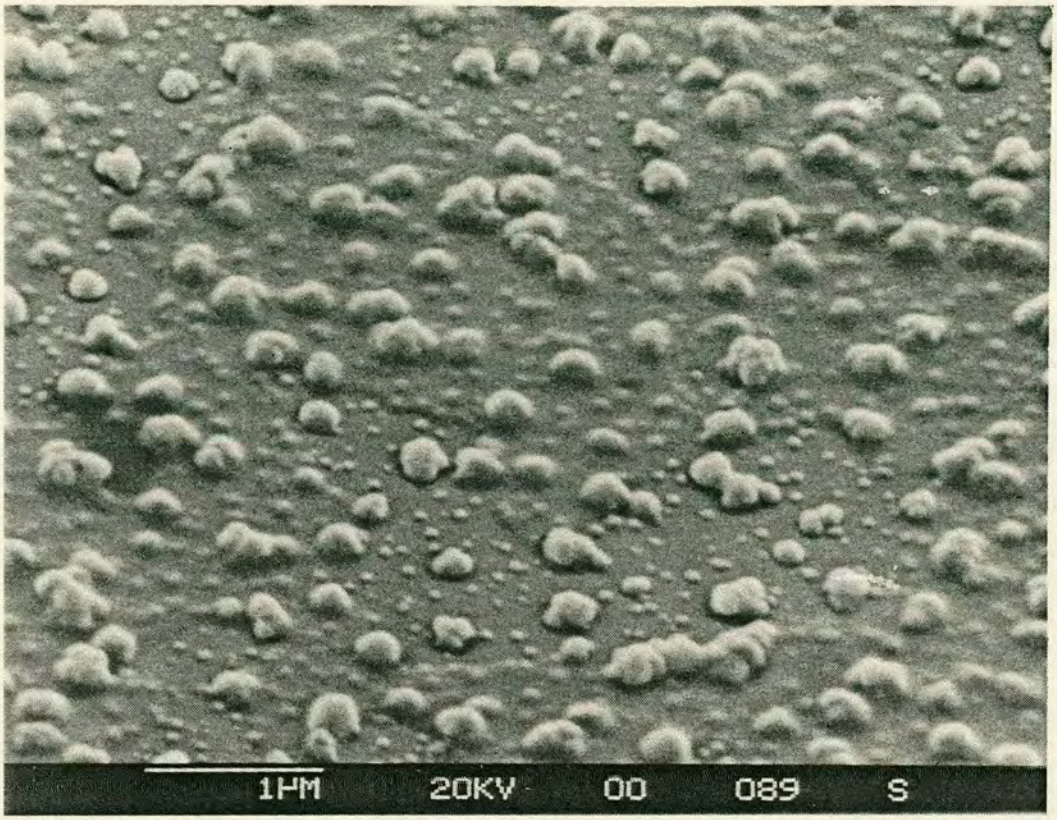

PLATE 4.4.3.1 SPAN-20 10 ppm. POLYMER BATCH 87

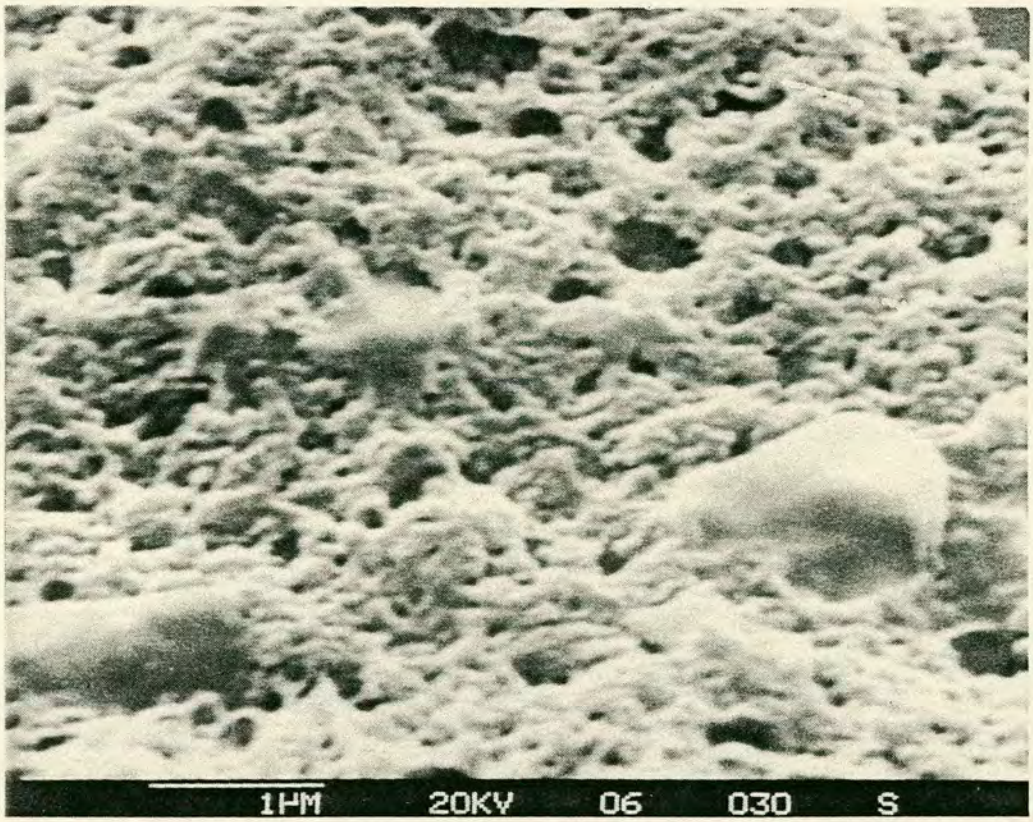

PLATE 4.4.3.2 SPAN-20 0.2 PER CENT. POLYMER BATCH 114

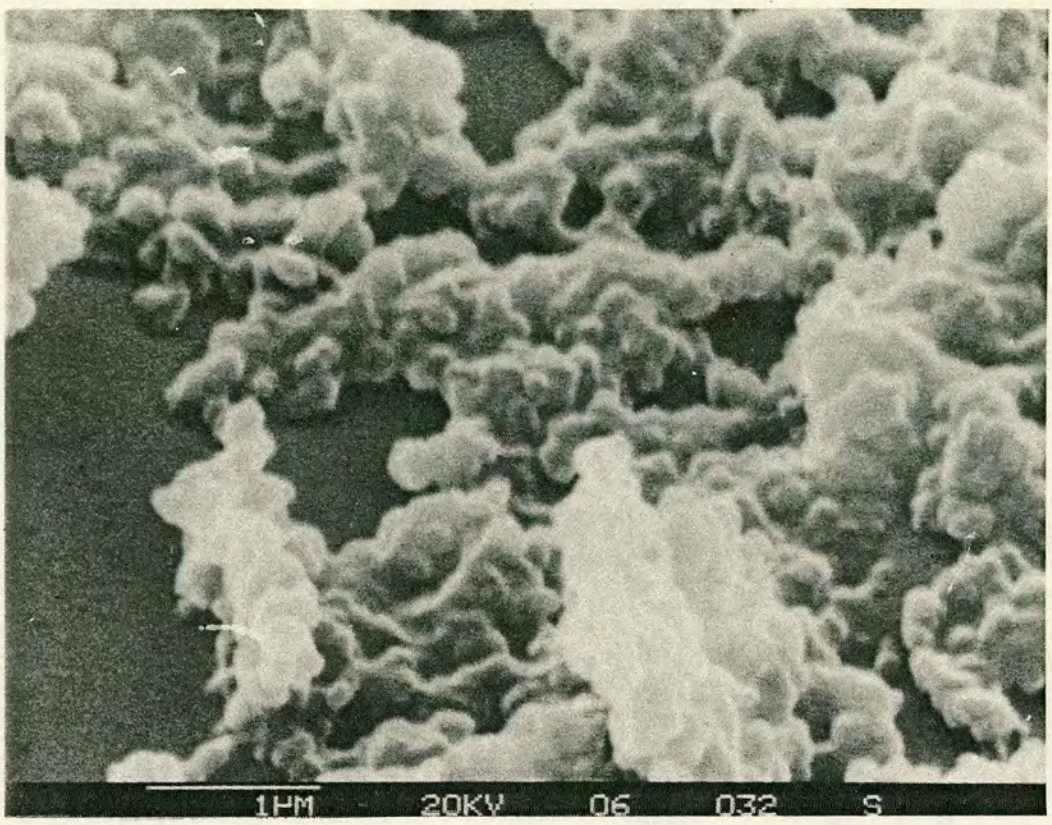

PLATE 4.4 3.3 SPAN-20 0.2 PER CENT. POLYMER BATCH 115

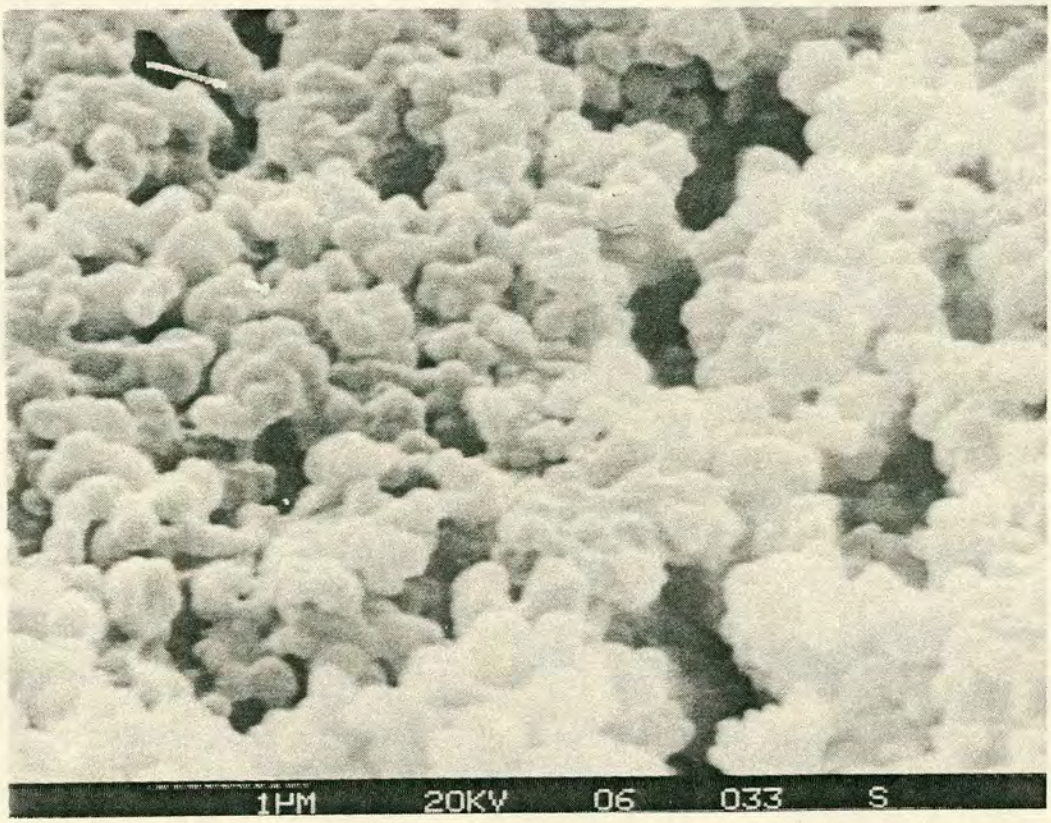

PLATE 4.4.3.4 SPAN-20 0.2 PER CENT. POLYMER BATCH 115

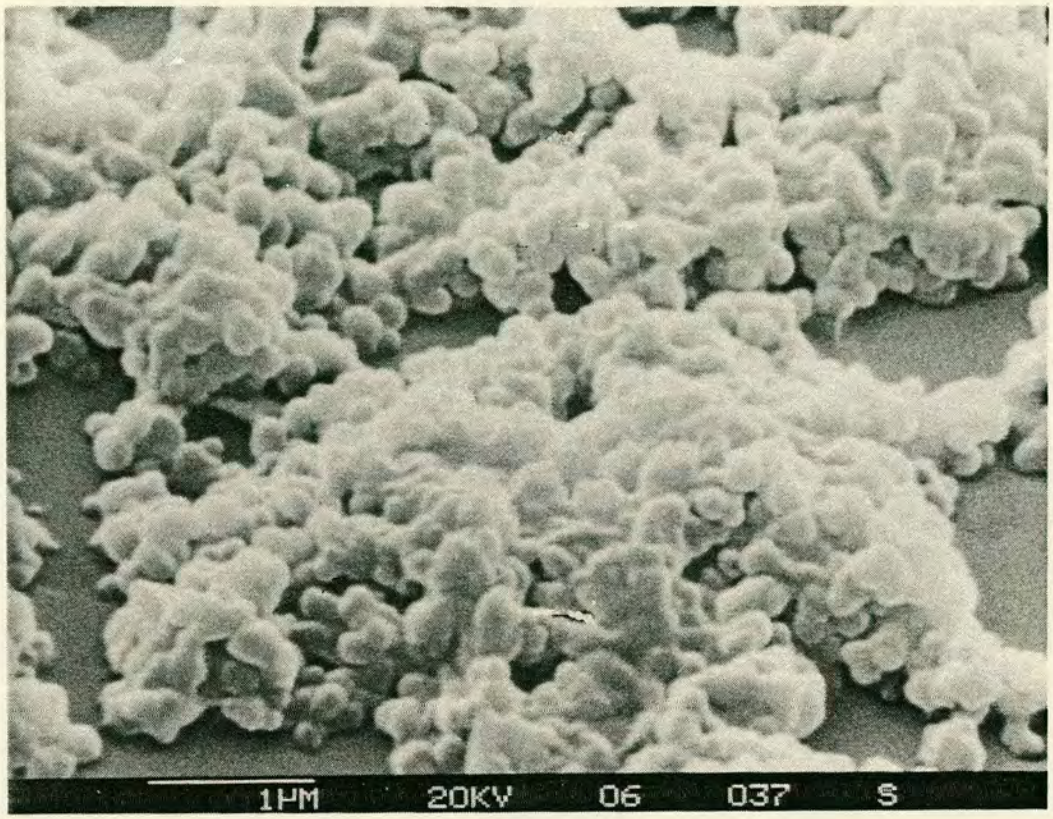

PLATE 4.4.3.5 SPAN-20 0.2 PEk CENT. POLYMER BATCH 116

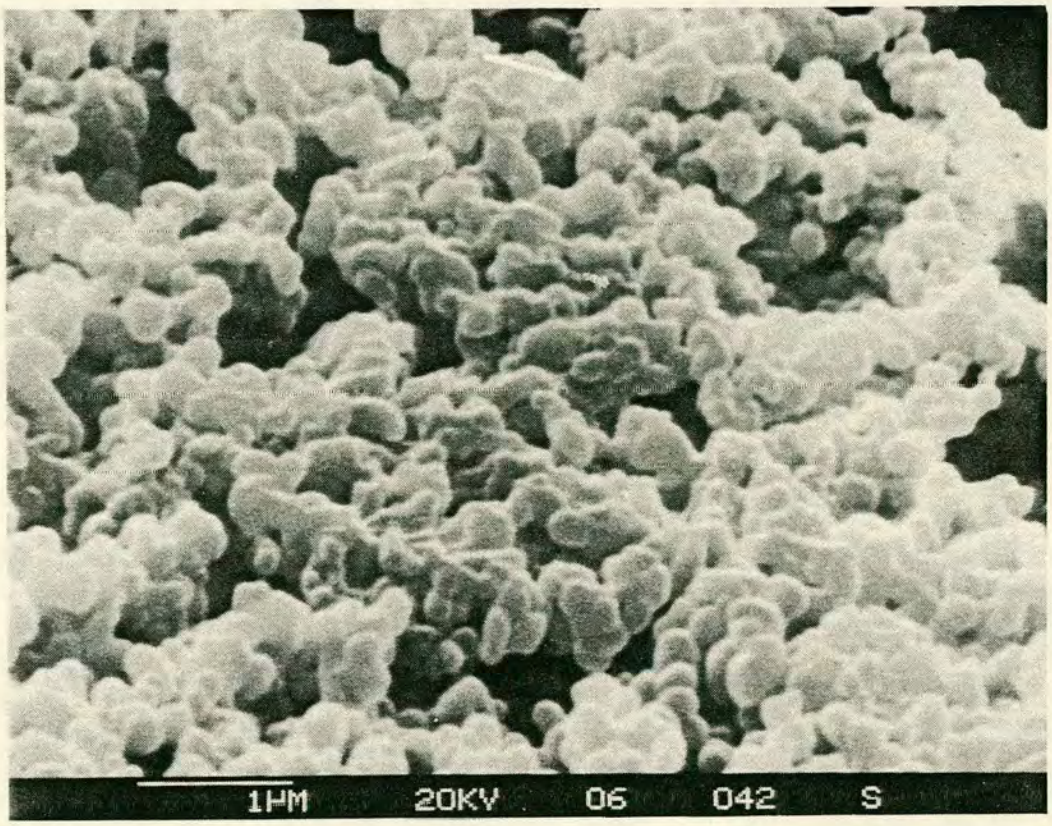

PLATE 4.4.3.6 SPAN-20 0.2 PER CENT. POLYMER BATCH 116

particle aggregates (Plates 4.4.3.5 and 4.4.3.6). However the early aggregation step appears to promote an open structure when the aggregates lock into a continuum. The fate of these micron sized voids and their effect on porosity could not be addressed by the present experimental technique.

From this study it is not possible to resolve conclusively the nature of the 0.2 μm near spherical particles observed at 1.4% (wt/vol) conversion. Either these particles have grown from the already aggregated primary particles observed in batch 114, which might account for the considerable fusion and intergrowth of the particles, or these particles are themselves the aggregates of the primary particles which have then undergone further polymerisation leaving a near spherical primary particle aggregate with concealed internal primary particle structure. The resolution of the scanning electron microscope used in this study was unable to resolve this question.

Tornell and Uustalu (66) considered polymerisations at 332 K containing 0.2% (vol/vol) Span-20. They describe a process similar to that observed here with aggregation of the primary particles occurring at much lower conversions than in polymerisations without additions of Span-20.

When attempts were made to measure the electrophoretic mobility of PVC dispersions containing Span-20, no primary particles could be observed by dark

field microscopy. At high monomer conversions aggregated material was observed but showed no regular electrophoretic mobility suggesting that the particles were of a low or uncharged nature.

Saharova et. al. (169) have reported that the primary particle number increases on the addition of sorbitan monolaurate. Using the procedure described in section 4.2.4 the primary particle concentration for this system at the point of aggregation was estimated to be about 9×10^{18} m^{-3}. In the absence of Span-20 the primary particle concentration is approximately 3×10^{17} m^{-3} indicating that Span-20 has a significant influence on the primary particle concentration.

According to the mechanism of Zichy (9), in the absence of additives the polymerisation contains a finite charge, distributed evenly amongst the particles. This total charge is given by the product of the number of charges associated with each particle (Q = 20) and the particle concentration (3×10^{17} m^{-3}). If it is assumed that the non-ionic Span-20 does not contribute to the finite charge in the system and only influences the dispersion through increasing the number of primary particles 30 fold, then an even distribution of the available charge would result in each primary particle carrying in the region of 1 elementary charge per particle. Such a particle would be expected to exhibit minimal electrostatic stabilisation to coagulation and thus account for low particle charge and early particle

coagulation behaviour observed experimentally.

The mechanism by which Span-20 influences the primary particle concentration is unknown. It is however known that Span-20 can initiate VCM polymerisation (66) and this was confirmed by polymerising batch 137 in the absence of the normal lauroyl peroxide initiator. The combined presence of two VCM initiators may well lead to an increase in the number of oligomers produced and hence a larger number of primary particles.

A much more thorough investigation would be required to characterise, in detail, the colloidal events occurring in the initial stage of the PVC polymerisation containing Span-20. This study would require the use of techniques which can detect colloidal particles below the resolution of the SEM equipment available during this investigation and may well be more suited to experiments followed by technique such as photon correlation spectroscopy.

The addition of sorbitan monolaurate to polymerisations at 323 K has been shown to modify the morphology of the PVC polymer produced. This arises from the lack of a stabilising moiety on the growing PVC particles and has been shown to correspond to a reduction in the magnitude of the electrostatic charge on the PVC particles.

The addition of this non-ionic low molecular mass compound can therefore indirectly modify the charge on the growing particle by influencing the concentration of

primary particles in the dispersion. This may represent a method of controlling the morphological properties of the commercially produced PVC polymer.

4.4.4 Bis-(2-hydroxyethyl)-aminohexadecane

Preliminary polymerisations using this basic low molecular mass monomer soluble additive indicated that it could modify both the electrophoretic behaviour and polymer morphology in the early stages of VCM polymerisations.

Two experimental programmes were devised to characterise the influence of this molecule on the polymerisation process. Firstly, at a constant monomer conversion, to evaluate the electrophoretic mobility as a function of additive concentration. A low monomer conversion was envisaged where electrophoresis measurements would not be hampered by the formation and presence of primary particle aggregates. This should reveal a suitable treatment level to bring about major changes in particle charge. The second series of experiments would then investigate the particle size and polymer morphology as a function of monomer conversion at a constant additive concentration. This should help to elucidate the development of the particulate PVC structures formed.

Initial polymerisations revealed that a monomer conversion of about 0.15% (wt/vol) produced suitably sized

particles for observation by dark field microscopy. Polymer batches 99 and 91 to 95 were polymerised to approximately 0.15% (wt/vol) conversion. These contained bis-(2-hydroxyethyl)-aminohexadecane at concentrations ranging from 1 to 100 ppm. Polymerisation details and the experimentally determined parameters are summarised in Table 4.4.4.1.

Using equation (4.2.5.1) the electrophoretic data and image analysis results were combined to give Q the experimentally determined number of elementary charges per particle. Figure 4.4.4.1 is a plot of Q as a function of additive level for polymerisations quenched at a constant monomer conversion of about 0.15% (wt/vol). It reveals that the addition of bis-(2-hydroxyethyl)-amino hexadacane increases the number of charges per particle from around 20 in the absence of additives, to about 45 in the presence of this molecule. This encouraging result would suggest that the primary particles produced at 0.15% (wt/vol) monomer conversion should be highly stable to coagulation and, if so, continue to grow by polymerisation rather than coagulation. The second part of the investigation, polymer morphology as a function of monomer conversion should reveal any such behaviour.

A further feature of Figure 4.4.4.1 is that the number of charges per particle appear to be reasonably independent of the concentration of bis-(2-hydroxyethyl)-aminohexadecane over the 1 to 100 ppm range. This would suggest that the number of charges per particle is limited

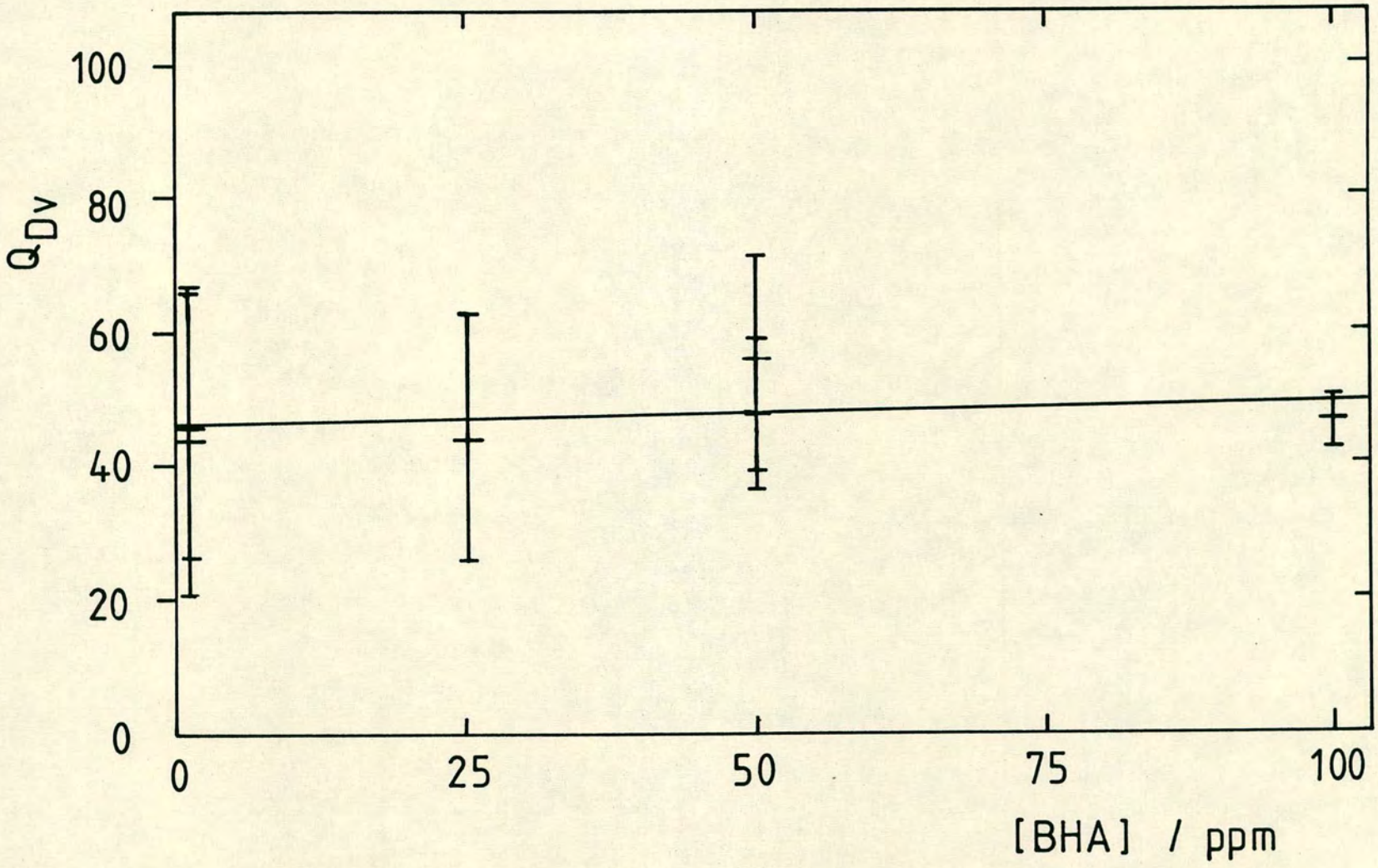

Fig.4.4.4.1. Nº charges per particle Q against concentration of BHA at constant conversion.

Table 4.4.4.1. Summary table for polymerisation at 323 K containing various concentrations of Bis-(2-hydroxyethyl)-aminohexadecane.

Batch No.	% Conversion (wt/vol)	Additive level /ppm	Mean and Standard Deviation shrunken diameter				- Zeta Potential /mV	Q_{Dv}
			Dn/μm	σn/μm	Dv/μm	σv/μm		
93	0.16	1	0.156	0.085	0.273	0.088	91	46±20
94	0.19	1	0.143	0.056	0.218	0.084	109	44±23
95	0.13	25	0.180	0.055	0.218	0.041	106	43±20
91	0.15	50	0.132	0.044	0.167	0.035	154	48±11
92	0.16	50	0.164	0.055	0.201	0.035	149	56±15
99	0.15	100	0.152	0.053	0.190	0.034	130	46± 4
90	0.10	1	0.100	0.047	0.168	0.058	76	24±12
111	0.26	10	0.203	0.078	0.266	0.053	169	84±27

by some, as yet unknown, mechanism. Some evidence to suggest that the number of charges per particle increased during polymer growth was obtained from polymer batches 90 and 111 in which polymerisations were quenched at monomer conversions of 0.1 and 0.26% (wt/vol). For these dispersions Q_{Dv} values of 24 and 84 charges per particle were evaluated suggesting that as the surface area of the particles increased so did the particle charge. If this was occurring, the primary particles would become very stable to coagulation. Growth by polymerisation would continue in the absence of an aggregative step resulting in primary particles attaining a large critical diameter before coagulating to form primary particle aggregates.

A more extensive investigation of particle charge as a function of monomer conversion was envisaged to assess the surface charge density on the particles during growth. Unfortunately this proved impossible, a secondary nucleation of particles occurred at higher monomer conversions which rendered the electrophoresis measurements invalid, the nature of the particles observed being in doubt.

Polymer batches 99 to 110 were polymerised in the presence of 100 ppm bis-(2-hydroxyethyl)-aminohexadecane to various monomer conversions up to 4% (wt/vol). The morphological development of PVC particles at increasing monomer conversion is shown in a series of SEM micrographs, Plates 4.4.4.1 to 4.4.4.12. (Where bis-(2-hydroxyethyl)-aminohexadecane has been abbreviated to

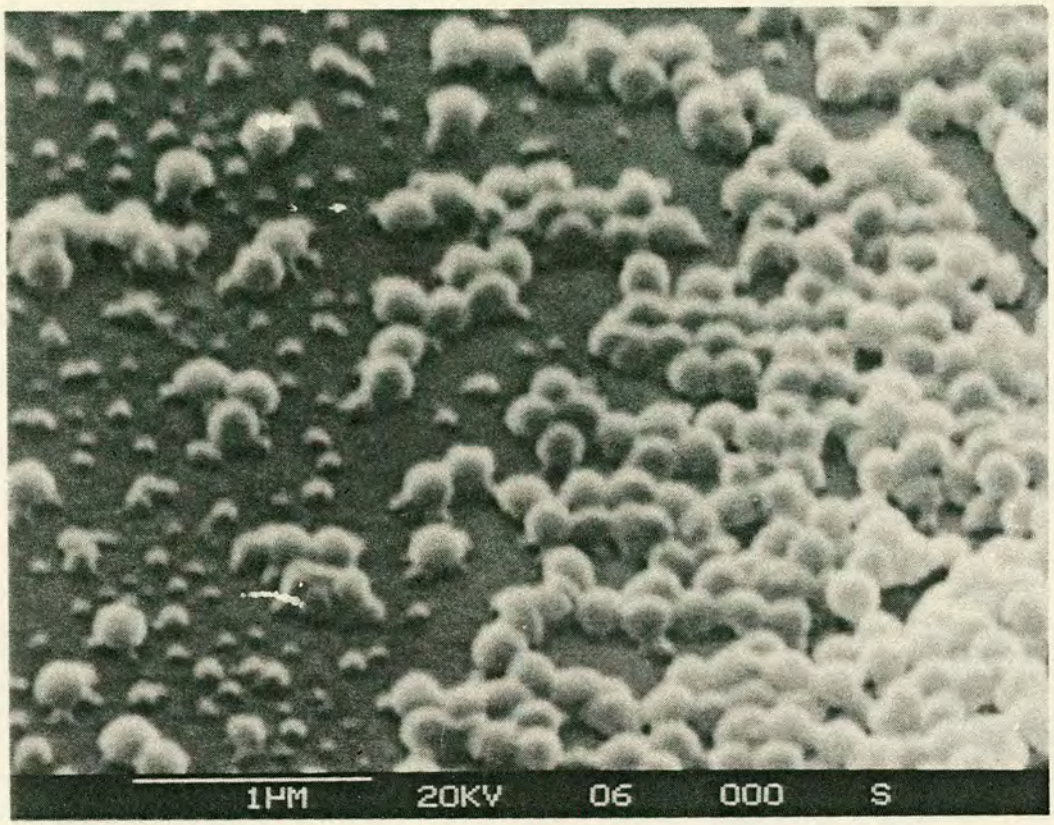

PLATE 4.4.4.1 BHA 100 ppm. POLYMER BATCH 99

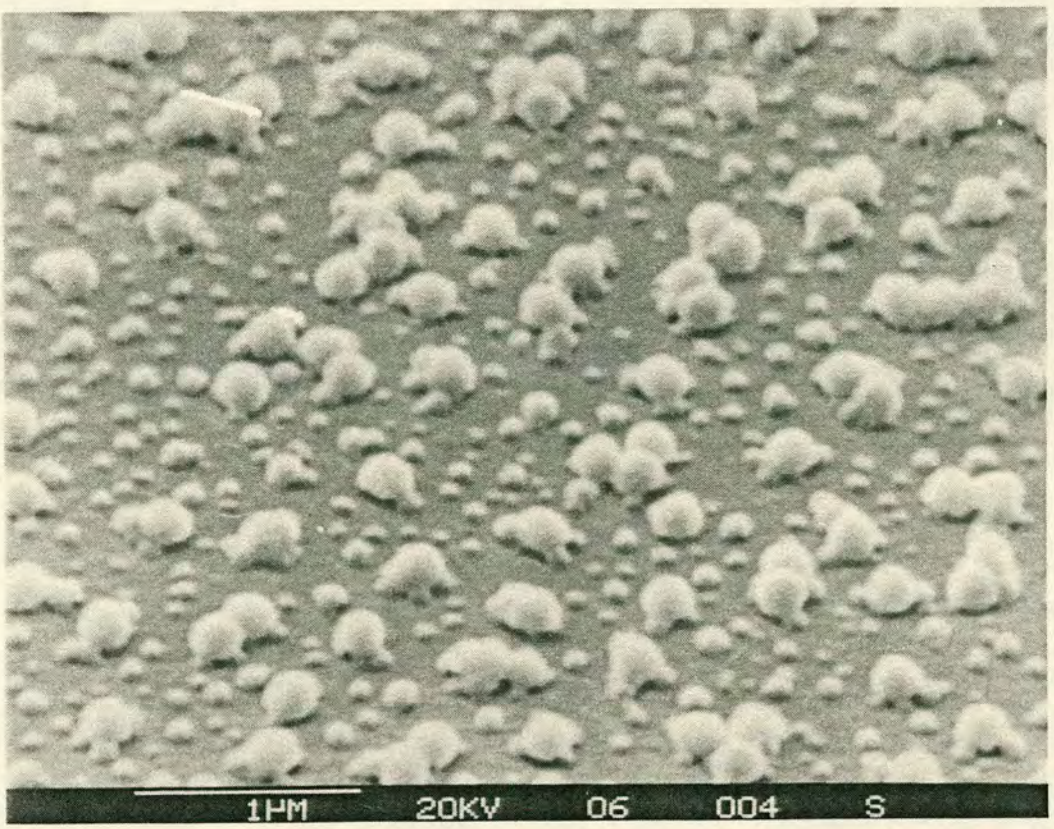

PLATE 4.4.4.2 BHA 100 ppm. POLYMER BATCH 99

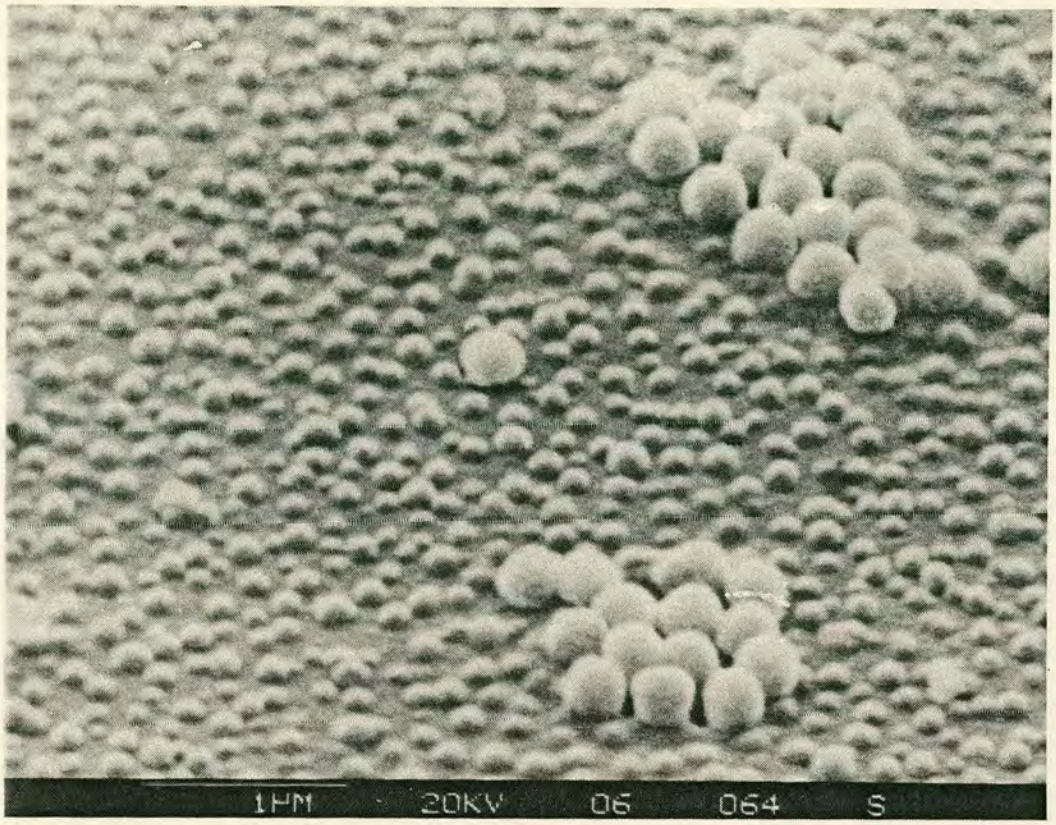

PLATE 4.4.4.3 BHA 100 ppm. POLYMER BATCH 106

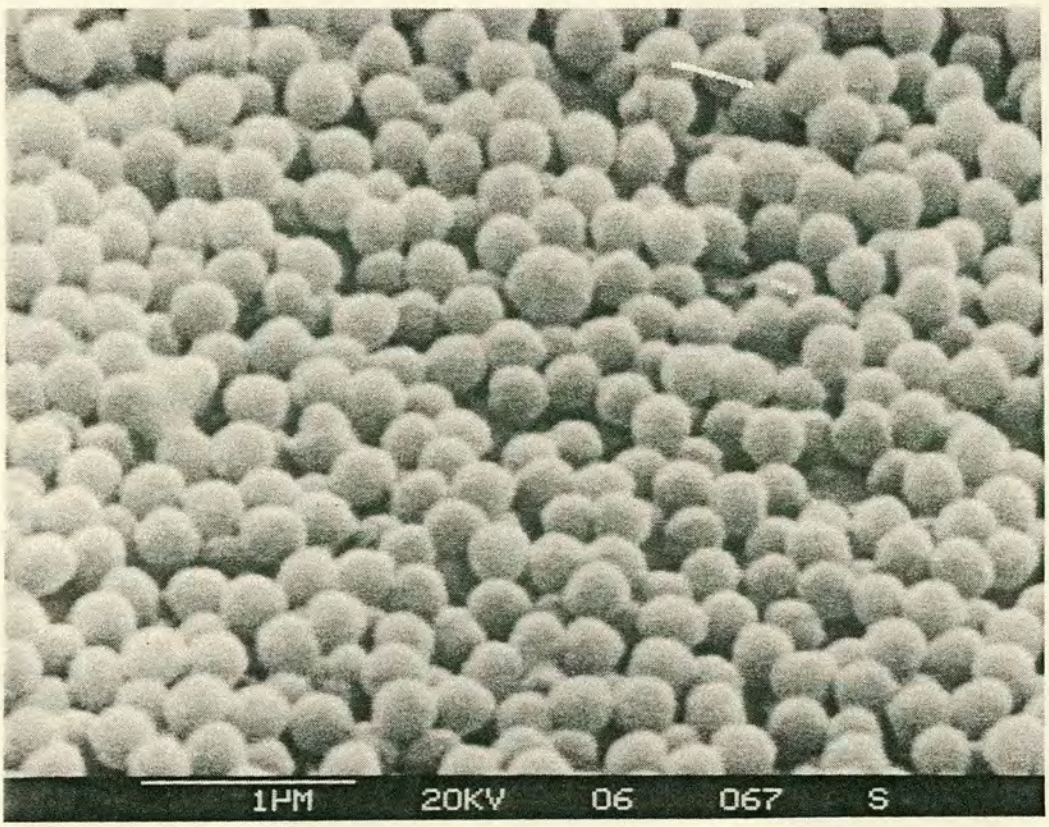

PLATE 4.4.4.4 BHA 100 ppm. POLYMER BATCH 106

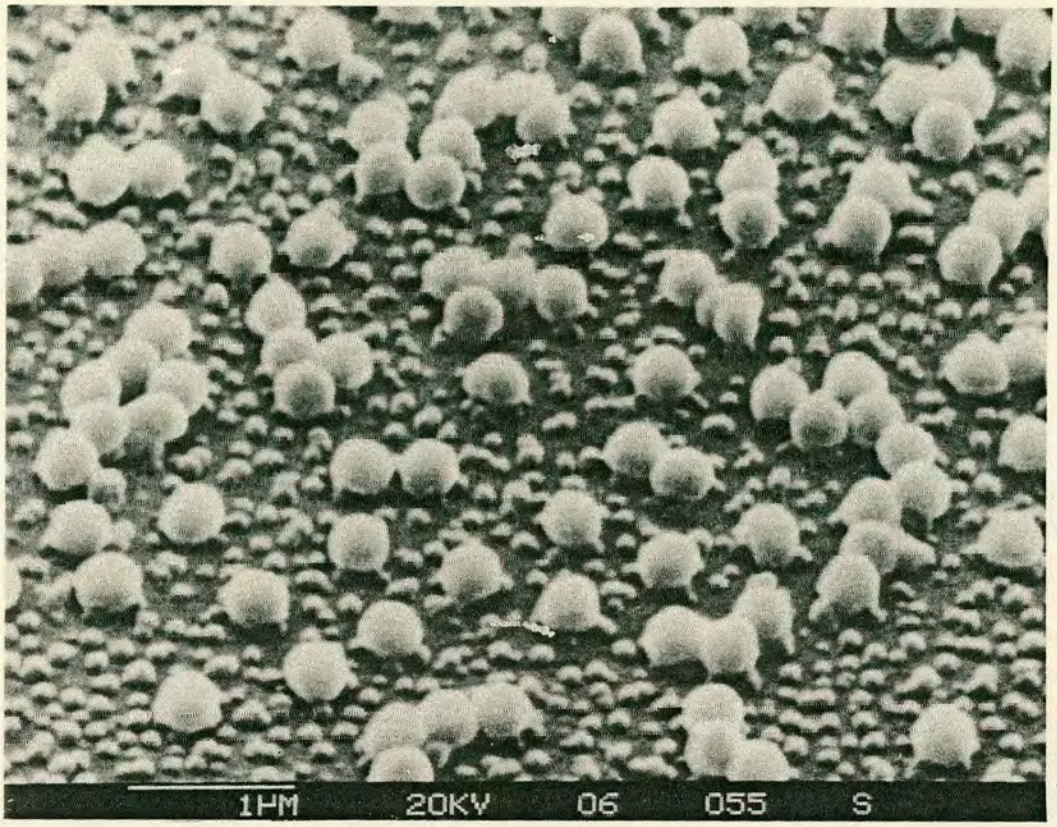

PLATE 4.4.4.5 BHA 100 ppm. POLYMER BATCH 103

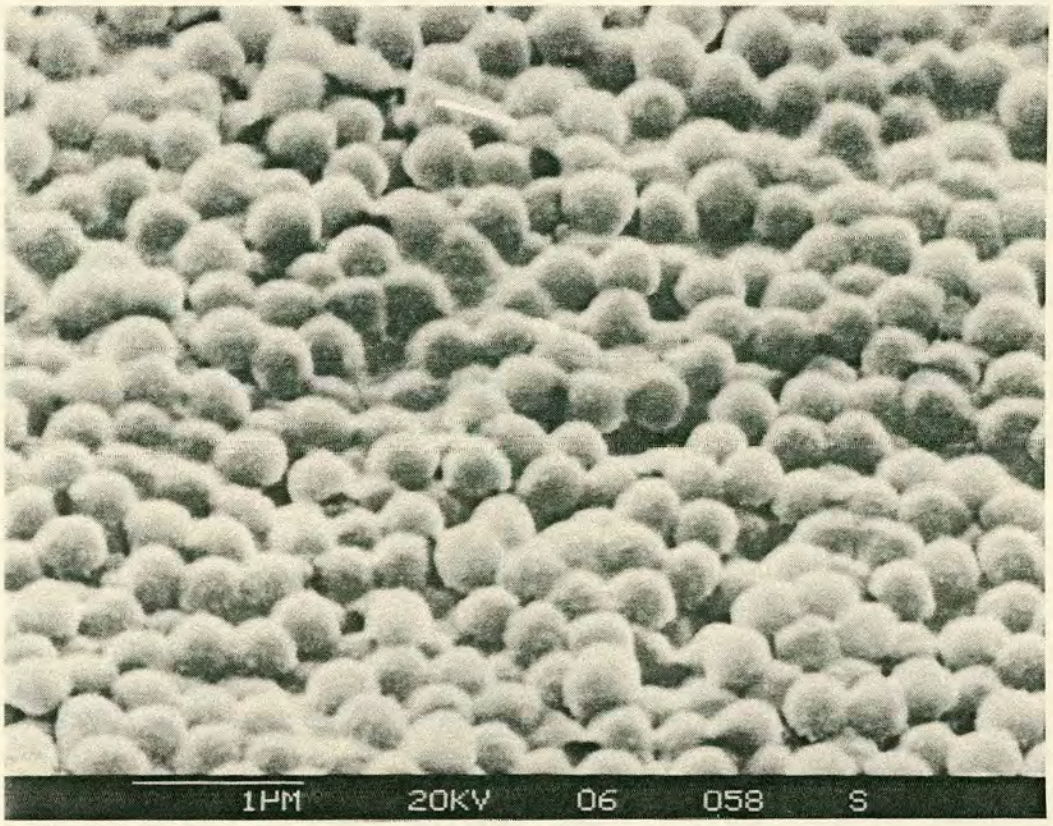

PLATE 4.4.4.6 BHA 100 ppm. POLYMER BATCH 103

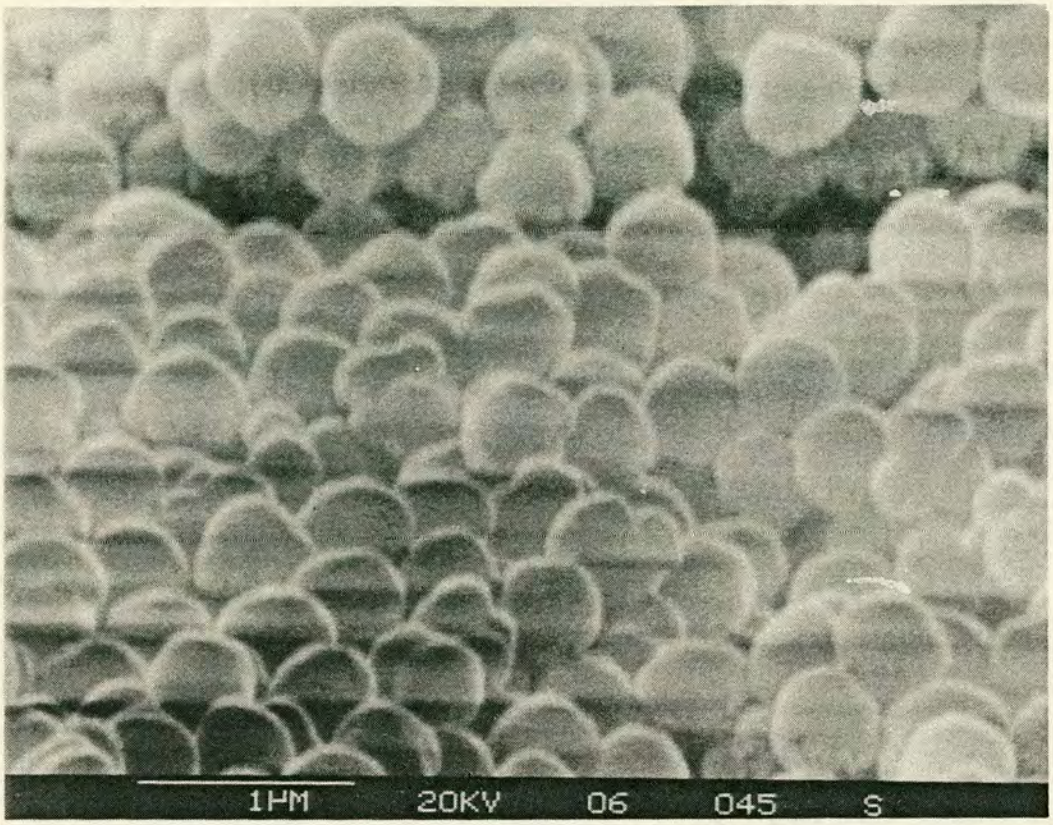

PLATE 4.4.4.7 BHA 100 ppm. POLYMER BATCH 100

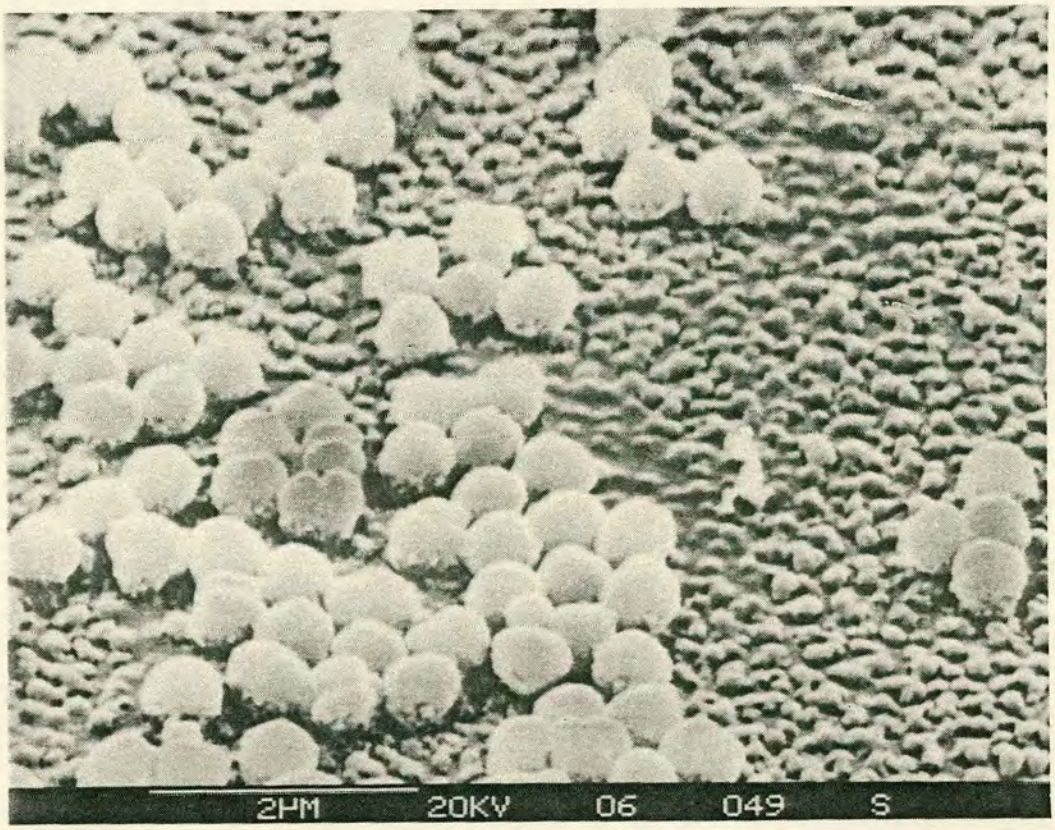

PLATE 4.4.4.8 BHA 100 ppm. POLYMER BATCH 100

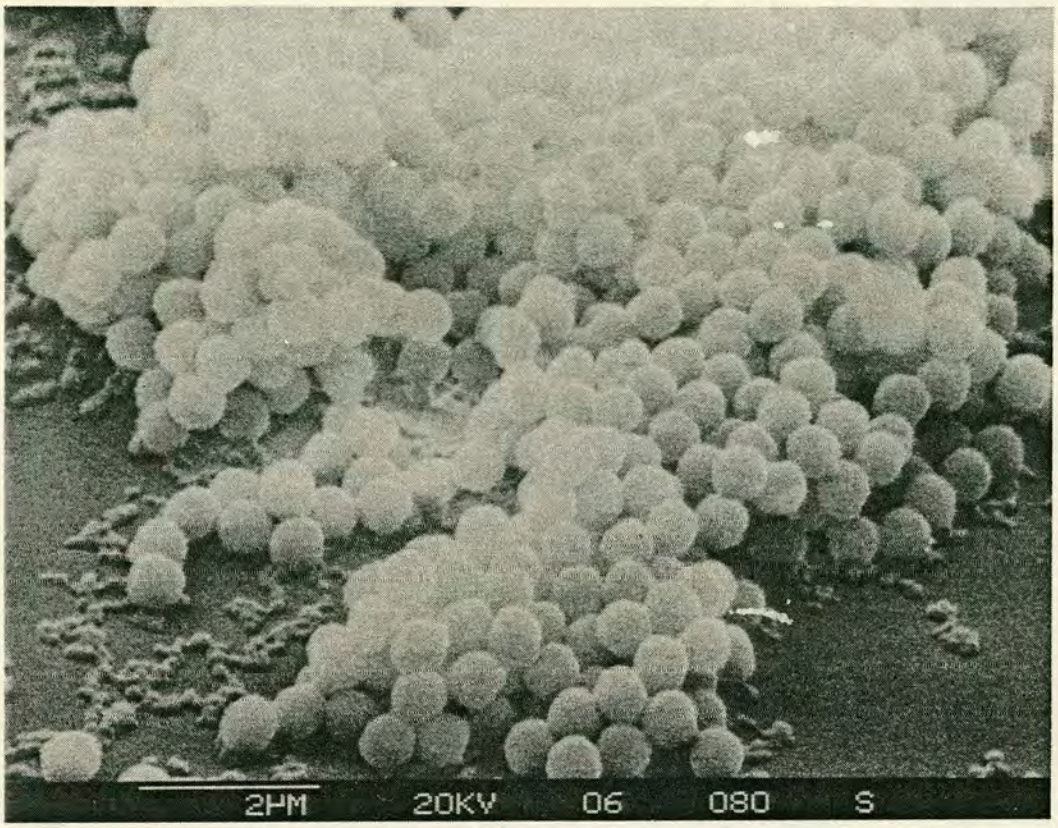

PLATE 4.4.4.9 BHA 100 ppm. POLYMER BATCH 109

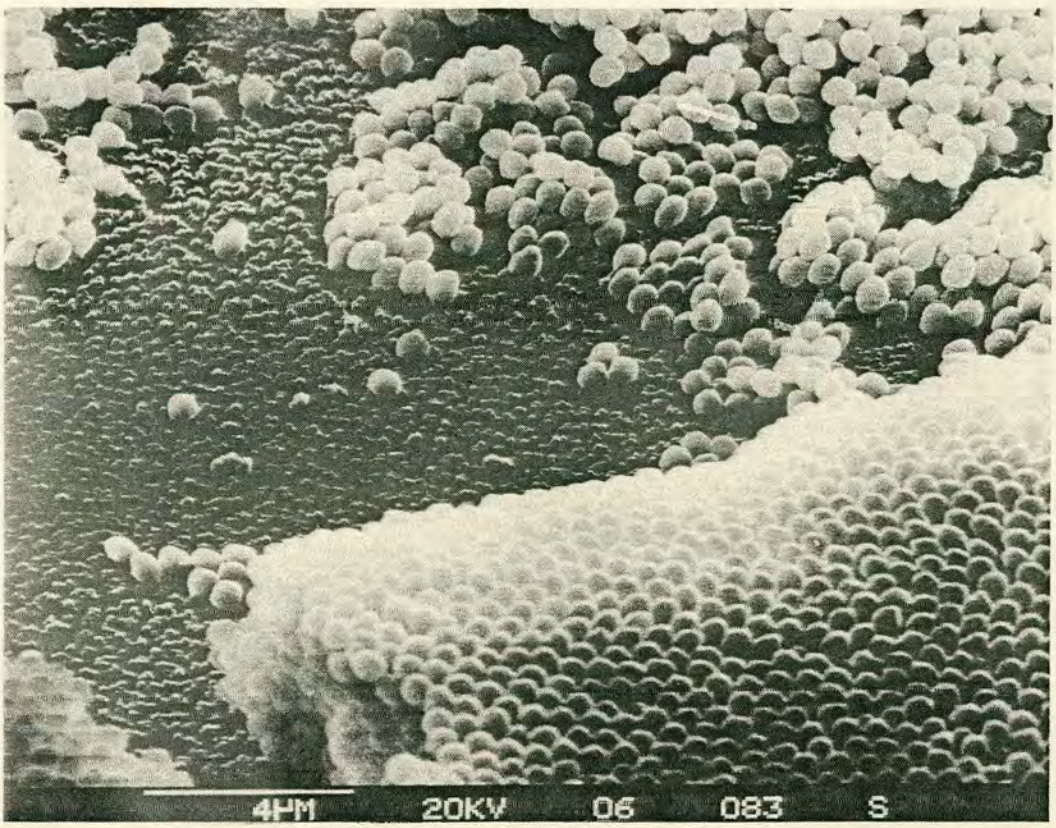

PLATE 4.4.4.10 BHA 100 ppm. POLYMER BATCH 109

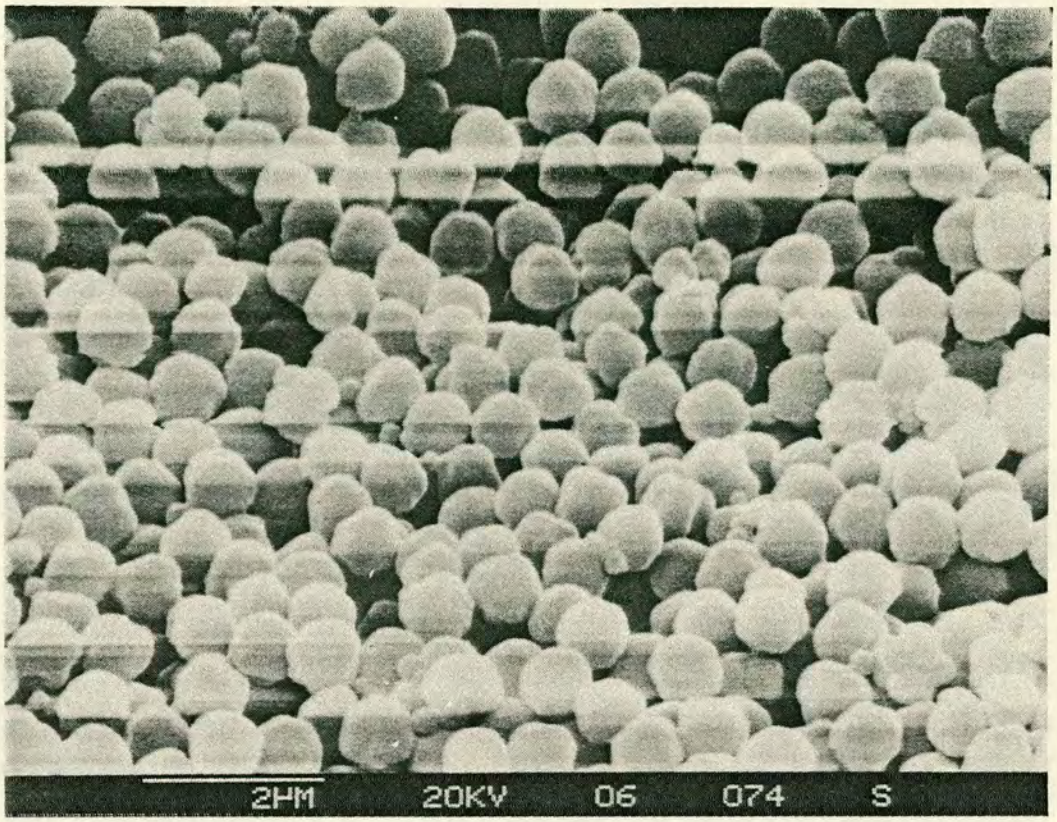

PLATE 4.4.4.11 BHA 100 ppm. POLYMER BATCH 107

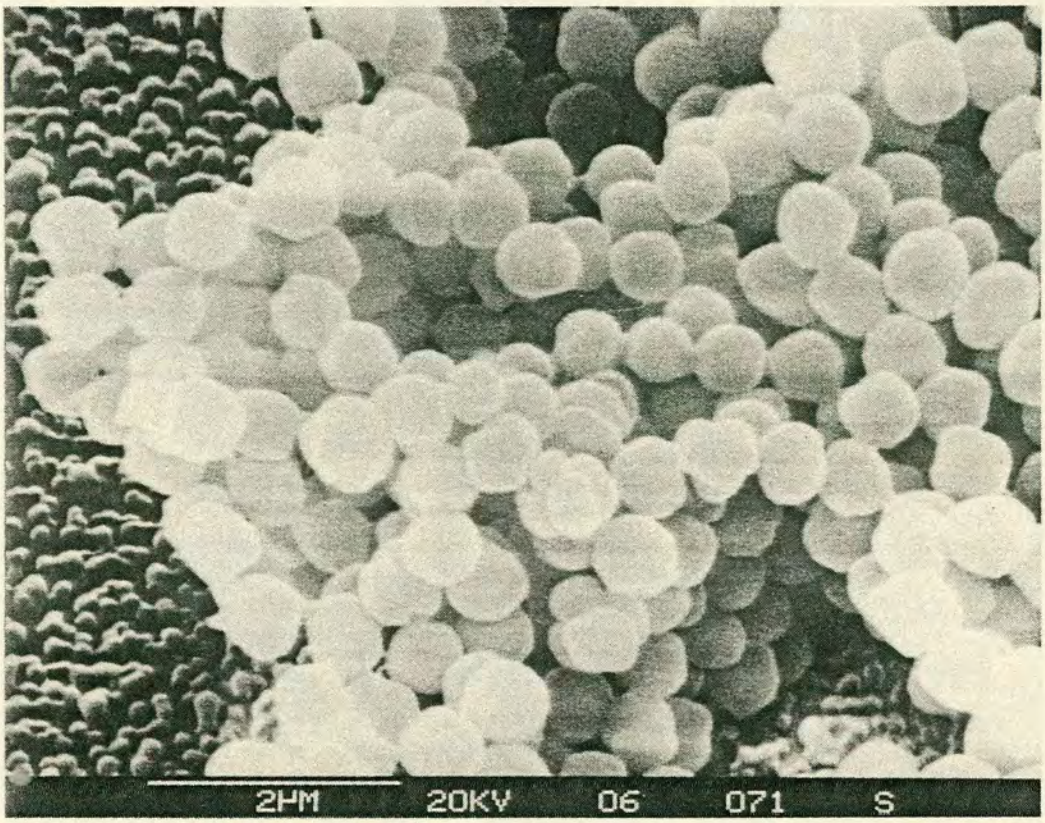

PLATE 4.4.4.12 BHA 100 ppm. POLYMER BATCH 107

Table 4.4.4.2. Polymerisation and shrunken particle size data for polymerisations of 323 K containing 100 ppm bis-(2-hyroxyethyl)-aminohexadecane.

Batch No.	Conversion percent (wt/vol)	Overall diameter mean & std. deviation		Primary diameter mean & std. deviation		Secondary diameter mean & std. deviation	
		Dn/μm σn/μm	Dv/μm σv/μm	Dn/μm σn/μm	Dv/μm σv/μm	Dn/μm σn/μm	Dv/μm σv/μm
99	0.15	0.152 0.053	0.190 0.034	0.176 0.031	0.192 0.038	0.070 0.018	0.081 0.015
106	0.39	0.202 0.091	0.290 0.061	0.275 0.046	0.299 0.049	0.111 0.031	0.134 0.028
103	0.70	0.262 0.127	0.366 0.052	0.355 0.042	0.370 0.042	0.106 0.039	0.152 0.047
110	0.96	0.289 0.138	0.399 0.059	0.385 0.048	0.403 0.049	0.110 0.034	0.141 0.038
100	2.39	0.407 0.179	0.537 0.077	0.509 0.076	0.540 0.069	0.136 0.038	0.163 0.032
109	2.90	0.395 0.206	0.562 0.076	0.537 0.074	0.565 0.066	0.126 0.033	0.152 0.037
107	3.99	0.438 0.290	0.743 0.111	0.702 0.106	0.747 0.096	0.144 0.038	0.174 0.042

BHA). Details of the various polymer batches and results of the image analysis are tabulated in Table 4.4.4.2.

Particle size analysis of the PVC dispersions produced indicated that two types of particles form in the presence of bis-(2-hydroxyethyl)-aminohexadecane. The majority of particles appear to grow uniformly without coagulating to form the 13 particle primary particle clusters observed in polymerisations in the absence of stabiliser. These spherical particles were observed to remain as separate entities up to 4% (wt/vol) monomer conversion, the maximum conversion possible with this type of apparatus. At this conversion the primary particles had attained a shrunken diameter of 0.75 μm, approximately 5 times the diameter observed in polymerisations without a primary particle stabiliser. See Figure 4.4.4.2.

Far fewer particles (about 1%) were found to be of a secondary type. These particles exhibited a mean diameter of approximately 0.15 μm and did not appear to grow significantly over the polymerisation range investigated. See Figure 4.4.4.2. Several mechanisms for their appearance can be suggested; Boisell and Fischer (26), working on the bulk polymerisation of VCM, found evidence of a secondary nucleation stage. Perhaps these smaller particles observed here arise from such a secondary nucleation. Alternatively, these particles may have originated from normal primary particles whose radicals became poisoned or chain transferred from the PVC

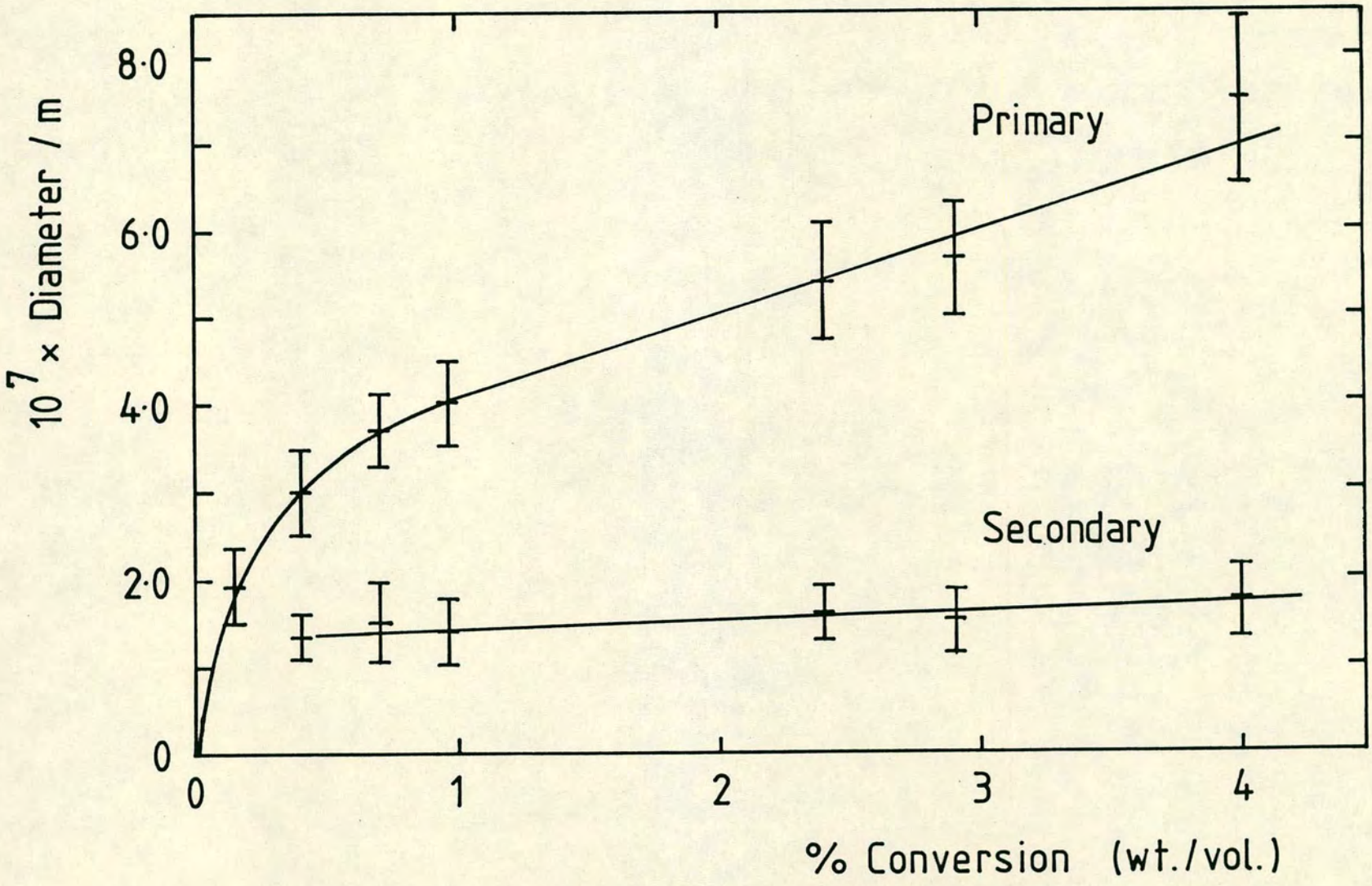

Fig. 4.4.4.2 Particle diameter (shrunken Dv) as a function of monomer conversion for polymerisations containing 100 ppm BHA.

particle to the monomer. This would leave a stable but "dead" polymer particle which would not increase in size. A third mechanism can be proposed in which the initial flux of primary particles consume all the stabilising additive, leaving, in effect, a normal polymerisation in which secondary particles would carry a much lower charge and coagulate at the previously determined shrunken diameter of about 0.15 μm. This would result in the formation of the primary particle aggregates as were shown to exist in section 4.2.2. Some evidence for this type of structure can be observed in the micrographs, amongst the predominately spherical primary particles.

By investigating the primary particle concentration during polymerisation, it was confirmed that, unlike Span-20, the mechanism by which bis-(2-hydroxyethyl)-amino hexadecane modified the electrostatic charge on the particles, was not through a change in primary particle concentration.

Using the procedure described in section 4.2.4, the primary particle concentration was found to remain reasonably level at $2.3 \pm 0.4 \times 10^{17}$ m^{-3} for polymerisations containing 100 ppm stabiliser. This compares favourably with the value of 3×10^{17} m^{-3} found in the absence of stabiliser. Thus the increased electrostatic charge on the particles cannot simply be explained in terms of modifying the particle concentration. The mechanism by which bis-(2-hydroxyethyl) aminohexadecane increases the particle charge and hence

primary particle stability has not yet been elucidated. It has however been reported (170) that this primary particle stabilizer does affect the bulk properties of large scale VCM polymerisations, resulting in both increased polymer porosity and hot and cold plasticiser adsorption. These properties are lost if the hydroxyl group is removed from bis-(2-hydroxyethyl)-aminohexadecane. This suggests a method by which the charge producing species could be identified. By systematically varying the constituents of this low molecular mass additive it may be possible to determine the active functional groups responsible for the increase in electrostatic charge on the primary particles. From this type of investigation optimised primary particle stabilisers could be synthesised.

4.5 VCM polymerisation reaction kinetics.

4.5.1 Introduction.

Polymerisation temperature and initiator concentration are known to affect the granule morphology of PVC. This final section discusses the results of kinetic studies on the polymerisations carried out during this study. It also provides the foundations for further investigations of the influence of reaction kinetics on polymer morphology.

Sanderson (1) has illustrated the effect of polymerisation temperature on the PVC granules, showing that as the reaction temperature of the suspension

polymerisation is increased from 323 K to 343 K the porosity of the granules decreases from about 30% to less than 10%. Although lowering polymerisation temperature may appear, at first sight, a method of increasing granule porosity, it is found that the molecular mass of the polymer produced is inversely proportional to temperature. Thus, when all reaction variables, other than temperature, are constant polymerisations at lower temperatures yield only high molecular mass polymers.

Carenza et. al. (43) have investigated PVC particle morphology at 323 K and 343 K in small scale bulk polymerisations. They report that at the lower temperature the coagulation of spherical particles to form a primary particle aggregate occurs, but at the higher temperature no transition was observed. This was interpreted as arising from a higher plasticisation level of the polymer particles favouring a coalescence process of the agglomerated units.

Bort et. al. (36) have investigated the correlation between PVC particle morphology and polymerisation parameters. A progressive decrease in size and structural complexity of the primary particle aggregate was found at increasing initiator concentration or temperature. This was accounted for by a mechanism in which the occurrence of a flocculation process became less probable the more rapidly the particle size increased.

From these two examples it can be seen that the

rate of polymerisation plays an important role in the development of a particulate structure in the PVC granule. To investigate whether the morphological changes, brought about by the low molecular mass additives, were an artifact of modifying rate of polymerisation, kinetic studies were performed for each of the reaction conditions studied.

4.5.2 Calculation of polymerisation rates.

The kinetics of VCM polymerisation are complex, the various models proposed having been reviewed in Chapter 1. Fortunately the initial stage of VCM polymerisation follows first order kinetics (171), the auto-acceleration effect only becoming significant at monomer conversions higher than 8% conversion. For first order reaction kinetics

$$\frac{-d[VCM]}{dt} = k[VCM] \qquad (4.5.5.1)$$

which on integration yields

$$\ln [VCM_o]/[VCM] = kt \qquad (4.5.5.2)$$

where $[VCM_o]$ is the initial concentration of VCM at time, t, and k is the rate of reaction.

Using graphical procedures a plot of $\ln[VCM_o]/[VCM]$ against t should, if first order kinetics apply, yield a straight line of gradient k. The concentration of VCM at

Table 4.5.2.1 Summary of kinetic data for polymerisations at 323 K containing 0.1% (wt/vol) lauroyl peroxide

Batch No.	% Conversion (wt/vol)	Polymerisation time/s	10^3 x ln([VCM_o]/(VCM]
23	0.54	1200	4.73
24	0.96	2400	9.21
26	1.20	3600	11.79
27	0.24	600	1.53
29	1.60	4800	16.09
31	3.37	9600	35.36
32	2.03	6000	20.79
33	0.49	1200	4.12
36	2.71	7200	28.20
41	0.42	1200	3.41
58	0.89	1800	8.42
59	0.16	600	0.60
61	0.19	300	0.94
62	0.52	1200	4.52
66	0.78	2160	7.28
68	0.13	600	0.32
69	0.17	180	0.77
70	0.40	1200	3.22
71	0.16	1190	0.66

Table 4.5.2.1 Summary of kinetic data for polymerisations at 323 K containing 0.1% (wt/vol) lauroyl peroxide (cont.).

Batch No.	% Conversion (wt/vol)	Polymerisation time/s	10^3 x ln([VCM_o]/(VCM]
105	0.75	2430	6.90
132	2.05	7200	21.01
133	1.01	3600	9.73
134	0.19	600	1.00
151	0.16	600	0.66
152	0.13	300	0.28
153	0.29	900	2.02

time, t, was calculated from the mass of polymer extracted less the mass of initiator and any additive included in the polymerisation.

Table 4.5.2.1 records the polymerisation data for polymer batches produced at 323 K containing 0.1% (wt/vol) lauroyl peroxide. The first order kinetic plots are shown in Figure 4.5.2.1; for polymer batches up to 96, 97 onwards, and for all polymer batches. A slight decrease in rate of polymerisation was noted for polymer batches 97 onwards, which coincided with the replacement of the polymerisation limb on Quartz cell mark 8. Examination of Figure 4.5.2.1 reveals straight line plots confirming first order reaction kinetics. The calculated rates of polymerisation at 323 K containing 0.1% (wt/vol) initiator are given in Table 4.5.2.2.

Table 4.5.2.2 Polymerisation rates for reactions at 323 K containing 0.1% (wt/vol) initiator.

Polymer Batch	10^6 x k / s^{-1}
Up to batch 96	3.74 ± 0.09
Batch 97 onwards	3.02 ± 0.05
Overall	3.59 ± 0.12

The initial rate compares favourably with the value

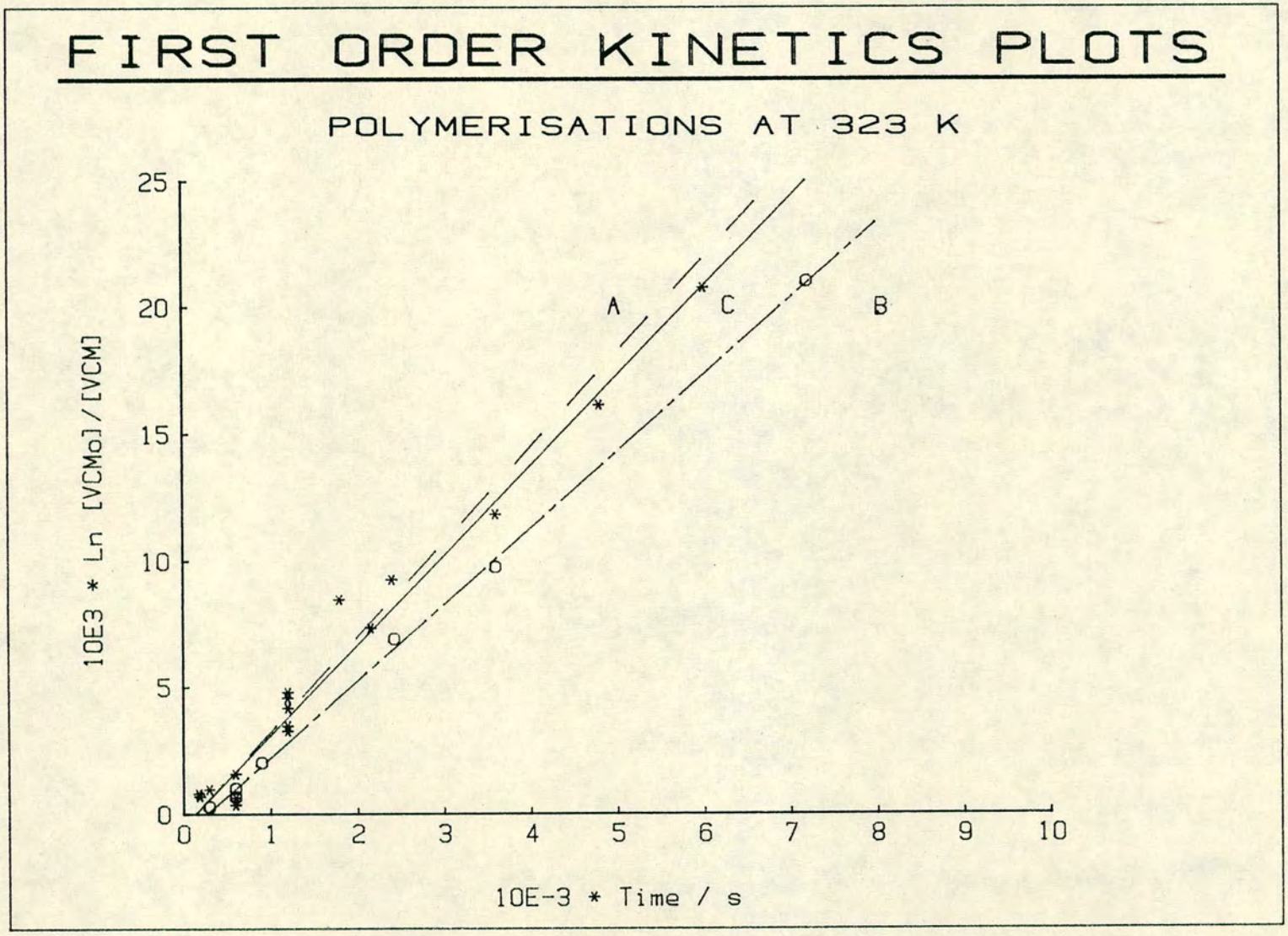

KEY

A = UP TO BATCH 96

B = BATCH 97 ONWARDS

C = ALL BATCHES

BEST FIT LINES SHOWN FOR ALL DATA

Figure 4.5.2.1

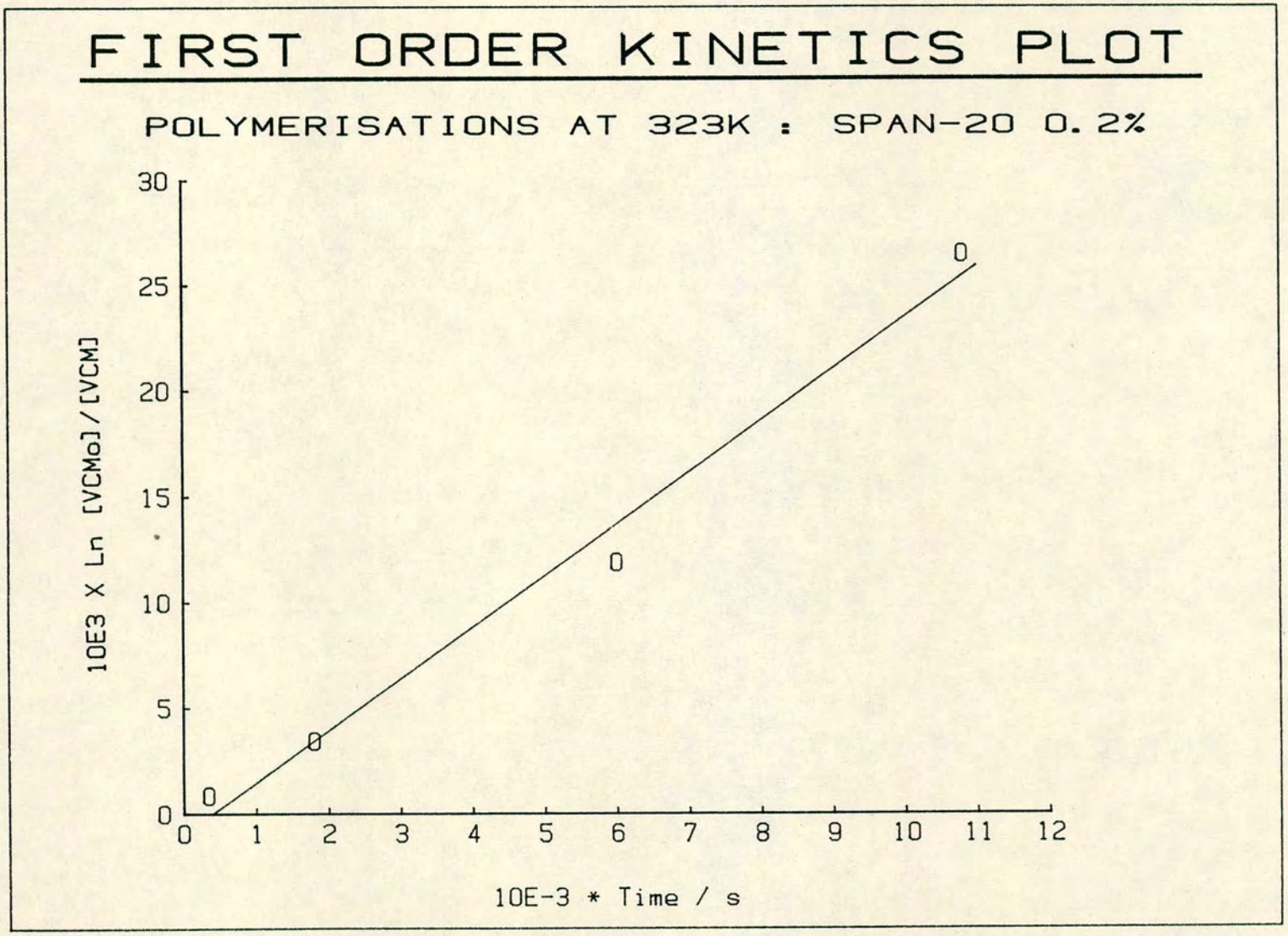
FIRST ORDER KINETICS PLOT
POLYMERISATIONS AT 323K : SPAN-20 0.2%
10E3 X Ln [VCMo]/[VCM]
30
25
20
15
10
5
0
0
1
2
3
4
5
6
7
8
9
10
11
12
10E-3 * Time / s

Figure 4.5.2.2

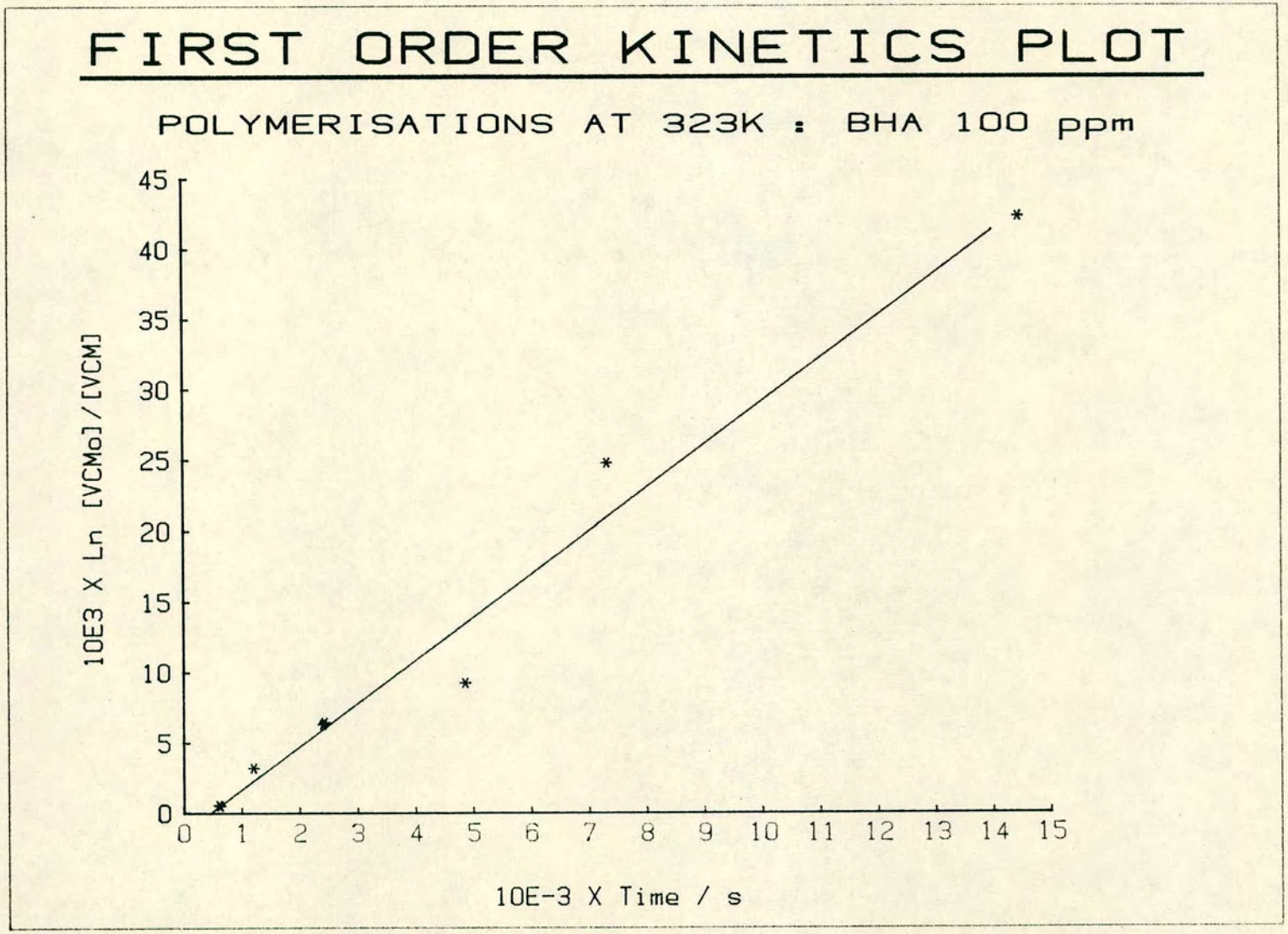
FIRST ORDER KINETICS PLOT
POLYMERISATIONS AT 323K : BHA 100 ppm
10E3 X Ln [VCMo]/[VCM]
0
5
10
15
20
25
30
35
40
45
0 1 2 3 4 5 6 7 8 9 10 11 12 13 14 15
10E-3 X Time / s

Figure 4.5.2.3

of 3.80×10^{-6} s^{-1} quoted by Rance and Zichy (42).

For polymerisations containing Span-20 (0.2% (vol/vol)) the relevant polymerisation data and kinetics plot are given in Table 4.5.2.3 and Figure 4.5.2.2 respectively. Assuming first order reaction kinetics, a polymerisation rate of $(2.46 \pm 0.14) \times 10^{-6}$ s^{-1} was found. This value is significantly lower than in the absence of Span-20. This rate reduction may have arisen from Span-20 taking part in a radical termination step or following the mechanism of Cotman (20) the early coagulation of the small primary particles could have resulted in radical occlusion and a subsequent reduction in polymerisation rate. This proposal could be checked by determining whether the rate remains dependent on the square root of the initiator concentration in the presence of Span-20.

Table 4.5.2.3 Summary of kinetic data for polymerisations at 323 K containing Span-20 at 0.2% (vol/vol).

Batch No.	% Conversion (wt/vol)	Polymerisation time/s	$10^3 \times \ln([VCM]/(VCM]$
114	0.38	345	0.81
115	1.39	6000	11.86
116	2.76	10800	26.43
138	0.62	1800	3.37

Table 4.5.2.4 Summary of kinetic data for polymerisations at 323 K containing bis-(2-hydroxyethyl)-aminohexadecane at 100 ppm.

Batch No.	% Conversion (wt/vol)	Polymerisation time/s	10^3 x ln([VCM_o]/(VCM]
96	0.14	624	0.45
99	0.15	610	0.53
100	0.12	7320	24.71
102	0.68	2400	6.23
103	0.70	2430	6.38
106	0.34	1200	3.13
107	3.99	14460	42.24
110	0.99	4860	9.17

The kinetic data for polymerisations at 323 K containing 100 ppm bis-(2-hydroxyethyl)-aminohexadecane are given in Table 4.5.2.4. The first order kinetic plot is linear and presented in Figure 4.5.2.3. The rate of polymerisation was determined from the gradient, $k = (3.05 \pm 0.19) \times 10^{-6}\ s^{-1}$. As these polymer batches were prepared in the new polymerisation limb this value compares well with the rate of $3.01 \times 10^{-6}\ s^{-1}$ found in the absence of stabiliser. It can therefore be concluded that a change in polymerisation rate was not responsible for the morphological changes observed on the addition of bis-(2-hydroxyethyl)-aminohexadecane.

Preliminary experiments were completed to allow an investigation of polymer morphology as initiator concentration and polymerisation temperatures were varied systematically. Guidelines for this are discussed in Section 4.8.

4.6 Summarising remarks.

The previous work of Speirs (58) at Edinburgh University laid the foundations for this study. The initial objective of this present C.A.S.E. Award was to confirm Speirs' finding that the PVC particles carried a net negative charge and, if possible, quantify the magnitude and sign of this charge as polymerisation conditions were systematically varied. The outcome of this study might indicate that the observed behaviour of

primary particle stability prior to the rapid onset of coagulation could be successfully explained in terms of electrostatic stabilisation. Then, by the addition of low molecular mass compounds, it was hoped that the magnitude of the charge on the primary particles could be varied to control the onset of primary particle aggregation. This control could then be utilised to produce a polymer with a wide variety of morphologies and lead to a PVC polymer with greater porosity and more consistent processing properties.

In this study at Edinburgh a combined polymerisation/electrophoresis cell has been evolved to overcome the previous difficulties in polymerisation, transference, dilution and measurement of the electrophoretic mobility of PVC particles dispersed in a liquified monomer. The observation of particle charge required designing a microelectrophoresis apparatus, constructed from quartz, capable of withstanding the autogeneous pressure of VCM at temperatures up to 343 K and yet still possess optical characteristics suitable for dark field microscopy.

The early stage of precipitation polymerisation of VCM has been elucidated by a combination of SEM microscopy and image analysis techniques. The morphological development of the particulate PVC structure has been revealed and illustrated in a series of micrographs as a function of monomer conversion (see Plates 4.2.3.1 to 4.2.3.12).

No photomicrographic evidence of the basic particles was obtained in this study. Under the conditions employed in this investigation, the coagulation of the basic particles to primary particles was estimated to occur within 10 to 20 seconds of initiating the polymerisation (42). Consequently, the first particles observed were already primary particles, the basic particles being too short lived to be detected.

Primary particles were found to be of a substantially spherical nature, with an initial concentration in the region of 3×10^{17} m^{-3}. This particle concentration was reduced rapidly once the primary particle diameter exceeded a mean critical size of 0.19 μm and coagulation occurred to form primary particle aggregates.

Analysis of the primary particle size distribution, within the primary particle aggregates, indicated that the aggregates only contain primary particles that have exceeded the critical primary particle diameter. This suggested that the smaller primary particles were indeed stable to coagulation until the critical diameter had been exceeded. The primary particle aggregates were observed to increase in size, reaching approximately 0.8 μm diameter at 2% (wt/vol) conversion.

It was confirmed that reliable electrophoresis could be performed on dispersions of primary particles in VCM in the combined polymerisation/electrophoresis cell. The particles remained net negatively charged throughout

the observable portion of the polymerisation. In addition, the number of charges per primary particle was found to remain reasonably constant throughout their lifespan, typical values being in the region of 16 to 20 charges per particle.

Theoretical calculations were performed to predict the stability behaviour of the primary particles at typical radius and charge found experimentally. It was found that the particle concentration effect was less important than previously thought (58). However, it was confirmed that the measured primary particle charge was sufficient to account for the known stability behaviour of the primary particles assuming purely electrostatic stabilisation. The actions of three potential low molecular mass monomer soluble additives were considered. Both Span-20 and bis-(2-hydroxyethyl)-aminohexadecane were found to modify the morphology of the PVC polymer produced. It was found that the rate of polymerisation was reduced in the presence of Span-20. This was accompanied by about a 30 fold increase in primary particle concentration and a near zero electrophoretic mobility. The primary particles were observed to aggregate much sooner in polymerisations containing Span-20, and this coincided with a reduction in the magnitude of the electrostatic charge on the PVC particles. It was concluded that one mechanism of controlling the morphology of commercially produced PVC polymer might be the modification of primary particle concentration and charge

by the addition of non-ionic low molecular mass monomer soluble compounds.

Bis-(2-hydroxyethyl)-aminohexadecane was discovered, at low treatment concentrations, not to significantly modify the rate of polymerisation or primary particle concentration. The colloidal events and structural development of PVC polymer in the presence of this additive have been elucidated and illustrated as a function of monomer conversion in Plates 4.4.4.1 to 4.4.4.12.

At 0.15% (wt/vol) monomer conversion the primary particles were found to be net negatively charged and to carry in the region of 45 elementary charges. These particles were observed to be stable to coagulation. At the highest monomer conversion possible, the primary particles attain a diameter in excess of 0.75 μm. No coagulation step was observed, unlike polymerisations carried out in the absence of polymer stabilisers. The increased electrostatic charge and primary particle stability could not be accounted for by a change in polymerisation rate nor decreased primary particle concentration. The origin of the extra charge on the particles has not been elucidated. However, the presence of the hydroxyl functional group has been reported to be necessary to bring about morphological changes in suspension polymerisations.

A mechanism for VCM bulk polymerisation, consistent with the above evidence must now be proposed, the results

of which will be directly applicable to the industrially more important suspension polymerisation (10).

4.7 Proposed mechanism for the precipitation polymerisation of VCM.

The morphogenesis of the VCM/PVC system comprises of three processes:-

a) Phase separation of swollen polymer gel particles from the VCM.
b) Multiple aggregation of the gel particles.
c) Growth of the gel by polymerisation.

Each of these occur simultaneously and interact to govern the life cycle of this two phase system from its phase separation to its ossification at around 40% conversion. The mechanism assumed for the morphogenesis of PVC during bulk or suspension polymerisation was outlined in section 1.2.

The decomposition of a VCM soluble free radical initiator produces two radicals, which by transfer to the monomer generates as many as 20 polymer chains each. These remain soluble in the monomer and grow until they contain roughly 10 monomer units and phase separate at about 0.001% conversion. The chains then coil with each other to form basic particles containing about 20 polymer chains. Assuming a degree of polymerisation of 1000 it has been estimated (42) that a basic particle would have a

diameter of 18 nm. These basic particles are colloidally unstable and continue to coagulate rapidly until a primary particle carrying sufficient surface charge to prevent further coagulation is formed. The subsequent colloidal stability of the primary particles then plays an important role in the processing properties of the final PVC product.

It is now necessary to augment this mechanism to account for the appearance of charged PVC particles and to rationalise the changes in polymer morphology which arise from modifying polymerisation conditions.

The origin of charge on the PVC particles is still the subject of speculation. Both Rance and Zichy (61) and Davidson and Witenhafer (60) have proposed that the most probable source of negatively charged ions in VCM at the start of polymerisation is chloride ions, which may specifically adsorb at the VCM/PVC interface. The chloride ions may be present either by the dehydrochlorination of PVC or from the hydrochloric acid produced through a side reaction. It has been shown (62) that residual oxygen present in the reactor readily reacts with VCM in the presence of radicals to produce vinyl chloride peroxide which subsequently decomposes to give hydrochloric acid as one of the products. Once all the oxygen has been consumed it was suggested that the ionic species present in the system (Cl^-,OH^-,H_3O^+ ions) will remain constant thus giving rise to a constant total charge to be distributed amongst the fixed number of PVC particles.

Further evidence to suggest that the chloride ion is responsible for the observed electrophoretic behaviour has been obtained (60) by an aqueous extraction of the charging species from initially stable particles produced in bulk polymerisation. This resulted in the aggregation of the particles and hydrochloric acid being detected in a suspension polymerisation. The charging species were not lost to the aqueous phase but retained by the pericellular membrane which surrounds the polymerising droplets.

An alternative explanation for the negative charge has been provided by Fowkes and Heilscher (63) in terms of "anion states" on the polymer resulting from electron injection from "donor states" of the surrounding medium.

Rance and Zichy (42) have proposed a mechanism similar to that of Fitch (53) for the formation of primary particles from basic particles. It is assumed that polymer is generated continuously in the early stages of polymerisation as a flux of basic particles. Two fates are available to the newly formed basic particle, it may either a) be captured by an existing primary particle or b) become the nucleus of a new primary particle. In the absence of any mechanism to confer colloidal stability to the basic particles they coagulate according to the Smoluchowski rate equation. In the initial stage of the polymerisation it is probable that the number of basic particles exceeds the available negative charge. The majority of basic particles are thus uncharged and coagulation of basics occurs rapidly to form aggregates

which increase in size with time to form primary particles. Eventually coagulation increases the average total charge per particle to a level sufficient to prevent coagulation with similarly charged particles, although coagulation with smaller, less highly charged particles, will still occur.

An equilibrium number of stable primary particles is formed within the first 10 to 20 seconds of polymerisation (42). The primary particles then grow at a constant charge and increase in size by the polymerisation of the monomer inside the gel phase and by the accretion of basic particles onto its surface. Eventually, at a critical primary particle radius, approximately 0.1 μm in the absence of stabilisers, the particle surface charge becomes too diffuse to confer stability and the primary particle coagulates to form the 13 particle primary particle aggregates observed in Plate 4.2.2.9.

Zichy (9) has considered particle stability as a function of particle growth in the initial stages of VCM polymerisation. The majority of basic particles when first formed, carry no charge, are therefore unstable and rapidly coagulate to give stable primary particles. These grow at constant total charge and exist in the stable region of their lifespan. Eventually the critical size is exceeded and the primary particles enter an unstable region in which the primary particle aggregates form by coagulation. This idealised mechanism is however, only strictly valid for monodisperse particle populations. As

was observed in this study, where the particle size distribution has a finite width, the individual aggregation steps run into each other resulting in both primary and primary particle aggregates existing simultaneously at low conversions. The stability of the clusters against coagulation between themselves is thought to arise from the fact that they can only make a few contacts of small area rather than from elecrostatic repulsion (42). The aggregates continue to grow by polymerisation and at around 40% conversion they lock into a continuum.

From this proposed mechanism it is apparent that, in the absence of added stabilisers, the total charge available to the system is the major factor controlling the stability of the PVC particles dispersed in the monomer. Two extremes can be considered. If the total charge available to the dispersion was high, the coagulation of basic particles to form primary particles would cease early in the polymerisation, giving rise to a high concentration of small primary particles. According to Speirs (58) the particle concentration effect would then exert a greater destabilising influence on the growing primary particles and coagulation would occur at a small particle size. Conversely, if the total charge in the system is low, extensive coagulation of basic particles would be required before the primary particles carried a sufficient charge for stability, so that a smaller concentration of particles would be formed. These

would then remain stable to a greater diameter before coagulating to form primary particle aggregates.

This proposed mechanism appears to be consistant with the experimentally observed morphogenesis of the VCM/PVC system in the absence of low molecular mass monomer soluble additives. It has not been possible to test this proposed mechanism further by the modification of total charge in the system through the addition of low molecular mass stabilisers. Although these additives have a significant influence on polymer morphology, which appears to be consistant with electrostatic stabilisation, they affect too many other polymerisation parameters to allow unequivocal proof of the mechanism. This would be better achieved by varying the levels of the proposed charging species, (Cl^-,OH^-) for example by the addition of hydrogen chloride gas, as discussed in the next section.

The influence of steric stabilistion on the stability of the nascent PVC particles in the absence of added particle stabilisers has been considered by several investigators (60) (155) (58) to be unimportant. None of the work described in this thesis can provide any evidence on the possible extent of any steric factors during the precipitation polymerisation of VCM. It has however shown that the observed stability behaviour can be adequately accounted for on the basis of an electrostatic mechanism alone.

The particle generation and charging mechanism for the low molecular mass polymers is less clear. In the case

of Span-20 the primary particle concentration was increased 30 fold over that observed in the absence of additives. It is known that Span-20 acts as a VCM initiator and thus two sources of basic particles result which increase the concentration of primary particles produced. The mechanism by which this occurs is open to conjecture, as no experimental evidence at this earliest stage of the polymerisation could be obtained using the present technique. A mechanism involving electrostatic stabilisation could however account for the early loss of primary particle stability if it is assumed that the non-ionic Span-20 does not contribute to the total charge in the system. An even distribution of the charge amongst more particles would reduce the level of electrostatic stabilisation. Particles would then aggregate at a small size at an early stage in the polymerisation.

For polymerisations containing bis-(2-hydroxyethyl) aminohexadecane, again the mechanism of particle formation is unclear. Here, the particles were found to exhibit increased colloid stability and this coincided with a higher number of charges per particle, again indicating the possible role of electrostatic stabilisation within the system.

To elucidate the mechanism of particle formation in the presence of low molecular mass monomer soluble additives a technique suitable for the investigation of the phase separation stage of the polymerisation is required. Possible options will be discussed in section

4.8. Although a detailed mechanism for the generation of charged primary particles cannot be given for polymerisations carried out in the presence of low molecular mass additives, this investigation has revealed methods of controlling the morphogenesis of PVC polymer which could potentially be used to modify the processing properties of commercially produced PVC.

In the industrial suspension polymerisation the control of the macroscopic polymer morphology is now fairly well understood (52). Subtle changes in the amount and type of suspending agent present and the degree of agitation (47) are used to produce polymers to a wide variety of bulk polymer properties. Some properties however, for example, surface area, porosity and processing characteristics appear to be independent of granule morphology and result from the submicroscopic structures within the granule. Methods of controlling these properties are much less well understood and, clearly, a greater insight into this area was desirable. The work described in this thesis was aimed at obtaining a more rational control over the micro and submicroscopic structures within the granule by controlling the colloidal stability of the growing polymer particles. Methods of modifying the stability of nascent PVC particles have been illustrated in this study.

In the absence of additives, it is proposed that the stability behaviour of the polymer particles is controlled by the total charge available within the

suspension droplets, and that the charging species are generated from side reactions involving residual oxygen (62) remaining in the reactor vessel after purging. By controlling the available charge it should therefore be possible to maximise the porosity of the polymer granule. Mechanisms by which this could be achieved have been proposed (58) and involved either a tighter control of residual oxygen levels or the introduction of small quantities of HCl gas with the monomer during the charging of the reactor.

Monomer soluble low molecular mass additives have been shown to drastically alter the morphology of the structures within the PVC granule. In this study the use of a non-ionic material resulted in the early coagulation of the primary particles yielding a highly aggregated polymer consisting of small particles. Conversely, the addition of bis-(2-hydroxyethyl)-aminohexadecane increased the electrostatic charge on the particles resulting in extremely stable primary particles which, over the permissible conversion range, did not appear to coagulate.

Using these types of techniques, control of the final granule morphology should be possible in the industrial process. However, the ideal stability behaviour to give optimum processing properties and allow the rapid degassing of residual toxic monomer is not yet apparent. This situation can only be resolved by performing carefully controlled polymerisations on a scale sufficient to produce enough polymer for porosity determinations.

The proposed mechanism to account for the origin of charge and action of low molecular mass additives, is unlikely to be complete. Due to the lack of experimental evidence some of the suggestions are necessarily tentative in nature. Nevertheless, considerable progress has been made in unravelling the complex nature of the initial stage of the VCM precipitation polymerisation. For example the morphological development of the primary particle cluster is now well documented and the original conjectures of Zichy (9) on primary particle stability have been shown to be correct. Suggestions for further work to enable a greater understanding of this industrially important area are discussed below.

4.8 Suggestions for future work.

4.8.1 Equipment

The apparatus evolved for this type of investigation has now been developed to provide a reliable pressure-tight combined polymerisation/electrophoresis cell. Only one further modification is considered necessary, that being a valve between the polymerisation limb and the electrophoresis cell to prevent unwanted distillation of monomer during polymerisation and, more importantly, allow the sampling of the PVC produced prior to electrophoresis.

The major disadvantage of the present technique is the time consumed in using a batch technique in which

dispersions can only be evaluated at one monomer conversion per polymerisation. If further work was invisaged on this topic I recommend that the present polymerisation/electrophoresis apparatus be abandoned in favour of a laser based combined electrophoresis/particle size apparatus such as the Malvern Particle Charge instrument. This would revolutionarise the investigations enabling continuous monitoring of both particle size and zeta potential. Such a system, once a suitable high pressure quartz cell had been constructed, would have the following advantages:-

a) Continuous particle sizing from the nanometer sized basics upwards. This was impossible with the SEM technique.

b) Continuous particle mobility measurements enabling particle charge to be measured as a function of extent of polymerisation.

c) Expand the observation window for both a and b.

d) Particle concentrations could be calculated accurately and continuously.

e) The onset of particle flocculation, critical primary particle size and an experimental stability ratio could be evaluated for each polymerisation.

The major advantage would however be the continuous measurement of polymerisation properties, eliminating the need for a batch process. This would allow the rapid

assessment of potential primary particle stabilisers, and enable studies as a function of polymerisation temperature

The current monomer purification and transfer arrangement worked well in this study and could be used without further refinement.

4.8.2 Experimental programme

Once the apparatus described above was commissioned evaluation of the colloidal aspects VCM/PVC system could follow several interesting pathways.

Bauer and Sabel (62) have indicated that certain free radical initiators generate a much higher concentration of HCl than lauroyl peroxide used in this study. By investigating a range of initiators it might be possible to elucidate the role of the chloride ion in the electrostatic stabilisation of PVC dispersions. It would also be interesting to carry out a study of polymerisations initiated in the absence of a monomer soluble initiator. This could be achieved by using a gamma ray Cobalt-60 source (43) or photochemical initiation. This would indicate whether the decomposition of the initiator molecule was involved in the generation of the charging species.

In this investigation the range of monomer soluble low molecular mass additives which could be evaluated was limited. With all the polymerisation parameters being available from a single experiment a far wider range of

additives could be assessed. Suitable candidate molecules could then be systematically modified, one functional group at a time, to elucidate the active components in terms of both modification of particle charge, and polymer morphology. Bis-(2-hydroxyethyl)-aminohexadecane would be a good starting point for this investigation as it is known that the molecule is rendered inactive if the hydroxyl group is absent (170).

It is known that the polymerisation temperature (1) influences the morphogenesis of the PVC granule. In any further investigation the polymerisation temperature should be raised to 333 K and the initiator concentration reduced to reproduce the same polymerisation kinetics studied at 323 K. The concentration of initiator required to achieve this is 0.022% (wt/vol) based on the known square root dependence on initiator concentration on polymerisation rate. Under these conditions, polymer is generated at the same rate as in the lower temperature polymerisations reported in this thesis. The influence of higher temperature but reduced initiator concentration on the colloidal aspects of PVC morphogenesis could then be assessed.

Finally it would be of interest to carry out polymerisations on a sufficiently large scale to enable porosity and plasticiser uptake studies. From these it would be possible to derive the optimum requirement for the colloidal events occurring in the initial stage of the VCM precipitation polymerisation.

References

1. A. K. Sanderson, The Brit. Polymer Journal, 1980, 12, 186.

2. D. V. Derjaguin and L. Landau, Acta Physiochem. U.R.S.S.,1941, 14, 633.

3. E. J. W. Verwey and J. Th. G. Overbeek, Theory of the Stability of Lyopohobic Colloids, Elsevier, Amsterdam, 1948.

4. G. Butters, ed., Particulate Nature of PVC; Formation Structure and Processing, Applied Science Publisers, 1982.

5. R. H. Burgees, ed., Manufacturing and Processing of PVC, Applied Science Publishers, 1982.

6. Pechiney-St. Gobain, Brit. Patent, 842690, 27th. July, 1960.

7. M. W. Allsopp, J. Macromol Sci.- Chem., 1977, A11(7), 1223.

8. P. H. Giel, J. Macromol Sci.- Phys., 1977, B14(1), 171.

9. E. L. Zichy, J. Macromol Sci.- Chem., 1977, A11, 1205.

10. A. Crosato - Arnaldi, P. Gasparini and G. Talamini, Makromol. Chem., 1968, 117, 140.

11. S. I. Kuchanov and D. N. Bort, Polymer Sci. (U.S.S.R.), 1973, 15, 2712.

12. R. G. W. Norrish and R. Smith, Nature, 1942, 150, 336.

13. W.J. Bengough and R. G. W. Norrish, Nature, 1949, 163, 325.

14. W. J. Bengough and R. G. W. Norrish, Proc. Roy. Soc., 1950, A200, 301.

15. J. Prat, Mem. Serv. Chim. Etat. (Paris), 1946, 32, 319.

16. J. Prat, C. R. J. Int. Plast., 1949, 58,

17. A. N. Levin and G. L. Fabrikant, Khimich. prom-st', 1947, 2, 48.

18. E. Jenckel, H. E. Eckmans and B. Rumbach, Makromolek. Chem., 1949, 4, 36.

19. H. S. Mickley, A. S. Michaels and A. L. Moore, J. Polymer Sci., 1962, 60, 121.

20. J. D. Cotman, H. M. F. Gonzales and G. C. Claver, J. Polymer Sci., Part A-1, Polymer Ciem., 1967, 5, 1137.

21. A. H. Abdel - Alim and A. E. Hamielec, J. Appl. Polym. Sci., 1972, 16, 783.

22. J. Ugelstad, H. Flogstad, T. Hertzberg and E. Sund, Makromol. Chem., 1973, 164, 171.

23. J. Ugelstad, J. Macromol. Sci. - Chem., 1977, A11, 1281.

24. O. F. Olaj, Angew. Makromol. Chem., 1975, 1, 47.

25. O. F. Olaj, J. Macromol. Sci. - Chem., 1977, A11, 1307.

26. J. Boisell and N. Fischer, J. Macromol. Sci., 1977, A11(7), 1249.

27. J. Ugelstad, P. C. Mork, F. K. Hanson, K. H. Kaggerud and T. Ellingoen, Pure Appl. Chem., 1981, 53, 323.

28. V. V. Kafarov, J. N. Dorokhov, H. Bulle and L. A. Artamonova, Doklady Akadem. Nauk (S.S.S.R.), 1978, 238, 380.

29. R. Thiele, J. Nelles and D. Rauchstein, Plaste und Kautschuk, 1978, 7, 395.

30. H. Bulle, W. Neumann, J. Schulz and R. Meinhard, Faserforsch. und Textiltechn., 1977, 28, 265.

31. W. H. Ray and S. K. Jain, J. Appl. Polym. Chem., 1975, 19, 1297.

32. H. Muller, Kolloid - Z., 1926, 38, 1.

33. V. A. Kargin, D. N. Bort, B. P. Shtarkman and K. S. Minsker, Polymer Sci. (U.S.S.R.), 1964, 6, 218.

34. D. N. Bort, Ye. Ye. Rylov, N. A. Okladnov, B. P. Shtarkman and V. A. Kargin, Polymer Sci. (U.S.S.R.), 1965, 7, 50.

35. D. N. Bort, Ye. Ye. Rylov, N. A. Okladnov and V. A. Kargin, Polymer Sci. (U.S.S.R.), 1967, 9, 334.

36. D. N. Bort, V. G. Marinin, A. I. Kalinin and V. A. Kargin, Polymer Sci. (U.S.S.R.), 1968, 10, 2989.

37. R. Tregan and A. Bonnemayre, Rev. Plast. Mod., 1971, 7, 230.

38. H. Behrens, Plaste u. Kautschuk, 1973, 20 (1), 2.

39. H. Behrens, Plaste u. Kautschuk, 1975, 22 (1), 2.

40. J. Boissel and N. Fischer, J. Macromol. Sci.-Chem., 1977, A11 (7), 1249.

41. M. Ravey, J. A. Waterman, L. M. Schorr and M. Kramer, J. Polym. Sci. - Chem. Ed., 1974, 14, 332.

42. D. G. Rance and E. L. Zichy, Pure Appl. Chem., 1981, 53, 377.(See Appendix (3))

43. M. Carenza, G. Palma, G. Talamini and M. Tavan, J. Marcromol. Sci.- Chem., 1977, A11, 1235.

44. L. M. Barclay, Agnew. Mackromol. Chem., 1976, 52, 1.

45. C. Singleton, T. Stephenson, J. Isner, P. H. Geil and E. A. Collins, J. Macromol. Sci.-Phys., 1977, B14, 29.

46. P. L. Soni, E. A. Collins and P. H. Geil, Abstracts 3rd. Int. Symposium on PVC, Cleveland, Ohio, U.S.A., 1980, 105.

47. L. M. Barclay, Agnew. Makromol. Chemie., 1976, 52, 1.

48. R. J. Krzewki and C. L. Sieglaff, Polymer Engineering and Science, 1978, 18, 1174.

49. A. R. Berens, Pure Appl. Chem., 1981, 53, 365.

50. D. N. Bort, V. S. Zavyalova,Yu. Vol'fkovich, E. I. Shkolnikov and E. P. Rybkin,Vysokomol. Soedin. Ser. A., 1980, 22 (8), 1736.

51. G. R. Johnson, "The effect of a Modified Weber Number on Resin Properties during VCM Suspension Polymerisation.", 71st. meeting American Institute of Chem. Engineers, Miami, 1978, Paper 12a.

52. M. W. Allsopp, Pure Appl. Chem., 1981, 53, 449.

53. R. M. Fitch, Polymer Colloids, Proc. A. C. S. Symp., Chicago, 13 - 18th. Sept., 1970, p. 73.

54. M. R. Hoare, Adv. Chem. Phys., 1979, XL, 90.

55. A. S. Dunn and C. H. Chong, Br. Polym. J., 1970, 2, 49.

56. J. W. Goodwin, R. H. Ottewill, R. Pelton, G. Vianello and D. E. Yates, Br. Polym. J., 1978, 10, 173.

57. J. C. Wilson and E. L. Zichy, Polymer, 1979, 20, 264.

58. R. M. Speirs, Ph.D. Thesis, University of Edinburgh, 1980.

59. W. D. Cooper, R. M. Speirs, J. C. Wilson and E. L. Zichy, Polymer, 1979, 20, 265.

60. J. A. Davidson and D. E. Witenhafer, J. Polymer Sci., Polym. Phys. Ed., 1980, 18, 51.

61. D. G. Rance and E. L. Zichy, Polymer, 1979, 20, 266.

62. J. Bauer and A. Sabel, Angew, Makromol. Chem., 1975, 47, 15.

63. F. M. Fowkes and F. H. Hielscher, A. C. S. Surface Coat. and Plastics, 1980, 42, 169.

64. M. Carenza, G. Palma, G. Talamini and M. Tavan, J. Macromol. Sci. Chem., 1977, A11, 1235.

65. D. N. Bort, Z. S. Zakharova, E. P. Shvaren, and S. A. Nikitina, Vysokomol. Soedin. Ser. A. 1976, 18(6), 1334.

66. B. E. Tornell and M. Uustalu, Lund Institute of Technology, personal communication via D. G. Rance, I.C.I. plc. Plastics and Petrochemicals Division.

67. J. L. van der Minne and P. H. J. Hermanie, J. Colloid Sci., 1952, 7, 600.

68. R. H. Ottewill, Colloid Science, Volume 1, Specialist Periodical Reports, The Chemical Society, 1973.

69. R. H. Ottewill, J. Colloid Interface Sci., 1977, 58, 357.

70. J. Th. G. Overbeek, J. Colloid Interface Sci., 1977, 58, 408.

71. D. H. Napper, J. Colloid Interface Sci., 1977, 58, 390.

72. G. D. Parfitt, Ann. Reports (A), 1967, 64, 125.

73. J. Lyklema, Adv. Colloid Interface Sci., 1968, 2, 65.

74. G. D. Parfitt and J. Peacock, J. Surface Colloid Sci., 1978, 10, 163-226.

75. B. Vincent, Colloid Science, Volume 1, Specialist Periodical Reports, The Chemical Society, 1973.

76. A. Kitahara, Progress in Organic Coatings, 1973/74, 2, 81.

77. V. T. Crowl, J. Oil Colour Chemists' Assoc., 1972, 55, 388.

78. R. H. Ottewill and J. N. Shaw, Disc. Faraday Soc., 1966, 42, 154.

79. C. A. Kraus and F. A. Fuoss, J. Am. Chem. Soc., 1933, 55, 21.

80. V. K. La Mer and H. L. Downes, J. Am. Chem. Soc., 1931, 53, 888; 1933, 55, 1840.

81. H. Koelmans and J. Th. G. Overbeek, Disc. Faraday Soc., 1954, 18, 52.

82. D. N. L. McGown, G. D. Parfitt and E. Willis, J. Colloid Interface Sci., 1965, 20, 650.

83. L. A. Romo, J. Phys. Chem., 1963, 67, 386.

84. G. Gouy, J. Phys., 1910, 9, 457.

85. D. L. Chapman, Phil. Mag., 1913, 25, 475.

86. T. H. Gronwall, V. K. La Mer and K. Sandved, Physik. Z., 1928, 29, 358.

87. F. Booth, J. Chem. Phys., 1951, 19, 821.

88. S. Levine, J. Chem. Phys., 1939, 7, 831.

89. J. -Y. Parlange, J. Chem. Phys., 1972, 57, 376.

90. L. R. White, J. Chem. Soc. Faraday II, 1977, 73, 577.

91. A. L. Loeb, P. H. Wiersema and J. Th. G. Overbeek, The Electric Double Layer Around a Spherical Colloidal Particle, M. I. T. Press, Cambridge, Mass., 1961.

92. S. S. Dunkhin, Special Discussion Faraday Soc., 1970, 1, 158.

93. O. Stern, Z. Electrochem., 1924, 30, 508.

94. D. C. Grahame, Chem. Rev., 1947, 41, 441.

95. F. P. Buff and N. S. Goel, J. Chem. Phys., 1969, 51, 4983 and 5363.

96. S. Levine, J. Colloid Interface Sci., 1971, 37, 619.

97. K. Robinson and S. Levine, J. Electroanal Chem., 1973, 47, 395.

98. R. J. Hunter, Zeta Potential in Colloid Science, (Colloid Science a series of Monographs), Academic Press, 1981.

99. B. V. Derjaguin, Kolloid-Z., 1934, 69, 155; Acta physiochimica U. S. S. R., 1939, 10, 333.

100. R. Hogg, T. W. Healy and D. W. Fuerstenau, Trans. Faraday Soc., 1966, 62, 1638.

101. O. F. Devereux and P. L. de Bruyn, Interaction of Plane Parallel Double Layers, M. I. T. Press, Cambridge, Mass., 1963.

102 D. W. J. Osmond, Disc. Faraday Soc., 1966, 42, 247, (discussion remark).

103. L. N. McCartney and S. Levine, J. Colloid Interface Sci., 1969, 30, 345.

104. G. M. Bell, S. Levine and L. N. McCartney, J. Colloid Interface Sci., 1970, 33, 335.

105. J. D. van der Waals, Ph.D. Thesis, University of Leiden, 1873.

106. J. Gregory, Adv. Colloid Interface Sci., 1969, 2, 396.

107. J. Visser, Adv. Colloid Interface Sci., 1972, 3, 331.

108. J. N. Israelachvili and D. Tabor, Prog. Surt. Memb. Sci., 1973, 7, 1.

109. V. A. Parsegian, Physical Chemistry: Enriching Topics from Colloid and Surface Sci., Ed. H. van Olphen and K. J. Mysels, Theorex, Calafornia, 1975.

110. D. Tabor, Colloidal Dispersions, Special Publication No. 43, The Royal Society of Chemistry, 1982.

111. P. Debye, Phys-Z, 1920, 21, 178.

112. W. H. Keeson, Phys-Z, 1921, 22, 129.

113. F. London, Z. Phys., 1930, 63, 245.

114. S. C. Wang, Phys-Z, 1927, 28, 663.

115. H. C. Hamaker, Physica, 1937, 4, 1058.

116. R. Eisenshchitz and F. London, Z. Phys., 1930, 60, 491.

117. E. A. Moelwyn-Hughes, Physical Chemistry, 2nd. Ed., Pergamon, 1961, 383.

118. W. Kauzmann, Quantum Chemistry, Academic Press, 1957, 692.

119. J. H. Schenkel and J. A. Kitchener, Trans. Faraday Soc., 1960, 56, 161.

120. E. M. Lifshitz, Sov. Phys., J. E. T. P., 1956, 2, 73.

121. H. G. B. Casimir and D. Polder, Phys. Rev., 1948, 73, 360.

122. I. E. Dzyaloshinskii, E. M. Lifshitz and L. P. Pitaerskii, Adv. Phys., 1961, 10, 165.

123. V. A. Parsegian and B. Ninham, Nature, 1969, 224, 1197; J. Chem. Phys., 1970, 52, 4578; J. Colloid Interface Sci., 1971, 37, 332.

124. D. Gingell and V. A. Parsegian, J. Theor. Biol., 1972, 36, 41.

125. P. Richmond and B. W. Ninham, J. Colloid Interface Sci., 1972, 40, 406.

126. G. D. Parfitt, Dispersions of Powders in Liquids, ed. G. D. Parfitt, Elsevier, Amsterdam, 1969.

127. M. von Smoluchowski, Physik. Z., 1916, 17, 557, 585; Z. Physik. Chem., 1917, 92, 129.

128. J. Th. G. Overbeek, Colloid Sci., vol. 1, ed. H. R. Kruyt, Elsevier, 1952.

129. H. Muller, Kolloidchem. Beihefte, 1928, 27, 223.

130. N. Fuchs, Z. Physik, 1934, 89, 736.

131. D. N. L. McGown and G. D. Parfitt, J. Phys. Chem., 1967, 71, 449.

132. L. A. Spielman, J. Colloid Interface Sci., 1970 33, 562.

133. M. Stimson and G. B. Jeffery, Proc. Roy. Soc., 1926, A111, 110.

134. J. Happel and H. Brenner, Low Reynolds Number Hydrodynamics, Prentice Hall, New Jersey, 1965.

135. R. Hogg, T. W. Healy and D. W. Fuerstenau, Trans. Faraday Soc., 1966, 62, 1638.

136. W. D. Cooper, P. Fearson, G. D. Parfitt, J. Chem. Soc., Faraday Trans. 1, 1973, 69, 1261.

137. W. D. Cooper, Kolloid z. z. Polym. 1972, 250, 38.

138. D. C. Prieve and M. M. J. Lin, J. Colloid Interface Sci., 1982, 86, 17.

139. U. S. A. Federal Register 39, October 4, No. 194, Part II. Title 29 - Labor, Chapter XVII - OSHA, Dept. of Labor, Part 1910 - OSHA Standards. Standards for exposure to vinyl chloride, p. 35890 (1974).

140. E. Huckel, Physik. Z., 1924, 25, 204.

141. D. J. Shaw, Elecrophoresis, Academic Press, London, 1969, p. 21.

142. R. W. O'Brian and L. R. White, J. Chem. Soc., Faraday II, 1978, 74, 1607.

143. G. E. van Gils and H. R. Kruyt, Kolloid-Beihefte, 1936, 45, 60.

144. S. Mattson, J. Phys. Chem., 1928, 32, 1532; 1933, 37, 223.

145. D. C. Henery, J. Chem. Soc.,1938, p.997.

146. E. S. Hall, Nature, 1964, 203, 1371.

147. A. L. Smith, Dispersions of Powders in Liquids, ed. G. Parfitt, 1973, Ch. 3, Applied Science Publishers.

148. R. M. Fitch, Charged React. Polym., 1975, 2, 51.

149. E. B. Bradford and J. W. Vanderhoff, J. Appl. Phys., 1955, 26, 864.

150. E. B. Bradford and J. W. Vanderhof, The Use of Monodisperse Latex Particles as Calibration Standards, 151st. ACS Meeting, Pittsburgh, 1966, unpublished manuscript available.

151. J. A. Davidson and E. A. Collins, J. Colloid Interface Sci., 1972, 40, 437.

152. S. A. McDonald, C. A. Daniels and J. A. Davidson, J. Colloid Interface Sci., 1977, 59, 342.

153. C. A. Daniels, S. A. McDonald and J. A. Davidson, Emulsions, Latices, Dispersions, ed. P. Becher, M. N. Yudenfreund, Deckker, New York, 1978, 175.

154. G. Herdan, Small Particle Statistics, Butterworths, 1960.

155. D. G. Rance and E. L. Zichy, personal communication.

156. H. A. Pohl, J. Appl. Phys., 1951, 22, 869.

157. H. C. Parreira, J. Chem. Phys., 1968, 49, 4711; J. Colloid Interface Sci., 1969, 29, 432.

158. A. D. Robertson, D. J. Fabian, A. J. Crocker and J. Dewing, Laboratory Glass-working for Scientists, Butterworths, London, 1957, Ch. 2.

159. A. R. Berens, Angew. Makromol. Chemie, 1975, 47, 97.

160. H. R. Kruyt, Colloid Science, Volume 1, Elsevier, 1952, Ch. 1.

161. G. D. Parfitt, J. A. Wood and R. T. Ball, J. Chem. Soc. Faraday Trans. 1, 1973, 69, 1908.

162. Ref. 160, Ch. 2.

163. I. R. Schmolka, Nonionic Surfactants, Surfactant Science Series, ed. M. J. Schick, Marcel Dekker, New York, 1967, Vol. 1, Ch. 10, p. 353.

164. W. Albers and J. Th. G. Overbeek, J. Colloid Sci., 1959, 14, 510.

165. C. S. Chen and S. Levine, J. Colloid Interface Sci., 1973, 43, 599; G. R. Feat and S. Levine, J. Chem. Soc., Faraday Trans. 2, 1975, 71, 102; J. Colloid Interface Sci., 1976, 54, 34; J. Chem. Soc., Faraday Trans. 2, 1976, 72, 501.

166. M. J. Vold, J. Colloid Interface Sci., 1961, 16, 1.

167. V. T. Crowl and M. A. Malati, Discussions Faraday Soc., 1966, 42, 301.

168. G. R. Wiese and T. W. Healy, Trans. Faraday Soc., 1970, 66, 490.

169. E. S. Saharova et. al., Vysokomal. Soedin, 1972, B19, 350.

170. Personnal communication, C. A. S. E. Award review meeting with members of I. C. I., Petrochemicals and Plastics Division, held at Bristol University, 8th. September 1982.

171. J. C. Koleske and L. H. Wartman, Poly(vinyl chloride), Its Preparation and Properties, Macdonald Polymer Monographs, 1969, p. 13.

Appendixes

Appendix 1 PVC Nomenclature.

The terminology used in the literature to describe PVC morphology is inconsistant and very confusing. In this work the polymer structures observed by electron microscopy have, in general, assigned the terminology proposed by Allsopp (7), whose nomenclature is best suited to describe the colloidal events occurring during the formation of the particulate polymer grain. This terminology, along with the recently proposed IUPAC nomenclature is given in Table 1 overleaf. Other nomenclature frequently used in the scientific literature is also given for cross referencing purposes.

Table 1. Nomenclature for the Sub-units of a PVC Grain.

Nomenclature of PVC Sub-units Appropriate To Colloid Formation	Approx. monomer Conversion (%) at First Appearance Of Sub-units	Approximate Particle Diameter /μm	IUPAC Nomenclature	Other Nomenclature In Frequent Use
Basic Particle	0.001 - 0.005	0.02	Microdomain	Particle
Primary Particle	0.005	0.08	Domain	Primary nucleus, Granule
		0.2 - 1	Primary Particle	Microgranule, Granule, Microglobule.
Primary Particle Aggregate	0.02 - 0.1%	2 - 5	Agglomerate	Cluster, Macroglobule.
Sub-grain			Sub-grain	Sub-granule, Unicell.
Grain			Grain	Granule, Cellular grain.

Appendix 2 Statistics of particle size distributions.

S.E.M. micrographs of the PVC polymer produced during experimental studies were evaluated on a Vickers Magiscan Image Analyser. When the polymer batch contained both primary and primary particle aggregates the Magiscan output an overall particle size distribution. To obtain particle size statistics for the individual polymer types within the overall distribution a computer programme "Diameter" was developed, a copy of which appears overleaf. "Diameter" makes use of the following statistical relationships.

$$\text{Number average} \quad D_n = \frac{\Sigma\, n_i\, D_i}{\Sigma\, n_i}$$

$$\text{Surface area average} \quad D_{sa} = \frac{\Sigma\, n_i\, D_i^3}{\Sigma\, n_i\, D_i^2}$$

$$\text{Volume (weight) average} \quad D_v = \frac{\Sigma\, n_i\, D_i^4}{\Sigma\, n_i\, D_i^3}$$

$$\text{Number standard deviation} \quad \sigma_n = \frac{\Sigma\, n_i\, D_i^2}{\Sigma\, n_i} - D_n^2$$

$$\text{Volume standard deviation} \quad \sigma_v = \frac{\Sigma\, v_i\, D_i^2}{\Sigma\, v_i} - D_v^2$$

where n_i is the number of particles of class diameter D_i

The degree of skewness = (mean - mode)

The programme, written in Basic Language, prompts the user for lower and upper particle size limits. The particle frequency is then input as the programme increments the particle diameter in step with the Magiscan output.

```
 10  REM *** DIAMETER ***
 20  REM *** INPUT UPPER AND LOWER SIZE LIMITS ***
 30  REM ***INPUT FREQUENCY DATA WHEN REQUESTED ***
 40 DIM Di(50):DIM ni(50):DIM VOLSUMVOL(50)
 50 INPUT"UPPER RANGE LIMIT ",URL
 60 sumni=0:sumniDi=0:sumniDi2=0:sumniDi3=0
 70 sumniDi4=0:SUMVOL=0:sumviDi=0: sumviDi2=0:sumvi=0
 80 CLASSINTERVAL=URL/49
 90 MIDINTERVAL=CLASSINTERVAL/2
100 INPUT "MAX DIA MEASURED ",MAXDIA
110 X=1
120 FOR DIA=0 TO MAXDIA STEP CLASSINTERVAL
130   PRINT"DIA" DIA
140   INPUT"FREQUENCY "ni(X)
150   Di(X)=DIA+MIDINTERVAL
160   sumni=sumni+ni(X)
170   sumniDi=sumniDi+(ni(X)*Di(X))
180   sumniDi2=sumniDi2+(ni(X)*Di(X)*Di(X))
190   sumniDi3=sumniDi3+(ni(X)*Di(X)*Di(X)*Di(X))
200   sumniDi4=sumniDi4+(ni(X)*Di(X)*Di(X)*Di(X)*Di(X))
210   X=X+1
220   NEXT
230 Dn=sumniDi/sumni
240 SIGMAn=SQR((sumniDi2/sumni)-(Dn*Dn))
250 Dsa=sumniDi3/sumniDi2
260 Dv=sumniDi4/sumniDi3
270 PRINT
280 @%=&2030A
290 PRINT"Dn "TAB(12); Dn
300 PRINT"SIGMA Dn "TAB(12);SIGMAn
310 PRINT
```

```
320 PRINT"Dsa "TAB(12);Dsa
330 PRINT
340 PRINT"Dv "TAB(12);Dv
350 X=1
360 FOR DIA=0 TO MAXDIA STEP CLASSINTERVAL
370   VOLSUMVOL(X)=ni(X)*Di(X)*Di(X)*Di(X)/sumniDi3
380   SUMVOL=SUMVOL+VOLSUMVOL(X)
390   X=X+1:NEXT
400 X=1
410 FOR DIA=0 TO MAXDIA STEP CLASSINTERVAL
420   VOL=SUMVOL*VOLSUMVOL(X)
430   sumviDi=sumviDi+VOL*Di(X)
440   sumviDi2=sumviDi2+VOL*Di(X)*Di(X)
450   sumvi=sumvi+VOL
460   X=X+1
470   NEXT
480 Dvol=sumviDi/sumvi
490 SIGMADvol=SQR((sumviDi2/sumvi)-(Dvol*Dvol))
500 SIGMADv=SQR((sumviDi2/sumvi)-(Dv*Dv))
510 PRINT"SIGMA Dv "TAB(12); SIGMADv
520 PRINT
530 PRINT"Dvol "TAB(12); Dvol
540 PRINT "SIGMA Dvol "TAB(12);SIGMADvol
550 PRINT
560 INPUT "Dn MODE" SMODEDN
570 INPUT "Dv MODE" SMODEDV
580 PRINT
590 PRINT"MODE Dn = "TAB(12);SMODEDN+MIDINTERVAL
600 PRINT"MODE Dv = "TAB(12);SMODEDV+MIDINTERVAL
610 PRINT
620 PRINT"Dn SKEW "TAB(12); (Dn-(SMODEDN+MIDINTERVAL))/SIGMAn
630 PRINT"Dv SKEW "TAB(12);(Dv-(SMODEDV+MIDINTERVAL))/SIGMADv
```

Appendix 3. Revised PCS data for reference (42)

A personal communication from Dr. D. G. Rance, Petrochemicals and Plastics Division, I. C. I. plc., indicated that the preliminary results reported in reference (42) have been recalculated. Although previous and present results agree in broad outline, there are numerical discrepancies which arose from different values for the physical properties of VCM and PVC being used in the interpretation of light scattering data.

As some of these values have been quoted in this thesis parts of the revised data are summarised overleaf.

Note added in proof. The revised data has now been published. F. M. Willmouth, D. G. Rance and K. M. Henman, Polymer 1984, 25, 1185.

Revised results for vinyl chloride polymerisations containing 0.1% (wt/vol) lauroyl peroxide reported in reference (42).

Polymerisation temperature (°C)	Rate of increase of gel volume fraction ($sec^{-1} \times 10^{-6}$)	Initial particle number per unit volume ($m^{-3} \times 10^{17}$)	Agglomeration onset time (secs)	Particle diameter at agglomeration onset (μm)
35.0	0.53	0.7	450	0.19
45.3	1.53	1.0	270	0.19
50.0	2.90	2.9	290	0.18
50.6	2.74	2	160	0.18
55.1	5.28	2.8	190	0.19

Appendix 4. Programme ALOV.

ALOV is based on the model proposed by Albers and Overbeek (164) to calculate the stability ratio for the interaction of identical spheres in concentrated dispersions where the double layer thickness is of the order of the average interparticle separation. Two factors were considered to lower the potential energy barrier to coagulation. These are illustrated in Figure 1. Firstly, when the average interparticle separation approaches the double layer thickness, the particles in their equilibrium position already possess a potential energy with respect to infinite separation. This reduces potential energy barrier from E_1 to E_2. Secondly, if the simultaneous interaction of particle b with particles a and c is considered the potential energy barrier to coagulation is reduced to E_3.

In the model of Albers and Overbeek it is assumed that particle b interacts with 12 nearest neighbours situated on a spherical shell of radius R_1, the average interparticle separation. All other particles are homogeneously distributed outside a larger sphere of radius R_2, with R_2 chosen such that the volume within the sphere just corresponds to the volume available to 13 particles. This is illustrated diagramatically in Figure 2. According to the Albers and Overbeek model the stability of the dispersion is determined by the height of the potential energy barrier E_3. ALOV evaluates values of

V_A and V_R at the equilibriun separation and subtracts the result from the values of V_A and V_R calculated at each separation of particles b and c from the equilibrium separation up to a separation of 0.1 nm. Thus, this method shifts the zero of potential energy from infinite separation to the average separation.

The values of V_A were calculated using equation (2.3.5) and V_R from:-

$$V_R\,(\text{total}) = \varepsilon\psi_o^2 a^2 e^{2\kappa a}\left[8.88 \cdot \frac{1.3\kappa R_1 + 1}{\kappa^3 R_1^3} \cdot \frac{e^{\kappa q} - e^{-\kappa q}}{q} \cdot e^{-1.3\kappa R_1} + \frac{e^{-\kappa(R_1 - q)}}{R_1 - q} - \frac{6}{\kappa R_1 q}\left(e^{-\kappa(R_1+q)} - e^{-\kappa\sqrt{R_1^2 + q^2 - \frac{5R_1 q}{3}}} \right) \right]$$

where V_R (total) is the energy of repulsion between the central particle b and all other particles.

ε is the permittivity of the dispersion medium ($4\pi\varepsilon_o\varepsilon_r$).

ψ_o is the surface potential of the particles.

a is the radius of the particles.

κ is the reciprocal double layer thickness.

q is the distance of the central particle b from the centre of the sphere of radius R_1 (Fig. 3), so that $(R_1 - q)$ is the separation of particles b and c,

where c is the particle with which b possibly collides.

The total potential energy of repulsion, V_T, between particles b and c, allowing for the influence of all other particles was evaluated as a function of separation by a summation of V_A and V_R. W, the stability ratio, was calculated using equation (2.5.2.10).

The programme ALOV is derived from THICKDL, given by Speirs (58). The subroutine DLVO, which was written by Dr. W. D. Cooper, evaluates the Verwey and Overbeek β and γ parameters as a function of separation. The real function DSPIEL, written by Dr. G. C. Peterson formerly of Unilever Ltd., calculates the Speilman correction factor as a function of separation.

The programme considers a suspension polymerisation droplet of known volume and requests the number, radius and charge of the primary particles. Values for the Hamaker constant, temperature and dielectric constant are also required.

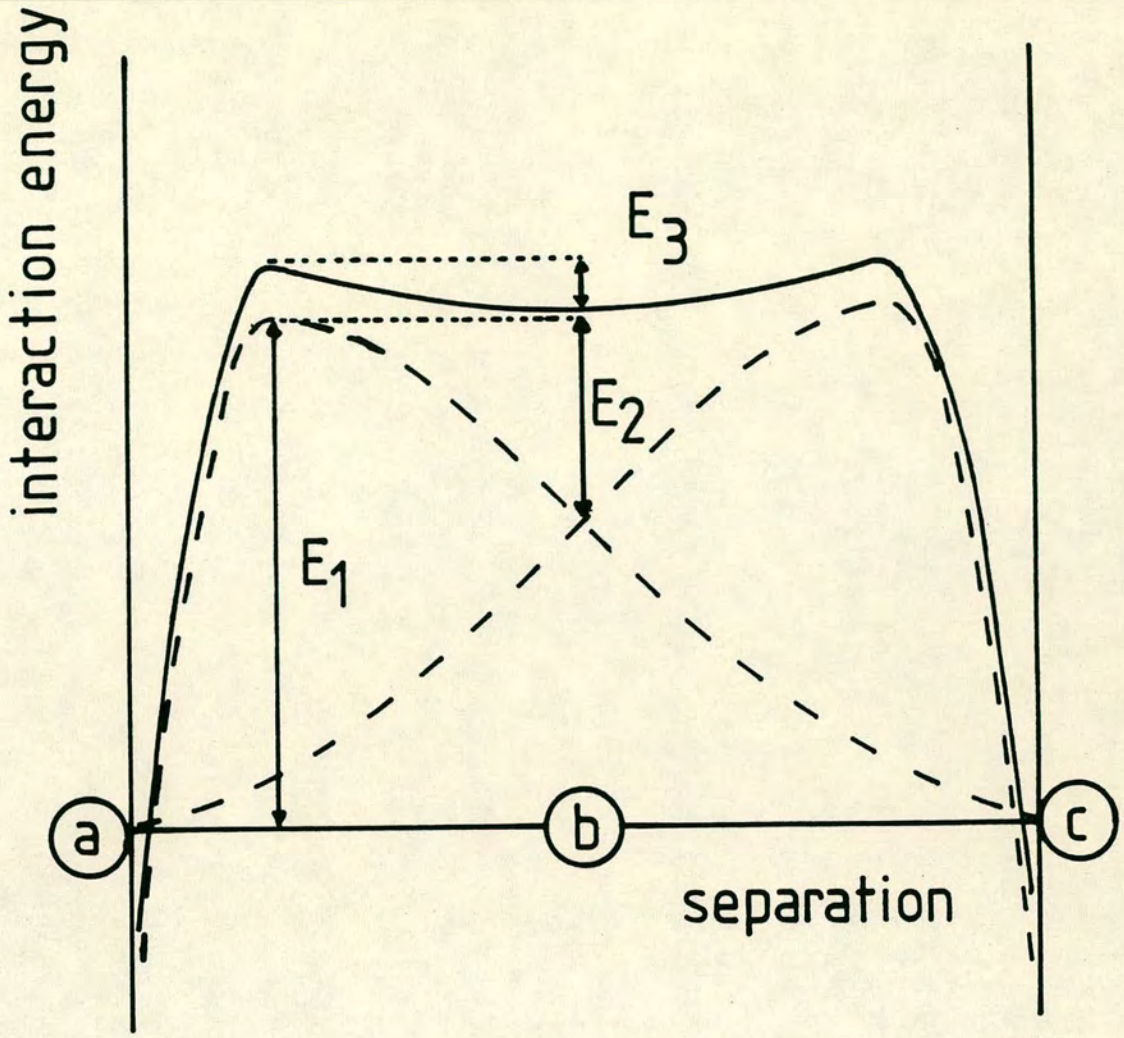

- - - Interaction between a and b, and between b and c, in the absence of the third particle.

_____ Interaction between the two pairs of particles when the simultaneous interaction with the third particle is included.

Fig.1 Diagram illustrating the reduction of the potential energy barrier to coagulation by the particle concentration effect.

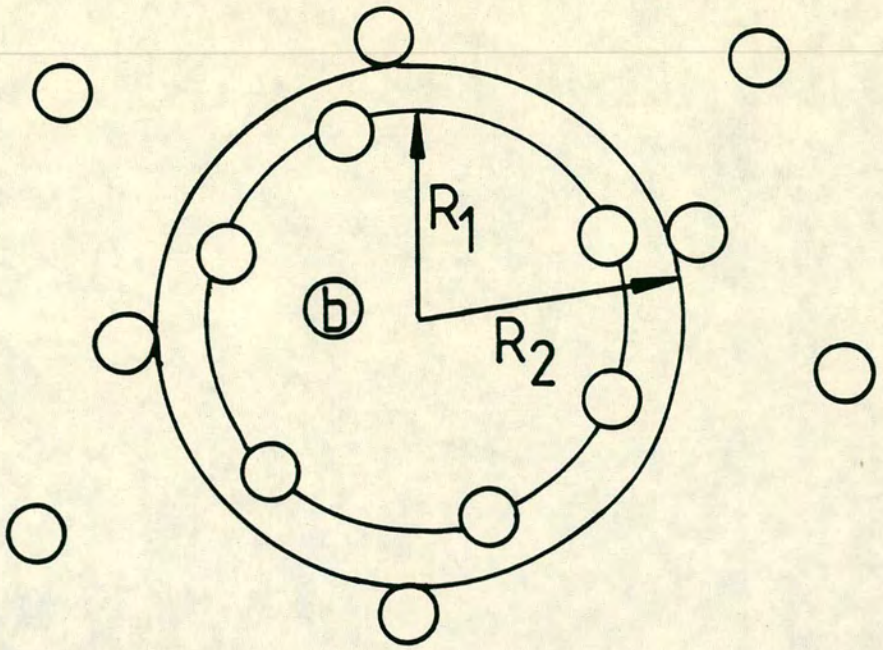

R_1 = average interparticle separation

R_2 contains the volume available to 13 particles.

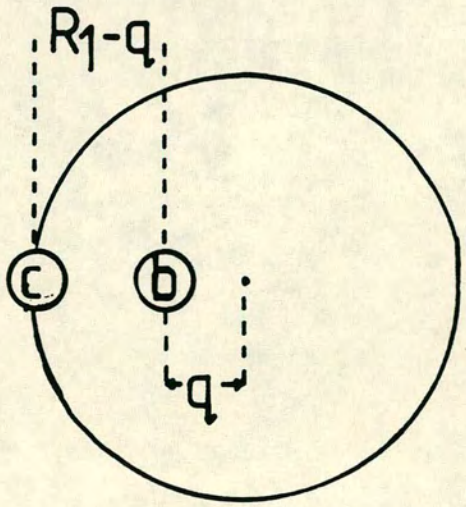

Figures 2 and 3 Diagrams illustrating the arrangement of particles assumed by Albers and Overbeek.

ALOV Compiled: 28/05/82 11.46.22

FORTRAN(G) COMPILER VERSION 70.1

```
C     THIS PROGRAM CALCULATES STABILITY RATIOS FOR CONCENTRATED
C     DISPERSIONS WHERE THERE IS INTERACTION BETWEEN SEVERAL DOUBLE
C     LAYERS. IT USES THE EXPRESSION OF ALBERS AND OVERBEEK.
      DOUBLE PRECISION PI,R1,KA,KT,EPS,APM,ELEM,Q1,PS1,NU,VOL,VOLFRA,
     2R3,RAD,AA,AB,AC,VA,Q,VRA,VRB,VRC,VRD,VRE,VRF,VRG,VRH,VRI,
     3VRTDL,VRTDLX,VRDLEX,VRDLGX,VTOT,STEP,ST,SUM,RP,VT,W,LOGW
     4,REVOL,VRTDLB,VRJ,FSTERM,SMAX,VRTDLG,VAX,HX,VRNORM,MAXH
     5,RAD1,F1,S,T,DF,GA,A21,SA,SB,XD,EP,VRJLIM,PARTVO,FREEVO,NUMCH,C
     6,Y,XX
      INTEGER INT,INT1,ISTEP,ICOUNT,I,CYCLE
      DIMENSION TOT(6),SUM(6),RP(6),W(6),LOGW(6)
      PI=3.141593
      WRITE(6,330)
  330 FORMAT('0',1X,'CALCULATION OF THE STABILITY RATIO IN',
     21X,'CONCENTRATED DISPERSIONS WITH THICK DOUBLE LAYERS')
    2 WRITE(6,100)
  100 FORMAT('0',1X,'DO YOU WANT TO CALCULATE ANOTHER W  Y=1 N=2')
      READ*,INT
      IF(INT.EQ.2) GOTO 60
      WRITE(6,120)
  120 FORMAT('1',1X,'DO YOU WANT TO INCLUDE THE SPIELMAN CORRECTION'
     2,1X,'  Y=1 N=2')
      READ*,INT1
      IF(INT1.EQ.2) GOTO 778
      WRITE(6,777)
  777 FORMAT('0',1X,'GIVE ME EP, THE SPIELMAN CONVERGENCE TERM')
      READ*,EP
  778 WRITE(6,101)
  101 FORMAT('0',1X,'GIVE ME THE PARTICLE RADIUS IN METRES')
      READ*,R1
      WRITE(6,102)
  102 FORMAT('0',1X,'GIVE ME KT,THE DIELECTRIC CONSTANT',1X,
     2'AND THE HAMAKER CONSTANT')
      READ*,KT,EPS,APM
      EPS=EPS*1.112D-10
      ELEM=1.6021D-19
      WRITE(6,207)
  207 FORMAT('0',1X,'GIVE ME THE TOTAL CHARGE ON EACH PARTICLE'
     2,1X,'IN NUMBERS OF ELEMENTARY CHARGES')
      READ*,Q1
      Q1=Q1*ELEM
      PS1=Q1/(R1*EPS)
      WRITE(6,104)
  104 FORMAT('0',1X,'HOW MANY STEPS DO YOU WANT BETWEEN EACH',1X,
     2'YR ETC PRINTOUT')
```

```
      READ*,ISTEP
      CYCLE=0
      ICOUNT=1
      PS1=PS1*1000.
      IF(PS1.GT.175.) PS1=175.
      WRITE(6,112)R1,PS1,Q1
  112 FORMAT('0',1X,'R1 =',1X,F11.4,1X,'METRES    PS1 =',1X,F6.2,1X,
     2'MILLIVOLTS    Q1 =',1Y,E12.5,1X,'COULOMBS')
      WRITE(6,113)APM
  113 FORMAT(' ',1X,'HAMAKER CONSTANT =',1X,F11.4,1X,'JOULES')
      WRITE(6,114)KT
  114 FORMAT(' ',1X,'KT =',1X,E11.4,1X,'JOULES')
      PS1=PS1/1000.
      WRITE(6,125)
  125 FORMAT('0','GIVE ME NU, THE (CONSTANT) PRIMARY PARTICLE',1Y,
     2'NUMBER IN EACH SUSPENSION DROPLET')
      READ*,NU
      VOL=5.236D-10
C     VOL IS THE VOLUME OF A MONOMER DROPLET IN A SUSPENSION
C     POLYMERISATION.  WE TAKE A 1MM DIAMETER
      VOLFRA=(NU*4.*PI*R1*R1*R1/3.0)/VOL
      REVOL=VOL-(1.68D-10*VOLFRA)
      VOLFRA=VOLFRA*VOL/REVOL
C     REVOL ALLOWS FOR SHRINKAGE AS POLYMERISATION PROCEEDS AND THE
C     VOLUME FRACTION IS RECALCULATED TO ALLOW FOR THIS
C     CALCULATION OF DOUBLE LAYER THICKNESS
      PARTVO=NU*4.0*PI*R1*R1*R1/3.0
      FREEVO=REVOL-PARTVO
      NUMCH=NU*Q1/ELEM
      C=NUMCH/FREEVO
      Y=(4.0*PI*ELEM*ELEM*C)/(EPS*KT)
      KA=DSQRT(Y)
      XX=1.0/KA
      WRITE(6,651)XX
  651 FORMAT('0',1X,'DOUBLE LAYER THICKNESS =',1X,E11.4,1X,'METRES')
      WRITE(6,115)VOLFRA
  115 FORMAT('0',1X,'VOLUME FRACTION =',1X,F9.6)
      RADI1=(1.61*R1)/(VOLFRA**0.333)
      WRITE(6,521)RADI1
  521 FORMAT('0',1X,'RADI1 =',1X,F11.4,1X,'METRES')
      WRITE(6,116)
  116 FORMAT('0',6X,'H',4X,'VRTIL',6X,'VRTDLR',4X,'VRTDLG',
     27X,'VA',8X,'VB',8X,'VA',8X,'VRNORM',7X,'VRI',12X,'VRE',12X,'VRJ')
      SMAX=RADI1/R1
      ESTERM=1./SMAX
         DO 56 I=1,6
         SUM(I)=ESTERM
   56    CONTINUE
C     WE FIRST CALCULATE THE POTENTIAL ENERGY OF THE PARTICLES
C     AT THEIR AVERAGE SEPARATION THEN CALCULATE FOR THIS
C     ENERGY CHANGES AS THE PARTICLES APPROACH AND COLLIDE
      R3=2.*R1
      Q=0.0
      H1=RADI1-R3
      RAD=R1+R1+H1
      S=(R3+H1)/R1
      T=KA*R3/2.0
      CALL DLVO(S,T,RE,GA)
      AA=2.*R1*R1
      AB=((2.*R3)+H1)*H1
      AC=AA+AA+AB
      VAX=-APM*(AA/AB+AA/AC+DLOG(AB/AC))/6.0
      VRA=EPS*PS1*PS1*R1*R1*DEXP(2.*KA*R1)
      VRB=(1.7*KA*RADI1)+1)/(KA*KA*KA*RADI1*RADI1*RADI1)
      VRC=2.0*KA
```

```
      VRI=0.00*VRB*VRC*DEXP(-1.3*KA*RADI1)
      VRB=DEXP(-KA*(RADI1-Q))/(RADI1-Q)
      VRJ=-11.0*DEXP(-KA*RADI1)/RADI1
      VRJLIM=VRJ
      VRTDLX=VRA*(VRD+VRE-VRJ)
      VRDLBX=VRA*(VRD+(VRE*BE)-VRJ)
      VRDLGX=VRA*(VRD+(VRE*GA)-VRJ)
      FX=F1
      H1=1.0D-10
    1 RAD=R1+R1+H1
      IF(F1.GT.(RADI1-R3)) GOTO 61
      S=(R3+H1)/R1
      T=KA*R3/2.0
      CALL DLVO(S,T,BE,GA)
      AP=((2.*R3)+H1)*H1
      AC=AA+AA+AB
      VA=-APM*(AA/AP+AA/AC+DLOG(AP/AC))/6.0
      IF(DABS(VA).LT.(1000.*KT)) GOTO 31
      VA=-1000.*KT
   31 VA=VA-VAX
      VA=VA/KT
      Q=RADI1-(R3+H1)
      IF(Q.LT.1.0D-10) GOTO 572
      VRC=(DEXP(KA*Q)-DEXP(-KA*Q))/Q
      GOTO 573
  572 VRC=2.0*KA
  573 VRI=0.98*VRB*VRC*DEXP(-1.3*KA*RADI1)
      VRE=DEXP(-KA*(RADI1-Q))/(RADI1-Q)
      IF(Q.LT.1.0D-10) GOTO 570
      VRF=DEXP(-KA*(RADI1+Q))
      VRG=(RADI1*RADI1)+(Q*Q)-(5.0*RADI1*Q/3.0)
      VRH=DSQRT(VRG)
      VRI=DEXP(-KA*VRH)
      VRJ=0.*(VRF-VRI)/(KA*RADI1*Q)
      GOTO 571
  570 VRJ=-11.0*DEXP(-KA*RADI1)/RADI1
  571 VRTDL=VRA*(VRD+VRE-VRJ)
      VRTDLB=VRA*(VRD+(VRE*BE)-VRJ)
      VRTDLG=VRA*(VRD+(VRE*GA)-VRJ)
      VRTDL=VRTDL-VRTDLX
      VRTDLB=VRTDLB-VRDLBX
      VRTDLG=VRTDLG-VRDLGX
      VRTDL=VRTDL/KT
      VRTDLB=VRTDLB/KT
      VRTDLG=VRTDLG/KT
      VRNORM=VRA*VRE/KT
      IF(ICOUNT.NE.ISTEP) GOTO 996
      H1=F1*1.0D10
      WRITE(6,117)F1,VRTDL,VRTDLB,VRTDLG,VA,BE,GA,VRNORM,VRD,VRE,VRJ
  117 FORMAT(' ',1X,F9.1,1X,F9.4,1X,F9.4,1X,F9.4,1X,F11.4,1X,
     2F9.4,1X,F9.4,1X,F9.4,4X,E11.4,4X,E11.4,4X,E11.4)
      H1=F1*1.0D-10
      ICOUNT=0
C     NOW FIX STEP SO THAT STEP IS SMALLEST WHEN THE TWO COLLIDING
C     PARTICLES ARE CLOSEST
  996 STEP=0.1*R3
      IF(H1-(2.5*R3)) 16,18,18
   16 IF(H1-R3) 17,32,32
   17 STEP=0.005*R3
      GOTO 19
   32 STEP=0.01*R3
   19 A21=1.0000
C     CALCULATION OF STABILITY RATIO
      SA=H1/R1
      SP=1.D3+A21+SA
      IF(INT1.EQ.2) GOTO 50
```

```
      XI=DSPIFL(SP,A21,FP)
      GOTO 51
   50 XI=1.0
   51 ST=STEP*XI*B3/(2.*RAD*RAD)
      IF(DABS(VA).GT.89.0) GOTO 25
      TOT(6)=ST*DEXP(VA)
      GOTO 26
   25 TOT(6)=ST*1.D-25
   26 SUM(6)=SUM(6)+TOT(6)
      RP(1)=VRTDL
      RP(2)=VRTDLB
      RP(3)=VRTDLG
      RP(4)=VRNORM
         DO 21 I=1,4
         VT=VA+RP(I)
      IF(VT.GT.89.0) VT=89.0
         IF(DABS(VT).GT.90.0) GOTO 27
         TOT(I)=ST*DEXP(VT)
         GOTO 28
   27    TOT(I)=ST*1.D-25
   28    SUM(I)=SUM(I)+TOT(I)
   21    CONTINUE
      MAXH=F1/B3
      H1=H1+STEP
      CYCLE=CYCLE+1
      ICOUNT=ICOUNT+1
      GOTO 1
   61 VRTDLX=VRTDLX/KT
      VRDLBX=VRDLBX/KT
      VRDLGX=VRDLGX/KT
      VAX=VAX/KT
      HX=HX*1.0D10
      WRITE(6,62)VRTDLX,VRDLBX,VRDLGX,VAX,HX,MAXH
   62 FORMAT('0',1X,'VRTDLX =',1X,F11.4,2X,'VRDLBX =',1X,F11.4,2X,
     2'VRDLGX =',1X,F11.4,2X,'VAX =',1X,F7.4,2X,'HX =',1X,F10.4,
     22X,'MAXH =',1X,F5.2)
      WRITE(6,715)VRJLIM
  715 FORMAT(' ',1X,'VRJLIM =',1X,E11.4)
      HX=HX*1.0D-10
      WRITE(6,500)CYCLE
  500 FORMAT('0',1X,'TOTAL NUMBER OF CYCLES =',1X,I4)
      WRITE(6,170)
  170 FORMAT('0',1X,'UNITS: H/ANGSTROMS')
      WRITE(6,171)
  171 FORMAT(' ',8X,'VR TERMS/UNITS OF KT')
      WRITE(6,172)
  172 FORMAT(' ',8X,'BE,GA/DIMENSIONLESS')
      WRITE(6,154)
  154 FORMAT('0',1X,'I=1, ALLOWING FOR ALL OTHER PARTICLES ASSUMING'
     2,1X,'BETA = 1')
      WRITE(6,520)
  520 FORMAT(' ',1X,'I=2, ALLOWING FOR ALL OTHER PARTICLES AND'
     2,1X,'MULTIPLYING TERM FOR COLLIDING PARTICIES BY BETA')
      WRITE(6,130)
  130 FORMAT(' ',1X,'I=3, ALLOWING FOR ALL OTHER PARTICLES AND'
     2,1X,'MULTIPLYING TERM FOR COLLIDING PARTICLES BY GAMMA')
      WRITE(6,140)
  140 FORMAT(' ',1X,'I=4, SIMPLE TWO PARTICLE INTERACTION',1X,
     2'WITH BETA AND GAMMA =1')
      WRITE(6,133)
  133 FORMAT('0',8X,'W',11X,'I',6X,'LOGW')
         DO 22 I=1,4
         W(I)=SUM(I)/SUM(6)
         LOGW(I)=DLOG10(W(I))
         WRITE(6,29)W(I),I,LOGW(I)
   29    FORMAT(' ',4X,E11.4,5X,I1,5X,F7.4)
```

```
 22     CONTINUE
        GOTO 2
 60     STOP
        END



        SUBROUTINE DLVO(S,T,BE,GA)
        DOUBLE PRECISION S,T,BE,GA,A,AL,A1,A2,B,C,D,E,F,G,H,L1,L2,X,Y
        A1=S*T
        A2=A1*A1
        A=DEXP(-T*(S-2.D0))/(2.D0*A1)
        B=1.D0+1.D0/A1
        C=2.D0*B-1.D0+2.D0/A2
        D=4.D0*B-3.D0+9.D0/A2+9.D0/(A2*A1)
        E=(T-1.D0)/(T+1.D0)+DEXP(-2.D0*T)
        F=(T*(T-3.D0)+3.D0)/(T*(T+3.D0)+3.D0)-DEXP(-2.D0*T)
        G=1.D0+3.D0/A1+3.D0/A2
        H=1.D0+6.D0/A1+24.D0/A2+54.D0/(A1*A2)+54.D0/(A2*A2)
        X=1.D0/3.D0+A*E*C
        Y=D*(1.D0/3.D0+A*(E*C-F*I))
        L2=-A*((F*G-E*B)*X+B*Y)/((1.D0/5.D0+A*(F*H-E*D))*X+A*D*Y)
        L1=-A*E*(B+D*L2)/X
        AL=L1*B+L2*G
        BE=(1.D0+AL)/(1.D0+A*(1.D0-DEXP(-T*2.D0))*(1.D0+AL))
        GA=(1.D0+AL)/(1.D0-A*F*(1.D0+AL))
        RETURN
        END



        REAL FUNCTION DSPIEL*8(S,A21,EPS)
C  THE DOUBLE PRECISION FUNCTION DSPIEL CALCULATES THE RATIO OF THE
C RELATIVE DIFFUSION COEFFICIENTS AT INFINITE AND FINITE SEPARATIONS
C FOR TWO DISSIMILAR SPHERES
C  S=R/A1 WHERE R=CENTRE TO CENTRE DISTANCE
C  A21=A2/A1 WHERE A1 AND A2 ARE THE RADII OF SPHERES,A2>A1.
C  I.E.  DSPIEL=D12(INFINITY)/D12(S) - L.A.SPIELMAN,
C  J.COLL.INT.SCI.,33,562,(1970)
C  EPS IS A CONVERGENCE PARAMETER
        DOUBLE PRECISION S,A21,EPS,AD,BD,A,B,AMB,APB,KS1,KS2,LS1,LS2,N2,N,
       1KN,RT2,AN,BN,CN,DN,AND,BND,CND,DND,DLTA,SAMB,SAPB,CAPB,FAMB,FBMA,
       2E1AMB,S1AMB,S1APB,C1APB,S2AMB,S2APB,C2APB,S3AMB,S3APB,C3APB,X1,X2,
       3X3,Y1,Y2,Y3,KNUD,KH1,KH2,LH1,LH2,SA,F,FH
         IF(S.LT.(5.D0+A21)) GOTO 70
        DSPIEL=1.D0
        RETURN
 70     IF(S-(1.11D0+A21))40,50,50
 40     DSPIEL=1.D0/((1.D0+1.D0/A21)*(S-1.D0-A21))
        GOTO 60
 50     AD=(S*S-A21*A21+1.D0)/(2.D0*S)
        AD=AD+DSQRT(AD*AD-1.D0)
        A=DLOG(AD)
        BD=(S*S+A21*A21-1.D0)/(2.D0*A21*S)
        BD=BD-DSQRT(BD*BD-1.D0)
        B=DLOG(BD)
        AMB=A-B
        APB=A+B
        KS1=0.D0
        KS2=0.D0
        LS1=0.D0
        LS2=0.D0
        RT2=1.41421356237309
        SAMB=DSINH(AMB)
        SAPB=DSINH(APB)
        CAPB=DCOSH(APB)
```

```
      EAMB=DEXP(AMB)
      EBMA=1.D0/EAMB
C  THE FOLLOWING LOOP CALCULATES THE TERMS OF THE SERIES FOR KS1,KS2,
C    LS1 AND LS2
      N1=0
   10 N1=N1+1
      N=DFLOAT(N1)
      M=N1+N1
      N2=DFLOAT(M)
      KN=N*(N+1.D0)/((N2-1.D0)*(N2+1.D0)*(N2+3.D0)*RT2    )
      X1=(N-0.5D0)*AMB
      Y1=(N-0.5D0)*APB
      X2=X1+AMB
      Y2=Y1+APB
      X3=X2+AMB
      Y3=Y2+APB
      S1AMB=DSINH(X1)
      S1APB=DSINH(Y1)
      C1APB=DCOSH(Y1)
      S2AMB=DSINH(X2)
      S2APB=DSINH(Y2)
      C2APB=DCOSH(Y2)
      S3AMB=DSINH(X3)
      S3APB=DSINH(Y3)
      C3APB=DCOSH(Y3)
      E1AMB=DEXP(-X2)
      DLTA=4.D0*S2AMB*S2AMB-((2.D0*N+1.D0)*SAMB)**2
      KNUD=KN/DLTA
      AN=(N2+3.D0)*(4.D0*E1AMB*S2AMB+(N2+1.D0)**2*EAMB*SAMB+
     1   2.D0*(N2-1.D0)*S2AMB*C3APB -2.D0*(N2+1.D0)*S3AMB*C1APB-
     2    (N2+1.D0)*(N2-1.D0)*SAMB*CAPB)*KNUD
      BN=-(N2+3.D0)*(2.D0*(N2-1.D0)*S2AMB*S2APB-
     1   2.D0*(N2+1.D0)*S3AMB*S1APB+(N2+1.D0)*(N2-1.D0)*SAMB*SAPB)*
     2    KNUD
      CN=-(N2-1.D0)*(4.D0*E1AMB*S2AMB-(N2+1.D0)**2*EBMA*SAMB+
     1   2.D0*(N2+1.D0)*S1AMB*C3APB-2.D0*(N2+3.D0)*S2AMB*C2APB+
     2   (N2+1.D0)*(N2+3.D0)*SAMB*CAPB)*KNUD
      DN=(N2-1.D0)*(2.D0*(N2+1.D0)*S1AMB*S3APB-
     1   2.D0*(N2+3.D0)*S2AMB*S2APB+(N2+1.D0)*(N2+3.I0)*SAMB*SAPB)*
     2    KNUD
      AND=(N2+3.D0)*(2.D0*(N2-1.D0)*S2AMB*S2APB-
     1    2.D0*(N2+1.D0)*S3AMB*S1APB-(N2+1.D0)*(N2-1.D0)*SAMB*SAPB)*
     2 KNUD
      BND=-(N2+3.D0)*(-4.D0*E1AMB*S2AMB-(N2+1.D0)**2*EAMB*SAMB+
     1 2.D0*(N2-1.D0)*S2AMB*C2APB-2.D0*(N2+1.D0)*S3AMB*C1APB+
     2    (N2-1.D0)*(N2+1.D0)*SAMB*CAPB)*KNUD
      CND=-(N2-1.D0)*(2.D0*(N2+1.D0)*S1AMB*S3APB-
     1    2.I0*(N2+3.D0)*S2AMB*S2APB-(N2+1.D0)*(N2+3.D0)*SAMB*SAPB)*
     2    KNUD
      DND=(N2-1.D0)*(-4.D0*E1AMB*S2AMB+(N2+1.D0)**2*EBMA*SAMB+
     1   2.D0*(N2+1.D0)*S1AMB*C3APB-2.D0*(N2+3.D0)*S2AMB*C2APB-
     2    (N2+1.D0)*(N2+3.D0)*SAMB*CAPB)*KNUD
      X1=(N2+1.D0)*(-AN+AND-BN+BND-CN+CND-DN+DND)
      X2=(N2+1.D0)*(-AN-AND+BN+BND-CN-CND+DN+DND)
      Y1=(N2+1.D0)*(+AN+AND+BN+BND+CN+CND+DN+DND)
      Y2=(N2+1.D0)*(+AN-AND-BN+BND+CN-CND-DN+DND)
      KS1=KS1+X1
      KS2=KS2+X2
      LS1=LS1+Y1
      LS2=LS2+Y2
      F=(KS1*KS2-LS1*LS2)/(KS1+KS2-LS1-LS2)
      IF(N1.GT.1)GOTO 30
   20 FH=F
      GOTO 10
   30 IF(DABS((F-FH)/FH).GT.EPS) GOTO 20
      SA=DSINH(A)
      ISPIEL=RT2*(1.D0+1.D0/A21)*SA*F/6.D0
   60 CONTINUE
      RETURN
      END
```